THE EFFECTS OF STRUCTURE AND LIGAND VARIATIONS ON THE LUMINESCENCE OF EUROPIUM(III) COMPLEXES

By

ORBETT T. ALEXANDER

A dissertation submitted in fulfilment of the requirements for the degree of

PHILOSOPHIAE DOCTOR

Faculty of

NATURAL AND AGRICULTURAL SCIENCES

In the

DEPARTMENT OF CHEMISTRY

At the

UNIVERSITY OF THE FREE STATE

Supervisor: Prof. Hendrik G. Visser

Co-Supervisor: Dr. Alice Brink

February 2018

Acknowledgements

I firstly would like to send my gratitude and appreciation to almighty God for granting me the wisdom, perseverance and understanding for all the years of my life. I would like to thank Him for giving me the strength that I needed throughout the trials and tribulations I underwent all my life. I am, that I am today because of His grace…..PSALM 23.

Thank you Prof. H.G. Visser for your guidance, understanding, patience, support and most of all; the challenges you threw at me to sharpen my understanding of the kind of science we were practicing. I am honoured to have worked with you.

Thank you Dr. A. Brink for the friend in science you were to me, the guidance, support, patience and encouragements that you gave me. I am very honoured to have worked with the person of your kind.

Thank you Prof. A. Roodt for the support and opportunities you gave me. I am forever grateful for them.

Thank you Prof. R.E. Kroon for the support, patience, understanding and guidance that you gave me. I am truly honoured to have crossed your path.

I am very happy to call these two friends of mine Dr. D.V. Kama and Dr. P.P. Mokolokolo as fellow doctors. We have laughed, fought, partied, comfort, cried, toured, studied, advised, encouraged, gin'ed, marrau'd and mostly cared for each other. That was due to the love we have for each other. May success be the only thing left for us in this lifetime!

I would like to thank the Inorganic Group for their support and crazy moments and lots of braai's we had. It was a wonderful journey we had fellows.

Thanks to my dear friend Dr. A. Frie all the way from Switzerland (Zurich). A good friend you've been to me so far regardless of the distance between us. Amongst all the craziness we did together….BUSH WALKING!!…..back in Kruger National Park was the craziest.

Vote of appreciation and gratitude to Mr. Mohammed Elmakki Azeez and Miss S. Xaba for always lending me your ears during tough times. Your encouragements and advices were of very high importance to me.

Special thanks and love to my family: Motshidisi, Ronnie, Ntsoaki and Tebogo….my lovely Fiance Thandiwe….our lovely daughter Olorato (God is love) and my mother in law Mannini and uncle Setjhele. My nephew Itumeleng and my two nieces Bokamosho and Palesa.

You guys have been the pillar of strength to me all the time. I really appreciate all the comforts, love, care, and encouragements you spoiled me with. This kind of achievement is the first one in the whole history of the family and therefore I did it for all of us.

To the late Mr Lice W. Alexander….i just wishes you were around Papa to celebrate this success with me. I know you would have been mad proud of me. I thank God for your life and being a good father to all of us.

Table of Contents

Abbreviations and Symbols

Abbreviation	Meaning
DMMP	3,3-Dimethyl-2,4-pentanedione
DMC	3-Chloro-2,4-pentanedione
TCPB	4,4,4-Trifluoro-1-chlorophenyl-butanedione
DBBrM	2-Bromo-1,3-diphenyl-propanedione
DBM	1,3-diphenyl-propanedione
BZAN	Benzoic Anhydride
TMHD	2,2,6-Tetramethyl-3,5-heptanedione
BCA	Benzene Carboxylic Acid
Z	Number of molecules in a unit cell
Å	Angstrom
NMR	Nuclear Magnetic Resonance spectroscopy
IR	Infrared spectroscopy
XRD	X-ray Diffraction
ν	Stretching frequency on IR
δ	Chemical shift
ppm	Units of chemical shift (parts per million)
π	pi
σ	Sigma
α	Alpha
β	Beta
γ	Gamma
λ	Wavelength
°	Degrees
°C	Degrees Celsius
K	Kelvin
ε	Extinction coefficient
g	Gram
M	Concentration ($mol.dm^{-3}$)
T	Temperature

UV	Ultraviolet region in light spectrum
Vis	Visible region in light spectrum
$CDCl_3$	Deuterated Chloroform
DMF	Deuterated Dimethylformamide
CSD	Cambridge Structural Database
s	Singlet in NMR spectroscopy
d	Doublet in NMR spectroscopy
m	Multiplet in NMR spectroscopy
d(···)	Distance
Hz	Hertz
PL	Photoluminescence
nm	Nano-meter

Summary

The chemistry of lanthanides has expanded immensely across many scientific fields over the years and that was mainly due to the rare versatility exhibited by the spectroscopic and magnetic nature of these metals in the series. With the coordination nature of these lanthanoids not governed by the orbital directionality, as is the case with transition metals, the relative coordination chemistry of this series becomes of great interest and therefore is susceptible to ground breaking science across many scientific disciplines. Europium (III) metal ion in particular, has been involved in many scientific fields due to its sterling spectroscopic properties. Its ternary analogues have been extensively employed as emitting layers in the edifice of optoelectronic devises. Moreover, its applications extend as far as tailoring active luminescence bioprobes in biomedical sciences which is a vast field with a lot of other related applications in it. The main interest has always been its red narrow emission spectral profile which is susceptible to any organic matrix it is submerged in.

The principle aim of this study was to gain insight into the chemistry, coordination and photoluminescence behaviour of ternary Eu^{III} based complexes. From this idea, it was decided to synthesize a few novel ligand systems. This include (*E*)-1-((9-ethylcarbazol-3-ylimino)methyl)-napthanol, *(E)*-2-(9-ethylcarbazol-3-yliminomethyl)-6- methoxy phenol, (*E*)-2-methoxy-(6-(phenyliminomethyl))-phenol, *(E)*-1-((2-(pyridin-2-yl)hydrazono) methyl) naphthalene-2-ol, *(E)*-2-methoxy-6-((2-(pyridin-2-yl)hydrazono)methyl)phenol, *(E)*-2-(2-((2-hydroxynaphthalen-1-yl)methylene)hydrazinyl) quinolin-8-ol and *(E)*-2-(2-(2-hydroxy-3-methoxybenzylidene)hydrazinyl) quinolin-8-ol characterized by means of IR, UV/Vis and NMR (^{1}H, ^{13}C) spectroscopy. Furthermore, the solid state structural characterization was carried out using single crystal X-ray diffraction spectroscopy for compounds with suitable single crystals X-ray diffraction collection. However, the intended tailoring of ternary Eu^{III} complexes with this novel ligand species was not successful. The ligand systems synthesized were designed with the idea to be potentially biologically active and fluorescent by itself. They were analysed for photoluminescence properties and were successfully found to be luminous and are to be sent for cell testing.

A range of ternary Eu^{III} based complexes, of the form [Eu(β-diketone)$_3$ X] (X = 1,10-phenanthroline), were synthesized by using selected acetyl acetone derivatives (β-diketone) as parallel ligand system used in this study. The bidentate β-diketone ligands

used are 1,3-Diphenyl-propanedione (DBM), 2) 4,4,4-Trifluoro-1-chlorophenyl-butanedione (TCPB), 3) 2-Bromo-1,3-diphenyl-propanedione (DBBrM), 4) 3-Chloro-2,4-pentanedione (DMC), 5) 3,3-Dimethyl-2,4-pentanedione (DMMP), and 6) Benzoic anhydride (BZAN). The Eu^{III} based analogues with the bidentate *β*-diketone ligand given above were successfully synthesized and characterized by means of IR, X-ray diffraction and Elemental Analysis spectroscopy. These obtained ternary Eu^{III} based complexes are [*tris*-(4,4,4-Trifluoro-1-chlorophenyl-butanedione) mono(1,10-phenanthroline) europium(III)], [*tris*-(2-Bromo-1,3-diphenyl-propanedione) mono(1,10-phenanthroline) europium(III)], [*tris*-(1,3-Diphenyl-propanedione) mono (1,10-phenanthroline) europium(III)], [*tris*-(3-Chloro-2,4-pentanedione) mono(1,10-phenanthroline) europium(III)], [*tris*-(2,2,6,6-Tetremethyl-heptanedione) mono(1,10-phenanthroline) europium(III)], *tris*-(Benzoic Anhydride)-*mono*-(1,10-phenanthroline) europium(III)] and {[*hexa*-(Benzyl carboxylic acid) *bis*-(1,10-phenanthroline) di-europium(III)]-*μ*-[κ^2-O,O'-(benzyl carboxylic acid)$]_2$}. These above stated ternary Eu^{III} complexes were analysed for photoluminescence and all proved to be luminous. However, there were significant differences in the spectral identity of these respective complexes and that was due to the ligand nature coordinated to the Eu^{III} metal ion. The observed spectral identities are defined in terms of relative Stark splitting of the complexes which is induced by the symmetry imposed on the Eu^{III} ion by the atomic orientations around the metal. The atomic orientations around the Eu^{III} metal ion are dictated by the steric hindrance imposed by the peripheral derivatization on the acetyl acetone back bone. It was crystallographically deduced that the high quantum yield (82%) of complex [*tris*-(4,4,4-Trifluoro-1-chlorophenyl-butanedione) mono(1,10-phenanthroline) europium(III)] was due to strong binding of the antenna ligand to the metal ion, facilitating efficient energy transfer to give high luminous efficiency.

There were successful correlations drawn between the photoluminescence and the crystallographic data obtained of the [Eu(*β*-diketone)$_3$ X] (X = 1,10-phenanthroline) complexes. The respective point groups from both disciplines could be matched. However, the polyhedron constructed for atoms directly bonded to the Eu^{III} metal ion indicates higher symmetry point groups due to observed polyhedral distortions therein. The correlation of data from these two scientific disciplines rubber stamp the proof of concept of using the method detailed in this study in analysis of the site symmetry of the Eu^{III} metal ion in bulk organic system, UPNP or any other organic system for that matter.

1 Introduction

In this chapter:
A brief overview of electronic properties of the lanthanide series. Brief discussions on relative applications in which this project can be relevant to. Detailed aims of this study.

1.1. A Brief Introduction on Lanthanides

The lanthanides are a series of elements comprising of 15 metals in the periodic table with atomic numbers from 57 through to 71. These elements range from lanthanum to lutetium with a general configuration of $[Xe]4f^n5d^16s^2$, they arguably holds rather a unique position in the periodic table which largely corresponds to the first period of the *f*-block elements. This series of lanthanoids, as alternatively called, is commonly known as rare earths.[1]

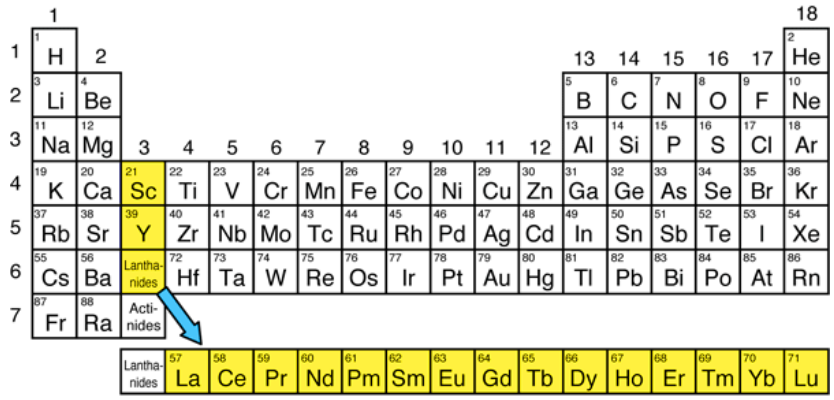

Figure 1.1: The periodic table highlighting the lanthanide series.

The series oxidation states are largely influenced by their specific electronic configurations and the low electronegativity causing them to lose three electrons from $5d^1$ and $6s^2$ orbitals attaining stable oxidation state in the process. The $4f^n$ Sub-shells lying inside the ion shielded by the $5s^2$ and $5p^6$ sub shells even if the 6s shell is removed, strongly suggests a very similar chemical behaviour of the series. The gradual $4f^n$ shell electron filling , with several unpaired electrons for some, dictates unique properties to the series and that is mainly translated to the spectroscopic (absorption and luminescent) and magnetic properties thereof. In this thesis, we will solely focus on the spectroscopic aspect of the selected lanthanide (Eu^{III}) of interest.1

[1] Moeller, T., (**1973**). *The Chemistry of the Lanthanides*, *Pergamon Texts in Inorganic Chemistry*, vol 25, Elsevier, New York.

1.2. Overview of Europium (III) Chemistry

1.2.1. Introduction

The brightly emitting europium doped phosphor (Y_2O_3:Eu^{III}) was discovered at the beginning of the 20th century. This europium (III) phosphor is still in use to date in fluorescent tubes, light emitting diodes (LED's) and TV screens. Therefore these lanthanide ions, with their rather unique spectroscopic and magnetic properties, are deemed ideal candidates for many other basic as well as sophisticated applications.[2,3,4,5]

Europium (III) metal ion and its chemistry have never looked back ever since its discovery and have been usefully tossed around many scientific fields. The advancement in its science went as wide as covering almost every aspect of our current high technology world. Amongst many other scientific fields it features in, europium (III) complexes are noted in optical and telecommunication systems, magnetic resonance imaging (MRI), economical lighting systems to mention a few.[6,7,8,9]

In addition, medical-oriented applications such as time-resolved luminescence immunoassays and bio-analytical sensing are now well established.[10,11] All this is stirring a great deal of research effort aimed at tailoring highly luminescent Eu^{III}-based molecular and polymeric compounds.

---

[2] Bunzli, J.G.; Eliseeva, S.V., (**2011**) *Lanthanide Luminescence: Photophysical, Analytical and Biological Aspects*; *Hanninen, P.; Harma, H., Eds*., Springer, Vol. 7, Springer Verlag: Berlin, 1-45.

[3] Ma,Y.; Wang,Y., *Coord. Chem. Rev*., **2010**, 254, 972-990.

[4] Justel, T.; Nikol, H.; Ronda, C., *Angew. Chem. Int. Ed*., **1998**, 37, 3085-3103.

[5] Armelao, L.; Quici, S.; Barigelletti, F.; Accorsi, G.; Bottaro, G.; Cavazzini, M.; Tondello, E., *Coord. Chem. Rev*., **2010**, 254, 487-505.

[6] Bradley, J. D. B.; Pollnau, M., *Laser Photonics Rev*. **2011**, 5, 368-403.

[7] Martín-Ramos, P.; Coya, C.; Alvarez, A. L.; Silva, M. R.; Zaldo, C.; Paixao, J.A.; Chamorro Posada, P.; Martín-Gil, J.J., *Phys. Chem. C.*, **2013**, 117, 10020-10030.

[8] Law, G.-L.; Kwok; Wong, W.-T.; Wong, K.-L.; Tanner, P.A., *J. Phys. Chem. B*., **2007**, 111, 10858-10861.

[9] Kido, J.; Okamoto, Y., *Chem. Rev*. **2002**, 102, 2357-2368.

[10] Bunzli, J.G.; Eliseeva, S.V., *J. Rare Earths*, **2010**, 28, 824-842.

[11] Bunzli, J.G., *Chem. Rev*., **2010**, 110, 2729-2755.

1.2.2. Europium Chemistry in Biological Sciences.

There is a vast need for the use of lanthanides in building efficient lanthanide luminescent bioprobes (LLB's). That is mainly because of their photogenic nature. These LLB's are essentially used in time-resolved luminescence immunoassays. Therefore, the sensitivity of this LLB's is somewhat better than that of radioactivity-based assays.

Eu^{III} based complexes plays and outstanding role in the biological field of study in terms of photoluminescence. The success in the use of Eu^{III} ion in this field depends hugely on the organic matrix in which it is submerged. The ligand design for building efficient and effective LLB's is governed by several requirements chemically, photo-physically and biochemically. [12,13,14]

The requirements to be met entail:

1. Efficient sensitization
2. Embedding of the emitting ion into a rigid and protective cavity minimizing non-radiative decay.
3. Complexes with long excited states lifetimes.
4. Water solubility
5. Whenever relevant, ability to couple to bioactive molecules while retaining their photo-physical properties and no altering the bio- affinity of the host.

It is worth noting that, quite a lot of times, number 1 and 5 are essentially vital and have been embarked on for decades in pursue for improved luminous Eu^{III} analogues across many scientific fields.[15,16] Informed ligand designs, in this case, would lead to useful Eu^{III} analogues for LLB's.

The depiction in **Figure 1.2** illustrates the versatility of the Eu^{III} based analogues in biosciences.

[12] Bunzli, J.G; Chauvin, A.S; Vandevyver, C.D.B; Song, B; Comby, S., (**2008**), *Lanthanide bimetallic helicates for in vitro imaging and sensing*. Ann New York, *Acad Sci*., 1130, 97-105.

[13] Pandya, S.; Yu, J.H.; Parker, D., *Dalton Trans.*, **2006**, 2757-2766.

[14] Hemmila, I.; Mukkala, V.M., *Crit. Rev. Clin. Lab. Sci*., **2001**, 38, 441-519.

[15] Eliseeva, S.V.; Bunzli, J.C., *Chem. Soc. Rev.*, **2010,** 39 (1), 189-227.

[16] Xu, H.; Sun, Q.; An, Z.; Wei, Y.; Liu, X., *Coord. Chem. Rev.*, **2015,** 293-294, 228-249.

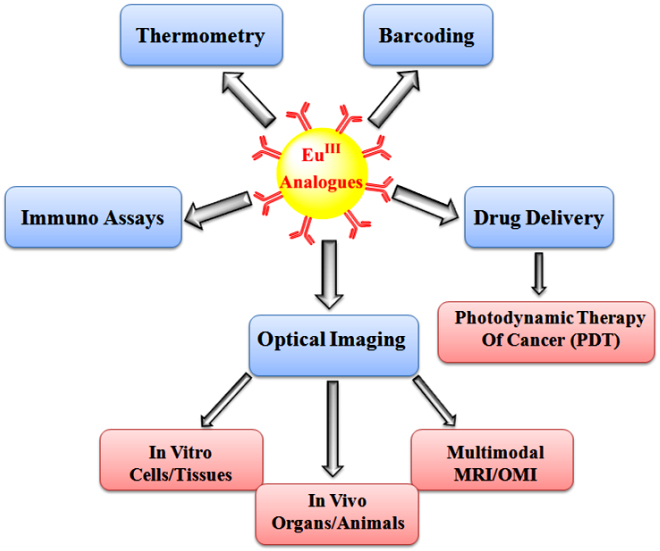

Figure 1.2: Diverse applications of Eu^{III} based analogues in biosciences. Adapted from[17]

The lanthanide and inorganic complexes are used, often conjugated to matrices like acadin, biotin, monoclonal antibodies or peptides; to ensure biochemical specificity. Subsequently, that has prompted investigations on luminescence spectra of Eu^{III} based complexes in bulk crystals. However, in UCNP (up-conversion nano-particles) Eu^{III} based analogues, the optical properties (e.g., excitation/emission wavelengths, quantum yield, and luminescence lifetimes) of Eu^{III} in the nanosized hosts may differ significantly from those of the bulk crystals. Therefore to overcome this, a comprehensive survey of the fundamental photo-physics, and other complementary scientific disciplines, of Eu^{III} -activated NP's is essential for optimizing their optical properties and exploring new applications.[18]

Furthermore, the main advantage for Eu^{III} complexes in bio-imaging is the dependence of the emission spectral pattern and lifetimes on the coordination environment. The sharp emission bands arising from Eu^{III} complex $^5D_0 \rightarrow {}^7F_J$ transitions that are subtly sensitive to the nature and type of ligand donor and the coordination geometry around the ion renders them the perfect imaging agents. It is these above stated properties that enable the rational design of responsive probes where binding events at the Eu^{III} ion can be interrogated directly using luminescence methods.[19]

[17] Bunzli, J.C., *J. Lumin.*, **2016**, 170, 866-878.

[18] Tu, D.; Zheng, W.; Huang, P.; Chen, X., *Coord. Chem. Rev.*, **2017**, https://doi.org/10.1016/j.ccr.2017.10.027.

[19] Amoroso, A.J.; Pope, S.J., *Chem. Soc. Rev.*, **2015,** 44 (14), 4723-4742.

1.2.3. Europium Chemistry in Optoelectronic Devices

It is the special spectroscopic, electronic and magnetic properties of lanthanide ions that render them particularly interesting. There are rather two main domains that which the lanthanide induced emissions are partitioned-in depending on the emission wavelength. The first domain is that of optical and electro-optical devices, where vast application cross-section addresses aspects like laser materials,[20] amplifiers,[21] organic light emitting diodes[22] (OLED's) to mention few. The second domain is of biosciences.

The use of Eu^{III} complexes as potential emitting agents in the edifice of optoelectronic devices comes a long way. That is mainly because of its sharp emissions with high colour purity and long lifetime radiations as a result of well shielded inner *f*-orbital's by the outermost *s* and *p* orbitals. [23]

The quest in attaining highly luminescent Eu^{III} complexes has increased drastically over the years. Through the antenna effect[24] (Eu^{III} ion luminescence triggered through the coordinated organic molecule via energy transfer), many exotic organic matrixes has been employed in trying to get high emitting complexes. The use of ternary Eu^{III} complexes (is exemplary) with an ancillary neutral ligand has given rise to further peripheral *pi*-conjugated extensions both on the anion and the neutral ligand. [25]

The ever evolving technology has equally enticed growth in the development of new and efficient organic LED's. The transition of technology for producing flexible colour displays from liquid-crystal to electroluminescent polymeric materials has prompted a lookout for improved phosphorescent metal complexes.[26,27] Therefore, apart from lanthanides unique *f*-electron configuration, Eu^{III} in particular, their other advantage lies with their ability to have slow fall-off of the luminescence intensity which can last tens of milliseconds and narrow

[20] Bradley, J.D.B.; Pollnau, M., *Laser Photonics Rev*. **2011**, 5, 368-403.

[21] Kuriki, K.; Koike, Y.; Okamoto, Y., Chem. Rev., **2002**, 102 (6), 2347-2356.

[22] Im, S.Y.; Go, D.H.; Ryu, J.G.; Kim, Y.S., *IEICE. Trans. Electr*., **2017**, E100–C (11), 1021-1025.

[23] Ahmed, Z.; Iftikhar, K., *Inorg. Chem.*, **2015,** 54 (23), 11209-21125.

[24] Weissman, S. I., *J. Chem. Phys.*, **1942,** 10 (4), 214-217.

[25] Xu, H.; Sun, Q.; An, Z.; Wei, Y.; Liu, X., *Coord.Chem. Rev.*, **2015,** 293-294, 228-249.

[26] Yakimanski, A.V.; Goıkhman, M.Y.; Podeshvo, I.V.; Ananeva, T.D.; Smyslov, R.Y. Nekrasova, T.N.; Loretsyan, N.L.; Bochkarev, M.N.; Il'ichev, V.A.; Konev, A.N., J. Opt. Technol., **2011**, 78 (7), 430-434.

[27] Kido J.; Okamoto Y., *Chem. Rev.*, **2002,** 102 (6), 2357-2368.

emission bands. It is therefore for those reasons that ternary Eu^{III} complexes are used as dopants or fluorescent tags on the polymeric matrices and thereby play a role of macromolecular ligand.[28,29,30]

1.3. Aim of this study

Considerable interest has been shown towards the organo-lanthanide complexes, due to the rich coordination chemistry therein and the wide range of spectroscopic properties they bring in the photoluminescence field of study. Particularly the use of Eu^{III} analogues with their desirable properties, are intensively used as key emitting agents in many basic lighting industry. Furthermore, these Eu^{III} based analogues are considered to have paved a successful tenure to date, as promising light emitting agents in the biomedical sciences. The concept of these organo-lanthanide complexes entails enhancing the nature of luminescence of the lanthanoids (destroying the spherical symmetry of the Ln-ion) by exciting the complex through the coordinated organic matrix via the intra-energy transfer. That approach is called antenna effect. The considerations and related examples will be discussed extensively in Chapter 2.

The luminance resultant of any Eu^{III} analogues using the antenna approach is subject to the energy transfer efficiency imposed by the nature of the organic matrix used. Sufficiently, the coordination modes dictated by the nature of these organic matrices somewhat defines the symmetry in which the Eu^{III} ion find itself in and therefore potentially influences the nature of luminescence thereof.

This study is concerned with investigating the solid state coordinative and luminescence behaviour of ternary Eu^{III} based complexes. It entails the investigations about the effect of the organic ligands toward both the intensity and the spectral identity of the Eu^{III} analogues in question. Furthermore, it entails the relative impact of the coordination nature of the surrounding organic ligands which is highly influenced by the steric and electronic effects therein. The main objectives of this study were focused on the synthesis and characterization of ternary Eu^{III} complexes based on the organic ligands of interest for this project.

[28] Weng, H.; Yan, B., *Inorg. Chem. Comm.* **2016,** 63, 11-15.

[29] Zhang, P.; Wang, Y.; Liu, H.; Chen, Y., *J. Mat.Chem.*, **2011,** 21 (45), 18462.

[30] Shi, M.; Li, F.; Yi, T.; Zhang, D.; Hu, H.; Huang, C., *Inorg. Chem*., **2005**, 44, 8929-8936.

The objectives are summarized as follows:

1. To synthesize a range of mono-negative bidentate ligands (L,L'-Bid) and tridentate ligands (L,L',L''-Trid). These ligands would allow convenient coordination of selected aromatic systems; ear-marked to be of great use in the photoluminescence fraternity. The synthesized ligands, according to Schiff's organic framework, are constituted by amine substituents with various steric and biological properties coordinated to the backbone forming the salicylidene bi- and tridentate ligands. (**SalH**). Investigate the spectroscopic nature of the synthesized ligands by conducting the absorption and photoluminescence experiments.

2. To synthesise complexes of $[Eu(L,L'\text{-}Bid)_n\ X]$ (X = 1,10-phenanthroline) with a variety of synthesized imino bi-functional chelators. This is to investigate the effect of the bi-functionality of these different Schiff base ligands coordinated to the Eu^{III} ion towards the luminescence thereof.

3. To synthesize Eu^{III} complexes of $[Eu(\beta\text{-diketone})_3\ X]$ (X = 1,10-phenanthroline) form, with selected β-diketone ligands comprising of both steric and electronic properties coordinated to the acetyl acetone backbone. This is to investigate the detailed ligand effect towards the respective luminescence behaviour of the complexes and the relative coordination modes therein.

4. To analyse all the synthesized ligands and Eu^{III} complexes for photoluminescence properties and measure quantum yields where possible.

5. To further characterise synthesized ligands and Eu^{III} complexes with single X-ray diffraction, IR and NMR spectroscopy.

6. To investigate any direct correlations between the photoluminescence results and the x-ray diffraction data. This is to investigate any correlation between the relative ligand orientations around the metal and the obtained luminescence spectral identity; together with luminescence intensities for all the Eu^{III} complexes.

7. A literature search on the Cambridge Structural Database (CSD) reveal that there are only four $[Eu(\beta\text{-diketone})_3\ X]$ (X = bidentate ligand) with *N,N'*-bidentate ancillary ligand and none of the structures has plain 1,10-phenonthroline ligand. Therefore

attempt to recrystallize single crystals suitable for X-ray diffraction would increase the CSD library on this type of complexes and further enable one to thoroughly investigate structural versus photoluminescence properties.[31]

In the following chapters, a brief literature review of luminous lanthanide chemistry, Eu^{III} based chemistry in particular, is presented and followed by the systematic presentation and discussion of experimental results.

[31] Cambridge Structural Database (CSD) Version 5.38, November 2016 update. Latest access date: 15/03/18.

2 Literature

In this chapter:
A brief history on the fundamentals of photoluminescence of lanthanides will be discussed. Discussion on relative applications of Euopium (III) based complexes in different scientific fields.

2.1. Introduction

Lanthanides have two distinct characteristics, amongst many, that are known to be of great interest for many years now. The first one is their magnetic properties and the second being their luminous abilities.[1] Both of these properties are the subject of the $4f^n$ shell electron filling and to some extent dictates the degree of strength in terms of magnetism and the relative emission colours for photoluminescence purposes across the series.[2,3,4]

Lanthanoids, as alternatively called, have very characteristic and very narrow line-like emission bands with radiative emissions ranging from the UV to near infrared regions (NIR). The latter statements holds for all metal ions in the series, except for those with completely filled 4f orbitals like lanthanum (La) and lutetium (Lu) resulting to non-radiative relaxations. Contrary to any other metals, lanthanides are known to exhibit intense luminescence with high colorimetric purity. With that mentioned, on the down side, they have a very low absorptivity for such good luminescence behaviour.[5,6,7] Majority of the trivalent lanthanides ions in the series are luminescent with corresponding transitions occurring as electronic rearrangement within the 4f orbitals. Some of these ions are found to be phosphorescent (e.g. Eu^{3+} and Tb^{3+}), some are fluorescent (e.g. Ho^{3+} and Yb^{3+}) while many of them are both (e.g. Pr^{3+} and Nb^{3+}).[8]

[1] Bunzli, J.G., *Inorg. Chimi. Acta*, **1987,** 139, 219-222.

[2] Ma, C.G.; Brik, M.G.; Liu, D.X.; Feng, B.; Tian, Y.; Suchocki, A., *J. Lumin.,* **2016**, 170, 369-374.

[3] Karroker, D. G., *J. Chem. Edu.*, **1970**, *47* (6), 424-430.

[4] Eliseeva S.V., Bunzli, J.C., *Chem. Soc. Rev.*, **2010,** 39 (1), 189-227.

[5] Bunzli, J.G.; Eliseeva, S.V.,*Comprehensive Inorganic Chemistry II*, Elservier, **2013**, 340-397.

[6] Bunzli, J.G., *Coord. Chem. Rev.,* **2015,** 293-294, 19-47.

[7] Ahmed, Z.; Iftikhar, K., *Inorg Chem.*, **2015,** 54 (23), 11209-11225.

[8] Bunzli, J.G., *Elsevier*, **2016**, 50, 141-176.

2.1.1. Lanthanide Luminescence

Lanthanides are widely known for their multi-spectral and characteristic narrow band emissions near-infrared regions. These narrow emissions certainly emerge from the intra-configurational f-f transitions. This is due to the moderate perturbations by their surroundings as a result of the 5s and 5p filled orbitals shielding to the 4f orbitals. These intra-configurational 4f-4f transitions are to some extent electric dipole (ED, odd parity) induced transitions, some are magnetic dipole (MD, even parity) induced or electric quadrupole dipole (QD).[9] The absorption of light by electrons moving around a nucleus is attributed to these operators which are linked to the nature of light.5 Moreover, the relative intensities of any lanthanide complexes are to some extent attributed to these operators with ED and MD being almost in the same measure of output. The intensities of the induced electric dipole f–f transitions can be derived from Judd–Ofelt theory. [10,11]

The relative intensities of lanthanide complexes are dictated by symmetry via the Laporte's parity rule. This spectroscopic selection rule forbids any centrosymmetric compounds that conserve parity. However, a ligand-field perturbed lanthanide ion can be partially allowed due to symmetry (non-centrosymmetric) assisted interactions allowing the mixing of electronic states of opposite parity into the 4f wave-functions.[12] The surrounding ligands (all electrons of the system except those of the lanthanide ion) to the lanthanide ion often destroy the spherical symmetry of the free ion. This observed effect is called the crystal field perturbation (CF). However, this crystal field effect should be the approximate of only the first coordination sphere in account to good shielding of the f-block electrons. Subsequently, the effect splits the individual *J*-levels only and permits the *J* mixing (see **Figure 2.1**) for its contribution to the wave-function.[13,14]

[9] Binnemans, K.; Van Herck, K.; GiSrller-Walrand, C., *Chem. Phys. Lett.*, **1997,** 266, 297-302.

[10] Gorller-Walrand, C.; Binnemans, K. (**1998**). *Handbook on the physics and chemistry of rare earths*, vol 25., Elsevier BV, Amsterdam.

[11] Walsh, B.M. (**2006**). *Judd–Ofelt theory: principles and practices*. Springer Verlag, Berlin.

[12] Liu, G.K. (**2005**). *In Spectroscopic Properties of Rare Earths in Optical Materials*; Springer, Vol. 83, Springer Verlag: Berlin**.**

[13] Souza, A.S., Couto dos Santos, M.A., *Chem. Phys. Lett.*, **2012**, 521, 138-141.

[14] Hernández, A.M.; de León Alfaro, M.A.; Villatoro, A.B.; Falcony, C.; Montalvo, T.R.; Medina, J.Z., *Open J. Synth.*, **2017,** 06 (1), 1-12.

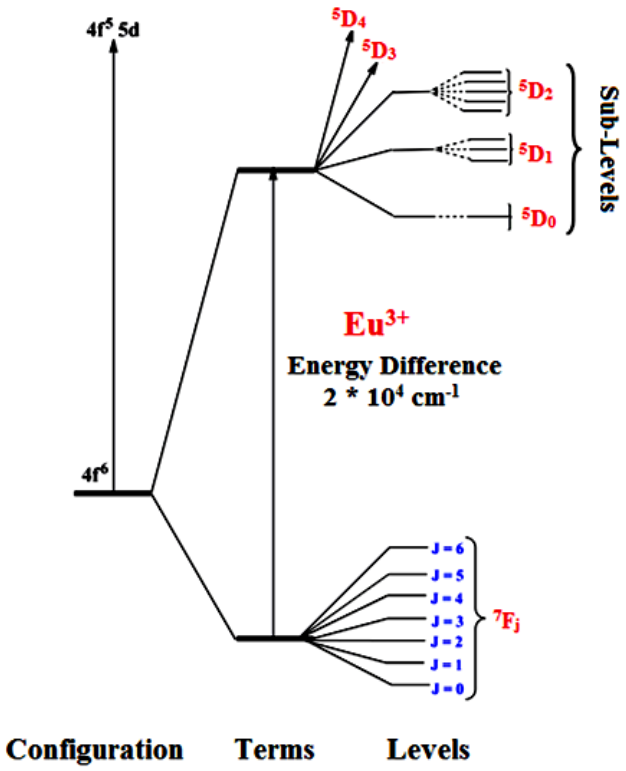

Figure 2.1: Splitting of energy levels for Europium (Eu^{3+}) ion. Redrawn from[15]

With the $5s^2 – 5p^6$ sub-shells protecting the 4f shell, all the observed transitions appear to be very narrow bands with their energy not being affected by any chemical environment of the ion. However, to gain some intensity, a transition between any two given sublevels must obey the symmetry-related selection rules.

Often, the analysis of the $^5D_0 \rightarrow {}^7F_j$ transitions gives away the local symmetry of the metal ion site. The complications arising from relative vibronic transitions, from the interactions between the phonon density of states and the electronic state and lastly from the energy migration from one site to another cannot be ruled out to make things a bit difficult in tracking the site symmetry of the metal ion. However, it is easy to recognize the existence of an inversion center since in this case the MD transitions are only transitions allowed and the $^5D_0 \rightarrow {}^7F_1$ transition tend to dominate in the emission spectral profile.[15,16.]

[15] Bunzli, J.G., *Inorg. Chimi. Acta*, **1987,** 139, 219-222.

[16] Bunzli, J.G.; Klein, B.; Wessner. D.; Alcock, N.W., *Inorg. Chimi. Acta***, 1982**, 59, 269-274.

2.1.2. Coordination Chemistry of Lanthanides

Lanthanides prefer hard donors like oxygen and that is due to the fact that they are strong Lewis acids. They mostly prefer negatively charged donor groups which to some extent hints at the importance of ionic bonding to lanthanides. The observed acid behaviour and the ionic character of the bonding correlates well with an increasing atomic number across the series and are more effective for the heavier lanthanide ions which possess smaller ionic radii (*see* **Figure 2.2**).

There are more complexes with oxygen (O) donors since they display the most effective coordinating properties towards lanthanides.[17] However, there are fairly enough N-based neutral ligands complexes with lanthanides in the literature.[18,19,20.] The coordination chemistry of lanthanides with S-donor and other chalcogens (Te, Se and Po) is hardly found in the literature.

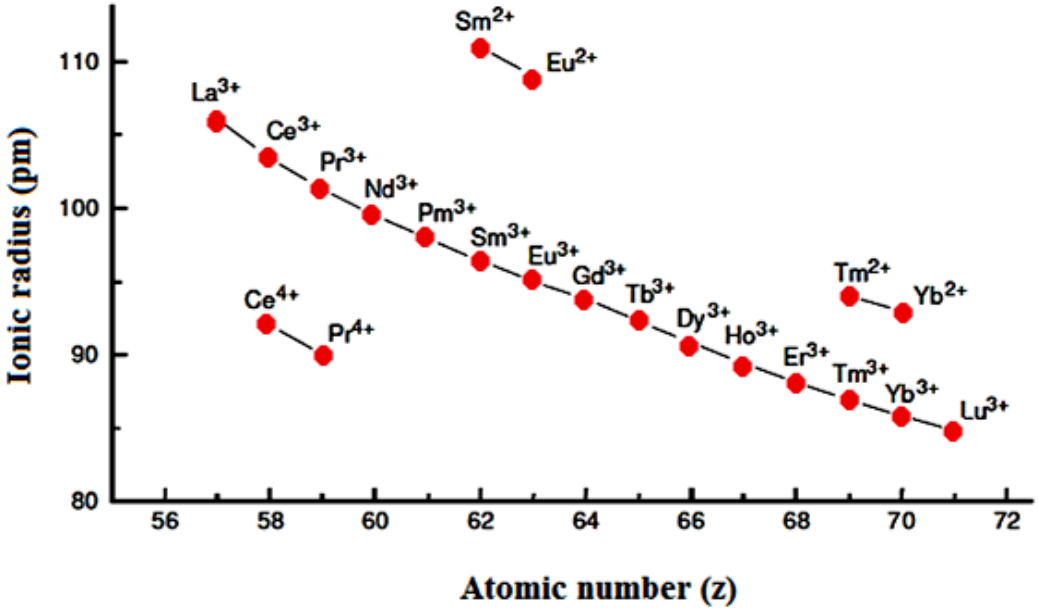

Figure 2.2: The ionic radii of the metals in the lanthanide series.

[17] Xu, H.; Sun, Q.; An, Z.; Wei, Y.; Liu, X., *Coord. Chem. Rev.*, **2015,** 293, 228-249.

[18] de Bettencourt-Dias, A.; Barber, P.S.; Viswanathan, S., *Coord. Chem. Rev.*, **2014,** 273, 165-200.

[19] Canard, G.; Koeller, S.; Bernardinelli, G.; Piguet, C., *J. Am. Chem. Soc*., **2008**, 130, 1025-1040.

[20] Dai, Z.; Tian, L.; Xiao, Y.; Ye, Z.; Zhang, R.; Yuan, J., *J. Mater. Chem*., **2013**, B1, 924-928.

Given the accentuated ionic nature, lanthanide ions possess the weak stereochemical preference and a labile coordination sphere. Consequential to the afore-stated character, results to variable coordination numbers and geometries (*see* **Figure 2.3**). Unlike the d-block transitions elements, given the diffuse radial dispersion of the core-like f-orbitals, the coordination geometry of the lanthanides is not governed entirely by the orbital directionality. It is however, ruled by ligand's orientation capacity imposed by the steric hindrance and to some extent the size of the cation. Subsequently, that dictates the coordination geometry of the complex which automatically advances to temper with the symmetry of the Eu^{III} ion therein.

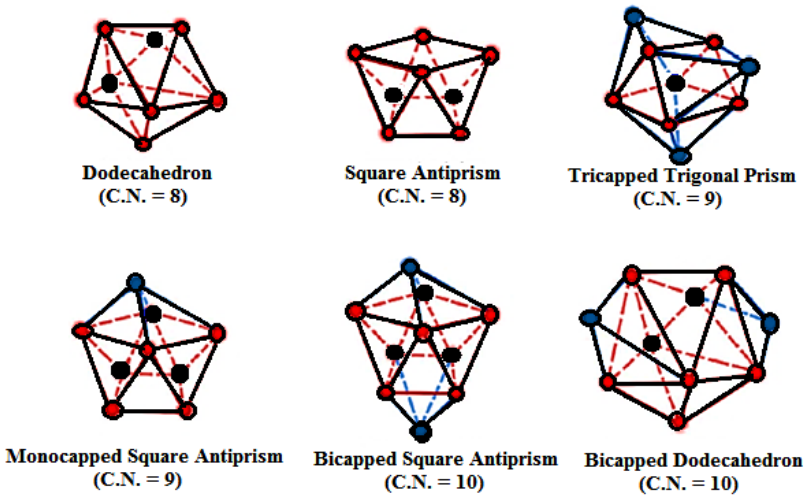

Figure 2.3: The typical coordination polyhedral for the lanthanide ions.

There are different coordination numbers of C.N. = 6 to C.N. = 12 depending likely on the size of the lanthanide ion. It is very hard or rather unusual to get C.N. = 6, only with ligands of particular steric hindrance. The first terms of the series (La and Nd) prefers the coordination number of C.N. = 9, whereas the heavier and smaller lanthanides ions (Gd-Lu) tend to heavily saturate their coordination spheres by reaching octa-coordination. [21,22.]

The following section entails the luminescence background of the Europium metal ion. Furthermore, the discussions of the luminescence sensitization of Eu^{III} based complexes across different scientific disciplines using different organic ligands.

[21] Karroker, D.G., *J. Chem. Edu.*, **1970**, 47 (6), 424-430.

[22] Bunzli, J.G.; Andre N.; Elhabin, M.; Muller, G.; Piguet, C., *J. Alloys Compd.*, **2000**, 66, 303-304.

2.2. The Chemistry of Europium(III) Metal

2.2.1. Introduction

Europium metal is one of the most interesting among the lanthanides, principally in its +3 (maximum anionic coordination points) oxidation state. Its spectrum of compounds represents several important properties across opto-electronic devices studies, [23,24] biological aspects[25], security[26], telecommunications[27] and many others. The main dominance of Eu^{III} complexes is in lighting devises and flouroimmuno luminescent probes as charted below.

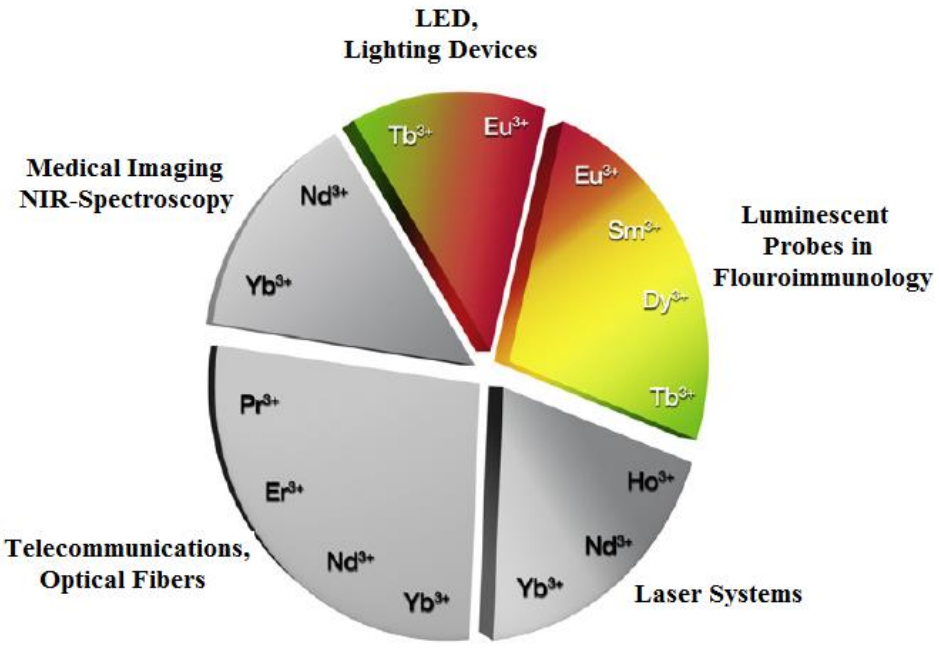

Figure 2.4: Type of emission and related application of lanthanides. Redrawn from.[28]

[23] Martín-Ramos, P.; Coya, C.; Alvarez, A.L.; Silva, M.R.; Zaldo, C.; Paixao, J.A.; Chamorro, P.; Martín-Gil, P.J.J., *Phys. Chem*., C, **2013**, 117, 10020-10030.

[24] Law, G.L.; Wong, K.L.; Tam, H.L.; Cheah, K.W.; Wong, W.T., *Inorg. Chem*., **2009**, 48, 10492-10494.

[25] Parker, D.; Williams, J.A.G., *Chem. Soc*., *Dalton Trans*, **1996**, 3613-3628.

[26] Kumar, P.; Singh, S.; Gupta, K.B., *Nanoscale,* **2016**, 8 (30), 14297-14340.

[27] Bradley, J.D.B.; Pollnau, M., *Laser Photonics Rev*., **2011**, 5, 368-403.

[28] Armelao, L.; Quici, S.; Barigelletti, F.; Accorsi, G.; Bottaro, G.; Cavazzini, M.; Tondello, E., *Coord. Chem. Rev*., **2010**, 254, 487-505.

2.2.2. Luminescence and Sensitization.

Europium metal is largely known for its red emission colour. It has five spectral emission lines near infrared region. These characteristic emission lines resonate at 580, 592, 612, 652 and 703 nm corresponding well with five europium spectral profile transitions of $^5D_0 \rightarrow {}^7F_0$, $^5D_0 \rightarrow {}^7F_1$, $^5D_0 \rightarrow {}^7F_2$, $^5D_0 \rightarrow {}^7F_3$, $^5D_0 \rightarrow {}^7F_4$. This multi-emitting metal ion is excited at one wavelength (traditionally at about 314 nm) to give the whole emission spectrum with the prime peak at about 612 nm. This 612 nm emission from the $^5D_0 \rightarrow {}^7F_2$ electric dipole transition is dominant and the monochromaticity is usually higher than 10 with respect to the $^5D_0 \rightarrow {}^7F_1$ electric dipole transition.[29]

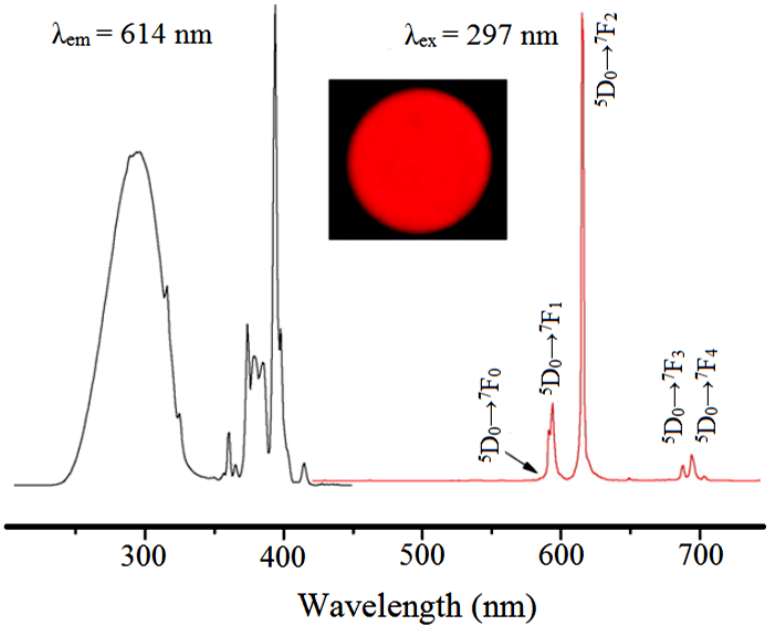

Figure 2.5: Typical Eu^{III} luminescence spectrum. Redrawn from[29]

The europium luminescent complexes are widely explored as potential luminescent layers in the edifice of opto-electronic devices for their red light emissions for two decades and more. The literature is filled with many of Eu^{III} based complexes with different organic chromophores to boost their luminous efficiencies. Subsequently, the trials in this luminous boosts using organic ligands has been tested with different exotic coordination modes and different donor atoms across many scientific fields; examples are portrayed in **Figure 2.6** below.

[29] Weng, H.; Yan, B., *Inorg. Chem. Comm.*, **2016**, 63, 11-15.

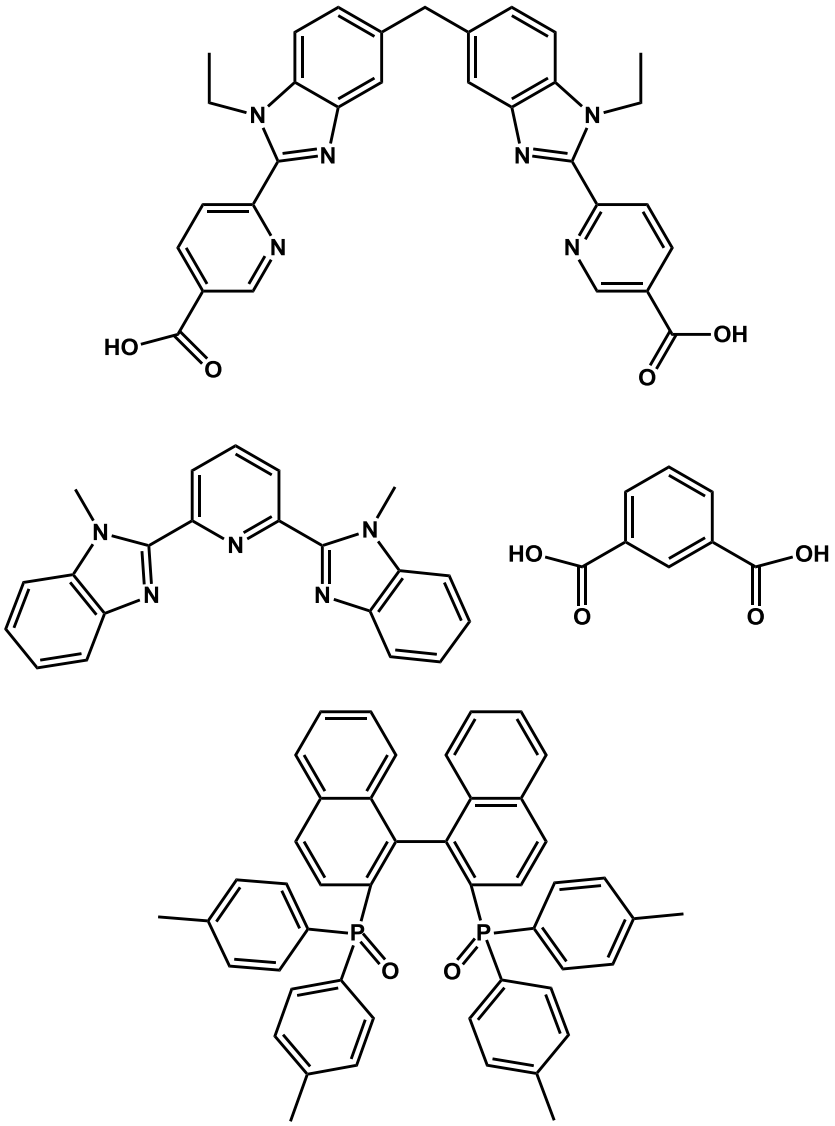

Figure 2.6: Typical examples of organic ligands used as luminescence sensitizers in Eu^{III} based complexes in different scientific fields.[30,31,32,33.]

The notion in using organic compounds to boost the luminescence of lanthanide ions was all birthed by an American chemist by the name of S.I. Weissman back in 1945.[34]

[30]Divya, V.; Freire, R.O.; Reddy, M.L.P., *Dalton Trans*, **2011**, 40, 3257-3268.

[31]Rodrigues, M.O.; da Costa, N.B.; de Simone, C.A.; Araujo, A.A.S.; Brito-Silva, A.M.; Paz, F.A.A.; de Mesquita, M.E.; Junior, S.A.; Freire, R.O., *J., Phys. Chem. B*, **2008**, 112 (14), 4204-4212.

[32]de Silva, G.; F.R., Malta O.L., Reinhard C., Gudel H.U., Piguet C., Moser J.E., Bunzli J.G., *J. Phys. Chem. A*, **2002**, 106, 1670-1677.

[33] Goncalves e Silva, F.R.; Longo, R.L.; Malta, O.L.; Piguet, C.; Bunzli, J.G., *Phys. Chem.*, **2000**, 2, 5400-5403.

[34] Weissman, S. I., *J. Chem. Phy.*, **1945**, 10 (4), 214-217.

With lanthanide ions rarely yielding highly luminescent materials even with direct excitation into their excited states, it was over-thought to trigger the luminescence of Eu^{III} ion via energy transfer by exciting through the ligand's energy states.[5,4] The concept was termed the antenna effect or luminescence sensitization.

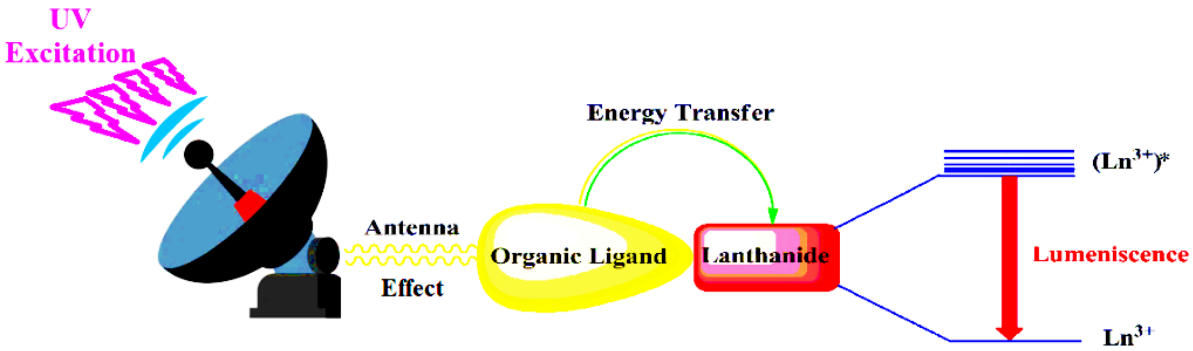

Figure 2. 7: Illustration of an antenna effect.

This phenomenon entails the embedment of a lanthanide ion into a matrix or an organic (chromophore) environment with good light harvesting properties.[35,36] The energy is transferred from the chromophore onto the metal ion, which eventually gives off its characteristic light as per their respective spectral profiles.

These organic ligands are used somewhat as ancillary ligands to prevent any water coordination to the first coordination sphere of the metal ion. Primarily, the aim is to saturate the metal ion core. That is because water molecules have high-energy vibrations from the O-H oscillations and they ultimately endorse quenching.[37] Hence these ancillary ligands enhance the overall luminescence outputs of the respective complexes.

The discussions in the next section entail reports of different applications in fields of interest wherein the organic scaffolds were used in sensitizing the luminescence of the Eu^{III} metal ion. The illustrations of different organic matrix systems used, as the scientific discipline requires, in enhancing the luminescence of the complex and/or using the system as an added feature for analytical analysis purposes (e.g. bio-imaging).

[35] Wefts, M.H.V.; Hofstraat, J.W.; Geurts, F.A.J.; Verhoeven, J. W., *Chem. Phys. Lett.*, **1997**, 276, 196-201.

[36] Alpha, B.; Ballardini, R.; Balzani, V.; Lehn, J.M.; Perathoner, S.; Sabbatini, N., *Photochem. Photobio.*, **1990**, 52 (2), 299-306.

[37] Dickins, R.S.; Packer, D.; de Sousa A.S.; Williams, J.A.G., *Chem. Commun.*, **1996**, 697-698.

2.2.3. Overview of Main Applications

2.2.3.1. Application on Sensitized Eu^{III} Luminescence by d-Orbitals Transition-Metal ions.

There has been a practice of making hetero-metallic d-f complexes. The interest in these types of complexes is aroused by the fact that the d- and f-metal ions display highly different stereo-chemical preferences. Interestingly, there are two synthetic paths in which these d-f compounds can be synthesized.[38] The path of interest, amongst the two, is the one that is kinetically controlled and it comprises of two steps:

- The first step entails the formation of a kinetically inert complex with either the d- or the f-block element.
- Followed by complexation with the more labile ion.

Therefore, in the case where the first step implies the f-ion, for instance, then Cyclen derivative (see **Figure 2.8**) is commonly used as the chelating agent; specifically in chemo-sensors for d-metal ions.[39]

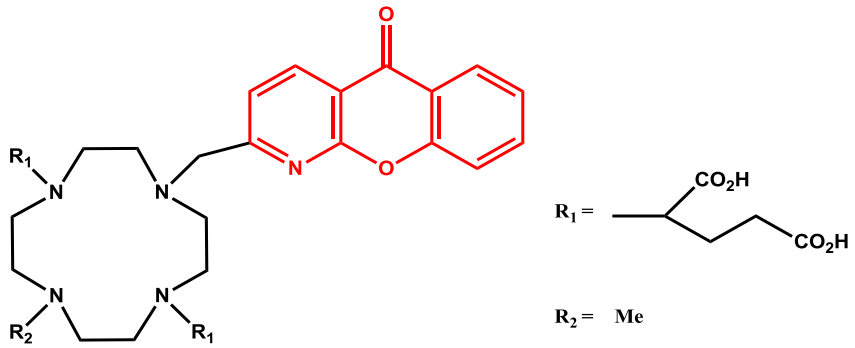

Figure 2.8: Typical example of a Cyclen derivative with a chromophore (attached in red).

The interest in these hetero-metallic d-f molecular compounds is fuelled by the electronic communication between metal ions which can be induced and controlled (see **Figure 2.9**).[38] To some extent, that enriches us with a tool for tuning the electronic (luminescence) properties of the lanthanide.[40,41.]

[38] Vigato, P.A.; Tamburini, S., *Coord. Chem. Rev*., **2004**, 248, 1717-2128.

[39] Faulkner, S.; Natraja, L.S.; Perry, W.S.; Sykes, D., *Dalton Trans.*, **2009**, 3890-3899.

[40] Chen, F.F.; Chen, Z.Q.; Bian, Z.Q.; Huang, C.H., *Coord. Chem. Rev*., **2010**, 254 (9), 991-1010.

[41] Ward, M.D., *Coord. Chem. Rev*., **2007**, 251, 1663-1677.

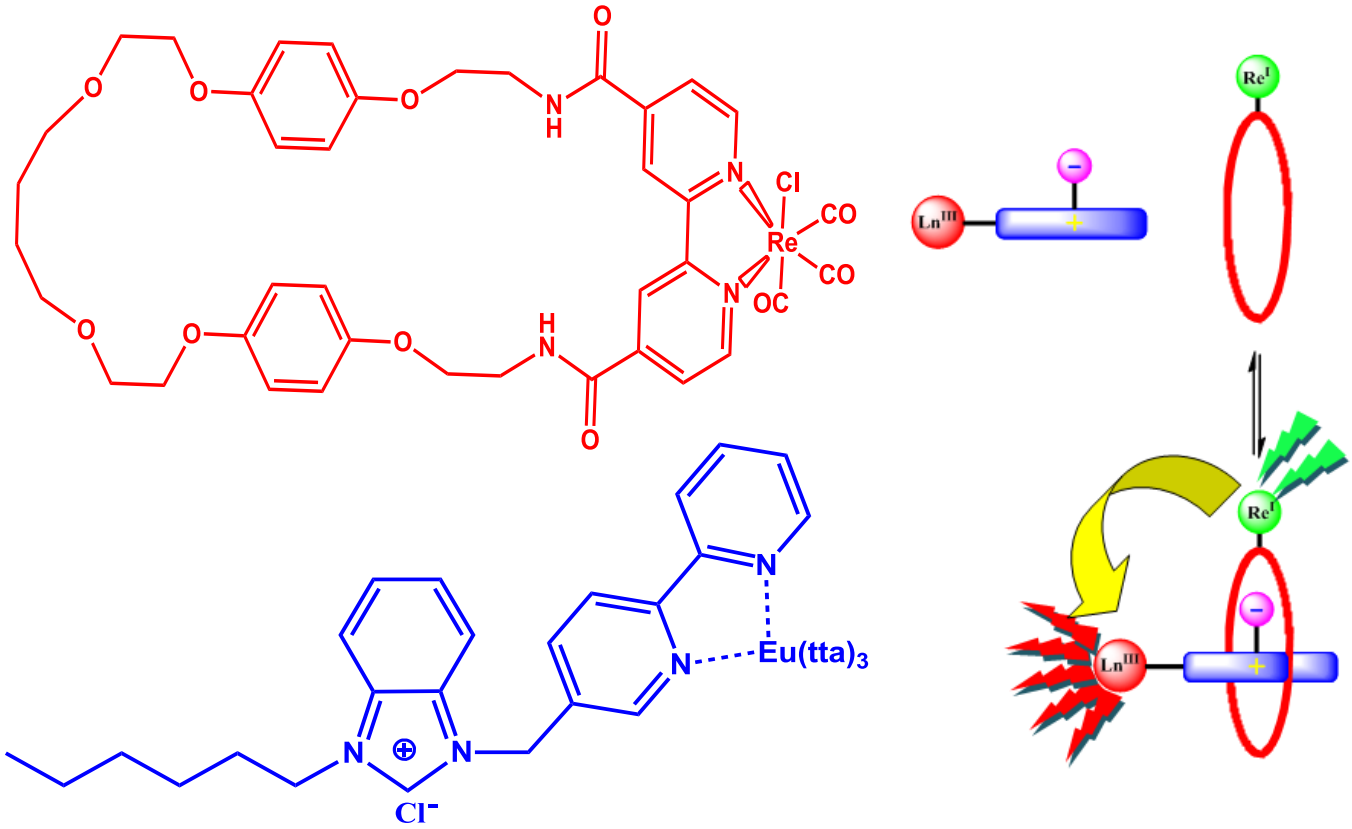

Figure 2.9: Illustration of a typical assembly of a Re^{I}-Ln^{III} hetero-nuclear complex. Redrawn from[42]

This type of complexes as exhibited in **Figure 2.9,** are potential therapeutic agents in radiopharmaceutical science with the lanthanide attachment as the switch on and off luminous emitting agent.[42] Moreover, they can further be considered for photodynamic therapy (PDT) in which rhenium complexes has been well featured for their anticancer activities.[43.]

Another type of switch on/off system is observed from the reports made by Lu's group about a Eu^{III} complex-based silica nanoparticle (see **Figure 2.10**) as luminescent probe for Calcium Dipicolinate (CaDPA) as a unique biomarker for Bicillus spores (a genus of gram-positive, rod shaped type of bacteria widely found in water and soil).[44] The $[Eu(EDTA)(H_2O)_3]$ complex is graphted onto the surface of uniform fluorescent isothio-cyanate (FITC) dye-doped silica nano-particles

[42] Sambrook, M.R.; Curiel, D.; Hayes, E.J.; Beer, P.D.; Pope, S.J.A.; Faulkner, S., *New J. Chem*., **2006**, 30, 1133-1136.

[43] Wahler, K.; Ludewig, A.; Szabo, P.; Harms, K.; Meggers, E., *Eur. J. Inorg. Chem*., **2014**, 5, 807-811.

[44] Ai, K.L.; Zhang, B.H.; Lu, L.H., *Angew. Chem. Int. Ed*., **2009**, 48, 304-308.

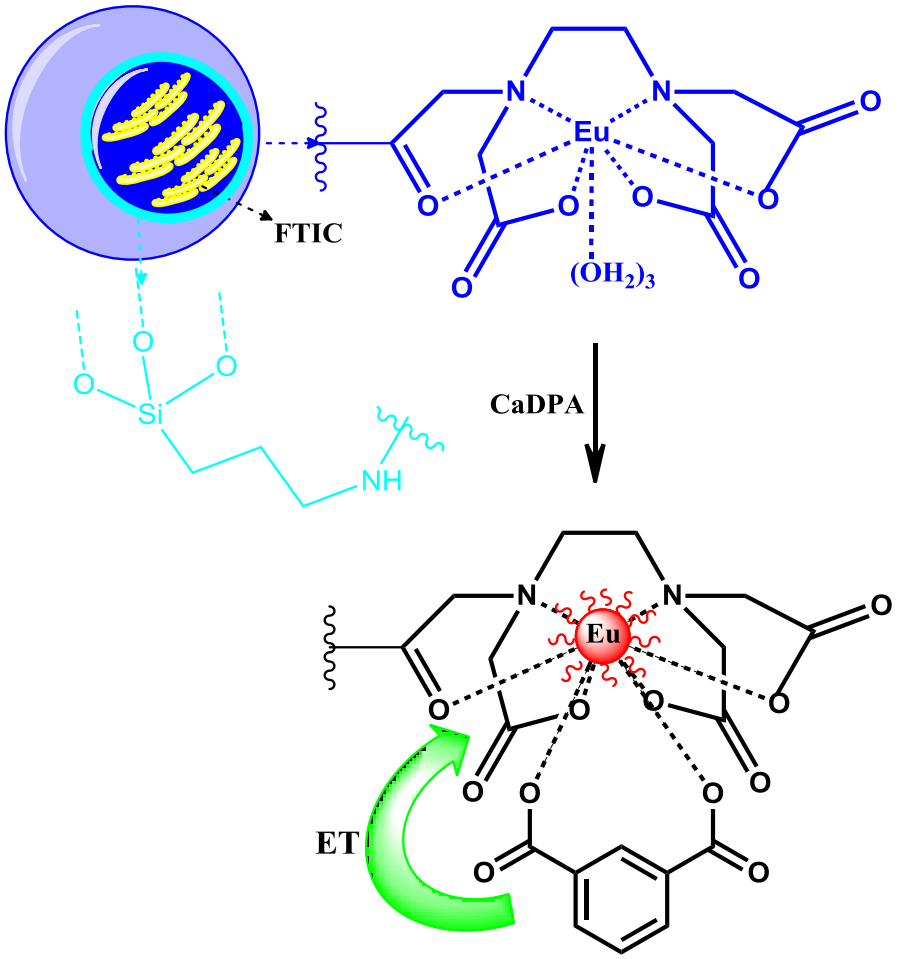

Figure 2.10: Illustration of spotted CaDPA via direct coordination of antenna with replacement of the coordinating water molecules.[43,45]

The quenching effect observed in this system is induced by the three monodentate water molecules coordinated in the first coordination sphere of the europium metal ion. This is a vivid example of quenching by overtones of high energy vibrations which is a great concern in the design of luminescent materials and probes. This behaviour of high energy oscillators can be somewhat modelled by the Foster mechanism.[46]

Therefore, the abrupt substitution of three water molecules coordinated to the Eu^{III} metal center by the CaDPA ligand, give rise to luminescence via energy transfer process.

[45] Wang, X.; Chang, H. Xie, J.; Zhaoa, B.; Liua, B.; . Xua, S.; Pei., W.; Rena, N.; Huanga, L., Huanga, W., *Coord. Chem. Rev.*, **2014,** 273-274, 201-212.

[46] Beeby, A.; Clarkson, I.M.; Dickins, R.S.; Faulkner, S.; Parker, D.; Royle, L.; de Sousa, A.S., Williams, J.A.G., Woods, M.J., *Chem. Soc. Perkin Trans*., **1999**, 2, 493-503.

2.2.3.2. Applications in Bio-analysis and Bio-imaging

The greater challenge over the years for biology and medicine is getting an insight into the functional properties of living systems. With cancer being the centre topic for many scientific entities across the world, the individualized approach (having a complex that diagnose and does therapy all at once; thera-nostic comlexes) to both diagnostic and therapy for its course seem to have attracted a lot of attention.[47] The intense focus on these approaches turns to necessitate better and faster pathological analyses and highly contrasted real time bio-images.[48]

It is without doubt that non-invasive methodologies are required for fewer perturbations on the investigated organs. So far, magnetic resonance imaging (MRI) and optical emissive probes emerges as indispensable techniques for this very purpose.[49] Lanthanide-based complexes in use for assays have become increasingly interesting over time. [50,51] That is largely attributed to their specific magnetic and photo-physical properties stemming from their $[Xe]4f^n$ electronic configurations; making them adequate for the afore-discussed purposes. Moreover, it is their long lifetimes of excited states that deem them integral entities in these luminescent bio-probes.[52]Looking at optical luminescent probes in particular, with substantial penetration depth (with suitable wavelengths), light can easily reach regions of cells and tissues that are not accessible to other molecular probes as illustrate below.[53]

Eu^{III} and Tb^{III} turn out to be the mostly used metal centres in the optical luminescence bio-probes science. Their authentic dominance is not only stamped by their less sensitivity towards vibrational quenching compare to others,[54] but also the lack of near-infrared detection cameras which to some extend limits the use of NIR emitting lanthanide ions.[55]

[47] Melancon, M.P.; Zhou, M.; Li, C., *Acc. Chem. Res*., **2011**, 44 (10), 947-956.

[48] Thompson, K.H.; Orvig, C., *Chem. Soc. Rev.*, **2006**, 35 (6), 499-499.

[49] Kobayashi, H.; Longmire, M.R.; Ogawa, M.; Choyke, P.L., *Chem. Soc. Rev*., **2011**, 40, 4626-4648.

[50] Evangalista, R.A.; Pollack, A.; Allor, B.; Templeton, E.F.; Morton, R.C.; Diamandis, E.P., *Clin. Biochem*., **1988**, 21, 173-178.

[51] Mathis, G., *Clin. Chem*., **1995**, 41 (9), 1391-1397.

[52] Faulkner, S.; Pope, S.J.A.; Burton-Pye, B.P., *App. Spec.Rev.,* **2005,** 40, 1-31.

[53] Lakowicz, J.R. (**2006**). *Principles of Fluorescence Spectroscopy*, Springer Science, New York.

[54] Montgomery, C.; Murray, B.; New, E.; Pal, R.; Parcker, D., *Acc. Chem. Res*., **2009**, 42, 925-937.

[55] Jin, D., *Cytometry: Part A*, **2011**, 79 (A), 392-397.

The Europium (III) ion in particular, prior to the series luminescent complexes hype, had clear precedence as optical label through their use over a number of decades in sensitive bio-analysis such as DELFIA (Dissociation Enhanced Flourometric Immuno Assay).[56] The imaging observed in **Figure 2.11** is of bone structure damage, medically termed micro-cracks wherein Eu^{III} complexes given below in **Figure 2.12** have been used to image and assess the extent of the fracture.

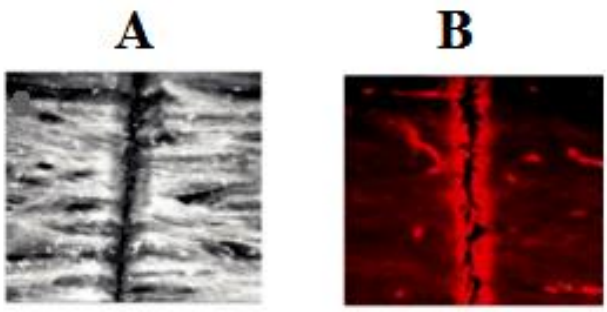

Figure 2.11: Microscopy images of bone sample A) Reflected light image: 0 hrs (B) 4hrs. Redrawn from.[57]

The exhibition in **Figure 2.12** indicates the organic groups marked with red as the antenna scaffolds and peripheral acetates and glucose active sites as target linkers to the protein. In the case of peripheral acetates groups where the amido-naphthalene is the antenna; hydroxyapatite lattice of the bone is targeted and results to the detailed bone surface morphology through the Eu (III)-based red emissions (as observed above).[50]

The cyclen approach in tailoring adequate LLB's (Lanthanoid Lumeniscent Bioprobes) has paid off over the years as a good approach. However, many have looked in macrocycle ligands attached with antenna chromophores. Interestingly, Parkers's group have established that the cell uptake and localization is primarily influenced by the nature of the chromophore and its attachment ode to the macrocycle and not the charge of the complex or its lipophilicity.[58]

[56] Braunwalder, A.F.; Yarwood, D.R.; Sills, M.A.; Lipson, K.E., *Anal. Biochem*, **1996**, 238, 159-164.

[57] Amoroso, A.J.; Pope, S.J., *Chem. Soc. Rev.*, **2015,** 44 (14), 4723-4742.

[58] New, E.J.; Parker, D., *Org. Biomol. Chem*., **2009**, 7, 851-855.

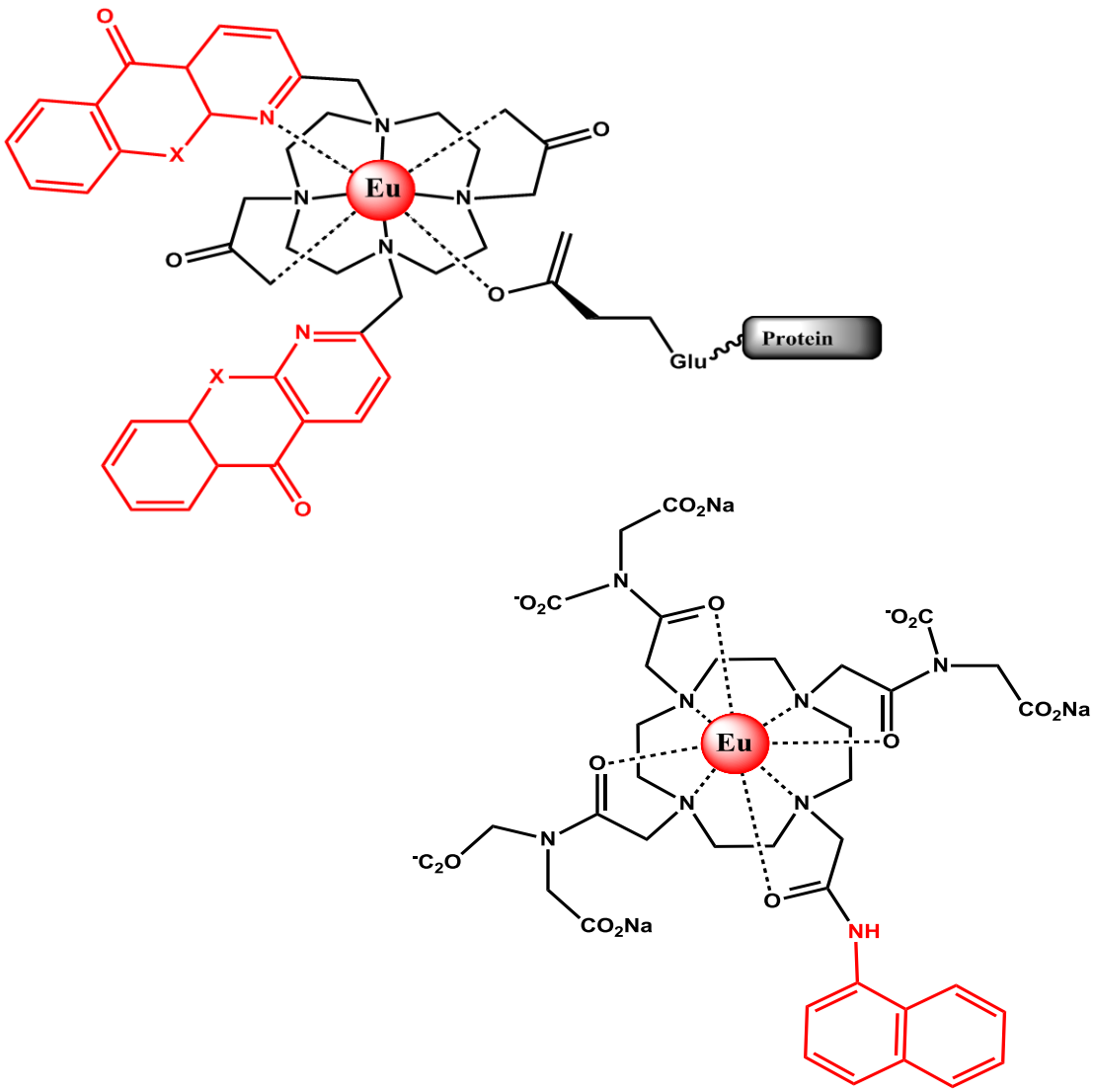

Figure 2.12: The illustration of chromophoric Eu-based complexes for bio-imaging.[56]

There are synthetic technicalities of note that needs to be practiced in tailoring these types of complexes. There are of certain stability aspects expected, as a form of routine, in the making of lanthanide complexes predominantly for labelling. Apart from having a good matching ligand which:

I. its singlet and triplet energy levels are suitable for the targeted cation,
II. have a strong coordination to the Ln cation,

It is expected to have complexes that could easily afford high thermodynamic and kinetic stabilities. There are essentially two ways to go about attempting to have this stabilization. The first way is to use highly pre-organized ligands featuring macrocycles as observed in **Figure 2.13**.

The second strategy is to include numerous negatively charged functions such as carboxylates, phosphonates or phophinates. Complexes with phophonate functions are among thermodynamically most stable complexes with lanthanide ions.[59,60]

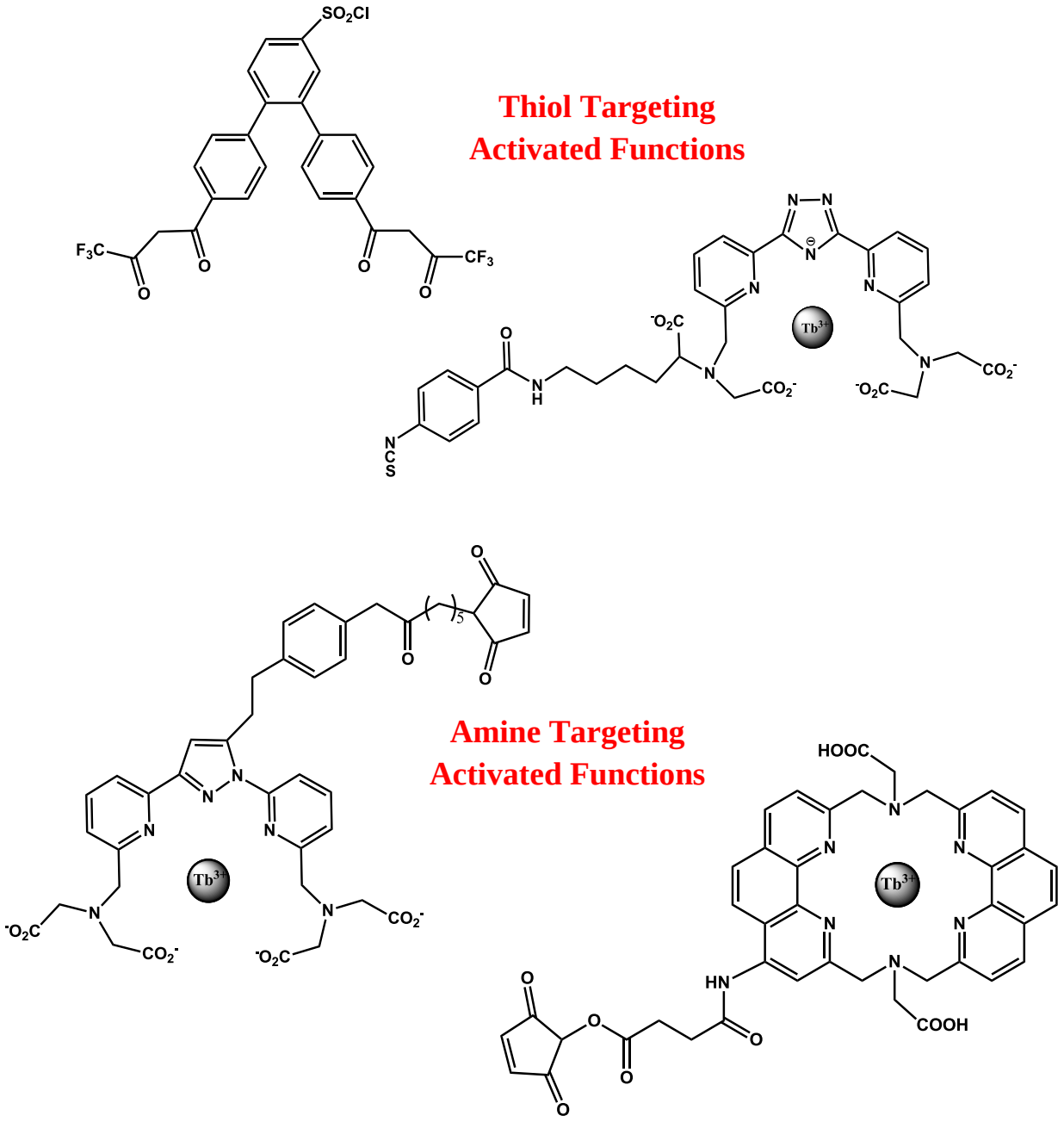

Figure 2.13: Illustration of ligands bearing amine- and thiol-targeting activated functions for bio-labelling.[62]

[59] Sherry, A.D.; Ren, J.; Huskens, J.; Brucher, E.; Toth, E.; Geraldes, C.G.; Castro, C.A.; Cacheris, W.P., *Inorg. Chem.*, **1996**, 35 (16), 4604-4612.

[60] Elhabiri, M.; Abada, S.; Sy, M.; Nonat, A.; Choquet, P.; Esteban- Gomez, D.; Cassino, C.; Platas-Iglesias, C.; Charbonniere, M.L.J., *Chem. Eur. J.*, **2015**, 21, 6535-65456.

However, there is a third route that which Piquet and Bunzli have developed. With the help of supramolecular chemistry, they engineered very stable lanthanide labels, assembling three ligand strands around two Ln cations in a dinuclear triple helix to obtain extremely stable water soluble edifices.[61]

With the feature of lanthanides in bio-labelling still in somewhat early stages, it is believed that their molecular based up-conversion (UP) labels are prone to cut through potentially as targets of choice in this field. If however there isn't any efficiency for these systems with regards to photon UC in solution, there is an ample room for improvements and relevant applications for bio-analysis.[62.]

2.2.4. Applications of Eu^{III} Complexes in Optoelectronic Devices.

One of many interesting characteristics of the lanthanide series in the edifice of opto-electronic devices is their sharp narrow spectral emissions lines.[63] With their emissions originating from the electronic transitions of the central ions, probed by the antenna organic scaffolds coordinated to it, their electroluminescent emissions are rendered potentially good agents within the OLED stacking and low cost flat panel display technology.[64.7] With the making of OLED's deemed very progressive over the years, there are still some fine aspects to be revisited. The struggle in finding common ground in simultaneous optimization of the emission colour, emission efficiency and the lifetimes of the conjugated organic polymers and small organic molecules makes the quest a little bit tedious.[65.]

Conjugated polymers, organic molecules and also phosphors often give off impure emission colours due to their emission spectra having a full width at half maximum (FWHM) of about 50-100 nm or more wider.[66,67.] The unwanted colours could ultimately be filtered out but the downside is that the OLED would be inefficient due to the fact that only certain part of their emission is utilized.

[61] Bunzli, J.C.; Piguet, C., *Chem. Soc. Rev.*, **2005**, 34 (12), 1048-1077.

[62] Sy, M.; Nonat, A.; Hildebrandt, N.; Charbonniere, L.J., **2016**, 52 (29), 5080-5095.

[63] Im, S.Y.; Go, D.H.; Ryu, J.G.; Kim, Y.S., *IEICE Transactions on Elect.*, **2017**, E100, C (11), 1021-1025.

[64] Kido, J.; Okamoto, Y., *Chem. Rev.*, **2002**, 102 (6), 2357-2368.

[65] Yu, D.X., *Int. J. Mol. Sci*., **2011**, 12 (3), 1575-94.

[66] Strobl, G.R., (**2007**). The Physics of Polymers: *Concepts for Understanding Their Structures and Behavior*, *Springer-Verlag*, Berlin Heidelberg.

[67] Hu, Y.; Zhuang, W.; Ye, H.; Zhang, S.; Fang, Y.; Huang, X., *J. Lumin.*, **2005**, 111 (3), 139-145.

Interestingly, the lanthanide luminescent complexes are believed to be promising candidates to solve the above discussed problem, hence the immense venture in the electroluminescence of lanthanide based complexes in the past two or more decades. The spectroscopic versatility induced by organic chromophores in the first coordination sphere renders them ideal entities for use in full colour display[68] as known from inorganic luminescent materials particularly in cathode ray and projection television tubes.[69,70,71.]

2.2.4.1. A Brief Construction of an Organic Light Emitting Diode (OLED).

Thin film OLED's devices usually consists of multiple organic and metallic layers on an indium tin oxide (ITO) covered glass plates.

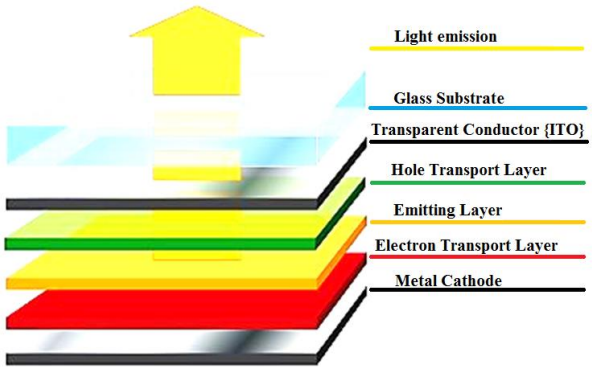

Figure 2.14: A typical multilayer structure of OLED stacking.

There are several processes with which the deposition of the layers on the substrate can take place. It can either be by thermal evaporation, plasma deposition, Langmuir-Blodget deposition and/or spin casting from the solution.[72,73.] Prior assembling the OLED stacking; all

[68] Weng, H.; Yan, B., *Inorg. Chem. Comm.*, **2016,** 63, 11-15.

[69] Ronda, C.R.; Kynast, U.H.; Dingen, W.P.M.; van Hal, H.A.M., *J. Alloys Compd.*, **1993,** 192, 55-56.

[70] Welker, T., *J. Lumin.*, **1991**, 48 & 49, 49-56.

[71] de Leeuw, D.M.; Mutsaers, C.A.H.A.; Mulder, H.; Klaassen, D.B.M., *J. Electrochem. Soc*., **1988**, 135 (4), 1009-1014.

[72] D'Arcya, J.M.; Tran, H.D.; Tang, V.C.; Tucker-Schwartza, A.K.; Wonga, R.P.; Yang, Y.; Kanera, R.B., *Proc. Natl. Acad. Sci. U.S.A.*, **2010**, 107 (46), 19673-19678.

[73] Li, J.C., *Condensed Matter: Materials Science*, **2009**, 11-13.

the segmented layers should be chemically stable and resistant to oxidation or photo-oxidation during operating conditions.

The optical properties of each layer should somehow be considered in the design of the OLED in that the layers should be transparent to the emitted radiation for higher efficiency light output. Along the OLED stacking, there should be an organic layer that serves as the emitting source for the device. This organic layer should therefore have high photoluminescence quantum efficiency. More importantly, the emissive layer must also have good bipolar charge transport properties allowing rapid transportation of the electrons and holes through the organic layer. The demonstrations in **Figure 2.15** show typical chemical structures of the hole and electron transporting materials.

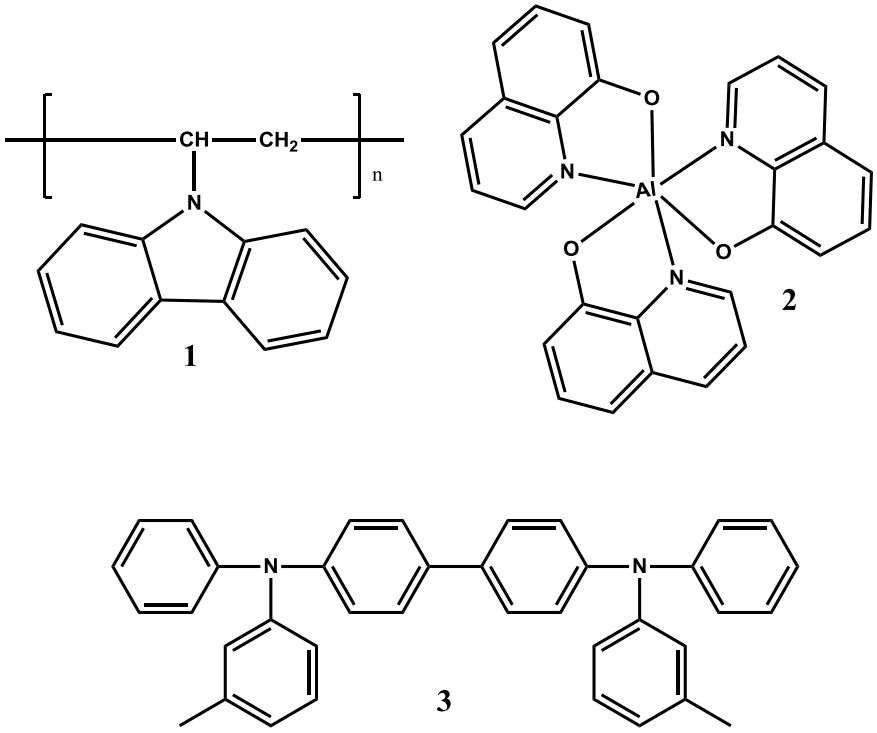

Figure 2.15: Chemical structures of commonly used hole-transporting materials: **1**. poly(*N*-vinylcarbazole), **PVK**; **2**. 8-hydroxyquinoline aluminum, $\mathbf{Alq_3}$ and **3**. *N*,*N*-diphenyl-*N*,*N*-bis-(3-methylphenyl)-1,1- biphenyl-4,4-diamine, **TPD** as an electron transporter.[64]

There are, however, several requirements needed to acquire a good light emitting material deducing from the OLED making discussions above:

- It should be an efficient luminophore
- A good charge transporter
- It must be capable of undergoing efficient charge transfer to an electrode

- ❖ Moreover, it must be thermally stable for small molecular materials to form a film by withstanding thermal evaporation in vacuum.

Many lanthanide complexes are highly luminescent, however, only a few of them can simultaneously satisfy these requirements for electroluminescence applications. Therefore, further developments should be focused on exploring new lanthanide complexes that satisfy the requirements listed above for this application.[64]

2.2.4.2. Specific Eu^{III} Complexes with Bidentate Ligands (*O,O' and N,O*) as Potential Emitting Agents for OLED's.

The molecular design of electroluminescence (EL) Eu^{III} complexes as emitters in OLED's, is mainly oriented towards enhancement of optical performance with simultaneous consideration of electrical modification and improvement of processability. To be specific, there are key features to be reckoned when tailoring this Eu^{III} based complexes for any luminous purposes, namely[74]:

1. Energy level compatibility
2. Ligand field effect
3. Electrical performance (in OLED's) and
4. Processability.

Keeping the above noted features in mind, it is believed that increasing organic proportions in ternary (see **Figure 16**) Eu^{III} based complexes, could enhances the energy harvesting ability which in turn helps further with the sensitization of the metal ion. That on its own, significantly impacts on the overall luminous output of the complex itself. The coordination sphere of this ternary Eu^{III} based complexes are often saturated by neutral ancillary ligands. (see **Figure 17**).

[74]Xu, H.; Sun, Q.; An, Z.; Wei, Y.; Liu, X., *Coord. Chem. Rev*., **2015**, 293–294, 228–249.

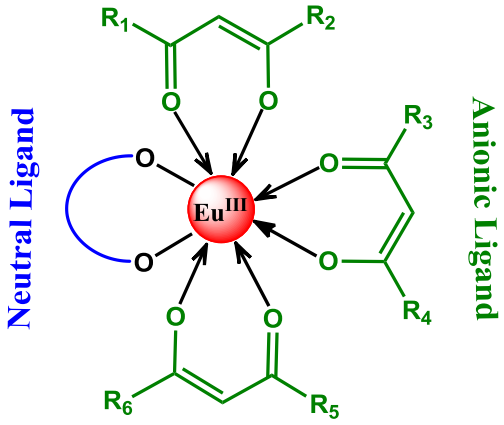

Figure 2.16: Chemical structures of typical ternary *β*-diketonate Eu^{III} complexes. With R_x substitutions on the periphery being either electron donating or withdrawing groups of choice.

The choice of ligand is learnt to be very crucial in engineering this ternary Eu^{III} complexes. The Judd-Ofelt theory[11] indicates the dictation of an organic ligand, with key aspects like crystal field effect, coordination strength, distance and steric shielding effect, towards the complexe's luminescence.

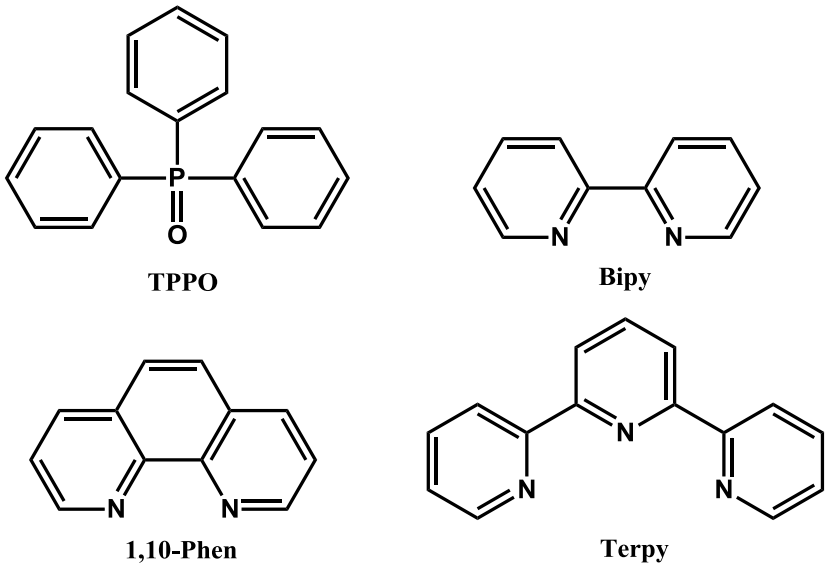

Figure 2.17: Illustration of common neutral ligands used as ancillary ligands in Eu^{III} β-diketonato type of complexes. [75,76.]

[75] Liang, H.; Xie, F., *Spectrochimica acta., Part A, Molecular and biomolecular spectroscopy*, **2009**, 73 (2), 309-312.

[76] Bortoluzzi, M.; Reolon, A.; Castro, J.; Enrichi, F.; Albertin, G.; Bragato, C., *RSC Advances*, **2016,** 6 (39), 32727-32739.

The first binary europium complex utilised in the edifice of OLEDs was a *tris*-(thienyltrifluoro-acetonato) europium (Eu(TTA) $_3$) as illustrated in **Figure 2.18**.[77] Despite the fact that Eu^{III} has great affinity for oxygen atoms, *β*-diketones systems are considered fit for the task, for they are quite versatile in that their polarizability can be tuned by choosing adequate ancillary ligands. Moreover, *β*-diketonate lanthanoid complexes have been explored because they give highly volatile, thermodynamically stable, and highly luminescent complexes, which are essential conditions for the fabrication of OLEDs. [78,79] The relative energy differences of *β*-diketones are well off to sensitize the Eu^{III} in particular, with fluorinated ones much interesting.[74]

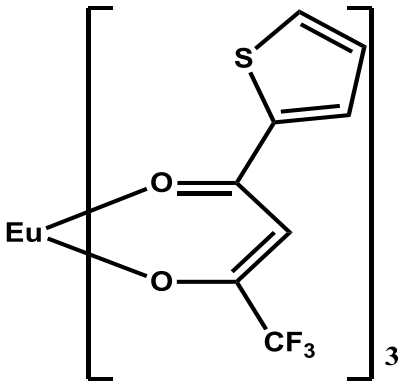

Figure 2.18: Fist binary Eu^{III} *tris*-(*β*-diketonate) complex.[77]

Following the shortcomings of this binary complex, most of EL Eu^{III} complexes now seem to have adopted a ternary configuration between the central metal ion, anionic and neutral ligands (see **Figure 2.19**) by taking advantage of superiority in ligand-to-metal ET-efficiency. [80,81,82,83,84,85]

[77] Kido, J.; Nagai, K.; Okamoto, Y., *J. Alloy Compd*., **1993**, 192, 30-33.

[78] Andreiadis, S.A.; Gauthier, N.; Imbert, D.; Demadrille, R.; Pecaut, J.; Mazzanti, M., *Inorg. Chem*., **2013**, 52, 14382-14390.

[79] Zheng, Y.; Lin, J.; Liang, Y.; Lin, Q.; Yu, Y.; Meng, Q.; Zhou, Y.; Wang, S.; Wang, H.; Zhang, H., *J. Mat. Chem*., **2001**, 11, 2615-2619.

[80] Robinson, M.R.; O'Regan, M.B.; Bazan, G.C., *Chem. Commun*., **2000**, 1645-1646.

[81] Li, S.; Zhong, G.; Zhu, W.; Li, F.; Pan, J.; Huang, W.; Tian, H., *J. Mater. Chem.*, **2005**, 15, 3221-3228.

[82] Liang, H.; Xie, F., *Spectrochim. Acta A*, **2010**, 75, 1191-1194.

[83] He, P.; Wang, H.H.; Liu, S.G.; Shi, J.X.; Wang, G.; Gong, M.L., *Inorg. Chem*., **2009**, 48, 11382-11387.

[84] Zhang, L.; Li, B.; Zhang, L.; Su, Z., *Appl. Mater. Interfaces*, **2009**, 1852-1855.

It is with saturated coordination sphere that high quantum yield were obtained. Below are ternary Eu^{III} based complexes with functionalised back bone of β-diketones ligand framework. There are also different or rather exotic derivatizations on the neutral position as ancillary ligands.

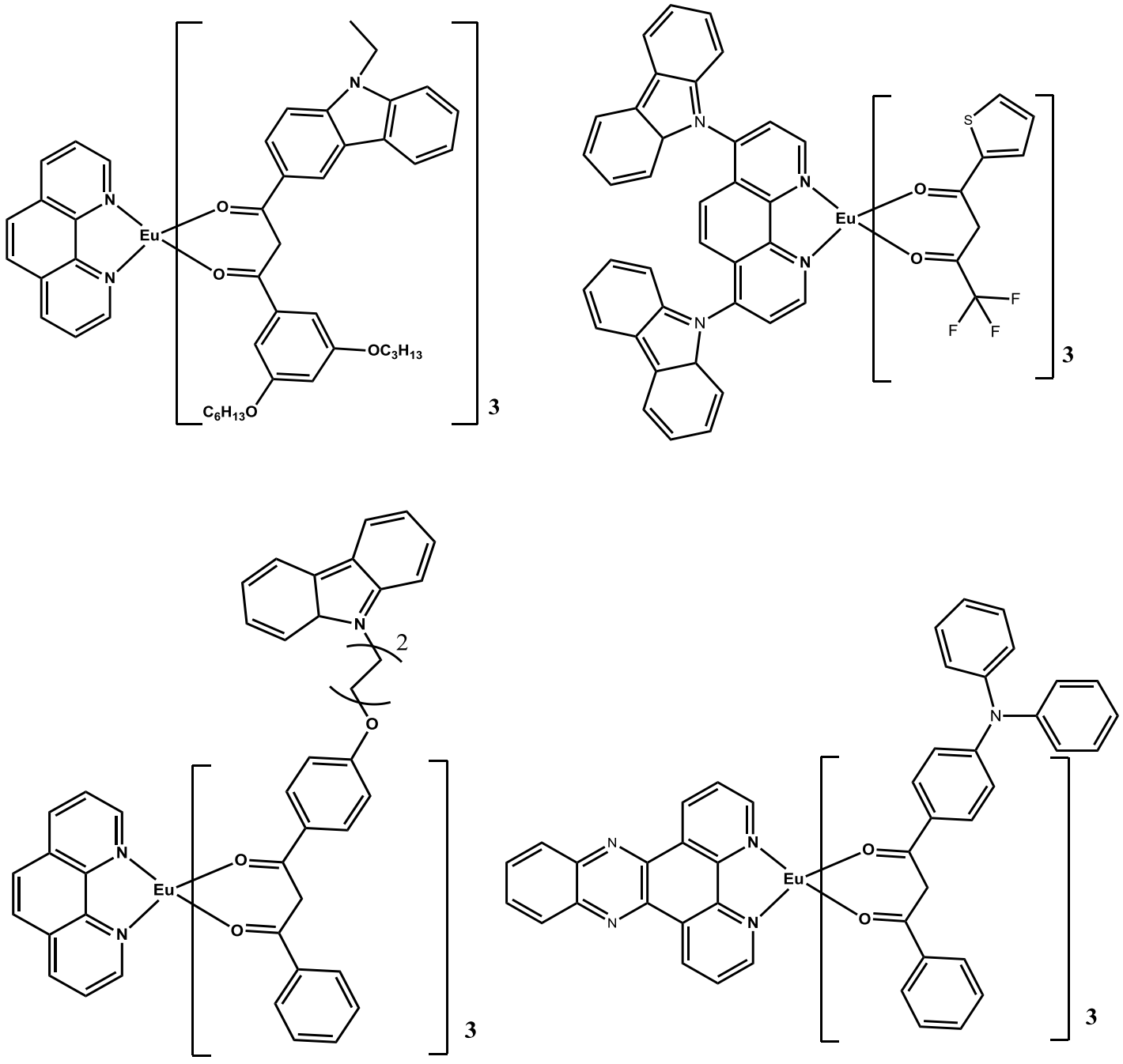

Figure 2. 19: Ternary luminous Eu^{III} based β-diketonate complexes.[80, 81, 82, 83, 84, 85]

[85] Zucchi, G.; Murugesan, V.; Tondelier, D.; Aldakov, D.; Jeon, T.; Yang, F.; Thuery, P.; Ephritikhine, M.; Geffroy, B., *Inorg. Chem.*, **2011**, 50, 4851-4856.

The later exhibited Eu^{III} based complexes shows an intense inclusion of carbazole moiety in the ternary complexes. It is because the carbazole moiety was found to be the best popular hole-transporting entity with low ionization potential and good host characteristics. This is complementary to what Bazan and co-workers have established in introducing the first carbazole with hexyloxyl functional group (**1** in **Figure 2.19)** into *β*-diketonate for enhance hole transportation and improved processability.[80] These characteristics of carbazole matches the stipulated requirements of a good chromophore as discussed in **Section 2.2.4.2.** It was Zheng et al. who further demonstrated the strong sensitizability of the carbazole with 1,10-phenonthroline group as the ancillary ligand.[86,87.]

However, there is an element of effectiveness from the ancillary ligands. Shi et al. opted for a completely different make up of the both the anion and the ancillary ligand using triphenyl phosphine oxide as the ancillary ligand and further incorporate pyrazole in the *β*-diketonate framework.[88]

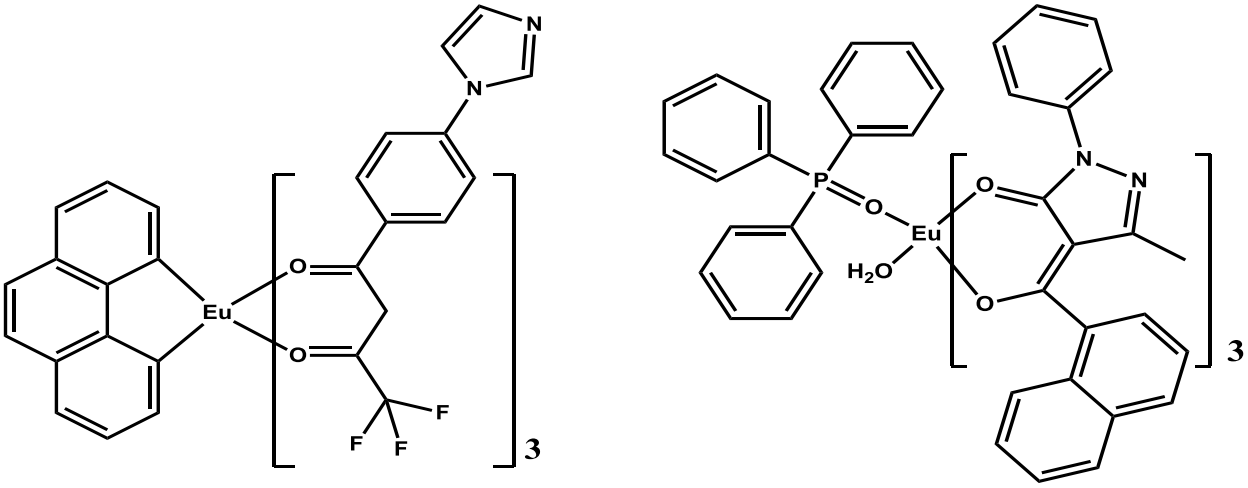

Figure 2.20: Ternary luminous Eu^{III} based *β*-diketonate complexes with different ancillary ligands

The quest for highly luminescent Eu^{III} based complexes is still relevant in that Xu and co-workers have demonstrated the first Wolf-III type Eu^{III} complex with a bidentate FDPO ligand for bridging $Eu(DBM)_3$ repeating units (see **Figure 2.21**).

[86] Zheng, Y.; Cardinali, F., Armaroli, N.; Accorsi, G., *Eur. J. Inorg. Chem*., **2008**, 2075-2080.

[87] Zheng, Y.; Zhou, Y.; Accorsi, G.; Armaroli, N., *J. Rare Earths*, **2008**, 26, 173-177.

[88] Shi, M.; Li, F.; Yi, T.; Zhang, D.; Hu, H.; Huang, C., *Inorg. Chem*., **2005**, 44, 8929-8936.

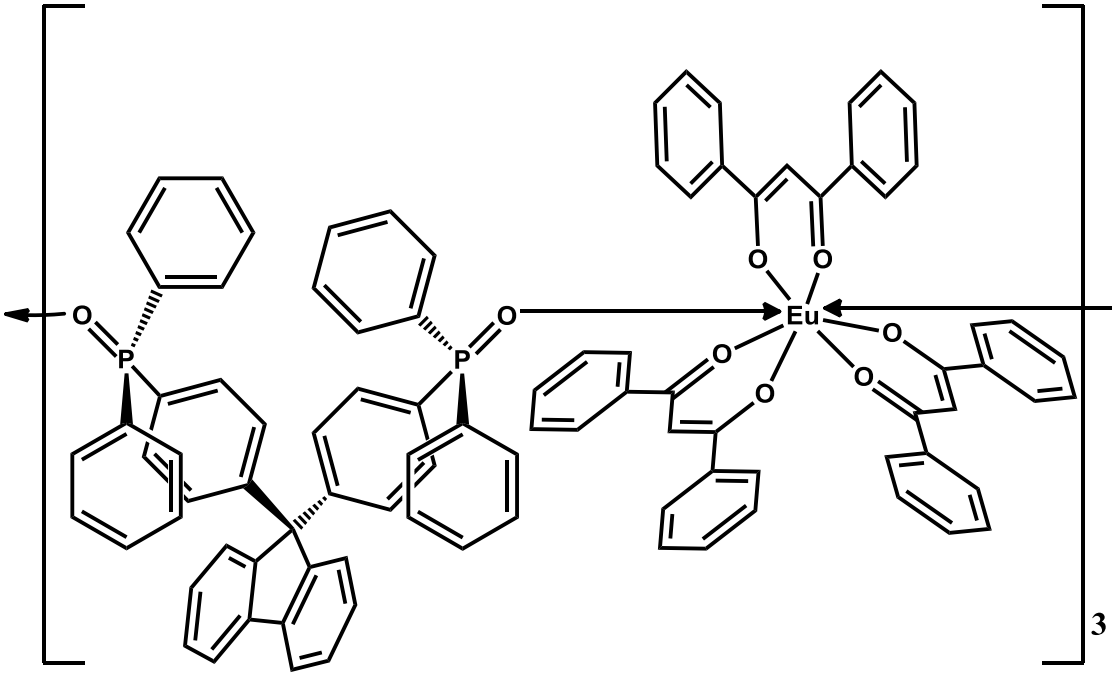

Figure 2.21: Illustration of Eu^{III} metal-polymers. Drawing format changed for clarity.[88]

The binding ability of the FDPO assisted with the stability of one dimensional chain structure by behaving as a bridge between the Eu^{III} ion of each $Eu(DBM)_3$ units. However, the observed electroluminescent of the polymer is lower than that of small molecular units.[89]

There is an element of symmetry in question for luminous output of these Eu^{III} based complexes. Many different organic groups pose a different environment to the metal ion and so that is translated through the symmetry which causes stark splitting of *J*-levels. Moreover, allowed electronic modes observed in the luminescent spectrum are a result of the conjugate matrices the metal finds itself in. [90]

[89] Xu, H.; Wang, J.; Wei, Y.; Xie, G.; Xue, Q.; Deng, Z.; Huang, W., *J. Mater. Chem. C*., **2015**, 3, 1893-1903.

[90]Binnemans, K., *Coord. Chem. Rev*., **2015**, 295, 1-45.

2.2.5. Organic Ligands

2.2.5.1. An overview of *β*-Diketone ligand Systems

The *β*-diketones have two carbonyl groups that are separated by one carbon atom. This carbon atom is the *α*-carbon. Traditionally in *β*-diketones, the substituents on the *α*-carbon are hydrogen atoms. There are cases where the *α*-substituted *β*-diketonates (substitution on the *α*-carbon of the *β*-diketone with either alkyls or halides or any other functional group but hydrogen) are known. These *β*-diketone bidentate ligands are used widely as a type of conjugated ligand system in organometallic chemistry.[91,92] The most common *β*-diketone is acetylacetone (Hacac), were the substituents on both carbonyl groups are methyl groups. All other *β*-diketones can be considered as derivatives of acetylacetone in substitution of the CH_3 groups by other functional groups ranging from electron donating to electron withdrawing groups.[93]

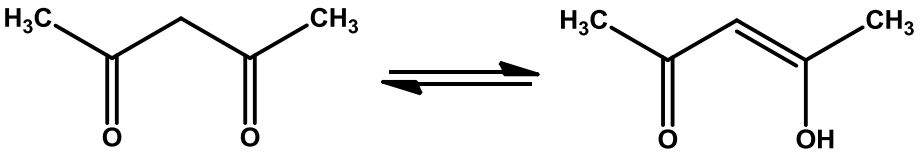

Figure 2.22: Keto-enol equilibrium in acetylacetone.Redrwan from.[94]

In solutions state, these *β*-diketones exhibit keto–enol tautomerism (see **Figure 2.22** above). The equilibrium in which the tautomerization is administered is often strongly shifted towards the enol form. That is because in tautomerism process, the hydrogen bonding to the carbonyl oxygen forms a pseudo aromatic ring (see **Figure 2.23**) which to some extend is stable enough to exist.[95,96]

[91] Padwa, A.; Hornbuckle, S.F.; Zhang, Z.; Zhi, L., *J. Org. Chem*., **1990**, 55(18), 5297-5299.

[92] Manicum, A.; Schutte-Smith, M.; Kemp, G.; Visser, H.G., *Polyhedron,* **2015,** 85, 190-195.

[93] Binnemans K., (**2005**). *Handbook on the Physics and Chemistry of Rare Earths: Rare-Earth Beta-Diketonates*, vol. 35, Elsevier B.V.

[94] Schematic of: *Keto-enol Tautomerism of a β-diketone*, adapted from: http://en.wikipedia.org/wiki/Beckmann_rearrangement: *Last accessed 15/12/2017.*

[95] Urbaniak, W.; Jurek, K.; Witt, K.; Goracko, A., *CHEMIK*, **2011**, 65, 273-282.

[96] Cullen, W.R.; Wickenheiser, E.B., *J. Organomet. Chem*., **1989**, 370, 141-148.

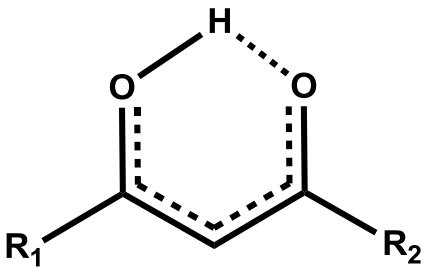

Figure 2.23: Resonance structure of a *β*-diketone ligand.[94]

As illustrated in **Figure 2.22** these *β*-diketones tend to undergo tautomerisation, the enol form the H-atom of the alcohol function is hydrogen-bonded to the carbonyl O-atom. These *β*-diketone bidentate ligands systems are of high use because of their highly coordinative nature, good solubility. One major factor that makes them easy to use is the feasibility to functionalize their backbone with various substituents on the carbonyl carbons.[97] Unsymmetrical ligands are also produced such as the substitution of a single methyl group with trifluoromethyl.[98] The ability to vary these substituents on the periphery significantly impacts on the absorption of the ligands and that could essentially affect the luminous output in E^{III} based *β*-diketonate complexes.

2.2.5.2. An overview of Schiff Base ligand System

Herein we look exclusively at the synthetic engineering of imino based type of ligands commonly known as Schiff bases. They are named after a German chemist called Hugo Schiff.[99] These organic scaffolds, alternatively known as aldeimine or azomethine, are nitrogen based analogues of an aldehyde or a ketone in which the carbonyl group (C=O) get replaced by an imine or azomethine group.

This ligand system can be functionalized on both ends of the salicylidene back-bone. Similar to *β*-diketones, one can get both symmetric and unsymmetrical Schiff base ligands. However, the unsymmetrical ligands looks to be interesting since there is a chance of dual absorption from both ends of the ligands and that could be observed in the luminescence behaviour.

[97] Viljoen J.A., (**2009**). *Speciation and Interconversion Mechanism of Mixed Halo O,O'- and N,O-Bidentate Ligand Complexes of Hafnium*, M.Sc. Dissertation, University of the Free State, South Africa.

[98] Lewis, F.D.; Miller, A.M.; Salvi, D.G., *Inorg. Chem*, **1995**, 34, 3173-3183.

[99] Schiff, H., *Eur. Journ. Org. Chem*., **1864,** 131(1), 118-119.

The scheme below illustrates relatively the general construction of the Schiff base ligand using an aldehyde and an amine.

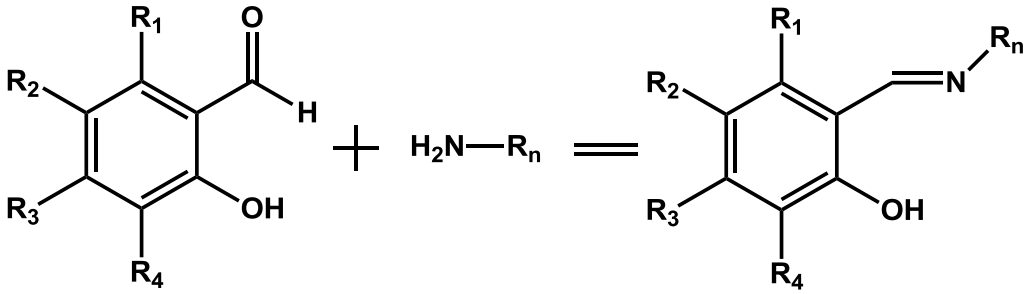

Figure 2.24: The schematic illustration of a typical Schiff base framework.

The general synthetic method of these Schiff base ligands entails the condensation reaction between the primary amine and a carbonyl precursor (either an aldehyde or a ketone). This reaction may require an acid catalyst; however, it is not always necessarily. Schiff bases are characteristic of their famous imine or azomethine functionality (C=N) to date. Schiff Bases can be tailored in such a way that are geometrically feasible to undergo a bidentate, tridentate or a tetradentate coordination mode. They often possess the nitrogen (N) and oxygen (O) as chelating donors. The most commonly known Schiff base is a tetradentate ligand named *N,N'*-ethylene-*bis*-(salicylidineiminato) [H_2Salen]. These class of O,N,N',O'-tetradentate Schiff base ligand are widely known as salenes.[100]

Schiff bases are suitable also in the photoluminescence studies[101] in that their photochromic and thermo-chromic properties are advantageous to their metal complex formation attracting a lot of focus in the photoluminescence field. Their ability to tautomerize[102] both in solid and solution state renders them perfect organic compounds to undergo the intra-ligand electron transfer and gives off light in the process. These are made possible by the existence of the *o*-hydroxy group forming a O-H…N and O…H-N giving rise to pseudo aromatic ring.[103] It is their synthetic versatility that renders them as potential chromophores to sensitize the luminescence of the Eu^{3+}-based complexes.

[100] Jurisson, K.; Dancey, K.; MacPartlin, M.; Tasker, P.A.; Deutsch, E., *Inorg. Chem*., **1984**, 23 (26), 4743-4749.

[101] Hai-Fu, G.; Xin, Z.; De-Yun, M.; Ai-Ping, X.; Wei-Bo, S., *Trans. Metal Chem.*, **2013,** 38 (3), 299-305.

[102] Temel, H.; Ilhan, S.; Sekerci, M.; Ziyadanogullari, R., *Spectrosc. Lett*., **2002**, 35 (2), 219-228.

[103] Bige, S.; Kilie, Z.; Hayvali, Z.; Hokelek, T.; Safran, S., *J. Chem. Sci*, **2009**, 121, 989-1001.

2.3. Conclusions.

The discussion outlaid in this chapter covered the basic lanthanide background, the introductory Eu^{III} luminescence and characteristics. It further covered the respective coordination modes influenced by the relative organic matrices coordinated to the Eu^{III} metal ion. Moreover, the relative sensitization methods across many scientific fields, from bio-imaging to organic light emitting diodes, using different types of ligand systems.

This chapter illustrated systems with much aromaticity. The aromaticity and structural rigidity are key aspects in giving off long and stable luminescence. With carbazole deemed the best organic framework in the luminescence of Eu^{III} based complexes as discussed above; it invited the effort of building organic ligands with carbazole moiety and also with other aromatic moieties as the main constituents. The easiest making of these organic scaffolds was the use of the Schiff base model with targeted constituents as part of the desired framework.

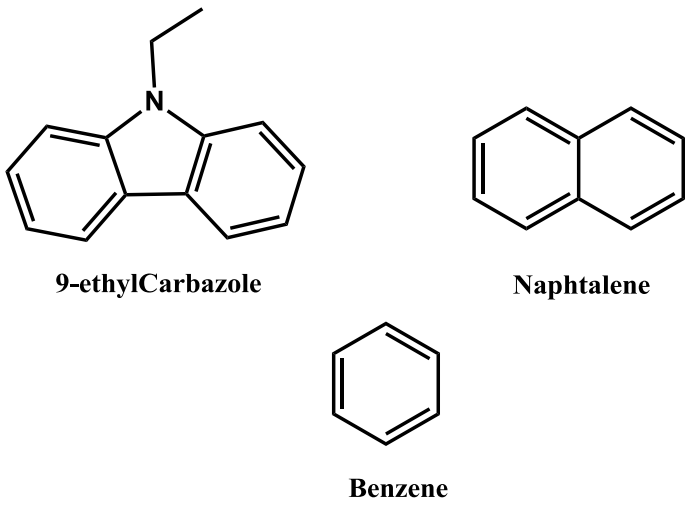

Figure 1: Organic units to be used in constructions of Schiff Bases.

On the contrary, there is very little literature reports on the bidentate Schiff base ligands with europium metal ion. This could mean two things, either the chemistry of bidentate Schiff base ligands with lanthanides haven't been explored, or, the chemistry of this ligand doesn't work at all. Nonetheless, none of the two has been reported also for clarity. There are however bidentate Schiff base ligands used for photoluminescence purposes with transition elements reported in the literature.[104,105,106,107,108,109.]

[104] Che C.M., Chan S.C., Xiang H.F., Chan M.C., Liu Y., Wang Y., *Chem. comm,.* **2004,** 13, 1484-1485.

There are some lanthanide complexes reported for NIR metal ions like Er and Yb and also Nd from the first part of the series for photoluminescence studies.[110,111]

Successful execution of this research endeavour necessitates full characterization of all synthesized Schiff base ligands and Eu^{III} based complexes obtained. This does not only include a full solid-state structural analysis by crystallographic methods but also photoluminescence studies on the complexes.

When all of these aspects are considered, it becomes quite obvious that this project constitutes a significant challenge of investigation of the effects of ligand coordination on the solid-state luminescence behaviour of Europium (III) complexes.

[105] Dong, Y.W.; Fan, R.Q.; Wang, P.; Wei, L.G.; Wang, X.M.; Zhang, H.J.; Gao, S.; Yang, Y.L.; Wang, Y.L., *Dalton Trans.,* **2015,** 44 (12), 5306-5322.

[106] Hai-Fu, G.; Xin, Z.; DeYun, M.; Ai-Ping, X.; Wei-Bo, S., *Trans. Metal Chem.,* **2013,** 38 (3), 299-305.

[107] Koh, L.L.; Ranford, J.O.; Robinson, W.T.; Svensson, J.O.; Tan, A.L.C.; Wu, D., *Inorg. Chem.,* **1996,** 35, 6466-6472.

[108] Tamami, B.l Ghasemi, S., *J. Organ. Chem.,* **2015,** 794, 311-317.

[109] Yu, T.; Su, W.; Li, W.; Hong, Z.; Hua, R.; Li, B., *Thin Solid Films,* **2007,** 515 (7-8), 4080-4084.

[110] Schuetz, S.A.; Day, V.W.; Sommer, R.D.; Rheingold, A.L.; Belot, J.A., *Inorg. Chem.* **2001,** 40, 5292-5295.

[111] Mohanan, K.; Subhadrambika, N.S.; Joseyphus, R.; Swathy, S.S.; Nisha, V.P., *J. Saudi Chem. Soc.,* **2016,** 20 (4), 379-390.

3 Synthesis of New Schiff Base Ligands

In this chapter:
We present the synthetic endeavours of Schiff base ligands as (N,O) bifunctional chelators with different coordinating modes induced by different organic constituents used on the salicylidene backbone.The systematic analysis of synthesized compounds with different techniques.

3.1. Introduction

Herein we look exclusively at the synthetic engineering of imino based type of ligands commonly known as Schiff bases. They are named after a German chemist called Hugo Schiff.[1] These salicylidene scaffolds, alternatively known as aldeimine or azomethine, are nitrogen based analogues of an aldehyde or a ketone in which the carbonyl group (C=O) get replaced by an imine or azomethine group

Schiff bases are used across many fields of science for various applications. [2,3,4,5] In this study we propose to synthesize both *bi*- and *tri*-dentate Schiff base ligands. These organic scaffolds, suspected to have luminous properties, will at a later stage be analyzed for luminescence properties and further used for the sensitization of Eu^{III} metal ion.

A range of *N,O*-bifunctional mono-negative ligands were synthesized. Both the two ends of the respective ligands consisting of aromaticity and aromatic amines were constructed on the salicylidene backbone via Schiff's synthetic routines. The selection of coordinated amines was based on their steric, electronic and luminous abilities.

The structure of the compounds were be confirmed by spectroscopic measurements of Infrared (IR), UV/Vis and Nuclear Magnetic Resonance (NMR).

---

[1] Schiff, H., *Eur. Journ. Org. Chem*., **1864,** 131(1), 118-119.

[2] Tamami, B.; Ghasemi, S., *J. Organometal. Chem*., **2015**, 794, 311-317.

[3] Zoubi, W.A.; Ko, Y.G., *Appl. Organometal. Chem*., **2016**, 31, 3574-3585.

[4] Dhar, D.N; Taploo, C.L., *J. Sci Ind Res.,* **1982,** 41(8), 501-506.

[5] Abuamer, K.M.; Maihub, A.A.; El-Ajaily, M.M.; Etorki, A.M.; Abou-Krisha, M.M.; Almagani, M.A., *Inte. J. Org. Chem*., **2014**, 4 (1), 7-15.

3.2. General Chemicals, Solvent and Analysis Techniques

3.2.1. Reagents and Solvents

All chemicals used for the synthesis and preparation of the complexes were of analytical grade and were purchased from Sigma-Aldrich, South Africa. Reaction solvents were of analytical grade and mostly used as received. In cases where anhydrous conditions were required, solvents were purified and dried according to literature procedures.[6]

3.2.2. Infrared Spectroscopy

Solid state FT-IR spectra of samples were recorded on a Bruker Tensor 27 Fourier transform spectrometer (ATR), utilizing a He-Ne laser at 632.6 nm, in the range of 3000 to 600 cm^{-1}.

3.2.3. Nuclear Magnetic Resonance Spectroscopy

The ^{1}H- and ^{13}C-FT-NMR solution-state spectra were recorded on a Bruker AVANCE II 600 MHz (^{1}H: 600.28 MHz; ^{13}C: 150.96 MHz) or Bruker DPX 300 MHz (^{1}H: 300.13 MHz; ^{13}C: 75.47 MHz) nuclear magnetic resonance spectrometer using the appropriate deuterated solvent. Chemical shifts, δ, are reported in ppm. ^{1}H NMR spectra were referenced internally using residual protons in the deuterated solvents, Chloroform-d_1 [$CDCl_3$ = 7.26(5) ppm]. ^{13}C NMR spectra were similarly referenced internally to the solvent resonance [$CDCl_3$ = 77.26(4) ppm] with values reported relative to tetramethylsilane (δ 0.0 ppm).

3.2.4. UV/Vis Spectroscopy

UV/Vis absorbance spectra were collected in a 1.000(1) cm tandem quartz cuvette on a Varian Cary 50 Conc. spectrophotometer, which was equipped with a Julabo F12-mV temperature cell regulator accurate within 0.1 °C. All λ_{max} values reported in this chapter were collected at 25.0 °C.

[6] Perrin, D.D.; Armarego, W.L.F., Purification of Laboratory Chemicals, *Pergamon Press, Oxford*, Great Britian., **1988**.

3.3. Experimental Procedure of Bidentate Schiff base Ligands

3.3.1. General Synthesis of n-Sal – "M" Bidentate Ligand Synthesis

The title compound was synthesized by the slow addition of an amine (1.0 mol) dissolved in methanol, to an aldehyde (1.0 mol). The reaction was gradually heated from room temperature and refluxed for 3 hrs. The solid was washed with cold methanol and filtered. The solvent was carefully removed under vacuum at 25.0 ˚C. Crystals, suitable for X-ray diffraction were obtained by the slow evaporation of the crude product.

All the synthetic procedures that follow below were carried out according to the general method described in **Section 3.3.1.**

3.3.1.1. The synthesis of *(E)*-2-(9-ethylcarbazol-3-yliminomethyl)-6-methoxyphenol-: **2oMe-SalH-Carba**

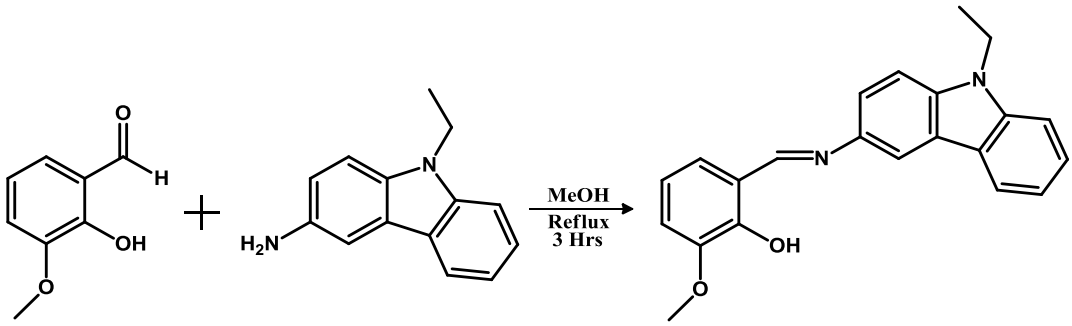

9-ethylcarbazole (1.382 g, 6.57 mmol) dissolved in methanol, was slowly added to 2-hydroxy-3-methoxybenzaldehyde (1.03 g, 6.76 mmol). After refluxing for 3 hrs, the mixture yielded an orange solid. Crystals suitable for X-ray diffraction were obtained by the slow evaporation of the filtrate. (Yield: 1.841 g, 80.09%),

IR (ATR, cm^{-1}) υ: 1625, 1569. λ_{max} = 290 nm, ε = 3.28 x 10^4 $M^{-1}.cm^{-1}$, **^{1}H NMR** (300 MHz, $CDCl_3$) δ 14.17 (s, 1H), 8.80 (s, 1H), 8.13 (d, *J* = 7.7 Hz, 1H), 8.07 (d, *J* = 1.8 Hz, 1H), 7.54 – 7.47 (m, 1H), 7.43 (d, *J* = 8.6 Hz, 1H), 7.08 (dd, *J* = 7.7, 1.5 Hz, 1H), 6.99 (dd, *J* = 8.0, 1.5 Hz, 1H), 6.90 (dd, *J* = 9.6, 6.1 Hz, 1H), 4.40 (q, *J* = 7.2 Hz, 1H), 3.96 (s, 1H), 1.46 (t, *J* = 7.2 Hz, 1H). **^{13}C NMR** (75 MHz, $CDCl_3$) δ 159.87, 146.93, 146.17, 140.62, 139.93, 139.17, 126.19, 123.61, 123.51, 122.90, 120.67, 119.99, 119.16, 118.36, 114.27, 112.41, 109.00, 108.80, 97.11, 56.24, 37.77, 13.84.

3.3.1.2. The synthesis of (*E*)-1-((9-ethylcarbazol-3-ylimino)methyl)-napthanol - : Napht-SalH-Carba

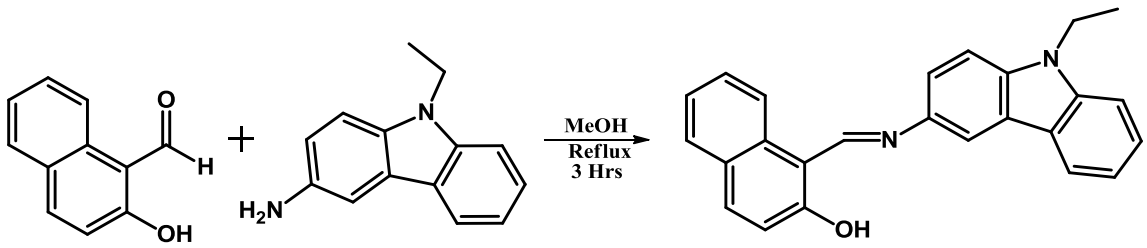

9-ethylcarbazole (1.22 g, 5.8 mmol) dissolved in methanol, was slowly added to 2-hydroxynaphthaldehyde (1 g, 5.81 mmol). After refluxing for 3 hrs, the mixture yielded a yellow-orange solid. Crystals suitable for X-ray diffraction were obtained by the slow evaporation of the filtrate. (Yield: 1.7257 g, 81.5%)

IR (ATR, cm^{-1}) υ: 1614, 1542. λ_{max} = 296 nm, ε = 5.7 x 10^4 $M^{-1}.cm^{-1}$, **^{1}H NMR** (300 MHz, $CDCl_3$) δ 16.02 (s, 1H), 9.50 (s, 1H), 8.22 – 8.12 (m, 3H), 7.81 (d, *J* = 9.1 Hz, 1H), 7.74 (d, *J* = 8.3 Hz, 1H), 7.59 – 7.49 (m, 4H), 7.45 (d, *J* = 8.0 Hz, 2H), 7.37 – 7.27 (m, 2H), 7.14 (d, *J* = 9.5 Hz, 1H), 4.41 (q, *J* = 7.2 Hz, 3H), 1.48 (t, *J* = 7.2 Hz, 5H). **^{13}C NMR** (75 MHz, $CDCl_3$) δ 189.43, 146.60, 140.68, 139.09, 135.90, 134.09, 132.58, 129.33, 127.82, 127.53, 126.36, 124.38, 123.77, 122.73, 120.73, 117.59, 115.74, 114.58, 114.16, 110.07, 108.89, 101.84, 100.30, 40.67, 13.86.

3.3.1.3. The synthesis of *((E)*-2-methoxy-(6-(phenyliminomethyl))-phenol-: 2oMe-SalH-Anil

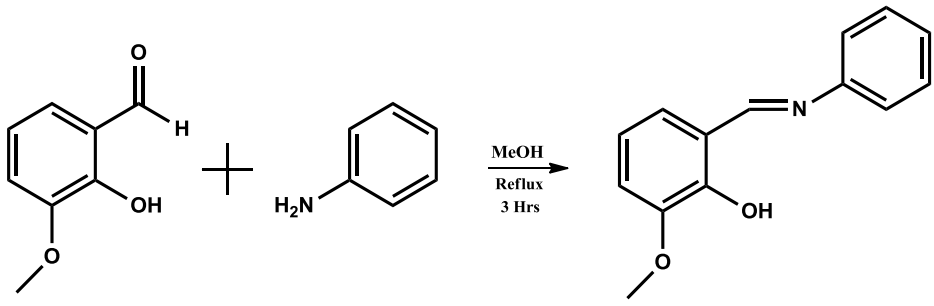

Benzenamine (0.612 g, 6.57 mmol) dissolved in methanol, was slowly added to 2-hydroxy-3-methoxybenzaldehyde (1.003 g, 6.59 mmol). After refluxing for 3 hrs, the mixture yielded a yellow-orange solid. Crystals suitable for X-ray diffraction were obtained by the slow evaporation of the filtrate. (Yield: 1.27 g, 85.06%)

IR (ATR, cm^{-1}) υ: 1614, 1588. λ_{max} = 314.3 nm, ε = 2.93 x 10^4 $M^{-1}.cm^{-1}$, **^{1}H NMR** (300 MHz, $CDCl_3$) δ 13.65 (s, 1H), 8.58 (s, 1H), 7.42 – 7.34 (m, 2H), 7.27 – 7.20 (m, 2H), 6.96

(ddd, *J* = 9.4, 7.9, 1.6 Hz, 2H), 6.87 – 6.80 (m, 1H), 3.89 (s, 3H). **^{13}C NMR** (75 MHz, $CDCl_3$) δ 162.64, 151.49, 148.51, 148.19, 129.44, 128.93, 127.00, 123.80, 121.18, 119.12, 118.54, 115.11, 114.79, 56.22.

3.3.1.4. The synthesis of *(E)*-1-((phenylimino)methyl)naphthalen-2-ol-: Napht-Sal-Anil

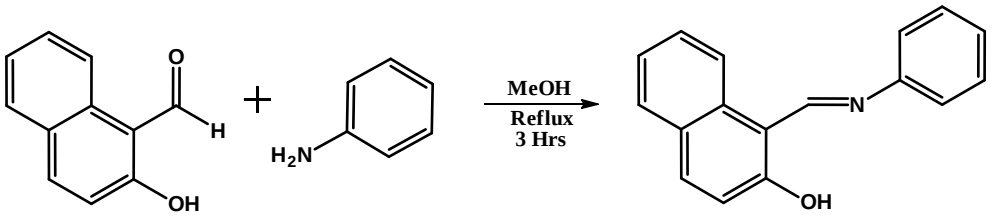

Benzeneamine (0.541 g, 5.81 mmol) dissolved in methanol, was slowly added to 2-hydroxynaphthaldehyde (1 g, 5.81 mmol). After refluxing for 3 hrs, the mixture yielded a yellow solid. Crystals suitable for X-ray diffraction were obtained by the slow evaporation of the filtrate. (Yield: 1.188 g, 87.2%)

IR (ATR, cm^{-1}) *υ*: 1620, 1578. λ_{max} = 245 nm, ε = 1.02 x 10^4 $M^{-1}.cm^{-1}$, **^{1}H NMR** (300 MHz, $CDCl_3$) δ 9.33 (s, 1H), 8.09 (d, *J* = 8.5 Hz, 1H), 7.80 (d, *J* = 9.2 Hz, 1H), 7.71 (d, *J* = 8.0 Hz, 1H), 7.56 – 7.44 (m, 3H), 7.42 – 7.29 (m, 4H), 7.08 (d, *J* = 9.2 Hz, 1H). **^{13}C NMR** (75 MHz, $CDCl_3$) δ 170.95, 154.45, 153.15, 145.03, 142.76, 136.89, 133.32, 129.71, 129.41, 128.13, 127.28, 126.53, 125.86, 123.55, 122.51, 120.24, 118.81.

3.4. Experimental Procedure of Tridentate Schiff base Ligands.

3.4.1. General Synthesis of n-Sal – "M" Tridentate Ligand Synthesis

The title compound was synthesized by the slow addition of an amine (1.0 mol) dissolved in methanol, to an aldehyde (1.0 mol). The reaction was gradually heated to room temperature and then stirred at 70.0 °C for 3 h. The solid was washed with cold methanol and filtered. The solvent was carefully removed under vacuum at 25.0 °C.

All the synthesis that follows below were carried out according to the general method described in **Section 3.4.1.**

3.4.1.2. The synthesis of *(E)*-2-methoxy-6-((2-(pyridin-2-yl)hydrazono)methyl)phenol -: 2oMe-Sal- Hydrapyrdin

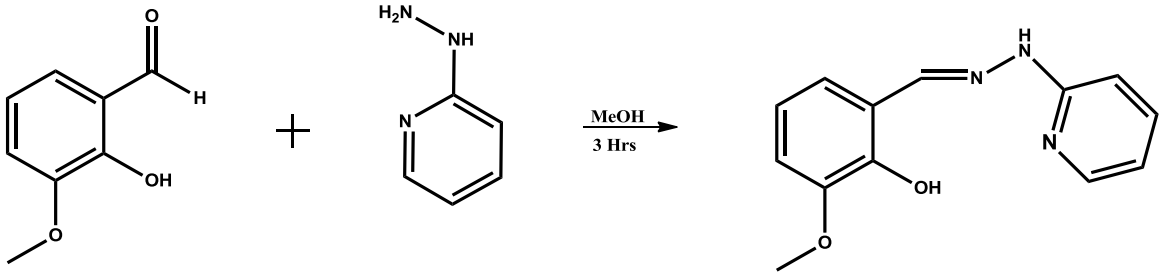

2-Hydrazinopyridine (0.9903 g, 9.07 mmol) dissolved in methanol, was slowly added to 2-hydroxy-3-methoxybenzaldehyde (1.387 g, 9.12 mmol). After refluxing for 3 hrs, the mixture yielded a pale yellow solid. (Yield: 1.311 g, 59.4%)

IR (ATR, cm^{-1}) υ: 1599, 1585. λ_{max} = 360.1 nm, ε = 4.53 x 10^4 $M^{-1}.cm^{-1}$, **^{1}H NMR** (300 MHz, $CDCl_3$) δ 8.18 (dd, *J* = 4.9, 1.0 Hz, 1H), 7.96 (s, 1H), 7.67 – 7.59 (m, 1H), 7.10 (d, *J* = 8.4 Hz, 1H), 6.95 – 6.75 (m, 4H), 3.93 (s, 3H). **^{13}C NMR** (75 MHz, $CDCl_3$) δ 155.70, 148.16, 147.62, 146.81, 142.30, 138.67, 121.45, 119.30, 118.50, 116.38, 112.59, 106.68, 56.16.

3.4.1.3. The synthesis of *(E)*-1-((2-(pyridin-2-yl)hydrazono)methyl)naphthalen-2-ol -: Naphth-Sal- Hydrapyrdin

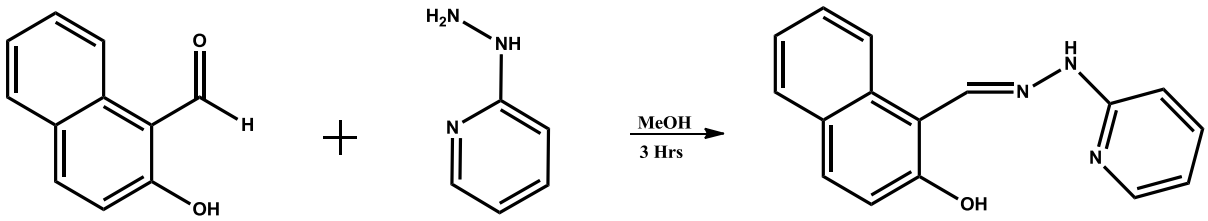

2-Hydrazinopyridine (1.04 g, 9.53 mmol) dissolved in methanol, was slowly added to 2-hydroxynaphthaldehyde (1.452 g, 9.54 mmol). After Refluxing for 3 hrs, the mixture yielded a pale yellow solid. (Yield: 1.5252 g, 60.74%)

IR (ATR, cm^{-1}) υ: 1620, 1595. λ_{max} = 475 nm, ε = 4.67 x 10^4 $M^{-1}.cm^{-1}$, **^{1}H NMR** (300 MHz, Acetone) δ 9.16 (s, 1H), 8.11 – 8.01 (m, 1H), 7.73 (dd, *J* = 8.4, 3.6 Hz, 1H), 7.61 (ddd, *J* = 8.3, 7.2, 1.8 Hz, 1H), 7.42 (ddd, *J* = 8.5, 6.9, 1.4 Hz, 1H), 7.25 (ddd, *J* = 8.0, 6.9, 1.0 Hz, 1H), 7.09 (d, *J* = 9.0 Hz, 1H), 6.91 (d, *J* = 8.4 Hz, 1H), 6.73 (ddd, *J* = 7.2, 4.9, 0.9 Hz, 1H). **^{13}C NMR** (75 MHz, Acetone) δ 184.42, 164.72, 157.04, 152.06, 148.39, 139.89, 138.16, 131.83, 131.22, 128.96, 127.19, 123.33, 120.32, 115.75, 109.27, 105.86.

3.4.1.4. The synthesis of *(E)*-2-(2-(2-hydroxy-3-methoxybenzylidene)hydrazinyl) quinolin-8-ol -: **2oMe-Sal-Quin**

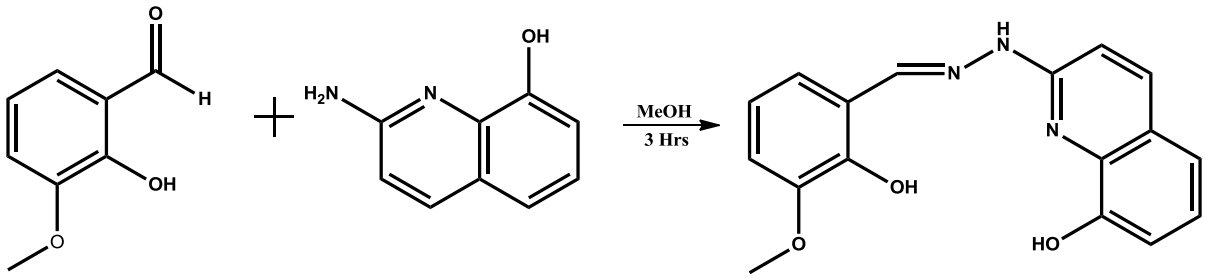

2-Aminoquinolin-8-ol (0.2507 g, 1.57 mmol) dissolved in methanol, was slowly added to 2-hydroxy-3-methoxybenzaldehyde (0.2375 g, 1.56 mmol). After refluxing for 3 hrs, the mixture yielded a dark orange solid. (Yield: 0.2965 g, 61.4%)

IR (ATR, cm^{-1}) υ: 1610, 1658. λ_{max} = 405 nm, ε = 2.901 x 10^4 $M^{-1}.cm^{-1}$, **^{1}H NMR** (300 MHz, $CDCl_3$) δ 9.52 (s, 1H), 8.26 (d, *J* = 8.6 Hz, 1H), 7.54 – 7.43 (m, 1H), 7.38 (dd, *J* = 8.3, 1.3 Hz, 1H), 7.23 – 7.15 (m, 1H), 7.03 – 6.92 (m, 1H), 6.75 (d, *J* = 8.8 Hz, 1H), 3.98 (s, 1H). **^{13}C NMR** (75 MHz, $CDCl_3$) δ 196.66, 165.85, 163.48, 155.27, 152.76, 152.03, 138.94, 127.86, 127.39, 125.05, 124.56, 119.58, 118.90, 117.98, 112.78, 110.85, 56.29.

3.4.1.5. The synthesis of *(E)*-2-(2-((2-hydroxynaphthalen-1-yl)methylene)hydrazinyl) quinolin-8-ol -: **Napht-Sal-Quin**

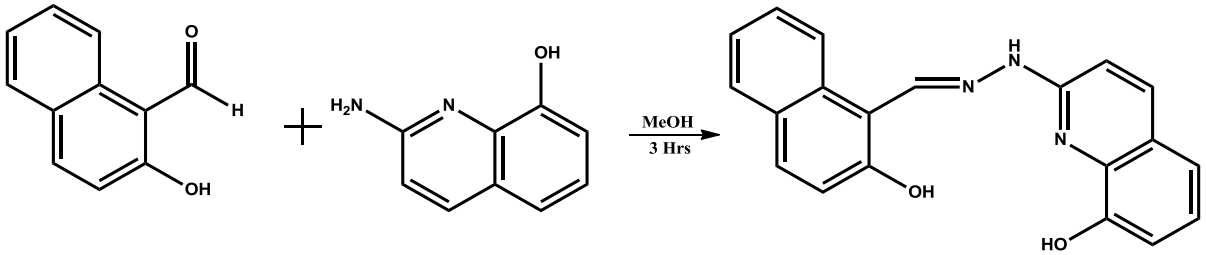

2-Aminoquinolin-8-ol (0.26 g, 1.62 mmol) dissolved in methanol, was slowly added to 2-hydroxynaphthaldehyde (0.2687 g, 1.77 mmol). After refluxing for 3 hrs, the mixture yielded a pale yellow solid. (Yield: 0.3279 g, 65.3%)

IR (ATR, cm^{-1}) υ: 1621, 1558. λ_{max} = 365 nm, ε = 1.68 x 10^4 $M^{-1}.cm^{-1}$, **^{1}H NMR** (300 MHz, $CDCl_3$) δ 10.76 (s, 1H), 8.29 (d, *J* = 8.6 Hz, 1H), 7.92 (d, *J* = 9.1 Hz, 1H), 7.81 (d, *J* = 8.8 Hz, 1H), 7.77 – 7.70 (m, 1H), 7.60 – 7.51 (m, 2H), 7.41 – 7.34 (m, 1H), 7.12 – 7.05 (m, 3H), 7.00 (q, *J* = 4.3 Hz, 1H), 6.66 (d, *J* = 8.8 Hz, 1H), 4.66 (s, 2H). **^{13}C NMR** (75 MHz, $CDCl_3$) δ 179.52, 164.98, 151.75, 149.18, 144.57, 143.40, 138.19, 129.51, 129.16, 124.53, 123.27, 119.22, 118.62, 117.79, 112.06, 110.49, 109.77, 109.45, 109.41, 102.11.

3.5. Conclusion

The synthesis of a range of Schiff base ligands has been successfully carried out. One main objective of this study is to design bi-functional ligands that are fluorescent with organic constituents known to have good characteristics needed in the making of organic light emitting diodes (OLED's). These designed ligands are to be later coordinated to the europium metal ion to have ternary Eu^{III} complexes with an ancillary ligand to saturate the coordination sphere of the europium ion in the process of luminescence enhancement and the coordinative nature therein.

The thought process behind the making of this ligand type entailed a relative comparison in the efficiency of the designed Schiff base ligands with other ligand models used in this project within one coordination mode.

A single crystal X-Ray diffraction study, focusing on crystallized ligand compounds, intra-inter-molecular interactions and crystal packing of the crystals obtained from the preceding sections is discussed in Chapter 5. Furthermore, in Chapter 7, a solid-state photoluminescence study of these Schiff base ligands is also evaluated.

4 Synthesis of Ternary β-Diketonate Eu^{III} Based Complexes

In this chapter:

The synthesis of a range of β-diketone ligands coordinated to Europium [Eu(III)] are described as well as the coordination modes thereof. The systematic analysis of synthesized complexes with different techniques.

4.1. Introduction

Herein we look to synthesize a range of ternary Europium (III) β-diketonate complexes. This lanthanide β-diketonate system with organic co-ligands as an ancillary fragment have emerged as a versatile class of compounds due to their multiple applications across many scientific stalls.[1,2,3,4.] The β-diketone ligands to be used have different substituents on the periphery of the ligand's core. The substituted derivatives on the ligands backbone cover steric and electronic properties aiding towards investigating their respective impact on the spectroscopic properties of the complexes of interest.

The reported versatility of the Europium (III) metal ion in array of applications (biosciences, magnetic and optoelectronics related applications), renders the metal ion the favourite across the series,[5,6] however, this study will solely look to investigate the luminescence aspect of the ternary europium complexes to be synthesized in this chapter.

The synthesized complexes will be further analysed in detail for photoluminescence and crystallographic properties.

The structure of the compounds will be confirmed by spectroscopic measurements of Infrared (IR) and Elemental Analyses techniques.

---

[1] Kumar, P.; Singh, S.; Gupta, K.B., *Nanoscale*, **2016**, 8 (30), 14297-14340.

[2] Bünzli, J.G.; *J. Lumin*., **2016**,170 (Part 3), 866–878.

[3] Bradley, J.D.B.; Pollnau, M., *Laser Photonics Rev*., **2011**, 5, 368−403.

[4] Martín-Ramos, P.; Coya, C.; Alvarez, A.L.; Silva, M.R.; Zaldo, C.; Paixao, J.A.; Chamorro, P.; Martín-Gil, P.J.J.; *Phys. Chem*., **2013**, 117, 10020−10030.

[5] Zhang, P.; Zhang L.; Tang J., *Dalton Trans*., **2015**, 3923–3929.

[6] Sun, J.; Song, B.; Ye Z.; Yuan J., *Inorg. Chem*., **2015**, 54, 11660–11668;

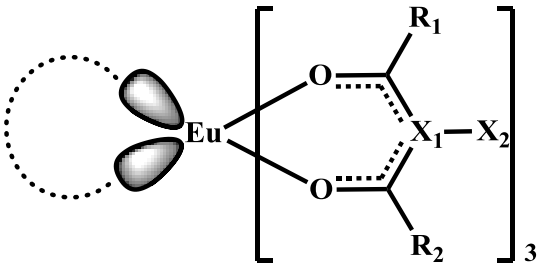

Figure 4.1: Skeletal representation of typical ternary Eu^{III} β-diketonate complexes.

Table 4.1: Tabled substituents on the backbone of the β-diketone ligands, as illustrated in **Figure 4.1.**

Substituents	R_1	R_2	X_1	X_2	β-Diketone Ligands
	Phenyl	Phenyl	O	Lone pair	**BZAN**
	Phenyl	Phenyl	C	Br	**DBBrM**
	Phenyl	Phenyl	C	H	**DBM**
	Chloro-Phenyl	CF_3	C	H	**TCPB**
	CH_3	CH_3	C	Cl	**DMC**
	CH_3	CH_3	C	$(CH_3)_2$	**TMHD**
	$(CH_3)_3$	$(CH_3)_3$	C	H	**DMMP**

4.2. General Chemicals, Solvent and Analysis Techniques

4.2.1. Reagents and Solvents

All chemicals used for the synthesis and preparation of the complexes were of analytical grade and were purchased from Sigma-Aldrich, South Africa. Reaction solvents were of analytical grade and mostly used as received. In cases where anhydrous conditions were required, solvents were purified and dried according to literature procedures.[7]

4.2.2. Infrared Spectroscopy

Solid state FT-IR spectra of samples were recorded on a Bruker Tensor 27 Fourier transform spectrometer (ATR), utilizing a He-Ne laser at 632.6 nm, in the range of 3000 to 600 cm^{-1}.

4.2.3. Elemental Analysis

A TruSpec Micro CHNS bought from LECO was used for elemental C, H and N analysis. The equipment calibration (EDTA, sulfamethazine and 3,4-dinitrobenzoic acid) standards, also bought from LECO, were used in quest to reach stable instrument conditions.

[7] Perrin D.D., Armarego W.L.F., **(1988)**, Purification of Laboratory Chemicals, *Pergamon Press, Oxford*, Great Britian.,

4.3. General Experimental Method

4.3.1. General Synthesis of *β*-diketonate Eu^{III} based Complexes

To a two-necked round bottom flask, the *β*-diketone ligand was dissolved in a ethanol (30 ml) and NaOH solution in stoichiometric proportions of 1:1 (L : OH). The solution was then left to stir for 30 min. The lanthanide ($LnCl_3 \cdot 6H_2O$) ion was dissolved in 5 ml of deionised water and added to the stirring ethanolic solution of the deprotonated ligand in a drop wise manner. The ancillary ligand, 1,10-Phenonthroline (10 ml, ethanol) was added to the solution. The reaction was left to reflux for about 4 hours and a white precipitate formed. The solution was filtered and the solvent was pressure evaporated. The solid product was washed with a cold ethanol:water (3:1) mixture to remove extra ligand and salts. The solvent was then removed under reduced pressure to yield the product in approximately 60% yields.

All the lanthanide complexes listed below were synthesised according to the general synthesis given in **Section 4.3.1** unless it is otherwise stated. All experiments were performed aerobically using double distilled water and ethanol. Unless otherwise stated, all chemicals were of reagent grade and purchased from Sigma Aldrich.

4.3.1.1. The synthesis of [*tris*-(2,2,6,6-Tetremethyl-heptanedione) mono(1,10-phenanthroline) europium(III)]: **[Eu(TMHD)$_3$Phen]**

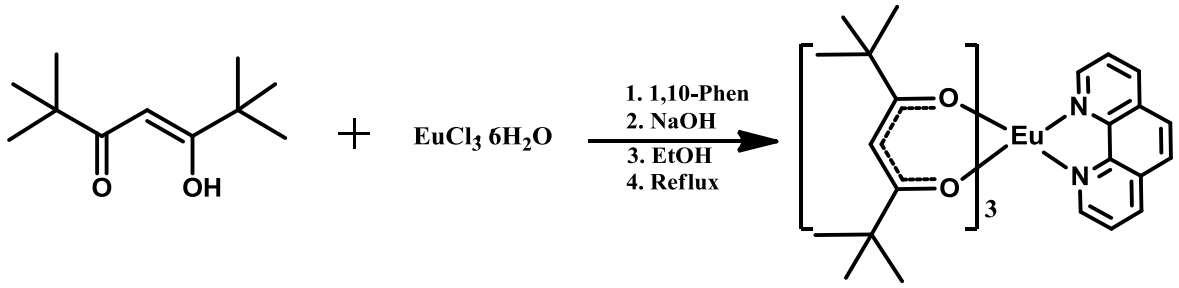

2,2,6,6-Tetamethyl-3,5-heptanedione (**HTMHD**) (150 mg, 0.819 mmol) was dissolved in NaOH a ethanolic solution. $EuCl_3 \cdot 6H_2O$ (100 mg, 0.273 mmol) dissolved in water was then slowly added to the stirring ethanolic solution wherein 1,10-phenonthroline (49.2 mg, 0.273 mmol) was later added. The reaction was left to reflux and a white precipitate formed. Yield = 0.1422, 56%

Anal. Calcd.: C, 61.28; H, 7.73; N, 3.18. **Anal**. Found: C, 63.60; H, 9.29; N, 3.99

IR (ATR, cm^{-1}) *υ*:1600, 1586.

4.3.1.2. The synthesis of [*tris*-(1,3-Diphenyl-propanedione) mono (1,10-phenanthroline) europium(III)]: **[Eu(DBM)$_3$Phen]**

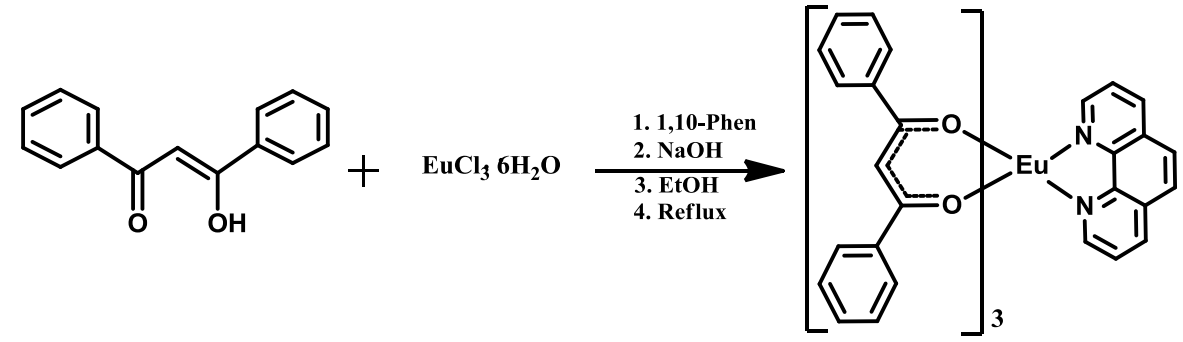

1,3-Diphenyl-propanedione (**HDBM**) (200 mg, 0.891 mmol) was dissolved in a NaOH ethanolic solution. $EuCl_3 \cdot 6H_2O$ (109 mg, 0.297 mmol) dissolved in water was then slowly added to the stirring ethanolic solution wherein 1,10-phenonthroline (53.6 mg, 0.297 mmol) was later added. The reaction was left to reflux and a yellowish precipitates formed. Yield = 0.1903, 61%

Anal. Calcd.: C, 68.33; H, 4.12; N, 2.80. **Anal**. Found: C, 69,64; H, 4.19; N, 2.84

IR (ATR, cm^{-1}) υ:1593, 1547.

4.3.1.3. The synthesis of [*tris*-(4,4,4-Trifluoro-1-chlorophenyl-butanedione) mono(1,10-phenanthroline) europium(III)]: **[Eu(TCPB)$_3$Phen]**

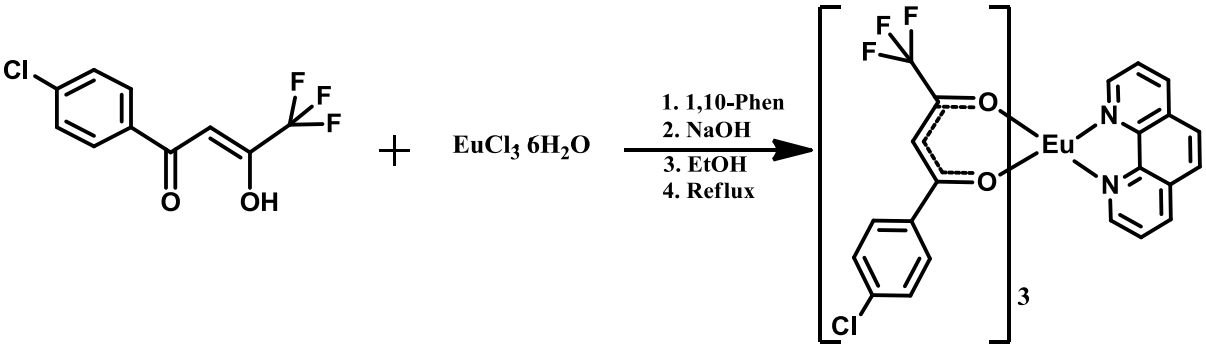

4,4,4-Trifluoro-1-chlorophenyl-butanedione (**HTCPB**) (200 mg, 0.798 mmol) was dissolved in a NaOH ethanolic solution. $EuCl_3 \cdot 6H_2O$ (97.5 mg, 0.266 mmol) dissolved in water was then slowly added to the stirring ethanolic solution wherein 1,10-phenonthroline (47.9 mg, 0.266 mmol) was later added. The reaction was left to reflux and a white precipitatesformed. Yield = 0.2376, 66%

Anal. Calcd.: C, 46.46; H, 2.14; N, 2.59. **Anal**. Found: C, 47.21; H, 2.15; N, 2.59

IR (ATR, cm^{-1}) υ: 1613, 1591.

4.3.1.4. The synthesis of [*tris*-(2-Bromo-1,3-diphenyl-propanedione) mono(1,10-phenanthroline) europium(III)]: **[Eu(DBBrM)$_3$Phen]**

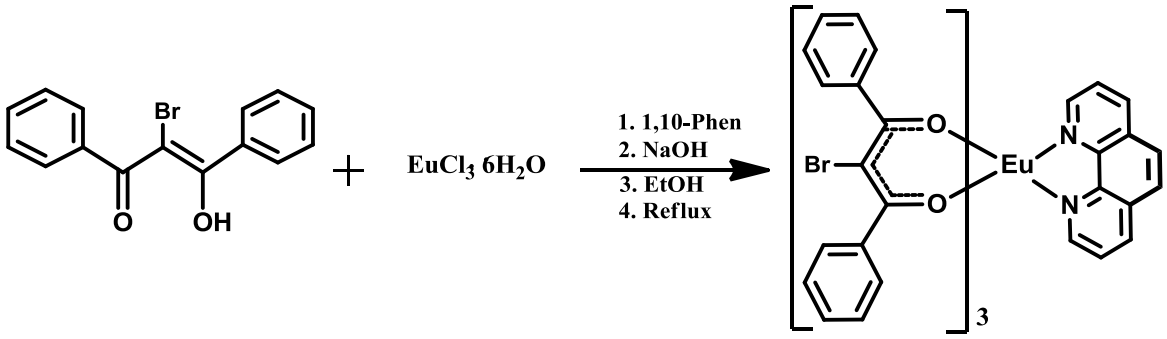

2-Bromo-1,3-diphenyl-propanedione (**HDBBrM**) (250 mg, 0.825 mmol) was dissolved in a NaOH ethanolic solution. $EuCl_3 \cdot 6H_2O$ (100 mg, 0.275 mmol) dissolved in water was then slowly added to the stirring ethanolic solution wherein 1,10-phenonthroline (49.5 mg, 0.275 mmol) was later added. The reaction was left to reflux and a white precipitate formed. Yield = 0.1839, 52%

Anal. Calcd.: C, 55.27; H, 3.04; N, 2.26. **Anal**. Found: C, 63.75; H, 4.30; N, 3.78

IR (ATR, cm^{-1}) *v*: 1703,1659,1672,1579.

4.3.1.5. The synthesis of [*tris*-(3-Chloro-2,4-pentanedione) mono (1,10-phenanthroline) europium(III)]: **[Eu(DMC)$_3$Phen]**

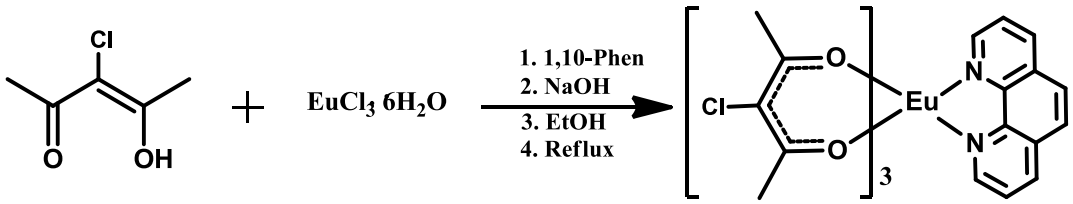

3-Chloro-2,4-pentanedione (**HDMC**) (200 mg, 1.486 mmol) was dissolved in a NaOH ethanolic solution. $EuCl_3 \cdot 6H_2O$ (182 mg, 0.495 mmol) dissolved in water was then slowly added to the stirring ethanolic solution wherein 1,10-phenonthroline (89.3 mg, 0.492 mmol) was later added. The reaction was left to reflux and a white precipitate formed. Yield = 0.2049, 53%

Anal. Calcd.: C, 44.25; H, 3.58; N, 3.82. **Anal**. Found: C, 45.44; H, 3.65; N, 3.97

IR (ATR, cm^{-1}) *v*: 1583, 1518.

4.3.1.6. The synthesis of [*tris*-(3,3-Dimethyl-2,4-pentanedione) mono(1,10-phenanthroline) europium(III)]: **[Eu(DMMP)$_3$Phen]**

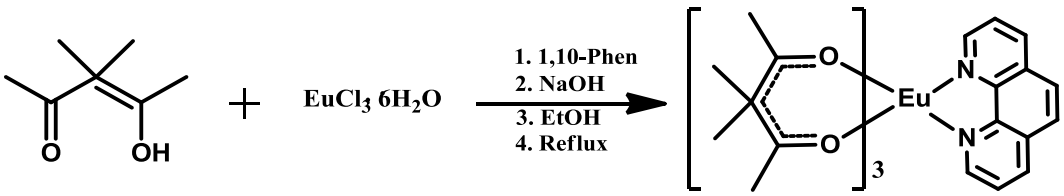

3,3-Dimethyl-2,4-pentanedione (**HDMMP**) (200 mg, 1.56 mmol) was dissolved in a NaOH ethanolic solution. $EuCl_3 \cdot 6H_2O$ (190 mg, 0.52 mmol) dissolved in water was then slowly added to the stirring ethanolic solution wherein 1,10-phenonthroline (93 mg, 0.52 mmol) was later added as the ancillary ligand. The reaction was left to reflux and a white precipitate formed. Yield = 0.2178, 55%

Anal. Calcd.: C, 55.30; H, 6.19; N, 3.91. **Anal**. Found: C, 59.58; H, 7.35; N, 4.57

IR (ATR, cm^{-1}) υ: 1598, 1576.

4.3.1.7. The synthesis of [*tris*-(Benzoic Anhydride) mono(1,10-phenanthroline) europium(III)]*:* **[Eu(BZAN)$_3$Phen]**

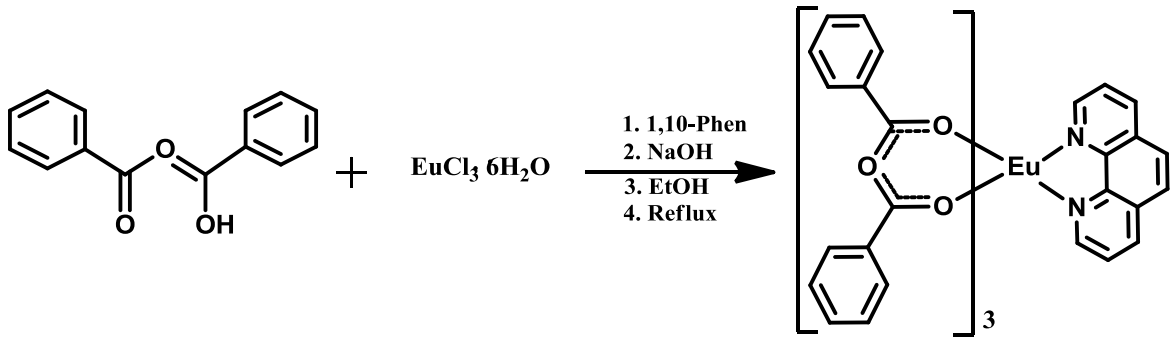

It however appears that the Benzoic Anhydride under high temperature easily breaks off to yield a pair of Benzyl Carboxylic Acid per ligand with respect to one Eu^{III} ion.

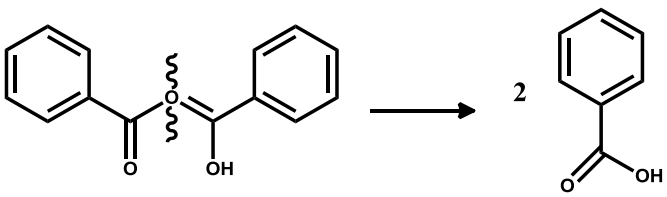

Therefore this reaction was done in duplicates with two different temperatures conditions and it resulted to different complexes:

4.3.1.7.1. The synthesis of {[*hexa*-(Benzyl carboxylic acid) *bis*-(1,10-phenanthroline) di-europium(III)]-μ-[κ^2-O,O'-(benzyl carboxylic acid)]$_2$} **: {[$Eu_2(BCA)_6(Phen)_2$]-μ-[κ^2-O,O'-(BCA)]} BCA)]}**

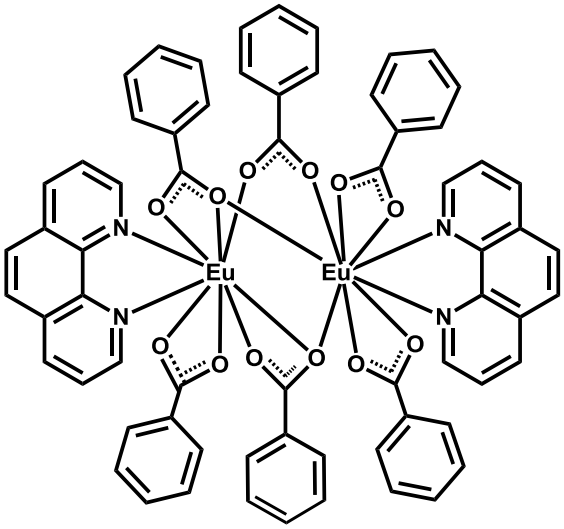

Benzoic anhydride (**HBZAN**) (350 mg, 1.54 mmol) dissolved in a NaOH ethanolic solution. $EuCl_3 \cdot 6H_2O$ (187 mg, 0.51 mmol) dissolved in water was then slowly added to the stirring ethanolic solution wherein 1,10-phenonthroline (92 mg, 0.511 mmol) was later added. The reaction was left to reflux and a white precipitate formed. Yield = 0.4855, 68%.

Anal. Calcd.: C, 56.99; H, 3.33; N, 4.03. **Anal**. Found: C, 60.88; H, 3.92; N, 4.46

IR (ATR, cm^{-1}) υ:1596, 1547.

4.3.1.7.2. The synthesis of [*tris*-(Benzyl Carboxylic Acid)-*mono*-(1,10-phenanthroline) europium(III)]*:* **[$Eu(BCA)_3Phen$]**

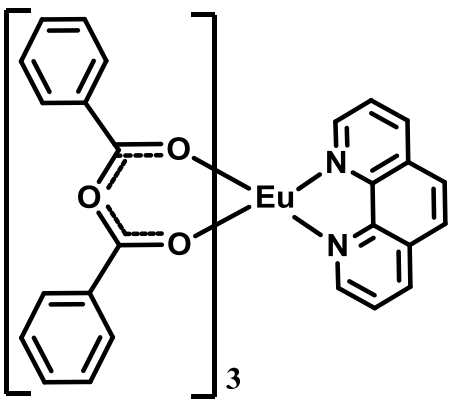

Benzoic anhydride (**HBZAN**) (350 mg, 1.54 mmol) dissolved in a NaOH ethanolic solution. $EuCl_3 \cdot 6H_2O$ (187 mg, 0.51 mmol) dissolved in water was then slowly added to the stirring ethanolic solution wherein 1,10-phenonthroline (92 mg, 0.51 mmol) was later added. The reaction was left to stir at room temperature and a white precipitate formed. Yield = 0.1389, 39%. **Anal**. Calcd.: C, 56.99; H, 3.33; N, 4.03. **Anal**. Found: C, 59.92; H, 3.43; N, 4.47
IR (ATR, cm^{-1}) *v*:1596, 1547.

4.4. Conclusions

The desired goal of synthesizing ternary Eu^{III} based complexes using the *β*-diketone derivatives has been archieved. The main aim is to sensitize the luminescence of the metal ion. These ligands are coordinated to the europium metal ion to have ternary Eu^{III} complexes with an ancillary ligand (1,10-phenanthroline) to saturate the coordination sphere of the europium ion to have an eight (8) coordinated europium metal complex. The compounds were synthesized with reasonably good yields in different solid forms.

With the *β*-diketone ligands having the liberty to have two different substitutions on the backbone, it is likely easy to control the relative nature of effect of the ligands based on how symmetric the ligands are. The luminescence results of the above tailored complexes will be compared to other bi-functional ligand systems used in this project.

The single crystal X-ray diffraction and photoluminescence properties of these complexes will be discussed in later chapters

5 Crystallographic Evaluation of New (*N*,*O*) Schiff Base Ligands.

In this chapter:
Crystal structures of Schiff base ligands (ScB) are presented. Various structural parameters, geometric orientations and molecular interactions are examined and compared to relevant compounds.

5.1. Introduction

It is in the salicylidene ligand system that the Schiff base ligands have found considerable growth and interest across many interdisciplinary areas of science like biomedical studies, catalysis and photo-chemistry since their discovery.[1,2,3] This system has been used quite extensively with transition elements with great success,[4,5] and now the same gesture is used to employ the nature of this ligand system in tailoring Eu^{III} based complexes with its derivatives for purposes that best suits the aim of this project.

It is their photochromic and thermo-chromic properties that deems them excellent candidates in the photoluminescence field. In their free ligand state, their ability to tautomerize[6] both in solid and solution state renders them perfect organic compounds to undergo the intra-ligand electron transfer and gives off light in the process. The existence of the *o*-hydroxy group forming an O-H…N and O…H-N giving rise to a resonance structure completed by the hydrogen atom mimicking a six member ring properties.[7],

Their synthetic versatility allows them to be utilizes as potential chromophores to sensitize the luminescence of the Eu^{III}-based complexes.

---

[1] da Silva, C. M.; da Silva, D. L.; Modolo, L. V.; Alves, R. B.; de Resende, M. A.; Martins, C. V. B.; de Fátima, Â., *J. Adv. Res.*, **2011,** 2 (1), 1-8.

[2] Dong, Y.W.; Fan, R.Q.; Wang, P.; Wei, L.G.; Wang, X.-M.; Zhang, H.J.; Gao, S.; Yang, Y.L.; Wang, Y.L., *Dalton Trans.* **2015,** 44 (12), 5306-5322.

[3] Gupta, K.C.; Sutar, A.K., Coord. Chem. Rec., 2008, 252 (12-14), 1420-1450.

[4] Mokolokolo, P. P.; Frei, A.; Tsosane, M. S.; Kama, D. V.; Schutte-Smith, M.; Brink, A.; Visser, H. G.; Meola, G.; Alberto, R.; Roodt, A., *Inorg. Chim. Acta*, **2018,** 471, 249-256.

[5] Tamami, B.; Ghasemi, S., *J. Org. Chem.*, **2015,** 794, 311-317.

[6] Temel, H.; Ilhan, S.; Sekerci, M.; Ziyadanogullari, R., *Spectrosc. Lett.*, **2002**, 35 (2), 219-228.

[7] Bige, S.; Kilie, Z.; Hayvali, Z.; Hokelek, T.; Safran, S., *J. Chem. Sci*, **2009**, 121, 989-1001.

The Schiff base ligands to be evaluated in this chapter are illustrated in **Figure 5.1** below.

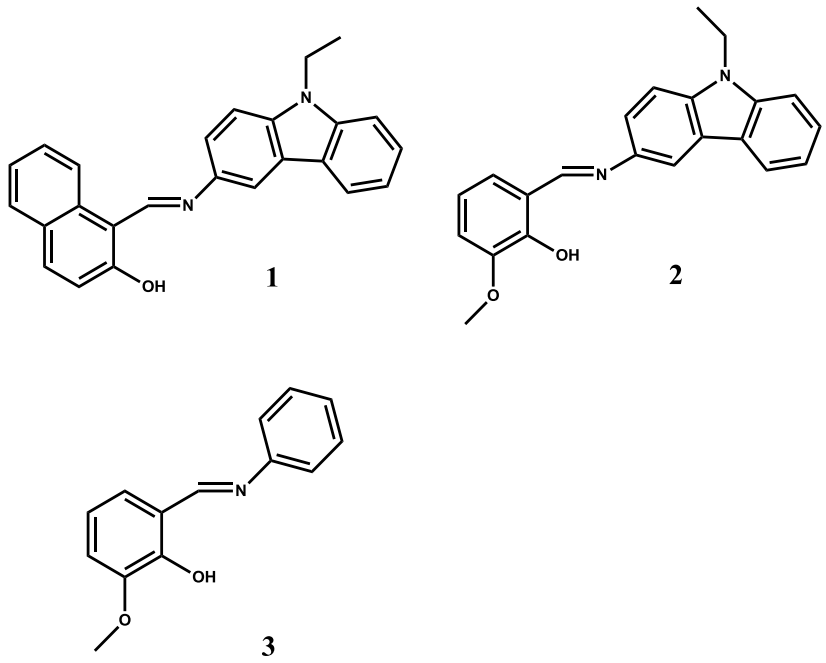

Figure 5.1: The sketched Schiff base molecules to be discussed in this single crystal x-ray diffraction chapter, **1** = (*E*)-1-((9-ethylcarbazol-3-ylimino)methyl)-napthanol; **2** = (*E*)-2-(9-ethylcarbazol-3-yliminomethyl)-6-methoxyphenol ; **3** = (*E*)-2-methoxy-(6-(phenyliminomethyl))-phenol

Various interesting aspects are envisaged in studying the solid state characteristics of these organic entities. Such as:

- Tautomerization in solid state,
- Planarity of the molecules,
- Intermolecular networking.

It is, in most cases, the molecular constituency that dictates the degree to which tautomerization will occur and that obviously translates to their planarity. Their photochromic strength from the ESIPT process[8,9] (excited state intramolecular proton transfer) depends hugely on their nature of geometry in that the more planer the molecule the more rigid the structure is to mimic a pseudo resonance of a six membered ring.[10]

[8] Chang, S.M.; Hsueh, K.L.; Huang, B.K.; Wu, J.H.; Liao, C.C.; Lin, K.C., *Surf. Coat. Technol.*, **2006,** 200 (10), 3278-3282.

[9] Zhao, J.; Ji, S.; Chen, Y.; Guo, H.; Yang, P., *Phys. Chem. Chem. Phys.*, **2012,** 14 (25), 8803-8817.

[10] Zborowski, K.K.; Solá, M.; Poater, J.; Proniewicz, L.M., *Cent. Eur. J. Chem*., **2013**, 11(5) , 655-663

All the afore-stated molecular geometry challenges in free salicylidene ligands will be discussed in this chapter.

5.2. Experimental

The X-ray intensity data was collected on a Bruker X8 ApexII 4K Kappa CCD area detector diffractometer, equipped with a graphite monochromator and MoKα fine-focus sealed tube (λ = 0.71069 Å, T = 100(2) K) operated at 2.0 kW (50 kV, 40 mA). The initial unit cell determinations and data collections were done by the SMART software package.[11] The collected frames were integrated using a narrow-frame integration algorithm and reduced with the Bruker SAINT-Plus and XPREP software packages respectively.[12] Analysis of the data showed no significant decay during the data collection. Data was corrected for absorption effects using the multi-scan technique SADABS, and the structure was solved by the direct methods package SIR97 and refined using the WinGX software incorporating SHELXL.[13,14,15,16] The final anisotropic full-matrix least-squares refinement was done on F^2. The methyl and aromatic protons were placed in geometrically idealized positions (C–H = 0.93 – 0.98 Å) and constrained to ride on their parent atoms with $U_{iso}(H) = 1.2U_{eq}(C)$. Non-hydrogen atoms were refined with anisotropic displacement parameters. The graphics were obtained with the DIAMOND program with 50% probability ellipsoids for all non-hydrogen atoms.[17]

[11] Bruker SMART-NT Version 5.050, *Bruker AXS Inc. Area-Detector Software Package*; Madison, Winconsin, United States of America, **1998**.

[12] Bruker SAINT-Plus Version 6.02 (including XPREP), *Bruker AXS Inc. Area-Detector Integration Software*, Madison, Winconson, United States of America, **1999**.

[13] Bruker SADABS Version 2004/1, *Bruker AXS Inc. Area Detector Absorption Correction Software*, Madison, Wisconsin, United States of America, **1998**.

[14] Altomare, A.; Burla, M.C.; Camalli, M.; Cascarano, G.L.; Giacovazzo, C.; Guagliardi, A.; Moliterni, A.G.G.; Polidori, G.; Spagna, R., *J. Appl. Cryst.*, **1999**., 32, 115-119.

[15] Farrugia, L.J, *J. Appl. Cryst.* **1999**, **32**, 837-838.

[16] Sheldrick G.M., (**1997),** SHELXL97, *Program for Crystal Structure Refinement*, University of Göttingen, Germany.

[17] Brandenburg, K.; Putz, H.; DIAMOND, *Release 3.3, Crystal Impact GbR*, Bonn, Germany, **2006**.

Table 5.1: Crystallographic and refinement details for structures discussed in this chapter.

Crystal Formula	Napht-SalH-Carba (1).	3Methoxy-SalH-Carb (2)	3Methoxy-SalH-Anil (3)
Empirical formula	C_{25} H_{20} N_2 O	$C_{88}H_{76}N_{12}O_{16}$	$C_{14}H_{13}NO_2$
Formula weight (g.mol^{-1})	364.43	1557.60	227.25
Crystal system, Space Group	Monoclinic, $P2_1/c$	Orthorhombic, $Pca2_1$	Orthorhombic, $P2_12_12_1$
***a, b, c* (Å)**	18.065(5), 6.010(5) 18.240(4),	24.399 (6), 5.2442 (12) 13.453 (4),	6.052(5), 9.072(4) 20.921(5),
α, β, γ (°)	90, 109.031(5), 90	90, 90, 90	90, 90, 90
Volume (Å^3),	1872.1(17)	1721.3 (8)	1148,6 (12)
Z	4	4	4
Density (calculated, Mg/m^3)	1.293	1.3328	1.314
Crystal colour	Orange	Orange	Orange
Crystal size (mm^3)	0.389x 0.159 x 0.105	0.186 x 0.102 x 0.102	0.46 x 0.14 x 0.10
Absorption coefficient μ (mm^{-1})	0.079	0.105	0.754
F(000)	768	732	480
Theta range	4.09 – 27.99°	1.669 – 20.816°	3.9 – 27.99°
Index ranges	-16<=h<=23, -7<=k<=7, -24<=l<=24	-24<=h<=24, -5<=k<=4, -13<=l<=13	-7<=h<=7, -11<=k<=11, -27<=l<=18
Reflections collected, Independent Reflections	44905, 4491	27139, 1794	17498, 2747
R_{int}	0.0510	0.0634	0.0354
Completeness to 2θ (°, %)	27.99, 99.7	25.242, 99.7	27.99, 99.8
Max. and min. transmission	0.7457 and 0.6818	0.7457 and 0.6826	0.7457 and 0.6855
Data, restraints, parameters	4491, 0, 255	1794, 1, 240	2751, 0, 65
Goodness-of-fit on F^2	1.025	1.061	1.047
Final R indices [I>2sigma(I)]	R_1 = 0.0431; wR_2 = 0.1006	R_1 = 0.0251; wR_2 = 0.0613	R_1 = 0.0294; wR_2 = 0.0768
R indices (all data)	R_1 = 0.0690; wR_2 = 0.1172	R_1 = 0.0277; wR_2 = 0.0636	R_1 = 0.0321; wR_2 = 0.0788
Largest diff. peak and hole (e.Å^{-3})	0.35, -0.23	0.093, -0.202	0.189, -0.171

(1) Napht-SalH-Carb = (*E*)-1-((9-ethylcarbazol-3-ylimino)methyl)-napthanol; **(2) 3Methoxy-SalH-Carb** = (*E*)-2-(9-ethylcarbazol-3-yliminomethyl)-6methoxyphenol;
(3) 3Methoxy-SalH-Anil =(*E*)-2-methoxy-(6-(phenyliminomethyl))-phenol

5.3. CRYSTAL STRUCTURE OF Napht-SalH-Carba (1).

The molecule, (*E*)-1-((9-ethylcarbazol-3-ylimino)methyl)-napthanol (Napht-SalH-Carba) (**1**) crystallizes in a monoclinic crystal system in the $P2_1/c$ space group with four (4) molecules per unit cell. The molecular framework is represented in **Figure 5.2** below with its atom numbering scheme.

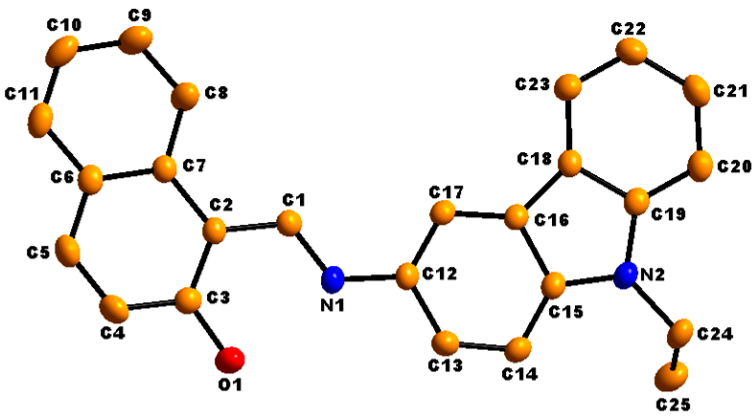

Figure 5.2: The molecular structure of Napht-SalH-Carba (**1**) exhibiting the atomic numbering sequence. Hydrogen atoms are omitted for clarity. Displacement ellipsoids are drawn at 50% probability level.

It was found that similar compounds to **1** undergoes tautomerization in solution, however, crystallized as the *trans* phenol-imine tautomer. [18] There is only one hydrogen bond interaction observed in **1**. The intra-molecular hydrogen bonding interaction is observed between O1-H1…N1 atoms with intra-distance of 1.769 (1) Å and the angle of 147.9 (10) ˚ (see **Figure 5.3** and **Table 5.3**).

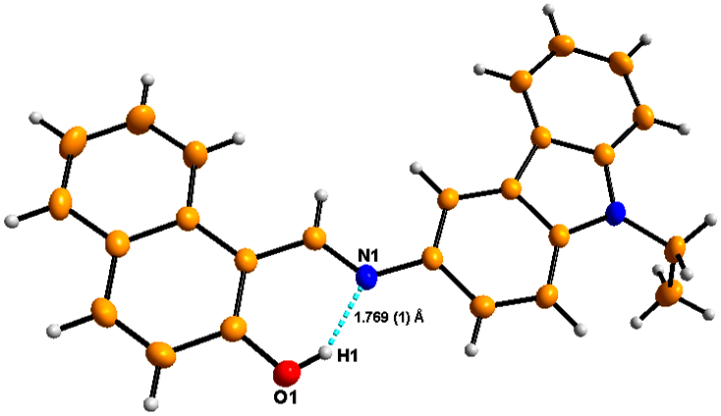

Figure 5.3: The molecular structure of **1** highlighting intra-molecular hydrogen bond interaction.

[18] Temel, H.; Ilhan, S.; Sekerci, M.; Ziyadanogullari, R., *Spectrosc. Lett.*, **2002**, 35 (2), 219-228.

Table 5.2: Selected bond lengths and bond angles for compound 3Methoxy-SalH-Carba [**Å and**°]

Atomic Bond Distances (Å)		Atomic Bond Angles (°)	
O1-C3	1.327(18)	**C1-N1-C12**	124.20(13)
N1-C12	1.414(2)	**O1-C3-C4**	117.46(13)
N1-C1	1.298(18)	**O1C3-C2**	122.31(14)
N2C24	1.457(19)	**C3-O1-H1**	109.5#
N2-C15	1.383(2)	**N1-C1-C2**	121.13(13)
N2-C19	1.386(19)	**C1-N1-C12**	124.20(13)
C3-C2	1.410(2)	**C15-N2-C24**	124.95(13)
C7-C2	1.444(2)	**C15-N2-C19**	108.96(12)
C1-C2	1.435(2)	**N2-C24-C25**	112.07(13)

#No e.s.d. as H-atom were all placed as riding on the parent atom.

Table 5.3: Hydrogen bonds for Napht-SalH-Carba [**Å and** °].

D-H...A	d(D-H) (Å)	d(H...A) (Å)	d(D...A) (Å)	<(DHA) (°)
O1-H1…N1 #1	0.840 (1)	1.769 (1)	2.520 (2)	147.9 (10)

Symmetry transformations used to generate equivalent atoms:
#1 x, y, z.

The C1-N1 bond distance, as tabled above, 1.298(18) **Å,** is indicative of a double bond (aromatic -C=N- is 1.34 **Å**) whereas the N1-C12 (1.414(2) **Å**) and O1-C3 (1.327(18) **Å**) bond distances are consistent with single bonds. All bond lengths and angles of **1** are within normal ranges.[19]

The measure of the dihedral angle between the planes (**Plane 1**: O1, O2, C1, C2, C3, C4, C6, C7, O8, C9, C10, C11 and **Plane 2**:, C12, C13, C14, C15, C16, C17, C18, C19, C20, C21, C22, C23, C24) constructed between two aromatic moieties of **1.** The measured dihedral angle constructed in **1** is 10.35 (4) °.The measured torsion angle is 178.61 (24) °between the C1-N1-C12-C17 atoms

[19] Bondi, A.; *J. Phys. Chem*., **1964**, 68, 441.

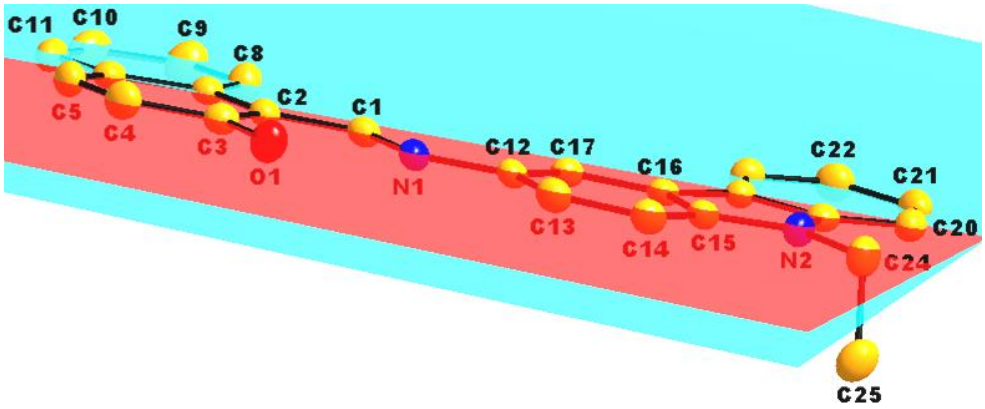

Figure 5.4: The graphical representation of Napht-SalH-Carba ligand indicating slight twisting of the C=N bond general co-planarity of the aromatic rings.

There are no classical intermolecular hydrogen interactions or any further type of molecular interaction occurring. The illustration in **Figure 5.5** is of the molecular packing pattern of **1** depicting six molecules along the *b-axis* with symmetry elements.

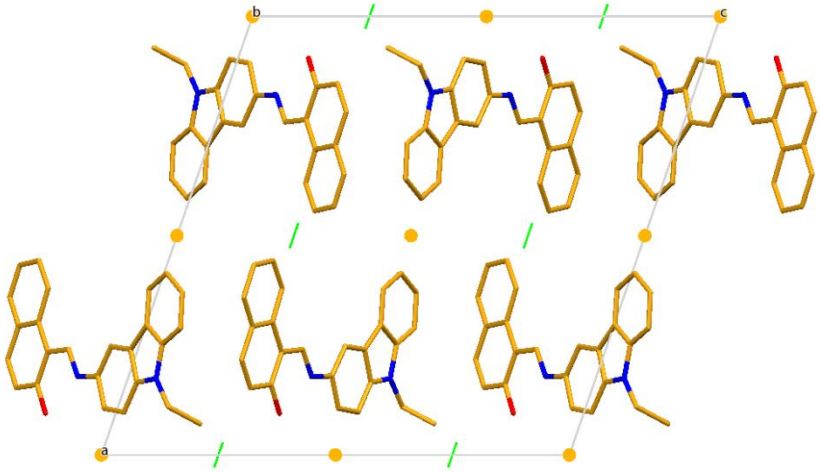

Figure 5.5: Graphical presentation of the molecular packing of **1** with the roto-inversion type of packing along the *b-axis*.

The packing seem to exhibit head to tail packing fashion portraying a zig-zag pattern (see **Figure 5.6**). The inversion centres are shown in yellow spots and the screw axes are in green lines.

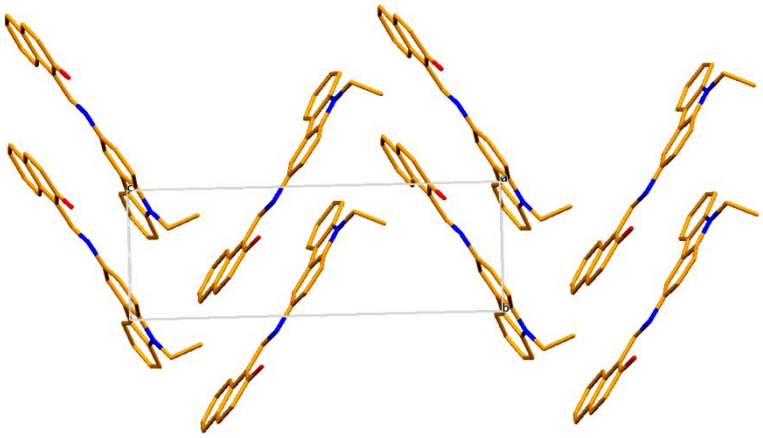

Figure 5.6: The illustration of the zig-zag packing of **1**.

5.4. CRYSTAL STRUCTURE OF 3Methoxy-SalH-Carba (2)

The molecule, (*E*)-2-(9-ethylcarbazol-3-yliminomethyl)-6-methoxyphenol (3Methoxy-SalH-Carba) (**2**) crystallizes in Orthorhombic crystal system in the *Pca2₁* space group with four molecules per unit cell (Z = 4). The molecular framework of **2** is represented in **Figure 5.8** below with its atom numbering scheme.

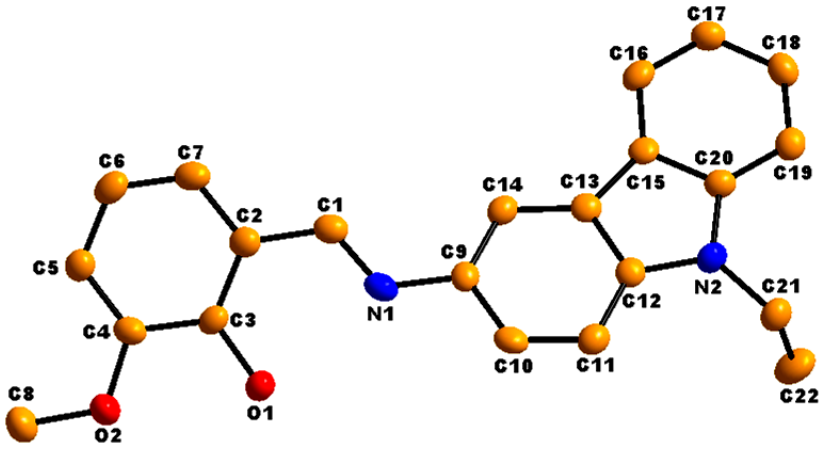

Figure 5.7: The molecular structure of 3Methoxy-SalH-Carba exhibiting the atomic numbering sequence. Hydrogen atoms are omitted for clarity. Displacement ellipsoids are drawn at 50% probability level.

The molecule crystallized as the *trans* phenol-imine tautomer. There is only one intra-molecular hydrogen bond interaction observed in **2**. The hydrogen bonding interaction is observed between O1-H1…N1 atoms with intra-distance of 1.86 (3) Å and the angle of 146.02 (3) ˚ (see **Figure 5.9** and **Table 5.5**).

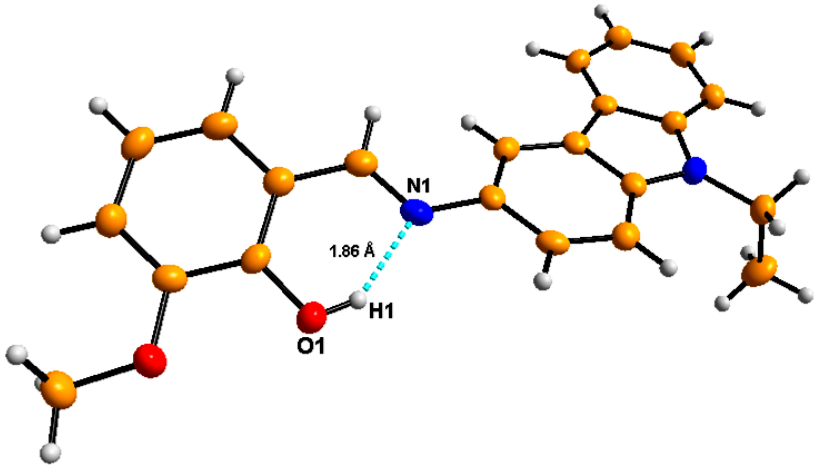

Figure 5.8: The molecular structure of **2** highlighting intra-molecular hydrogen bond interaction.

Table 5.4: Selected bond lengths and bond angles for compound 3Methoxy-SalH-Carba [**Å and**°]

Atomic Bond Distances (Å)		**Atomic Bond Angles (°)**	
N1-C1	1.282(4)	**O1-C3-C2**	122.3(3)
O1-C3	1.349(4)	**C1-N1-C9**	123.8(3)
C1-C2	1.451(5)	**N1-C1-C2**	122.2(3)
C7-C2	1.406(5)	**O1-C3-C4**	118.2(3)
C2-C3	1.401(5)	**C3-O1-H1**	146.02#
N1-C9	1.415(4)	**C12-C13-C15**	106.4(3)
N2-C20	1.390(5)	**C12-N2-C20**	108.0(3)
N2-C21	1.456(4	**C12-N2-C21**	125.7(3)
N2-C12	1.389(4)	**C20-N2-C21**	125.8(3)

#No e.s.d. as H-atom were all placed as riding on the parent atom.

Table 5.5: Hydrogen bonds for 3Methoxy-SalH-Carba [**Å and** °].

D-H...A	**d(D-H) Å**	**d(H...A) Å**	**d(D...A) Å**	**<(DHA) (°)**
O1-H1…N1 #1	0.840 (2)	1.864 (3)	2.604 (3)	146.02 (17)
C8-H8B…O1 #2	0.984 (4)	2.467 (2)	3.378 (4)	154.49 (21)

Symmetry transformations used to generate equivalent atoms:
#1 x, y, z; **#2** x, y-1, z.

The C1-N1 bond distance, as tabled above, 1.282(18) **Å** is indicative of a double bond (aromatic -C=N- is 1.34 **Å**) whereas the N1-C9 (1.415(4) **Å**) and O1-C3 (1.349(4) **Å**) bond distances are consistent with single bonds (typical bond distance of N-C and O-C are 1.47 and 1.43 **Å** respectively).

The rotation around the –C=N– bond induces a non-planar orientation of the moieties constructing **2**. The carbazolyl moiety is twisted out of the horizontal plane as exhibited in **Figure 5.10** below.

The measure of the dihedral angle between the planes (**Plane 1**: C1, C2, C3, C4, C5, C6, C7, O1, O2, and **Plane 2**: C9, C10, C11, C12, C13, C14, C15, C16, C17, C18, C19, N2, C20, C21) constructed between the two aromatic moieties of **2** is 26.535 (2) ° with a torsion angle of 157.49 (20) ° between C1-N1-C9-C10 atoms.

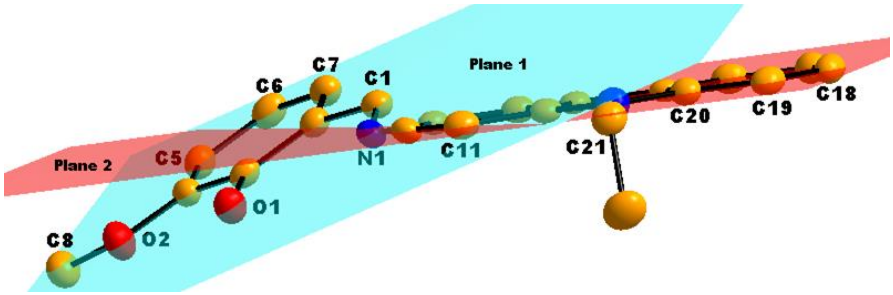

Figure 5.9: The graphical representation of 3Methoxy-SalH-Carba ligand indicating the twisting of the C=N bond general co-planarity of the aromatic rings. Hydrogen atoms are omitted for clarity.

There is one inter-molecular interaction observed in **2**. This inter-molecular hydrogen bond interaction C8-H8B…O1, with the distance 2.467 (2) **Å**, occurs between the terminal methyl of the methoxy group and the phenol oxygen O1 of the symmetry generated molecule (see **Figure 5.11** and **Table 5.5**).

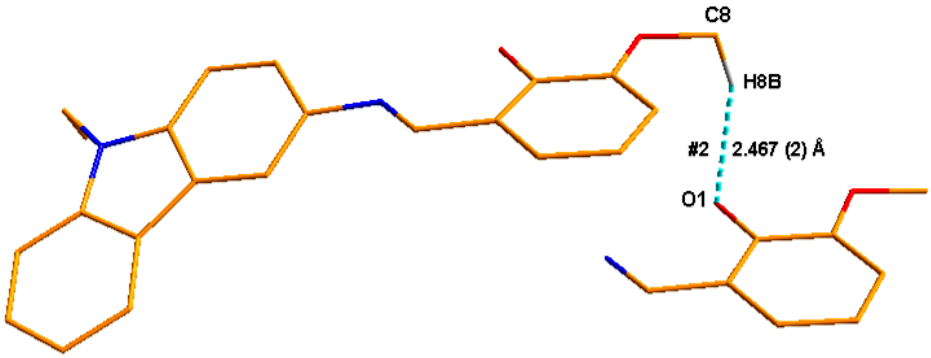

Figure 5. 10: Illustration of the intermolecular hydrogen bonding in **2**. Some H-atoms are omitted for clarity.

Observed below in **Figure 5.12** is the molecular packing of **2** depicting nine molecules along the *b-axis*. Along the *c-axis* there is a head to tail zig-zag type of packing (see **Figure 5.13**). The observed molecular packing is stabilized by inter- and intra-molecular hydrogen bonding as given in **Table 5.5**.

The packing in **Figure 5.12,** illustrates the screw axis in green lines with arrows assisting with rotational direction and the glide planes in purple along the *bc-axis* commending the $P2_1/c$ space group.

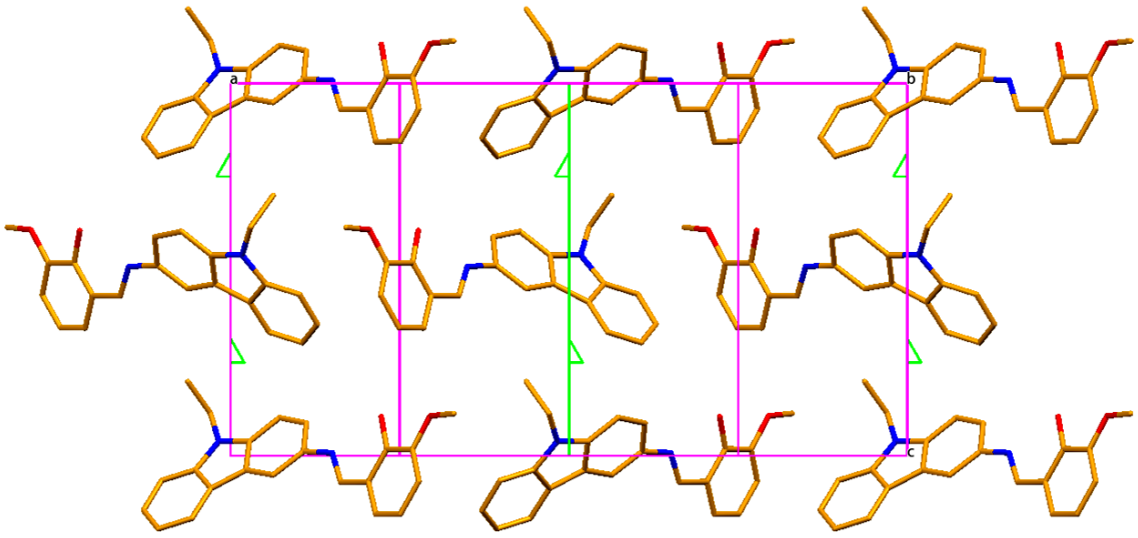

Figure 5.11: Graphical presentation of the molecular packing of **2** and its roto-inversion type of packing along the *b-axis* (z-90 rotation).

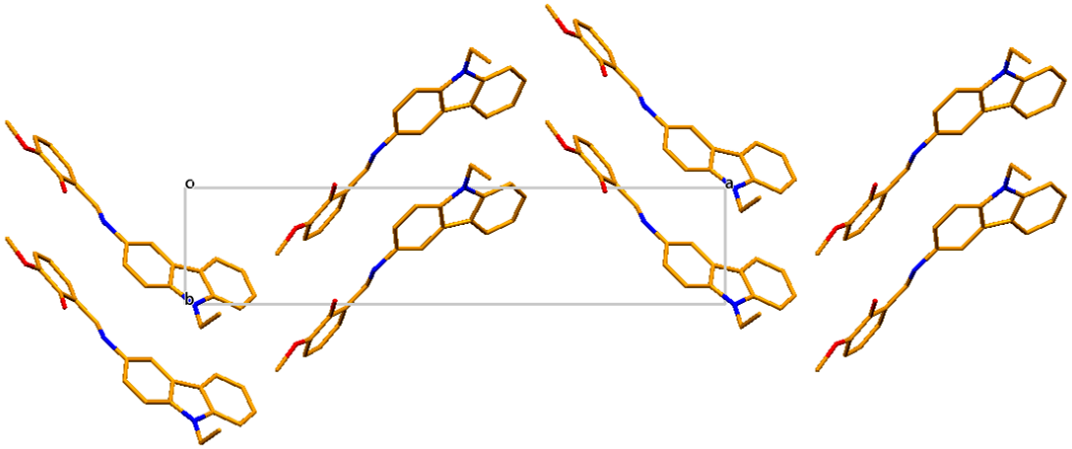

Figure 5. 12: The illustration of the zig-zag packing of **2** along the *c-axis*.

5.5. CRYSTAL STRUCTURE OF 3Methoxy-SalH-Anil (3)

The molecule, (*E*)-2-methoxy-(6-(phenyliminomethyl))-phenol (3Methoxy-SalH-Anil) (**3**) crystallizes in Orthorhombic crystal system in the $P2_12_12_1$ space group with four molecule per unit cell (Z = 4). The molecular framework of **2** is represented in **Figure 5.14** below with atom numbering scheme.

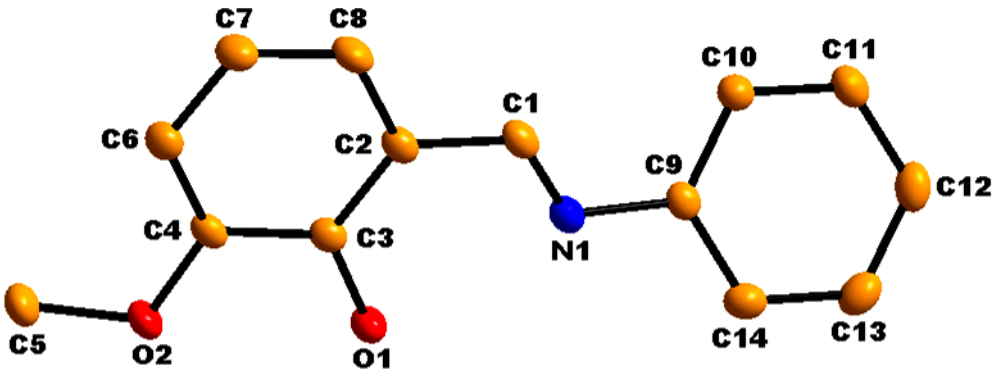

Figure 5.13: The molecular structure of 3Methoxy-SalH-Anil exhibiting the atomic numbering sequence. Hydrogen atoms are omitted for clarity. Displacement ellipsoids are drawn at 50% probability level.

The molecule crystallized as *trans*phenol-imine tautomer. There is only one intramolecular hydrogen bond interaction observed in **3**. The hydrogen bonding interaction is observed between O1-H1…N1 atoms with intra-distance of 1.904 (1) Å and the angle of 146.04˚ (see **Figure 5.15** and **Table 5.7**).

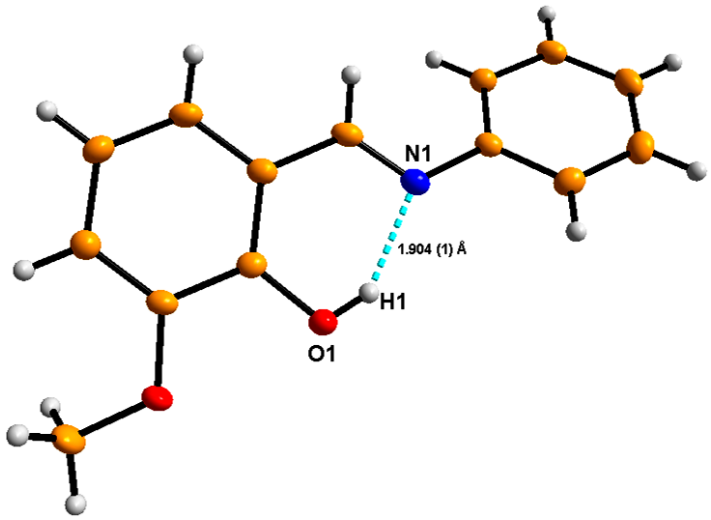

Figure 5.14: The molecular structure of **3** highlighting intra-molecular hydrogen bond interaction.

Table 5.6: Selected bond lengths and bond angles for compound 3Methoxy-SalH-Anil [**Å and**º]

Atomic Bond Distances (Å)		Atomic Bond Angles (˚)	
O1-C3	1.352(19)	**C1-N1-C9**	120.11(13)
N1-C9	1.420(2)	**N1-C1-C2**	122.42(14)
N1-C1	1.286(2)	**O1-C3-C2**	122.48(14)
C1-C2	1.450(2)	**C3-O1-H1**	146.04#
C8-C2	1.406(2)	**N1-C9-C10**	123.12(14)
C2-C3	1.408(2)	**N1-C9-C14**	117.05(14)

#No e.s.d. as H-atom were all placed as riding on the parent atom.

Table 5.7: Hydrogen bonds for Napht3Methoxy-SalH-Anil [**Å and** º].

D-H...A	d(D-H) Å	d(H...A) Å	d(D...A) Å	<(DHA) (˚)
O1-H1…N1 #1	0.820 (1)	1.904 (1)	2.624 (2)	146.04 (9)
C11-H11…O2 #2	0.930 (2)	2.506 (1)	3.420 (2)	167.43 (11)

Symmetry transformations used to generate equivalent atoms:
#1 x, y, z; **#2** -x,+y-1/2,-z+1/2+1.

The C1-N1 bond distance as tabled above, 1.286 (2) **Å** is indicative of a double bond (aromatic -C=N- is 1.34 **Å**) whereas the N1-C9 (1.420(2) **Å**) and O1-C3 (1.352(19) **Å**) bond distances are consistent with single bonds (typical bond distance of N-C and O-C are 1.47 and 1.43 **Å** respectively).

The rotation around the –C=N– bond induces a non-planar orientation of the moieties constructing **3**. The phenyl moiety is twisted out of the horizontal plane as exhibited in **Figure 16** below.

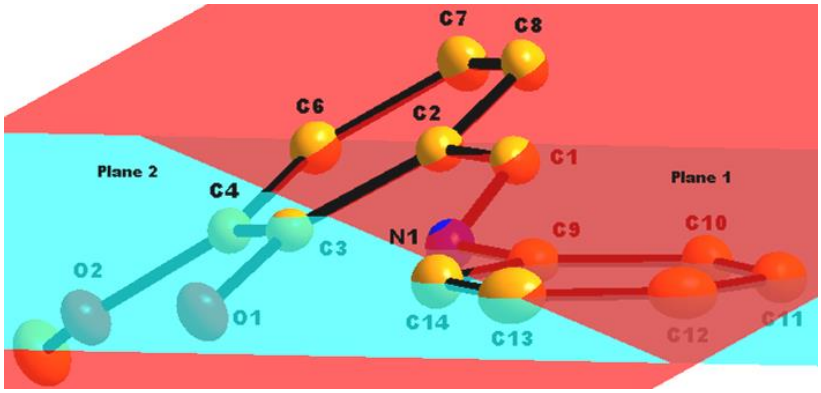

Figure 5.15: The graphical representation of 3Methoxy-SalH-Anil ligand indicating the twisting of the C=N bond general co-planarity of the aromatic rings. Hydrogen atoms are omitted for clarity.

The measure of the dihedral angle between the planes (**Plane 1**: O1, O2, C1, C2, C3, C4, C6, C7, O8, and **Plane 2**: C9, C10, C11, C12, C13, C14) constructed between two aromatic moieties of **2** is 32.018 (4) ˚ with a torsion angle of 150.856 (38) ˚ between C1-N1-C9-C14 atoms.

There is an inter-molecular interaction observed in **3**. This inter-molecular hydrogen bond interaction of C11-H11…O2, with the distance 2.506 (2) **Å**, occurs between the oxygen (O2) of the methoxy group and one of the phenyl carbons (C11) (see **Figure 5.17** and **Table 5.7**).

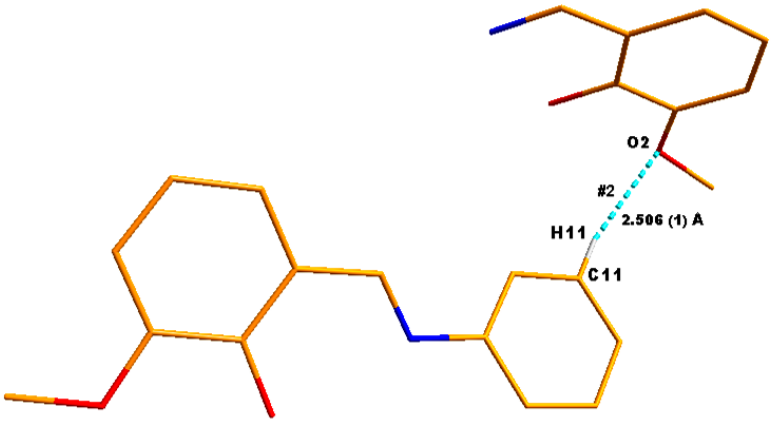

Figure 5.16: Illustration of the intermolecular hydrogen bonding in **3**. Some H-atoms are omitted for clarity.

The illustration in **Figure 5.18** is of the molecular packing of **3** depicting symmetry elements along the *a-axis*. With rotational axes passing through **C9** as shown in green lines below.

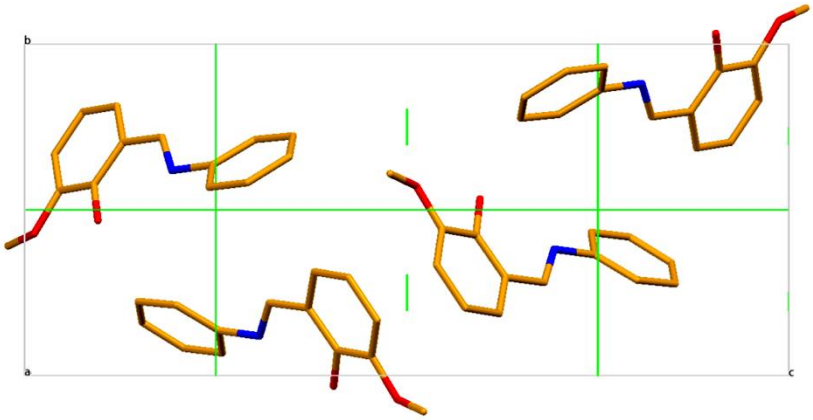

Figure 5.17: Graphical presentation of the molecular packing of **3** and its roto-inversion type of packing along the a-axis (z+90 rotation).

5.6. Discussions and Conclusion

The crystal structures of three salicyclidene derivatives were analysed and discussed in this section. Looking at **Table 5.8**, we find that these crystals were obtained in two different crystal systems which are monoclinic (**1**) and orthorhombic (**2** and **3**) and all appear to have 2-fold rotational axes.

Table 5. 8: Summary of structural cell dimensions of **1**, **2** and **3**.

Crystal Formula	Napht-SalH-Carba (1).	3Methoxy-SalH-Carb (2)	3Methoxy-SalH-Anil (3)
Empirical formula	C_{25} H_{20} N_2 O	$C_{88}H_{76}N_{12}O_{16}$	$C_{14}H_{13}NO_2$
Crystal system, Space Group	Monoclinic, $P2_1/c$	orthorhombic, $Pca2_1$	orthorhombic, $P2_12_12_1$
Temperature (K)	100 (2)	100 (2)	100 (2)
Unit Cell Demnsions			
***a* (Å)**	18.065(5)	24.399 (6)	6.052(5)
***b* (Å)**	6.010(5)	5.2442 (12)	9.072(4)
***c* (Å)**	18.240(4)	13.453 (4)	20.921(5)
α, β, γ (°)	90, 109.031(5), 90	90, 90, 90	90, 90, 90
Volume (Å^3), Z	1872.1(17), 4	1721.3 (8), 4	1148,6 (12), 4
Density (g/cm^3)	1.293	1.3328	1.314

The bond angle and distances of these three salicylidene molecules are within expected range.[20] These bond distance and angle are comparable to literature related structures.[21,22,23]
All the discussed molecules above crystallized as the phenol-imine tautomers exhibiting strong intramolecular hydrogen bonding.

The planarity of this compounds (**1**, **2** and **3**) where measured by constructing planes of the two constituent moieties on the opposites ends of the –C=N– "bridge" if you like. The higher the dihedral angle the less the planarity (see **Table 5.9**) in the molecular structure.

[20] Allen, F.H.; Kennard, O.; Watson, D.G.; Brammer, L.; Orpen, A.G.; Taylor, R., *J. Chem, Soc.*, Perkins Trans. II, **1987**, 0, S1-S19.

[21] Dey, D.K; Dey, S.P.; Elmah, A.; Elerman, Y., *J. Mol. Struct*., **2001**, 562, 177-184.

[22] Karakas, A.; Elmali, E.; Unver, H.; Svoboda, I., *J. Mol. Struct*., **2004**, 702, 103-110.

[23] Gakias, S.; Rix, C.; Fowless, A.; Wills,Johnson, G.; Latham, K.; White, J., *J. Mol. Struct*., **2005**, 737, 69-74.

Table 5. 9: Summary of selected geometric parameters of **1**, **2** and **3**.

		Bond Distance (Å)	
Atoms	**Napht-SalH-Carba (1).**	**3Methoxy-SalH-Carb (2)**	**3Methoxy-SalH-Anil (3)**
N1-C1	1.298(18)	1.282(4)	1.286(2)
N1-C9*	1.414(2)	1.415(4)	1.420(2)
C1-C2	1.435(2)	1.451(5)	1.450(2)
C3-O1	1.327(18)	1.349(4)	1.352(19)
N1…H1	1.769 (1)	1.86 (3)	1.904 (1)
		Bond Angles (°)	
O1- C3- C2	122.31(14)	122.3(3)	122.48(14)
N1- C1- C2	121.13(13)	122.2(3)	122.42(14)
C1- N1- C9*	124.20(13)	123.8(3)	120.11(13)
		Torsion Angle (°)	
C1-N1-C12-C17	178.61 (24)	157.49 (20)	150.856 (38)

∗In complex **1,** the imine bond of N1-C∗ has C∗= C12 whereas C∗ = C9 in complex **2** and **3**.

The interest in planarity of these complexes is coiled around the molecular ability to exhibit the photochromic and thermochromic properties in forming a pseudo six membered aromatic ring constituted by C1- C2-C3-O1-H1-N1. This pseudo aromatic resonance will contribute greatly in the solid state spectroscopic behaviour of the consent molecule.

The illustrations below on **Figure 5.19** are of structural overlays between all the discussed molecular structures in this chapter.

The salicylidene compounds **1**, **2** and **3** have two moieties to be matched with, the 3-methoxy-2-hydroxyphenyl end and the carbazolyl end of the respective molecules. All the molecules crystallized in different space groups, however, with same number of molecules per unit cell. Amongst all the molecular overlays, it is **C** that have the lowest overlay constant (**RMS = 0.135**) value suggesting the best structural overlay between complex **2** and **3.** However, it is in **A** and **B** that the RMS value has almost doubled with **RMS = 0.299** and **0.314** respectively.

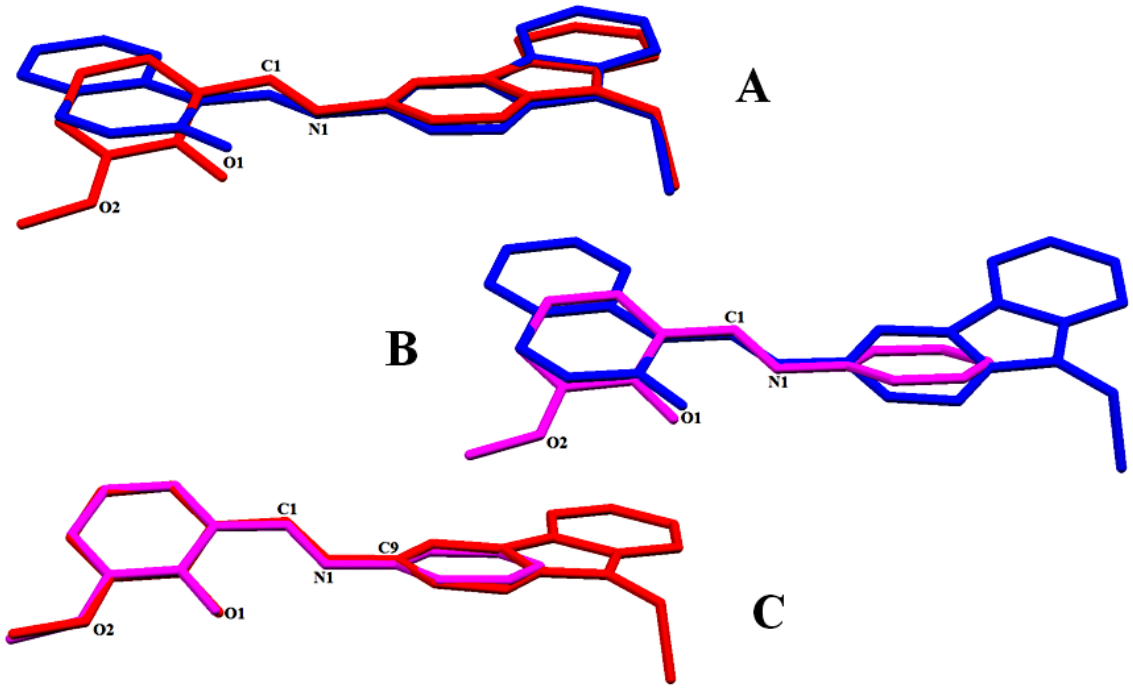

Figure 5.18: An Overlay of crystal structure to indicate the variation of rotation between the two opposite matching end aromatic moieties. (**A**) An overly of Napht-SalH-Carb (**1**) (indicated in blue) and 3Methoxy-SalH-Carb (**2**) (indicated in red) (**RMS = 0.299**); (**B**) Overlay of Napht-SalH-Carb (**1**) (indicated in blue) and 3Methoxy-SalH-Anil (**3**) (indicated in purple) (**RMS = 0.135**); (**C**) 3Methoxy-SalH-Anil (**3**) (indicated in purple) and 3Methoxy-SalH-Carb (**2**) (indicated in red) (**RMS = 0.314**).

The crystal structures of three salicylidene derivatives were analysed and discussed in this chapter. The above discussed ligand pieces will be further analysed, together with other synthesized ligands, for photoluminescence for they are deemed potential fluorophores in this in sensitizing the Europium luminescence in this project. Attempts in crystallizing the tridentate salicylidene derivatives proved to be unsuccessful.

6 Crystallographic Evaluation of Eu^{III} β-Diketonate Complexes.

In this chapter:
The crystallographic report on collected europium β-diketonate complexes and detailed discussions. Evaluation of different steric and electronic properties of the coordinated ligands towards the coordination modes and symmetry influence on the Eu^{III} metal ion.

6.1. Introduction

The use of β-diketone bidentate ligands has been explored widely across many scientific disciplines. This is merely because of their versatility which translates to their highly coordinative nature, good solubility and their corporative substitution on the periphery of the ligands backbone which ultimately significantly impacts on the spectroscopic nature of these ligands.[1]

One of the main goals of this project has been focused on employing selected commercially available β-diketone ligands, with varied substituents on the acetylacetone (acacH) back-bone and coordinating these systems to Eu^{III} metal ion. Not only the substituents alter the electronic characteristics of the ligand as a whole, but they could potentially translate that influence to the coordination pattern and the symmetry of the metal complexes with respect to their steric properties. Eventually, all this could potentially reflect in the luminescence properties of the respective complexes.[2,3,4,5]

Herein we look to outlay a detailed crystallographic discussion on the obtained Eu^{III} β-diketonate complexes which, together with the synthesized range, will be analysed for photoluminescence studies at a later stage. The obtained results in this chapter will be somewhat correlated to the obtained photoluminescence data looking exclusively at the ligands effects towards the respective luminescence spectra identities.

---

[1] Viljoen, J.A., (**2009**). *Speciation and Interconversion Mechanism of Mixed Halo O,O'- and N,O-Bidentate Ligand Complexes of Hafnium.* M.Sc. Dissertation, University of the Free State.

[2] Chauvin, A.; Gumy, F.; Matsubayashi, I.; Hasegawa, Y.; Bunzli, J.G., *Eur. J. Inorg.*, **2006**, 2, 473-480.

[3] Ahmed, Z.; Iftikhar, K., *Inorg. Chem.*, **2015,** 54 (23), 11209-11225.

[4] Manicum, A.; Schutte-Smith, M.; Kemp, G.; Visser, H. G., *Polyhedron,* **2015,** 85, 190-195.

[5]Tang, R.; Zhang,W.; Luo, Y.; Li, J., *J. Rare Earths*. **2009**, 27, 362–367.

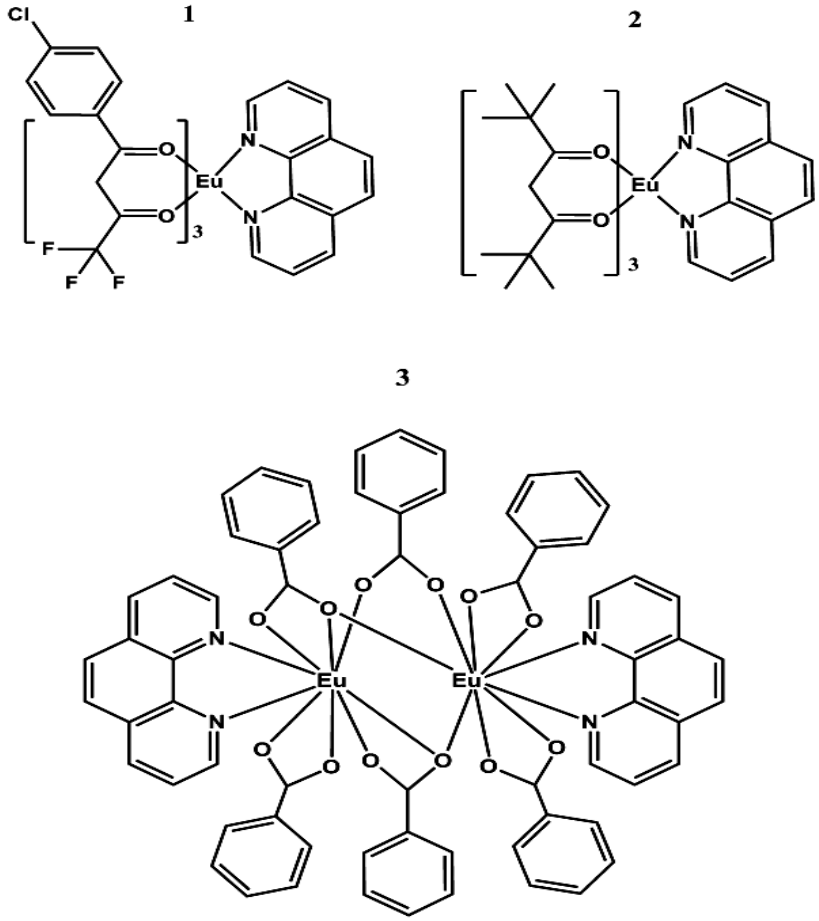

Figure 6. 1: Schematic illustration of Eu^{III} based complexes to be analyzed in this chapter.

The discussions below in this chapter entail the coordination geometry which to some extent is affected by the ligand effects imposed by the substitutions on the periphery of the acetylacetone (acacH) back-bone.

6.2. Experimental

The X-ray intensity data was collected on a Bruker X8 ApexII 4K Kappa CCD area detector diffractometer, equipped with a graphite monochromator and MoKα fine-focus sealed tube (λ = 0.71069 Å, T = 100(2) K) operated at 2.0 kW (50 kV, 40 mA). The initial unit cell determinations and data collections were done by the SMART software package.[6] The collected frames were integrated using a narrow-frame integration algorithm and reduced with the Bruker SAINT-Plus and XPREP software packages respectively.[7] Analysis of the data showed no significant decay during the data collection. Data was corrected for absorption effects using the multi-scan technique SADABS, and the structure was solved by the direct methods package SIR97 and refined using the WinGX software incorporating SHELXL.[8,9,10,11] The final anisotropic full-matrix least-squares refinement was done on F^2. The methyl and aromatic protons were placed in geometrically idealized positions (C–H = 0.93 – 0.98 Å) and constrained to ride on their parent atoms with $U_{iso}(H) = 1.2U_{eq}(C)$. Non-hydrogen atoms were refined with anisotropic displacement parameters. The graphics were obtained with the DIAMOND program with 50% probability ellipsoids for all non-hydrogen atoms.[12]

[6] Bruker SMART-NT Version 5.050, *Bruker AXS Inc. Area-Detector Software Package*; Madison, Winconsin, United States of America, **1998**.

[7] Bruker SAINT-Plus Version 6.02 (including XPREP), *Bruker AXS Inc. Area-Detector Integration Software*, Madison, Winconson, United States of America, **1999**.

[8] Bruker SADABS Version 2004/1, *Bruker AXS Inc. Area Detector Absorption Correction Software*, Madison, Wisconsin, United States of America, **1998**.

[9] Altomare, A.; Burla, M.C.; Camalli, M.; Cascarano, G.L.; Giacovazzo, C.; Guagliardi, A.; Moliterni, A.G.G.; Polidori, G.; Spagna, R., *J. Appl. Cryst.*, **1999**, 32, 115-119.

[10] Farrugia L.J, *J. Appl. Cryst.* **1999**, **32**, 837-838.

[11] Sheldrick, G.M., (**1997).** SHELXL97, *Program for Crystal Structure Refinement*, University of Göttingen, Germany.

[12] Brandenburg, K.; Putz, H., (**2006)**. DIAMOND, *Release 3.3, Crystal Impact GbR*, Bonn, Germany.

Table 6. 1: Crystallographic and refinement details for structures discussed in this chapter.

Crystal Formula	**[Eu(TCPB)$_3$Phen] (1)**	**[Eu(TMHD)$_3$Phen] (2)**	**{[Eu$_2$(BCA)$_6$(Phen)$_2$]- μ-[κ^2-O,O'-(BCA)]} (3)**
Empirical formula	$C_{42}H_{23}Cl_3EuF_9N_2O_6$	$C_{45}H_{65}EuN_2O_6$	$C_{66}H_{46}Eu_2N_4O_{12}$
Formula weight (g.mol^{-1})	1080.97	881.99	1390.99
Crystal system, Space Group	Monoclinic, $P2_1/n$	Triclinic, P-1	Triclinic, P-1
***a, b, c* (Å)**	12.0971 (3), 18.354(5), 21.031 (5)	10.860 (5), 12.285 (4), 18.398 (5)	10.761 (5), 11.865 (5), 12.275 (4)
α, β, γ (°)	90, 104.111(8), 90	80.396 (5), 87.575 (5), 68.761 (4)	105.044 (5), 93.811 (5), 112.902 (4)
Volume (Å^3), Z	4528.6 (16), 4	2255.3 (15), 2	1369.2 (10), 1
Density (calculated, Mg/m^3)	1.5853	1.2987	1.687
Crystal colour	Colourless	Colourless	Colourless
Crystal size (mm^3)	0.173 x 0.093 x 0.093	0.154 x 0.162 x 0.276	0.180 x 0.184 x 0.186
Absorption coefficient μ (mm^{-1}), F(000)	1.646, 2131.4	1.436, 920.4	2.341, 692
Theta range	4.11 – 20.82°	3.101 – 27.99	4.187 – 27.99°
Index ranges	-12<=h<=11, -18<=k<=18, -21<=l<=21	-10<=h<=10, -11<=k<=12, -18<=l<=18	-14<=h<=14, -15<=k<=11, -16<=l<=16
Reflections collected, Independent Reflections, R_{int}	48404, 4738, 0.0880	27072, 4707, 0.0306	37980, 6597, 0.0454
Completeness to 2θ (°, %)	20.82, 99.4	28.40, 99.9	25.24, 99.3
Max. and min. transmission	0.7457 and 0.4820	0.7457 and 0.7044	0.7457 and 0.662
Data, restraints, parameters	4738, 42, 567	4707, 55, 544	6597, 0, 380
Goodness-of-fit on F^2	1.660	1.021	1.090
Final R indices [I>2sigma(I)]	R_1 = 0.0634 wR_2 = 0.1566	R_1 = 0.0418 wR_2 = 0.12.67	R_1 = 0.0195 wR_2 = 0.0479
R indices (all data)	R_1 = 0.1514 wR_2 = 0.2116	R_1 = 0.0563 wR_2 = 0.1924	R_1 = 0.0215 wR_2 = 0.489
Largest diff. peak and hole (e.Å^{-3})	5.13, -3.48	0.74, -2.32	0.528, -0.570

6.3. CRYSTAL STRUCTURE OF [Eu(TCPB)$_3$Phen] (1)

The crystal structure of [*tris*-(4,4,4-trifluoro-1-chlorophenyl-butanedione-κ^2O,O') mono(1,10-phenanthroline) europium(III)] [Eu(TCPB)$_3$Phen] **(1)** forms part of an investigation which focuses on studying applied ligand chelation effects on Eu^{III} based complexes.

A summary of the general crystallographic data is given in **Table 6.2**, while the numbering scheme of the complex is shown in the perspective drawing in **Figure 6.2**., **Tables 6.2, 6.3** and **6.4** present selected bond lengths and angles of **1**.

[Eu(TCPB)$_3$Phen] **(1)** crystallizes in the monoclinic space group, $P2_1/n$, with four molecular entities in the unit cell (Z = 4). The asymmetric unit consists of a Eu(III) metal centre coordinated to three crystallographically independent *O,O'*-bonded 4,4,4-trifluoro-1-chlorophenyl-butanedione and *N,N'*-bonded 1,10-phenanthroline as an ancillary ligand.

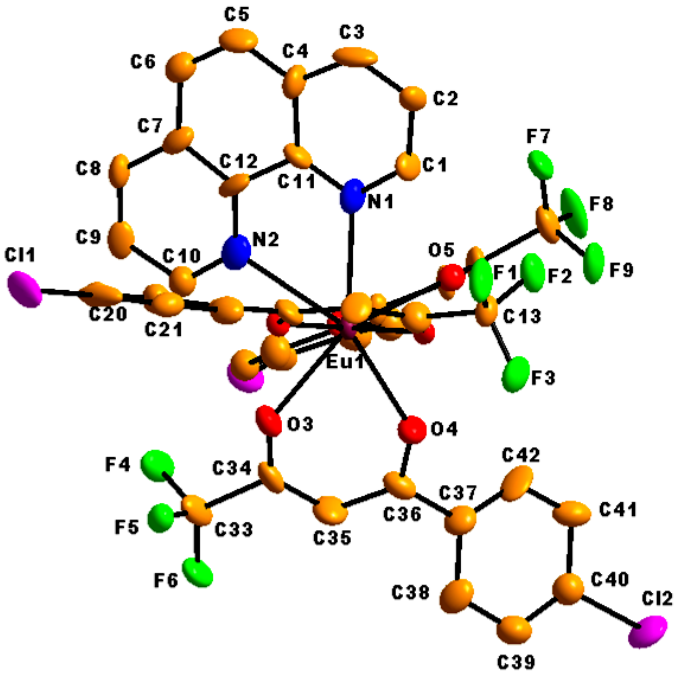

Figure 6.2: The molecular structure of [Eu(TCPB)$_3$Phen] (**1**) exhibiting the atomic numbering scheme. Hydrogen atoms are omitted for clarity. Displacement ellipsoids are drawn at 50% probability level.

The bond lengths and bond angles for discussion purposes are tabled below.

Table 6.2: Selected bond lengths and bond angles for compound [Eu(TCPB)$_3$Phen] (**1**).

Atomic Bond Distances		Atomic Bond Angles	
Atoms	**Length/Å**	**Atoms**	**Angle/°**
Eu1-O1	2.324 (4)	**O1-Eu1-O2**	71.94 (9)
Eu1-O2	2.382 (5)	**O3-Eu1-O4**	70.75 (6)
Eu1-O3	2.341 (2)	**O5-Eu1-O6**	70.89 (7)
Eu1-O4	2.395 (2)	**N1-Eu1-N2**	63.62 (4)
Eu1-O5	2.349 (4)	**C34-C35-C36**	123.5 (16)
Eu1-O6	2.399 (6)	**C24-C25-C26**	122.7 (13)
Eu1-N1	2.388 (1)	**C14-C15-C68**	122.4 (17)
Eu1-N2	2.399 (5)		

The molecular structure portrayed in **Figure 6.3** undergoes a range of inter- and intramolecular interactions. All of these intra- and intermolecular hydrogen contacts contribute to the strengthening and stabilization of the crystal lattice. Due to the fact that this intrinsic network will be difficult to graphically illustrate all at once, the various interactions will be illustated in bits, depending on the nature of the interaction. These interactions are observed in **Figures 6.3**, **6.4, 6.5** and **6.6**. The data related to these hydrogen contacts are given in **Table 6.3** and **6.4.**

Table 6. 3: Tabled intramolecular hydrogen bonding for [Eu(TCPB)$_3$Phen] (**1**)

D-H…A	d(D-H) (Å)	d(D-H) (Å)	d(D-H) (Å)	<(DHA) (°)
C10-H10...O3	0.95 (3)	2.567 (3)	3.20 (3)	125
C15-H15...F1	0.95 (3)	2.337 (6)	3.71 (3)	103
C35-H35...F6	0.95 (4)	2.427 (6)	2.80 (3)	103

Table 6. 4: Tabled intermolecular hydrogen bonding for [Eu(TCPB)$_3$Phen] (**1**)

D-H…A	d(D-H) (Å)	d(D-H) (Å)	d(D-H) (Å)	<(DHA) (°)
C9-H9…O1 #1	0.95 (4)	2.523 (5)	3.46 (3)	166
C29-H29…F1 #1	0.95 (4)	2.415 (6)	3.28 (3)	152
C32-H32…F3 #2	0.95 (4)	2.503 (2)	3.18 (4)	129

Symmetry transformations used to generate equivalent atoms:
#1:1/2 - x, -1/2 + y, 1/2 – z
#2 :1/2 + x, 3/2 - y, 1/2 + z

The intra atomic networking observed above is of C10-H10…O3 and C35-H35…F6 with bond distances of 2.565 (3) Å and 2.427 (6) Å respectively.

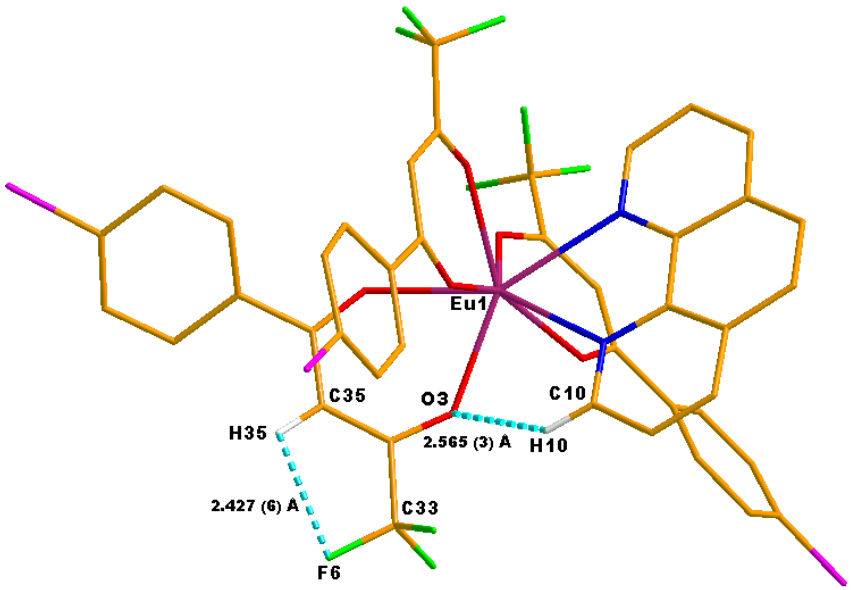

Figure 6.3: The graphical representation of occurring intramolecular molecular networking in **1**.

There are further intra and intermolecular interactions taking place stabilising the structure. The bifurcated fluorine (F1) atom undergoes hydrogen bonding (C-H…F) with C15 and C29 with bond distances of 2.337 (6) Å and 2.415 (6) Å respectively in **Figure 6.3.**

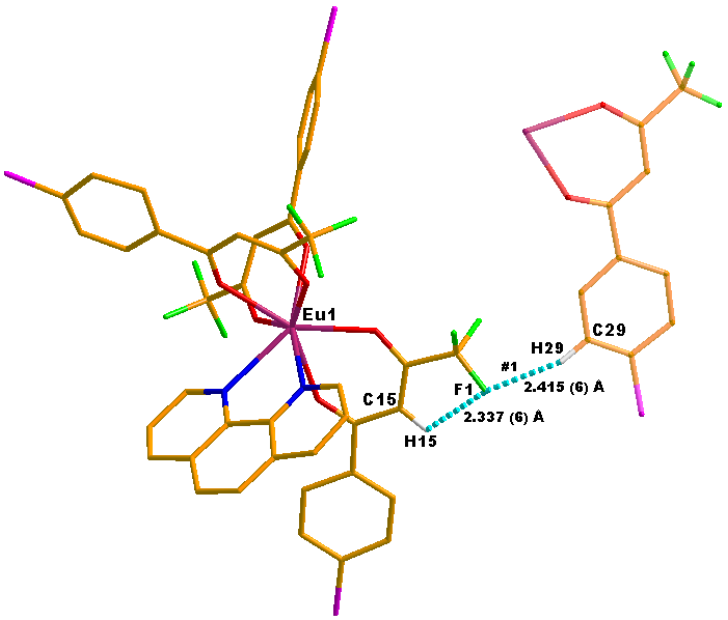

Figure 6.4: The graphical representation of inter- and intramolecular molecular networking in **1**.

Further intermolecular reinforcements, in stabilizing the complex, by another C9-H9…O1 interaction together with C32-H32…F3 are observed in **Figure 6.5** and **6.6** with bond distances of 2.523 (5) Å and 2.503 (2) Å respectively.

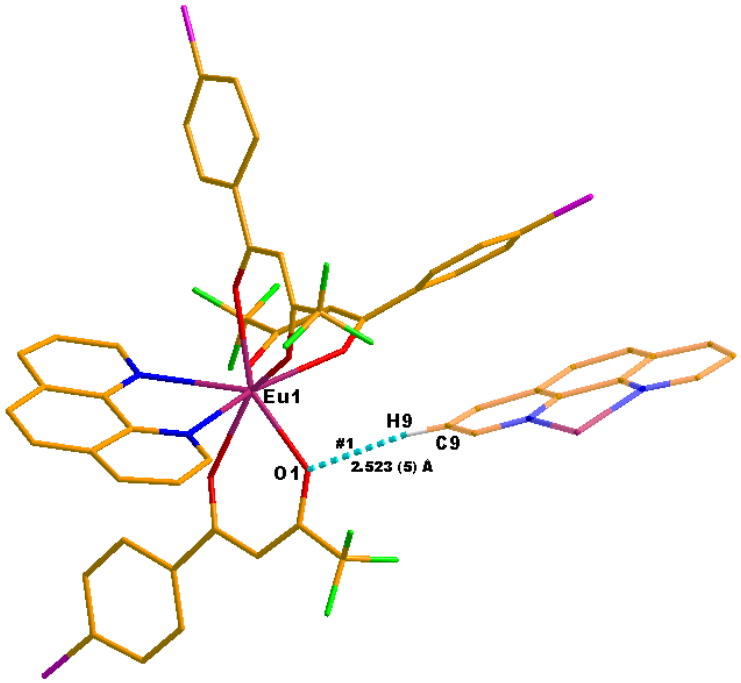

Figure 6.5: The graphical representation of intermolecular molecular networking in **1**.

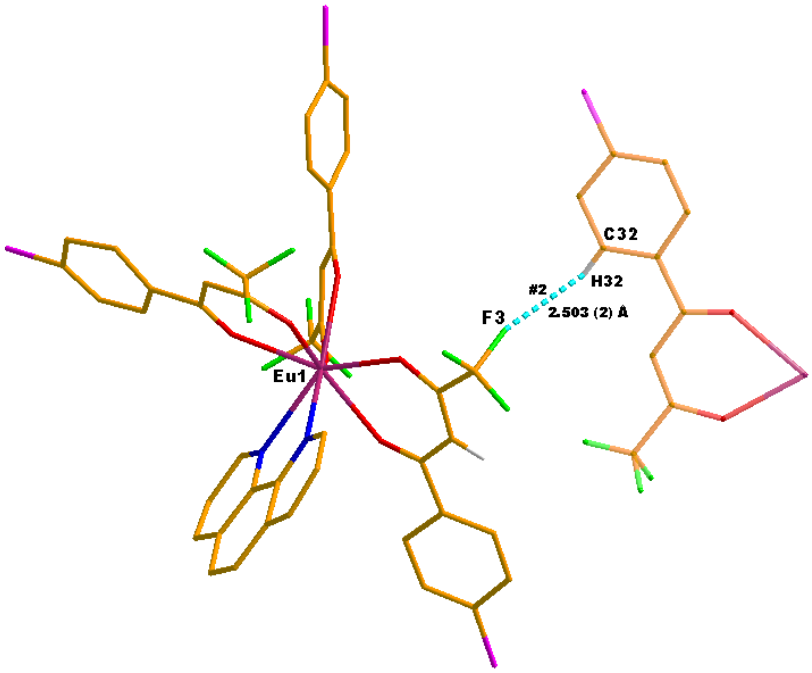

Figure 6.6: The graphical representation of further intermolecular molecular networking in **1**.

Constructed below is the polyhedral of coordination geometry around Eu^{III} metal ion. With eight coordinated atoms, consisting of six oxygen and two nitrogen atoms, it seem the coordination mode prefers either dodecahedron or squared antiprism as discussed in **Section 2.1.2.**

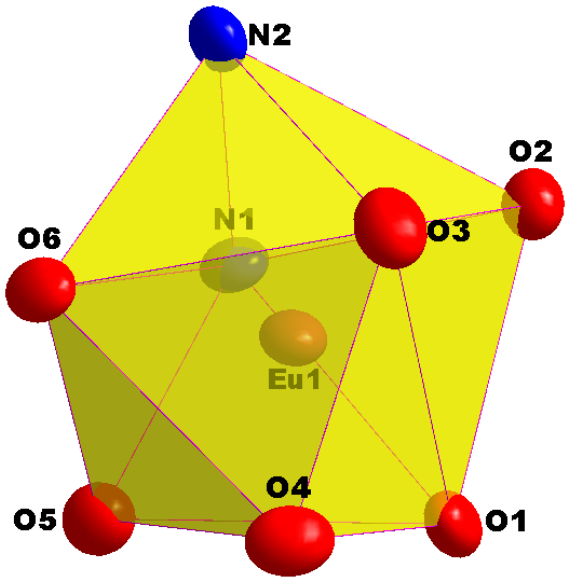

Figure 6.7: Schematic Illustration of coordination geometry of **1**.

The polyhedron is constructed around the six coordinated oxygens of three TCPB (4,4,4-trifluoro-1-chlorophenyl-butanedione) moeities and the two nitrogens of the 1,10-phenanthroline ancillary ligand. The above constructed polyhedral has 8 vertices with 12 triangle faces and 24 edges. The polyhedron conforms to be of *Snub Disphenoid* which is a sub class of dodecahedron polyhedron. [13]

Below in **Figure 6.8** is the molecular packing of **1** with occurring symmetry elements in the unit cell. The packing illustrates the screw axis in green lines with arrows assisting with rotational direction and the glide planes in purple along the *bc-axis*. There are also inversion centres at special positions (yellow spots) as per $P2_1/n$ space group requires.

[13] Merkens, C.; Englert, U., Dalton Trans., **2012**, 41, 4664-4673.

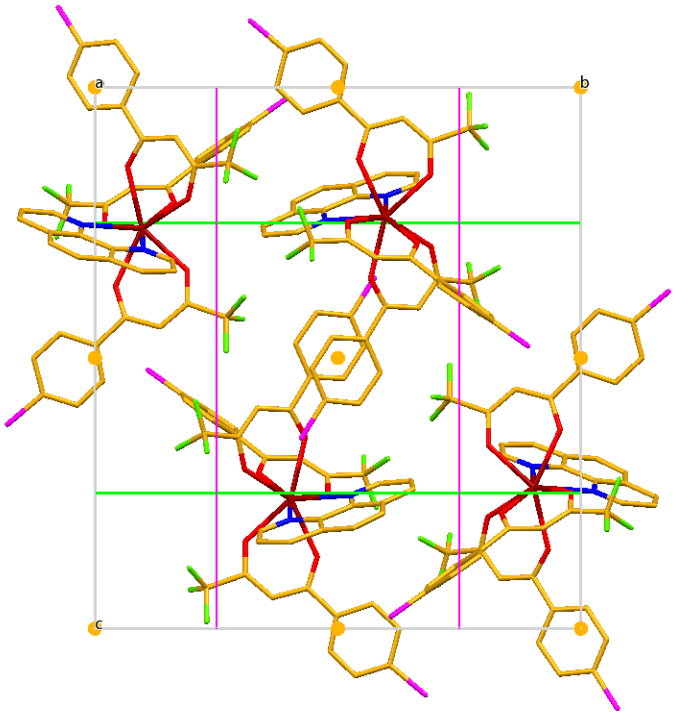

Figure 6.8: Graphical presentations of the molecular packing of **1** with the roto-inversion type of packing depicting symmetry elements thereof.

6.4. CRYSTAL STRUCTURE OF [Eu(TMHD)$_3$Phen] (2)

The crystal structure of [*tris*-(2,2,6-Trimethyl-3,5-heptanedione) mono (1,10-phenanthroline) europium(III)]: [Eu(TMHD)$_3$Phen] (**2**) also forms part of an investigation which focuses on studying applied ligand chelation effects on Eu^{III} based complexes.

A summary of the general crystallographic data is given in **Table 6.1**, while the numbering scheme of the complex is shown in the perspective drawing in **Figure 6.10**. **Tables 6.5** and **6.6** present selected bond lengths, angles and hydrogen bonding of **2** respectively.

[Eu(TMHD)$_3$Phen] **(2)** crystallizes in the triclinic space group, *P*-1, with two molecular entities in the unit cell (Z = 2). The asymmetric unit consists of a Eu(III) metal centre coordinated to three crystallographically independent *O,O'*-bonded 2,2,6-Trimethyl-3,5-heptanedione and *N,N'*-bonded 1,10-phenanthroline as an ancillary ligand.

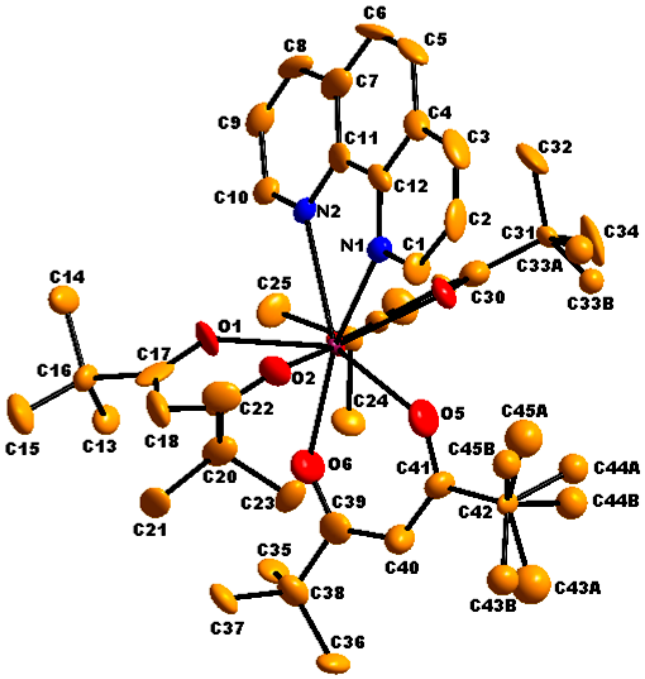

Figure 6.9: The molecular structure of [Eu(TMHD)$_3$Phen] (**2**) exhibiting the atomic numbering scheme. Hydrogen atoms are omitted for clarity. Displacement ellipsoids are drawn at 50% probability level.

The bond lengths and bond angles for discussion purposes are given in **Table 6.5**.

Table 6.5: Selected bond lengths and bond angles for compound [Eu(TMHD)$_3$Phen] (**2**)

Atomic Bond Distances		Atomic Bond Angles	
Atoms	**Length/Å**	**Atoms**	**Angle/°**
Eu1-O1	2.383 (7)	**O1-Eu1-O2**	71.64 (14)
Eu1-O2	2.369 (8)	**O3-Eu1-O4**	70.24 (15)
Eu1-O3	2.334 (7)	**O5-Eu1-O6**	70.48 (14)
Eu1-O4	2.357 (7)	**N1-Eu1-N2**	63.44 (11)
Eu1-O5	2.369 (6)	**C34-C35-C36**	124.8 (35)
Eu1-O6	2.327 (5)	**C24-C25-C26**	125.2 (36)
Eu1-N1	2.629 (9)	**C14-C15-C68**	125.7 (36)
Eu1-N2	2.620 (6)		

The molecular structure portrayed in **Figure 6.10** undergoes multiple intra-molecular interactions. These intra-molecular hydrogen contacts contribute to the strengthening and stabilization of the crystal lattice. There is also a pi-pi type interactions between one of the benzene rings of the 1,10-phenanthroline and the neighbouring benzene molecule. Due to the fact that this intrinsic network will be difficult to graphically illustrate at all once, the various interactions will be illustated in bits depending on the nature of the interaction. These interactions are observed in **Figures 6.11**, **6.12, 6.13**. The data related to these hydrogen contacts are given in **Table 6.6**.

Table 6.6: Tabled intra-molecular hydrogen bonding for [Eu(TMHD)$_3$Phen] (**2**)

D-H…A	d(D-H) (Å)	d(D-H) (Å)	d(D-H) (Å)	<(DHA) (°)
C13-H13A...O1	0.96	2.548 (10)	2.884 (1)	100.49 (33)
C14-H14B...O1	0.96	2.467 (7)	2.819 (1)	101.49 (24)
C22-H22B...O2	0.96	2.565 (7)	2.901 (1)	100.97 (27)
C35-H35B...O6	0.96	2.424 (10)	2.755 (1)	99.74 (24)
C45A-H45D...O5	0.96	2.467 (11)	2.812 (1)	100.82 (33)

Observed below in **Figure 6.11** is an illustration of bifurcated oxygen (O1) atom with two nearby hydrogen atoms of methyl carbon atoms C13 and C14 respectively. The respective distances appears to be 2.548 (10) Å and 2.467 (7) Å for C13-H13A...O1 and C14-H14B...O1 interactions respectively.

Further observed is an intra-atomic bonding of C22-H22B…O2 with the intra-molecular distance of 2.548 (10) Å.

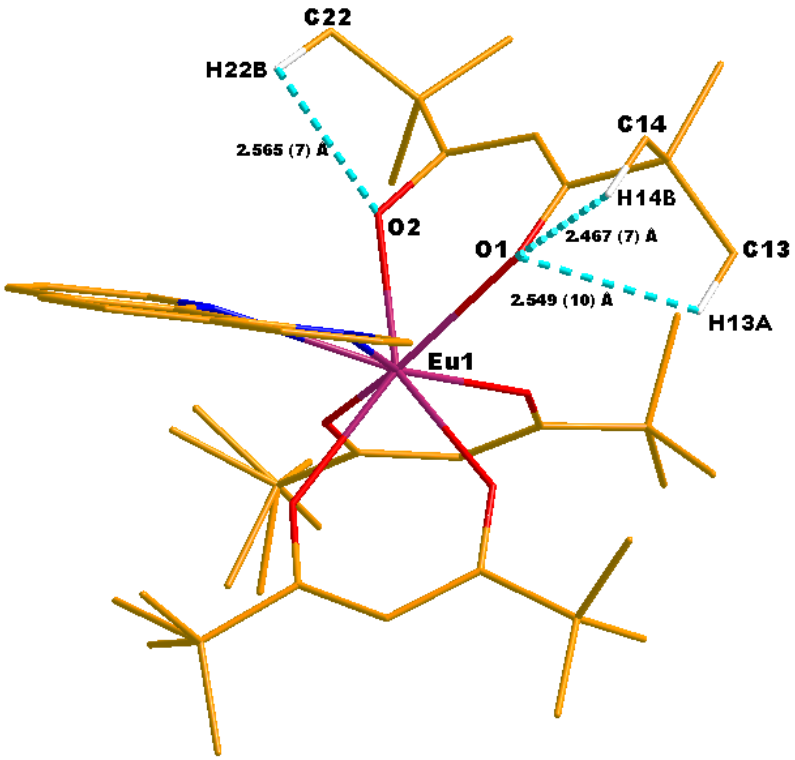

Figure 6.10: The graphical representation of occurring intra-molecular molecular networking in **2**.

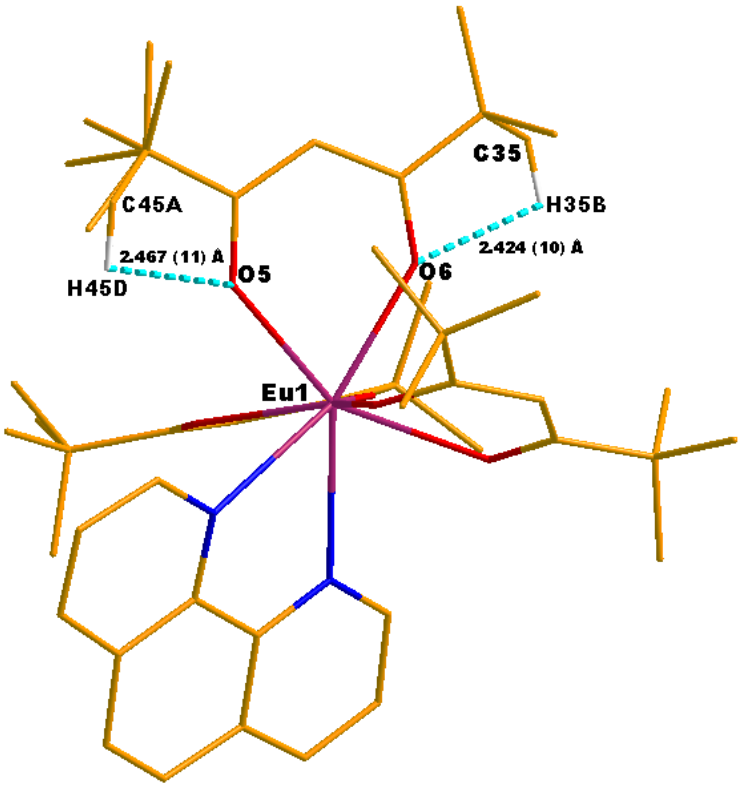

Figure 6.11: The graphical representation of further intra-molecular molecular networking in **2.**

The illustration below in **Figure 6.13** is of a sandwich centroid-to-centroid molecular interaction between Cg1 (C4-C5-C6-C7-C11-C12) with the same symmetry generated ring. This *pi*-stacking occurs between two 1,10-phenanthroline aromatic rings with the distance of 3.588 (10) Å.

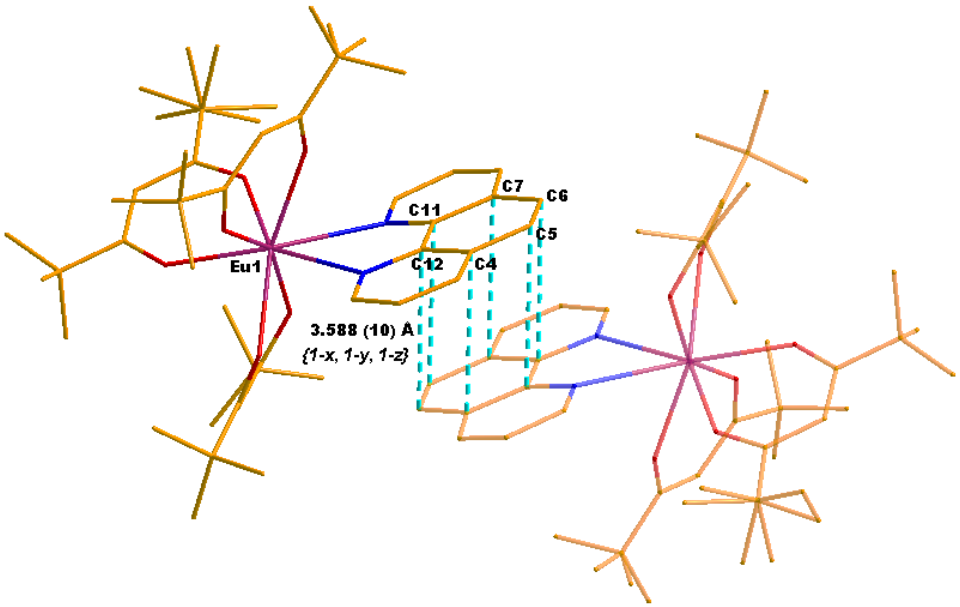

Figure 6. 12: Schematic Illustration of centroid-to-centroid intermolecular interaction in **2**.

The polyhedron constructed below in **Figure 6.14** is of coordination geometry of immediate atoms around Eu^{III} metal ion. The polyhedron consists of eight coordinated atoms, consisting of six oxygen and two nitrogen atoms.

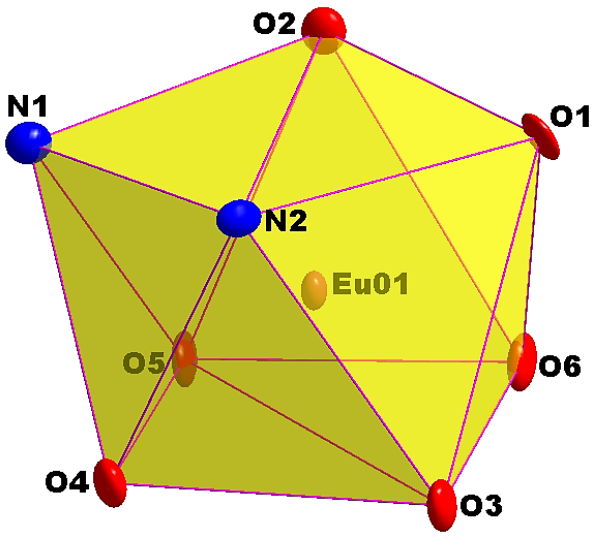

Figure 6.13: Schematic Illustration of coordination geometry of **2**.

The polyhedron is constructed around the six coordinated oxygens of three TMHD (2,2,6-Trimethyl-3,5-heptanedione) moieties and the two nitrogens of the 1,10-phenanthroline ancillary ligand. The above constructed polyhedral has 8 vertices with 12 triangle faces and 16 edges. The polyhedron conforms to be of *Square Antiprism* coordination mode.

Below in **Figure 6.15** is the molecular packing of **1** with occurring symmetry elements in the unit cell. There are 27 inversion centres at special positions as per *P-1* space group requires.

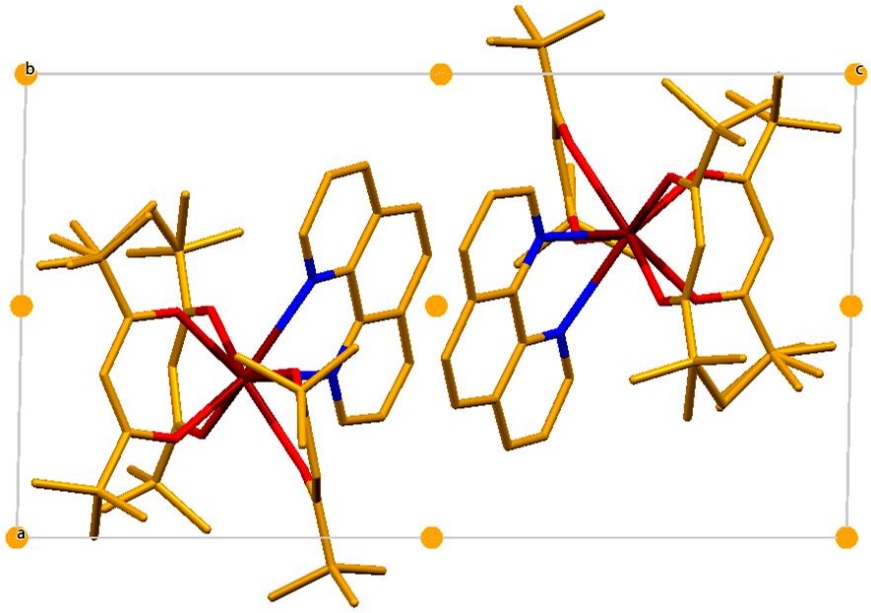

Figure 6.14: Graphical presentations of the molecular packing of **1**.

6.5. CRYSTAL STRUCTURE OF {[$Eu_2(BCA)_6(Phen)_2$]- μ-[κ^2-O,O'-(BCA)]$_2$} (3)

The crystal structure of {[*hexa*-(Benzyl carboxylic acid) *bis*-(1,10-phenanthroline) di-europium(III)]-μ-[κ^2-O,O'-(benzyl carboxylic acid)}: {[$Eu_2(BCA)_6(Phen)_2$]- μ-[κ^2-O,O'-(BCA)]$_2$} (**3**) also forms part of an investigation which focuses on studying applied ligand chelation effects on Eu^{III} based complexes.

A summary of the general crystallographic data is given in **Table 6.1**, while the numbering scheme of the complex is shown in the perspective drawing in **Figure 6.10**., **Tables 6.5, 6.6** and **6.7** present selected bond lengths and angles of **3**.

{[$Eu_2(BCA)_6(Phen)_2$]- μ-[κ^2-O,O'-(BCA)]$_2$} **(3)** crystallizes in the monoclinic space group, *P*-1, with four molecular entities in the unit cell (Z = 1). The asymmetric unit consists of a Eu^{III} metal centre coordinated to three crystallographically independent *O,O'* benzoic acid molecules and *N,N'*-bonded 1,10-phenanthrolineas as an ancillary ligand.

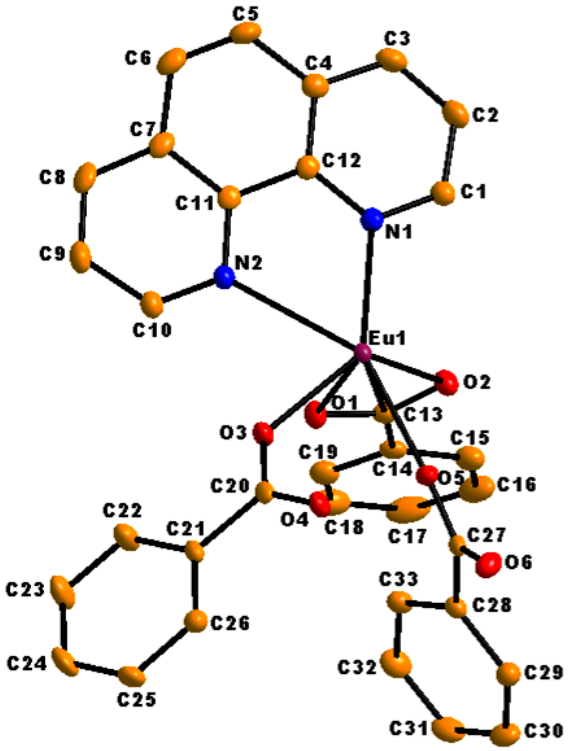

Figure 6.15: The molecular structure of {[$Eu_2(BCA)_6(Phen)_2$]- μ-[κ^2-O,O'-(BCA)]$_2$} (**3**) exhibiting the atomic numbering scheme. Hydrogen atoms are omitted for clarity. Displacement ellipsoids are drawn at 50% probability level.

There is half of the molecule in the asymmetric unit cell observed for **3** and the rest of the half is symmetry generated. The complex has an inversion center and therefore the symmetry generated half is the exact replica of the other half and that is observed via bond lengths and bond angles as tabled in **Table 6.5**. The molecular structure in discussion is a centrosymmetric complex.

The dimeric nature of **3** is constituted by six benzoic acid molecules and two 1,10-phenanthroline molecule all bonded to two Eu^{III} metal centers. The molecular structure is bridged by six oxygen atoms from four phenyl carboxylic acid molecules.

The respective coordination spheres of the two Eu^{III} centers are saturated with the coordinated organic molecules. The nature of coordination geometry for both the Eu^{III} centers observed in this molecular structure will be constituted by the nine coordination points per metal centres.

Below are the tabled selected atomic bond distances and bond angles of **3.**

Table 6.7: Selected bond distance and bond angles of **3**.

Atomic Bond Distances		**Atomic Bond Angles**	
Atoms	**Length/Å**	**Atoms**	**Angle/°**
Eu1-O1	2.419 (14)	**O1-Eu1-O2**	53.08 (49)
Eu1i-O1i	2.419 (14)	**O1i-Eu1i-O2i**	53.08 (49)
Eu1-O2	2.514 (17)	**O3-Eu1-O4**	134,69 (56)
Eu1i-O2i	2.514 (17)	**O3i-Eu1i-O4i**	134,69 (56)
Eu1-O3	2.367 (17)	**O5-Eu1-O6**	126.83 (58)
Eu1i-O3i	2.367 (17)	**O5i-Eu1i-O6i**	126.83 (58)
Eu1-O4	2.380 (16)	**N1-Eu1-N2**	62.47 (58)
Eu1i-O4i	2.380 (16)	**N1i-Eu1i-N2i**	62.47 (58)
Eu1-O5	2.336 (20)	**Eu1-O5i-Eu1i**	123.53 (16)
Eu1i-O5i	2.336 (20)	**Eu1-O5i-Eu1i**	123.53 (16)
Eu1-O6	2.429 (19)	**O5-C27-O6**	121.21 (19)
Eu1i-O6i	2.429 (19)	**O1-C13-O2**	121.48 (21)
Eu1-N1	2.591 (21)	**C20-O4-Eu1**	139.80 (15)
Eu1i-N1i	2.591 (21)		
Eu1-N2	2.655 (23)		
Eu1i-N2i	2.655 (23)		

The molecular structure portrayed in **Figure 6.10** undergoes multiple of inter- and intramolecular interactions strengthening and stabilizing the crystal lattice. Due to the fact

that this intrinsic network will be difficult to graphically illustrate at all once, the various interactions will be illustated bits ddpending on the nature of the interaction. These interactions are observed in **Figures 6.12**, **6.13**, **6.14** and **6.15**. The data related to the hydrogen bonding contacts is given in **Table 6.6** and **6.7**.

Table 6.8: Tabled intramolecular hydrogen bonding for **3**.

D-H…A	d(D-H) (Å)	d(D-H) (Å)	d(D-H) (Å)	<(DHA) (˚)
C10-H10...O3	0.93	2.478 (19)	3.08 (14)	123.32 (15)
C33-H33...O1	0.93	2.557 (19)	3.44 (16)	158.84 (15)

Table 6.9: Tabled intermolecular CH…π hydrogen bonding for $[Eu_2(BCA)_6(Phen)_2]$ (**3**)

X-H…Cg	d(H-Cg) (Å)	d(X-Cg) (Å)	<(XHCg) (˚)
C6-H6...Cg1 #1	2.89 (9)	3.47(16)	121
C17-H17...Cg2 #2	2.95 (10)	3.75(17)	144
C25-H25...Cg4 #3	2.77 (7)	3.68 (17)	169
C31-H31...Cg4 #4	2.82 (8)	3.67(17)	152

Symmetry transformations used to generate equivalent atoms:
#1: - x, - - y, 1 – z ; **#2**: - x, -y, – z
#3 : x, y, 1 - z ; **#4**:1 - x, 2 - y, 1 – z

There are observed intramolecular reinforcements stabilizing the crystal lattice from the C10-H10…O3 and C33-H33…O1 hydrogen interactions illustrated in **Figure 6.12** and **6.13** with bond distances of 2.478 (5) Å and 2.557 (2) Å respectively.

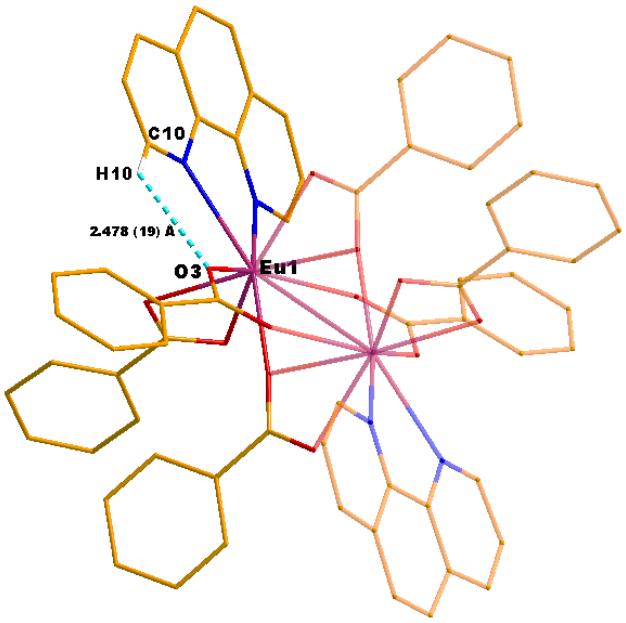

Figure 6.16: The graphical representation of occurring intramolecular molecular networking in **3**.

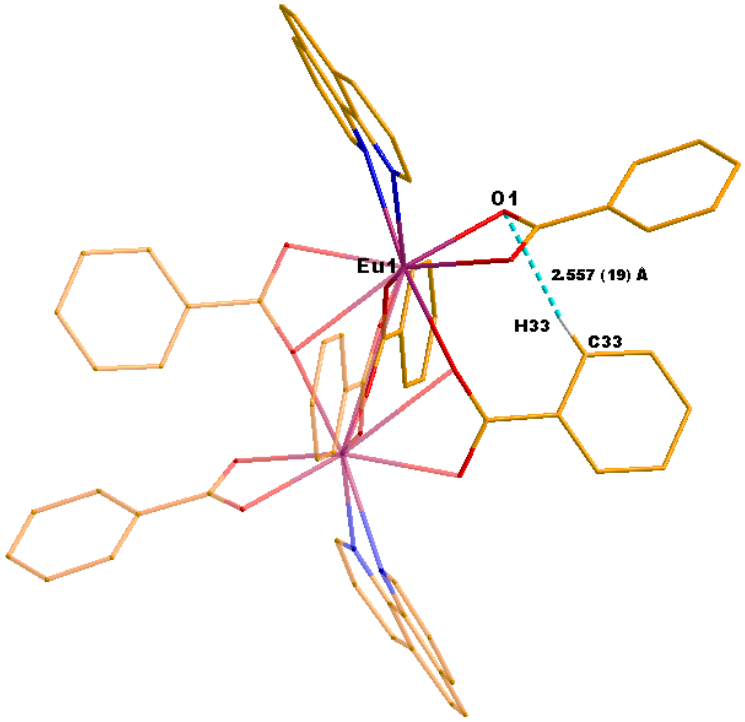

Figure 6.17: The graphical representation of occurring intramolecular molecular networking in **3**.

There are observed intramolecular reinforcements stabilizing the crystal lattice from the C6-H6…Cg1 (Cg1: N1, C1, C2, C3, C4, C12) and C17-H17…Cg2 (Cg2: N2, C10, C9, C8, C7, C11) hydrogen interactions illustrated in **Figure 6.14** and **6.15** with CH-centroid distances of 2.889 (9) Å and 2.995 (10) Å respectively.

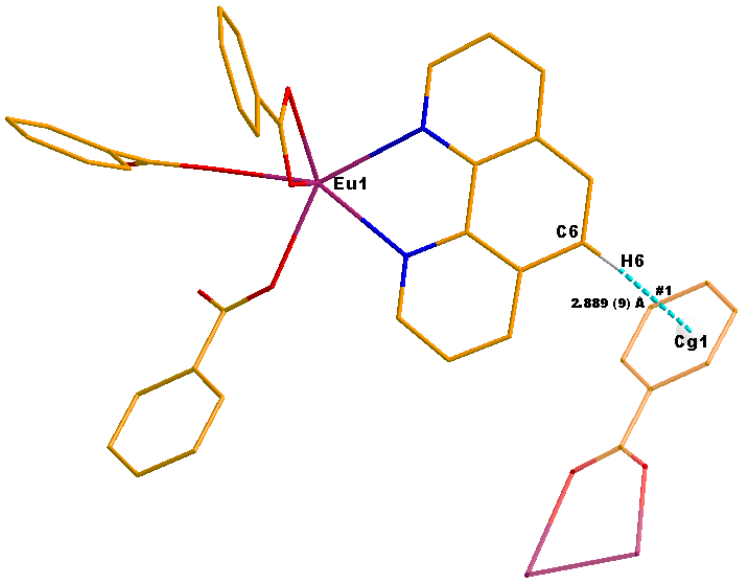

Figure 6.18: The Illustration of intermolecular CH…π hydrogen bonding for (**3**). Atoms constituting Cg1 are N1, C1, C2, C3, C4, C12 completing an aromatic ring.

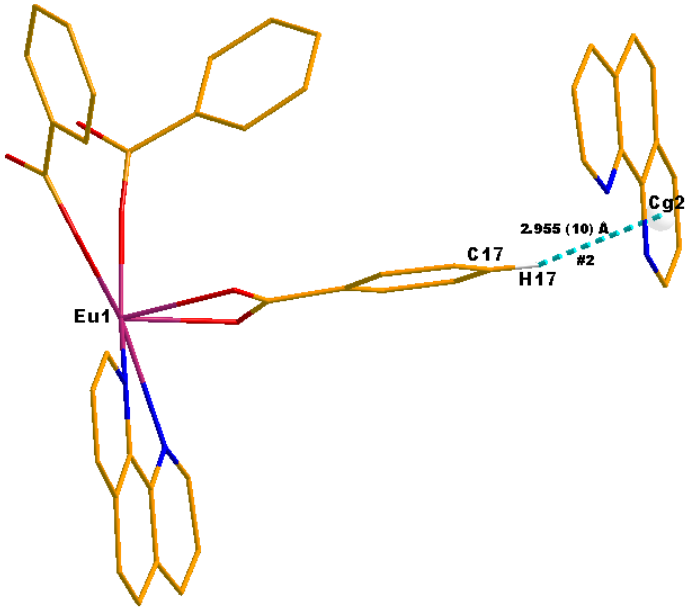

Figure 6.19: The illustration of intermolecular CH…π hydrogen bonding for (**3**). Atoms constituting Cg2 are N2, C10, C9, C8, C7, C11 completing an aromatic ring.

There are further observed intramolecular reinforcements stabilizing the crystal lattice from the C25-H25…Cg3 (Cg3: C14-C15-C16-C17-C18-C19) and C31-H31…Cg4 (Cg4: C21-C22-C23-C24-C25-C26) hydrogen interactions illustrated in **Figure 6.16** and **6.17** with CH-centroid distances of 2.767 (7) Å and 2.818 (8) Å respectively.

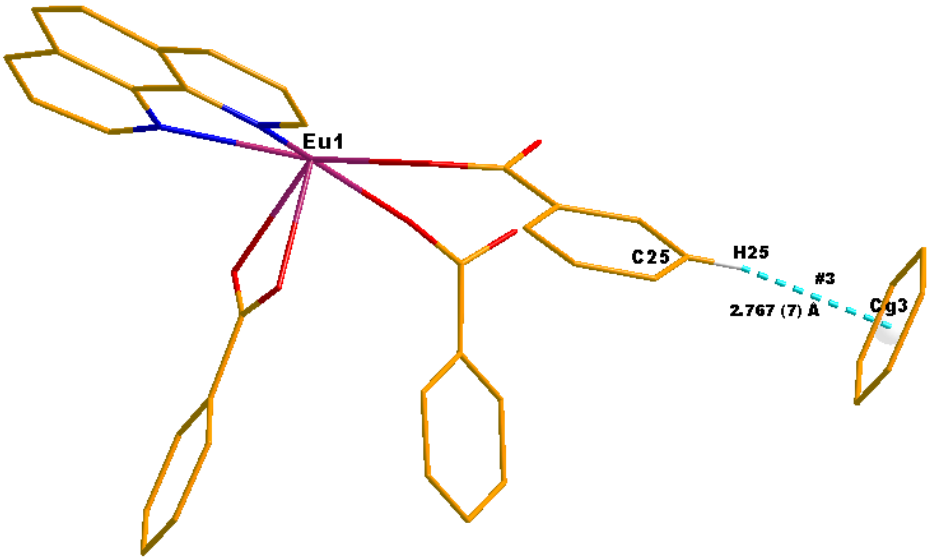

Figure 6.20: The Illustration of intermolecular CH…π hydrogen bonding for (**3**). Atoms constituting Cg3 are C14, C15, C16, C17, C18, C19 completing an aromatic ring.

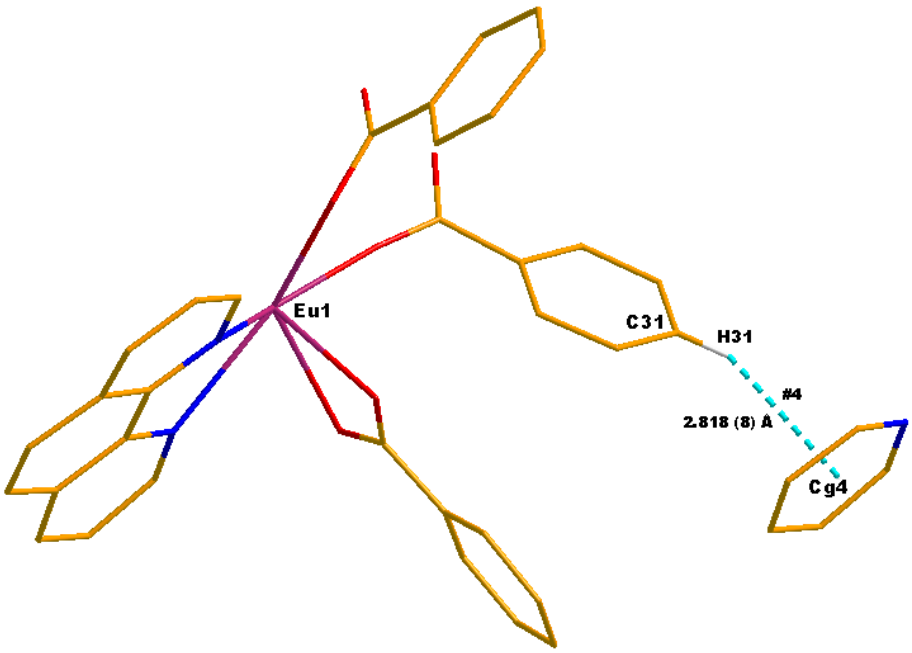

Figure 6.21: The Illustration of intermolecular CH…π hydrogen bonding for (**3**). Atoms constituting Cg4 are C21, C22, C23, C24, C25, C26 completing an aromatic ring.

Constructed below is the polyhedral of coordination geometry around the Eu^{III} metal centers. With nine coordinated atoms, consisting of seven oxygen and two nitrogen atoms, it seem the coordination mode prefers either monocapped square antiprism or tricapped trigonal prism as discussed in **Section 2.1.2.**

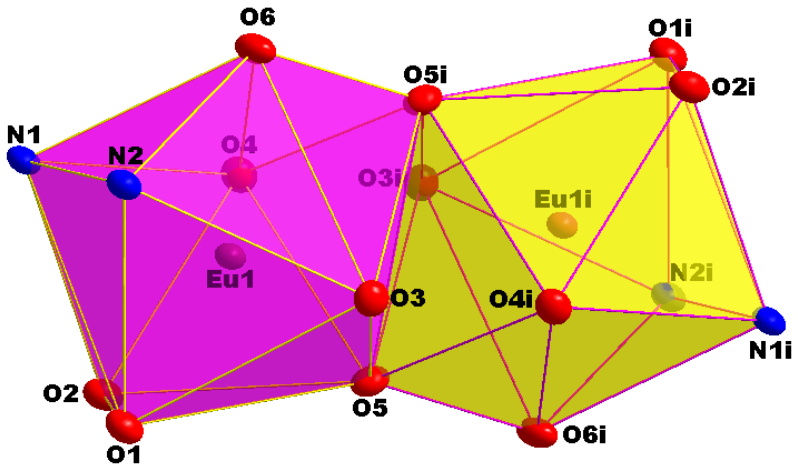

Figure 6.22: Schematic Illustration of coordination geometry of **3**.

The above constructed dual polyhedral both has 8 vertices with 10 faces and 16 edges, constructed by the atoms (C.N. 9) around the metal ion and is of *Monocapped Square Antiprism.*

Below in **Figure 6.19** is the molecular packing of **1** with occurring symmetry elements in the unit cell. There is a point of inversion between the two Eu^{III} centres.

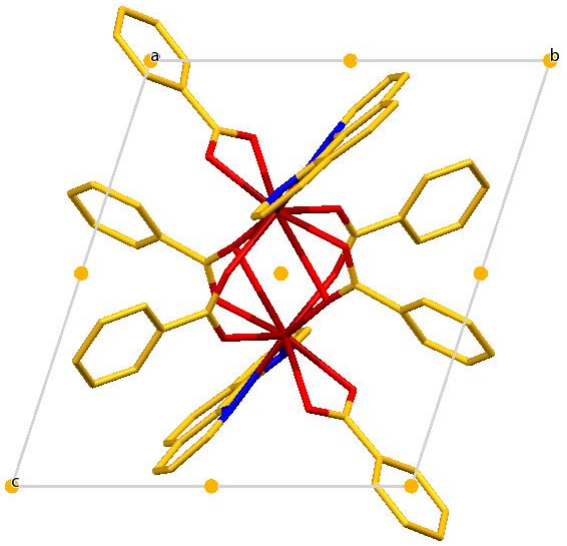

Figure 6.23: Graphical presentations of the molecular packing of **3** depicting symmetry elements thereof.

6.6. Discussion and Conclusions

This entire chapter was about crystallographic discussions and illustration of coordination modes of the respective Eu^{III} complexes as depicted in **Figure 6.1**. Amongst the array synthesized *β*-diketonate Eu^{III} complexes, only the above three discussed complexes crystallized despite many efforts and techniques used to obtain crystals from all of them. The obtained crystals were temperature sensitive and some decomposed during the crystal collection.

Tabled below are the basic crystal data for all the crystals discussed above depicting their respective crystal classes, number of molecules in unit cell, cell parameters and other features as given in **Table 6.10**.

Table 6.10: Summary of structural cell dimensions of **1**, **2** and **3**.

Crystal Formula	**[Eu(TCPB)$_3$Phen](1)**	**[Eu(TMHD)$_3$Phen]** (**2**)	**{[Eu$_2$(BCA)$_6$(Phen)$_2$]- *μ*-[κ^2-O,O'-(BCA)]$_2$} (3)**
Empirical formula	$C_{42}H_{23}Cl_3EuF_9N_2O_6$	$C_{45}H_{65}EuN_2O_6$	$C_{66}H_{46}Eu_2N_4O_{12}$
Crystal system, Space Group	Monoclinic, $P2_1/n$	Triclinic , *P*-1	Triclinic, *P*-1
Temperature (K)	100 (2)	100 (2)	100 (2)
Unit Cell Dimensions			
***a* (Å)**	12.097(3)	10.860 (6)	10.761 (5)
***b* (Å)**	19.354(5)	12.285 (4)	11.865 (5)
***c* (Å)**	21.031(5)	18.398 (4)	12.275 (4)
α, β, γ (°)	90, 104.11(5), 90	80.39 (5), 87.58 (5), 68.76 (4)	105.04 (4), 93.81(5), 112.9 (4)
Volume (Å^3), Z	4528.6(16), 4	2255.3 (15), 2	1369,2 (10), 1
Density (g/cm^3)	1.585	1.299	1.687

There are tabled bond distances and bond angles between all the discussed complexes in this chapter in **Table 6.11** and **6.12**.

There are two key observations noted on the bond distances of these complexes. The first observation is that the nature of the ligands affects the bond distance due to their respective steric hindrance. Subsequent to that, the coordination geometry of these respective complexes to the Eu^{III} metal ion is altered from one complex to the other. It is this bond elongation (e.g. **Eu1-O6** and **Eu1-N2**) effect that affects the coordination mode of these complexes.

Table 6.11: Summary comparisons of selected bond lengths of **1**, **2** and **3**.

	Atomic Bond Distances (Å)		
Atoms	**[Eu(TCPB)$_3$Phen] (1)**	**[Eu(TMHD)$_3$Phen] (2)**	**[Eu$_2$(BCA)$_6$(Phen)$_2$] (3)**
Eu1-O1	2.324 (4)	2.383 (7)	2.419 (14)
Eu1-O2	2.382 (5)	2.369 (8)	2.514 (17)
Eu1-O3	2.341 (2)	2.334 (7)	2.367 (17)
Eu1-O4	2.395 (2)	2.357 (7)	2.380 (16)
Eu1-O5	2.349 (4)	2.369 (6)	2.336 (20)
Eu1-O6	2.399 (6)	2.327 (5)	2.429 (19)
Eu1-N1	2.388 (1)	2.629 (9)	2.591 (21)
Eu1-N2	2.399 (5)	2.620 (6)	2.655 (23)

However, the **Eu1-N1** and **Eu1-N2** bonds of complex **1** are significantly smaller than those observed of complex **2** and **3** as depicted in **Tables 6.11**. The relative effect of this bond shortening for complex **1,** could be realised in the photoluminescence of the complex which will be discussed in chapter 8.

This observed bond elongation somewhat effect the bite angles of these respective complexes as depicted below in **Table 6.12**.

Table 6.12: Summary comparisons of selected bond angles of **1**, **2** and **3**.

	Atomic Bond Angles (˚)		
Atoms	**[Eu(TCPB)$_3$Phen] (1)**	**[Eu(TMHD)$_3$Phen] (2)**	**{[Eu$_2$(BCA)$_6$(Phen)$_2$]- μ-[κ^2-O,O'-(BCA)]$_2$} (3)**
O1-Eu1-O2	71.94 (9)	71.64 (14)	53.08 (49)
O3-Eu1-O4	70.75 (6)	70.24 (15)	134,69 (56)
O5-Eu1-O6	70.89 (7)	70.48 (14)	126.83 (58)
N1-Eu1-N2	63.62 (4)	63.44 (11)	62.47 (58)

All the complexes are reinforced by inter- and intra-molecular interactions. The obtained results in this chapter will be somewhat correlated to the obtained photoluminescence data. The obtained information about the coordination geometry, the crystal systems and the ligands effects will be further discussed in correlation with the luminescence results obtained of these very complexes.

7 Photoluminescence Study of New Schiff Base Ligands

In this chapter:
The spectroscopic analysis of several Schiff base ligands are presented. The absorption and emission nature of the above stated type of ligands.

7.1. Introduction

In this chapter we investigate the luminous abilities of an array of synthesized Schiff base ligands. These ligands were assumed to be the sensitizing organic scaffolds towards the tailoring of Eu^{III} based luminous complexes. The idea of using the Schiff's ligand framework is based on the fact that the two ends of the ligand, bridged by the –C=N– bond, can be custom-made to suit the desired design. The design in this project is based on the organic scaffolds that have luminescent substituents.

Aromaticity plays an integral role in the photoluminescence studies,[1] hence most of the ligands constituency are aromatic. Moreover, the use of the carbazole and naphthalene moiety is proven to have introduced interesting properties towards the luminescence of the Eu^{III} complexes.[2] It is for these reasons that most of the ligands are constructed with benzene, naphthalene or carbazole substituents respectively.

It has been discussed in previous chapters that these Schiff base ligands tend to undergo tautomerism between the enol-imino (O-H) and keto-amino (N-H) form.[3] Amongst the two tautomers, it is the enol-imino form that is highly preferred in solid state.[4] Therefore all the photoluminescence studies will be carried out in solid state form. However, the solution state UV/Vis experiments of the respective ligands will be carried out to investigate their relative absorption nature.

Figure 7.1 presents the structures of the Schiff bases to be analysed and discussed to understand their spectroscopic nature as free ligands.

---

[1] Bilge, S.; Kiliç, Z.; Hayvali, Z.; Hökelek, T.; Safran, S., *J. Chem. Sci.,* **2009,** 121 (6), 989–1001.

[2] Robinson, M.R, O'Regan, M.B., Bazan,G.C., *Chem. Commun.,* **2000**, 1645–1646.

[3] Mohanan, K., Subhadrambika, N., Selwin Joseyphus, R.; Swathy, S. S., Nisha, V. P., *J.Saudi Chem. Soc.* **2016,** 20 (4), 379-390.

[4] Pavlovic, G., Sosa, J.M., Vikic-Topic D., Leban, I., *Acta Cryst.,* **2002**, E58, o317-o320.

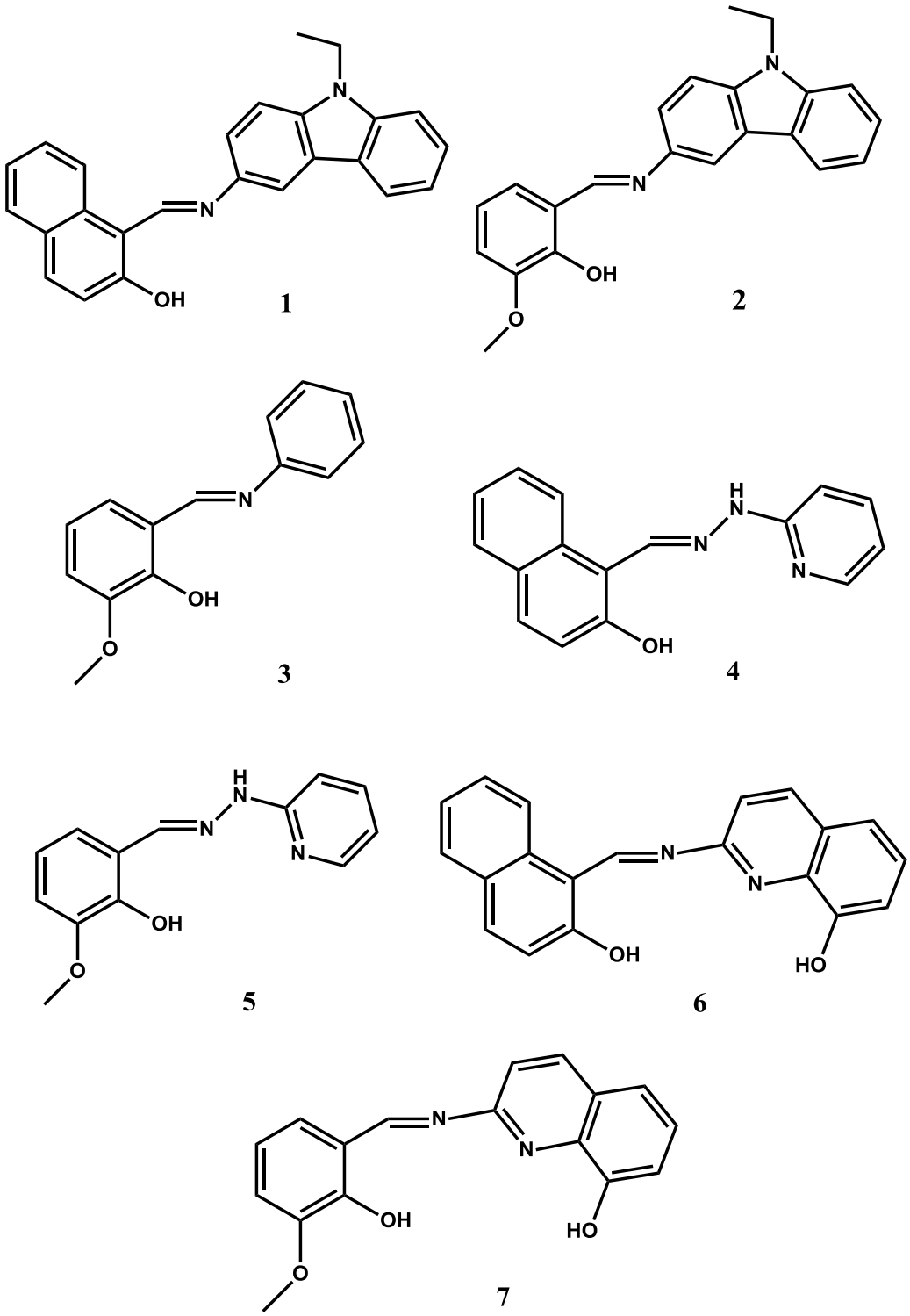

Figure 7. 1: Schematic illustration of the Schiff Base ligands to be photo-analysed. **1**) (*E*)-1-((9-ethylcarbazol-3-ylimino)methyl)-napthanol, **2**) *(E)*-2-(9-ethylcarbazol-3-yliminomethyl)-6- methoxy phenol, **3**) (*E*)-2-methoxy-(6-(phenyliminomethyl))-phenol, **4**) *(E)*-1-((2-(pyridin-2-yl)hydrazono) methyl)naphthalene-2-ol, **5**) *(E)*-2-methoxy-6-((2-(pyridin-2-yl)hydrazono)methyl)phenol, **6**) *(E)*-2-(2-((2-hydroxynaphthalen-1-yl)methylene)hydrazinyl) quinolin-8-ol, **7**) *(E)*-2-(2-(2-hydroxy-3-methoxybenzylidene)hydrazinyl) quinolin-8-ol.

7.2. Experimental

7.2.1. Reagents and Solvents

All chemicals used for the synthesis and preparation of the complexes were of analytical grade and were purchased from Sigma-Aldrich, South Africa. Reaction solvents were of analytical grade and mostly used as received. In cases where anhydrous conditions were required, solvents were purified and dried according to literature procedures.[5]

7.2.2. UV/Vis Spectroscopy

UV/Vis absorbance spectra were collected in a 1.000(1) cm tandem quartz cuvette on a Varian Cary 50 Conc. spectrophotometer, which was equipped with a Julabo F12-mV temperature cell regulator accurate within 0.1 °C. All λ_{max} values reported in this chapter were collected at 25.0 °C. The solution state experiments were done in Chloroform ($CHCl_3$) and some in Dimethylformamide (DMF).

7.2.3. Photoluminescence

The measurements were made using an Edinburgh Instruments FLS980 photoluminescence spectrometer with double monochromators. Samples were excited by a 450 W xenon lamp and the luminescence was measured using a Hammamatsu R928P photomultiplier tube. All spectra were corrected for the spectral response of the system. The quantum yield was measured using an integrating sphere. The total excitation light was recorded using a reflective spectralon sample, after which the excitation light reflected from the sample and the luminescence were measured under identical conditions. The luminescence output (integrated area under the emission curve) was divided by the absorbed light (integrated difference of the reflection from the spectralon and the sample) to give the quantum yield.

[5] Perrin D.D., Armarego W.L.F., Purification of Laboratory Chemicals, *Pergamon Press, Oxford*, Great Britian., **1988**.

7.3. Results and Discussion

7.3.1. Analysis of **Napht-SalH-Carba [1]** and **2oMe-SalH-Carba [2]**

Figure 7.2 depicts the respective absorption spectra of **Napht-SalH-Carba [1]** and **2oMe-SalH-Carba [2].** The absorption nature of both **1** and **2** looks to be very broad, ranging from 290 nm to 490 nm for **1** and from 290 nm to about 380 nm for **2**.

The depicted spectra for **1** and **2** in **Figure 7.2** are indicative of the same absorption identity. However, it was noticed that there are two sets of absorption spectra for **1** (**A**) with the wavelength shift of 24 nm between the absorption maxima peaks. This behaviour in solution state is known to be tautomerization.[6,7]

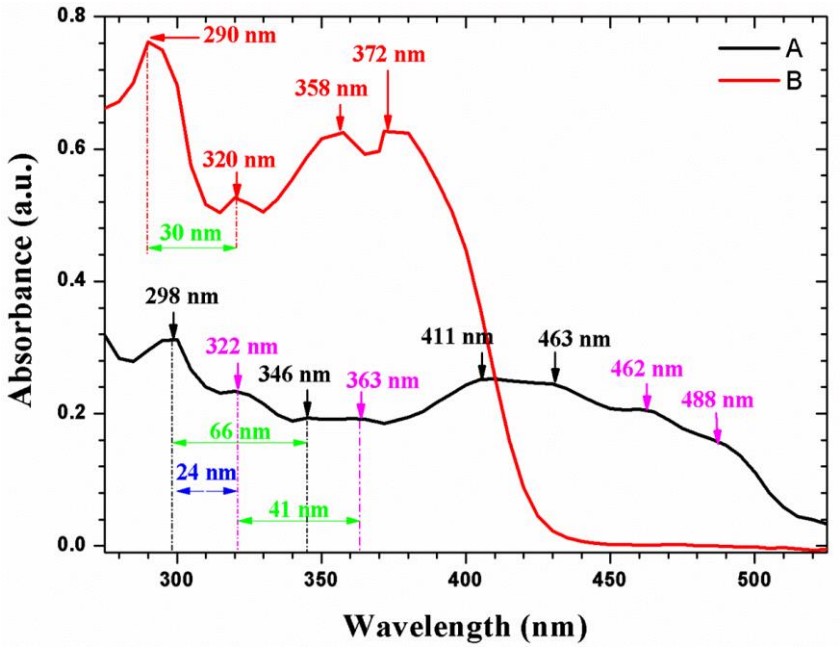

Figure 7.2: Illustration of the absorption spectra of (**A**) **Napht-SalH-Carba** [**1**] (**5.5 x10^{-6} M**) and (**B**) **2oMe-SalH-Carba** [2] (**2.32 x10^{-5} M**) both in chloroform.

The spectral shift between the two compounds is inevitable since an increase in the extent of the π-electron system leads to a shift of the absorption spectra to longer wavelengths. Subsequently, the broadness of the respective spectra depends on the π-conjugation of the two compounds. Therefore the Napht-SalH-Carba **[1]** compound, due to the naphthalene

[6] Temel, H.; Ilhan, S.; Sekerci, M.; Ziyadanogullari, R., *Spectrosc. Lett.*, **2002**, 35 (2), 219-228.

[7] Barbatti, M., *Phys. Chem. Chem. Phys*., **2011**, 13, 4686-4692.

moiety, is expected to red shift compared to the 2oMe-SalH-Carba **[2]** with the methoxy moiety.

Moreover, it was learnt from Temel et al. that the naphthalene Schiff entities prefers planar (see **Section 5.3**) structural conformations6 and to some extent increases the π-electron cloud with the construction of the pseudo aromatic ring constituted by the O-H…N intramolecular interaction. It was further observed by Zhang and co-workers that the existence of the enol-imino form in solution is confirmed by the appearance of the O-H peak resonating at roughly 14 ppm in the ^{1}H-NMR spectrum[8] and this behaviour was also observed in **Section 3.3.1.1** and **3.3.1.2**.

The luminescence spectra in Figure **7.3** and **7.4** are the spectroscopic representation of the excitation and emission of **1** and **2** respectively.

Compound **1** is a multi emitter; having multiple excitation wavelengths from 400 to 524 nm. The 522 nm peak appears to be the most prominent excitation peak giving rise to the maximum emission at 565 nm for **1** as shown in **Figure 7.3**.

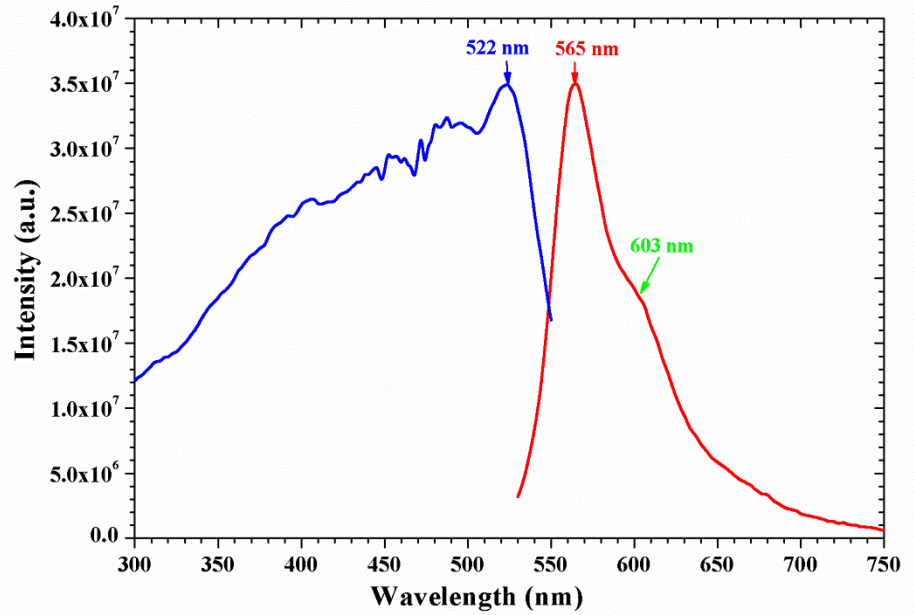

Figure 7.3: Excitation and emission spectra of **Napht-SalH-Carba** [**1**].

It was further observed that the emission peak at 565 nm has a shoulder peak resonating at 603 nm in **Figure 7.3**.

[8] Zhang, X.; Shi, J.; Shen G.; Gou, F.; Cheng, J.; Zhou, X.; Xiang, H., *Mater. Chem. Front.*, **2017**, 1, 1041-1050.

The multiple excitation wavelengths for **2** range from 400 to 500 nm. The 433 nm peak is the most prominent peak giving rise to the maximum emission of 608 nm for **2** as exhibited in **Figure 7.4**.

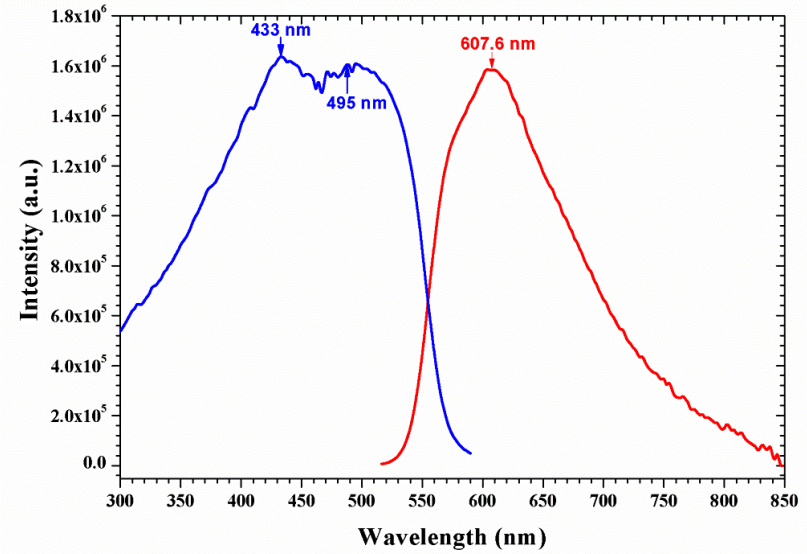

Figure 7.4: Excitation and emission spectra of **2oMe-SalH-Carba** [**2**].

It was learnt from Valeur et al. that substituted electron withdrawing groups, like methoxy (-OMe) group in this case, are responsible for increasing the molar absorptivity of the molecule, however, they are somewhat characteristic of derailing planarity in molecular structures and that was observed in **Section 5.4**. Furthermore, they are also characteristic of broad absorption and fluorescence spectra as observed in **Figure 7.4**. Nevertheless, it is the degree of π-conjugation in the molecule that highly influences the fluorescence quantum yields.[9]

It was also learnt from Valeur et al. that heterocyclic nitrogen atoms have low-lying *n*-π transitions; hence their relatively low fluorescent quantum yields in hydrocarbons. However, when a hetero-nitrogen is singly bonded to carbon atom in a heterocyclic system, the transitions involving the non-bonding electrons have properties similar to those of π-π* transitions.

Therefore, the combined π-conjugation from the two end moieties of the salicylidene back-bone in **1** and the efficient π-π* transitions from both the naphtha- and carbazol- moieties, gives high quantum yields in **1** compared to low quantum yield obtained for **2** as discussed in **Section 7.4.2**.

[9] Valeur, B., (**2001**). *Molecular Fluorescence: Principles and Applications*, *Wiley-VCH Verlag*, New York, 54-61.

7.3.2. Analysis of *2oMe-SalH-Anil* [3].

Figure 7.5 depicts the absorption spectrum of **2oMe-SalH-Anil [3].** The absorption nature of **3** also looks to be broad, ranging from 280 nm to 360 nm. There are two observed prime peaks absorbing at 280 and 314 nm respectively.

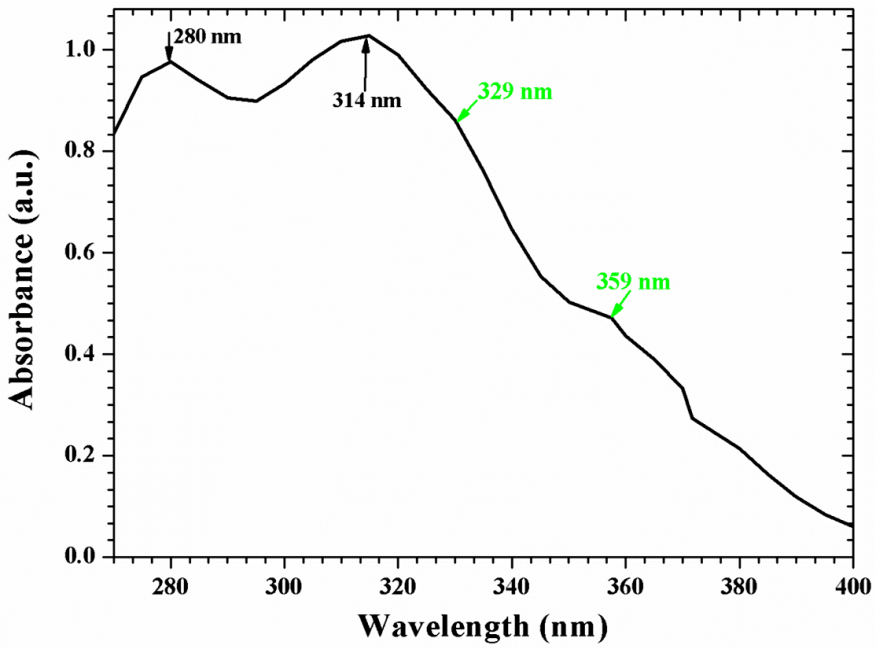

Figure 7.5: Absorption spectrum of **2oMe-SalH-Anil** [**3**] in chloroform (**3.52 x10^{-5} M**).

However there are other two shoulder peaks observed, that absorbs at 329 and 359 nm respectively. The observed broad band absorption spectrum is the result of the substituted electron withdrawing group, like methoxy (-OMe) group, on the phenol moiety.

With the methoxy (-OMe) substitution known to affect the planarity of the molecules, both the organic moieties in **3** are not coplanar and have the biggest dihedral angle when compared to **1** and **2** as discussed in **Section 5.5**.

The luminescence spectrum in **Figure 7.6** is the spectroscopic representation of the excitation and emission of **3**

The multiple excitation wavelengths potentially range from 400 to 500 nm. The 496 nm peak appears to be the most prominent peak giving rise to the maximum emission peak at 523 nm for compound **3** as exhibited in **Figure 7.6**.

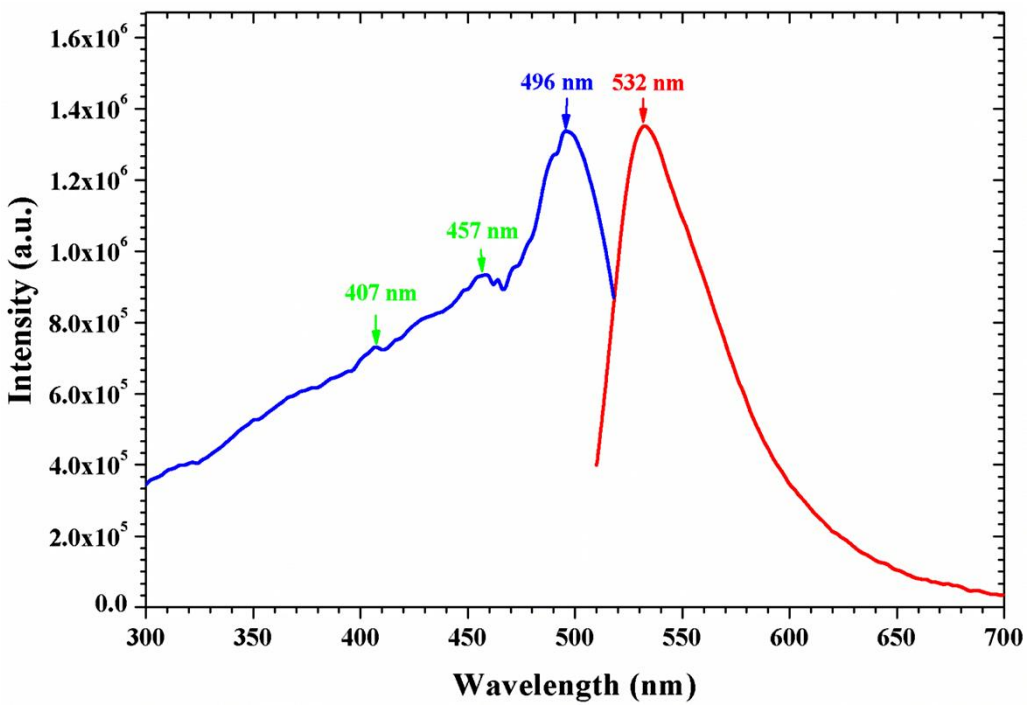

Figure 7.6: Excitation and emission spectra of **2oMe-SalH-Anil** [**3**].

The luminescence intensity and quantum yield of compound **3** is somewhat attributed to the aromatic character of aniline moeity attached to the salicylaldehyde backbone.

The emission intensity of **1** and **3** is, to some extent, incomparable relative to the organic constituency found in both respective molecules. The observed π –conjugation between both the molecules cannot be matched and therefore it is accepted that the emission intensity for **1,** with greater π –conjugation, surpass that of **3** by far.

However, the molecules **2** and **3** can be compared to one another via the molecular constituency thereof in their respective compounds. With the aniline moiety having real efficient π-π^* transitions compared to the carbazol moiety, which is somewhat mimicking the π-π^* transitions, result to **3** having higher emission intensity compared to **2**.

7.3.3. Analysis of **Naphth-SalH-Hydrapyrdin [4]** and **2oMe-SalH-Hydrapyrdin [5]**

Figure 7.7 depicts the respective absorption spectra of **Naphth-SalH-Hydrapyrdin** [**4**] and **2oMe-SalH- Hydrapyrdin [5].** The absorption nature of both **4** and **5** looks to be very broad, ranging from 365 nm to about 475 nm for **4** and 360 nm to 440 nm for **5**.

The depicted spectra for **4** and **5** in **Figure 7.7** are indicative of the same absorption identity. **Figure 7.7** clearly shows the three prominent absorption peaks from both the **4** and **5**. The three observed prime peaks in **4**, indicated with black arrows, absorbs at 365, 435 and 475 nm respectively. The corresponding three prominent peaks in **5**, indicated in red arrows are 360, 370 and 434 nm.

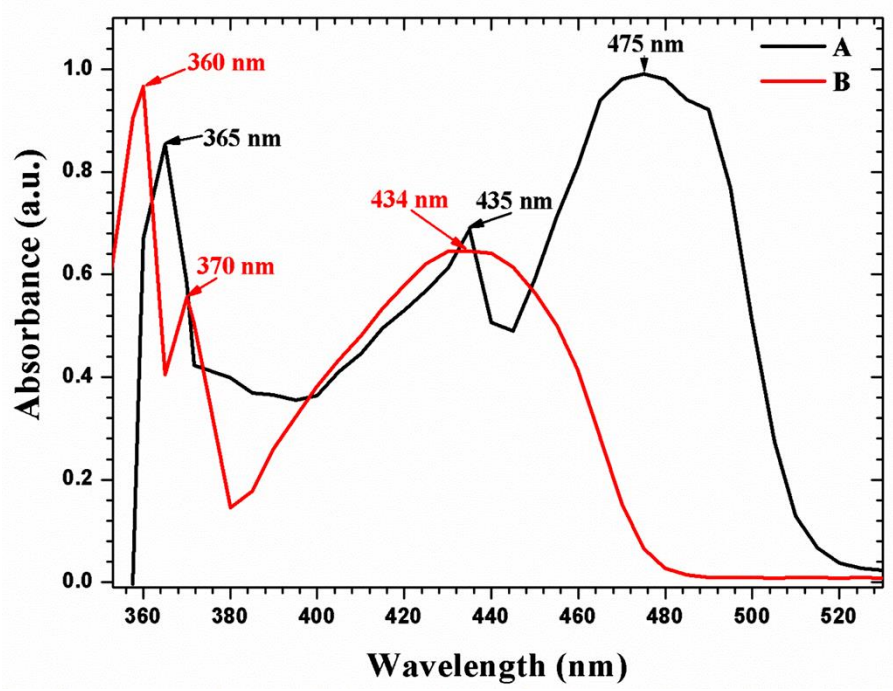

Figure 7.7: Absorption spectra of (**A**) **Naphth-SalH- Hydrapyrdin** [**4**] (**2.28 x10^{-5} M**) and (**B**) **2oMe-SalH-Hydrapyrdin** [**5**] (**2.13 x10^{-5} M**) in Dimethylformamide (DMF).

Due to the extended π-conjugation imposed by the naphathyl moeity observed in **5**, it was observed that the spectrum is red shifted to longer wavelengths. Subsequently, the Napht-SalH-Hydrapyrdin [**4**] compound, due to the naphthyl moiety, is expected to red shift compared to the 2oMe-SalH-Hydrapyrdin [**5**] with the methoxy (-OMe) moiety.

The luminescence spectra in **Figure 7.8** depicts the spectroscopic representation of the excitation and emission of **4**

The multiple excitation wavelengths potentially range from 420 to 490 nm. The 452 nm peak appears to be the most prominent peak giving rise to the maximum emission of 537 nm of compound **4** as exhibited in **Figure 7.8**.

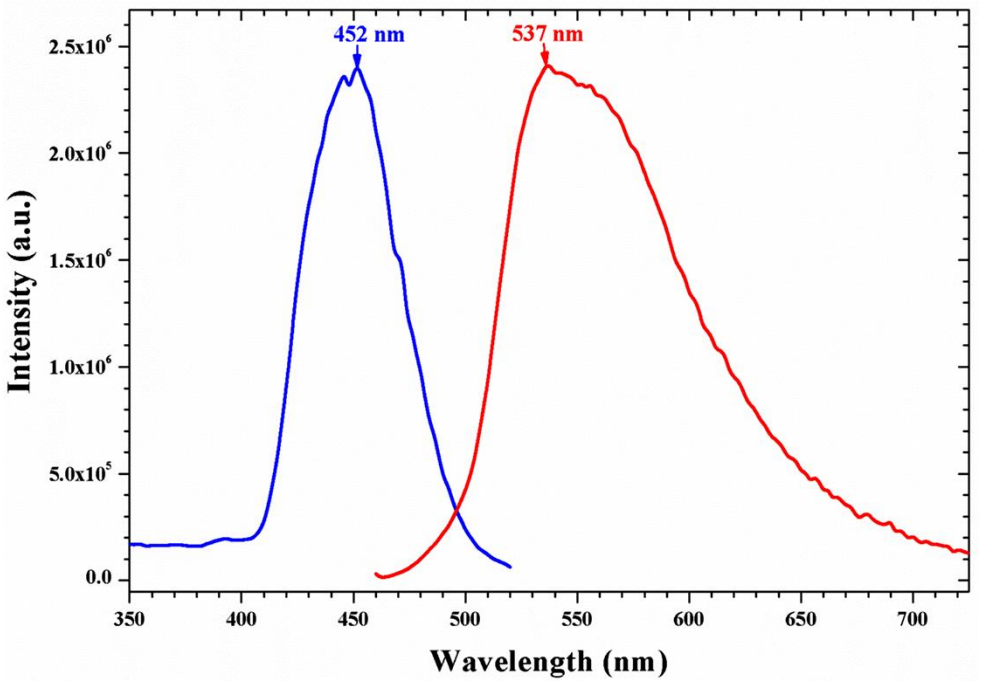

Figure 7.8: Excitation and emission spectra of **Naphth-SalH-Hydrapyrdin** [**4**].

There are no observed shoulder peaks on the excitation spectrum resonating. The emission spectrum of **4** is noticed to be less red shifted with the emission maxima of 537 nm compare to the spectrum of **5**.

The luminescence spectrum in **Figure 7.9** depicts the spectroscopic representation of the excitation and emission of **5**

The multiple excitation wavelengths potentially range from 400 to 500 nm. The 486 nm peak appears to be the most prominent peak giving rise to the maximum emission of 612 nm of compound **5** as exhibited in **Figure 7.9**.

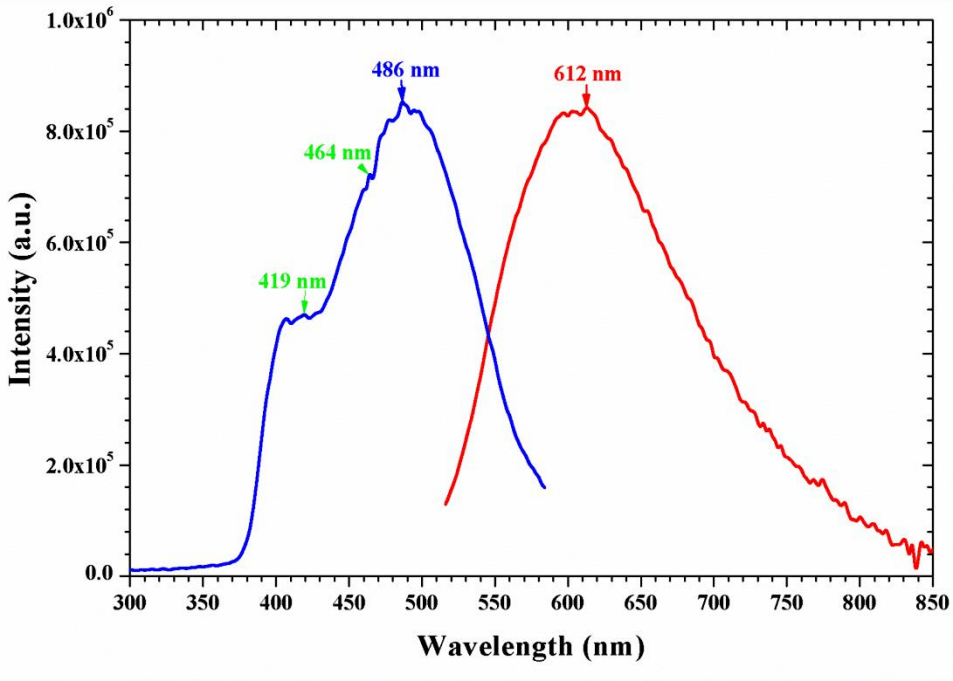

Figure 7.9: Excitation and emission spectrum of **2oMe-SalH-Hydrapyrdin [5]**.

Unlike in **4** which has no shoulder peaks on excitation spectrum**,**There are observed shoulder peaks on the excitation spectrum resonating at 419 and 464 nm. The emission spectrum of **5** is noticed to be red shifted with the emission maxima of 612 nm. It is also noticed that the electron donating ability of the methoxy is responsible for the emission spectral shift compared to the naphthyl moiety.

The organic constituency of **4** and **5** is somewhat the same as those observed above in terms of the naphthyl and the methoxy moieties. However, the other end of the Schiff base in **4** and **5** is the hydrazine moiety. The hydrazinopyridine is employed in this **Section 7.3.3**.

This hydrazinopyridine moiety has an extended π –conjugation via the extension imposed by the secondary (N̈H) amine. It is this extended π-system needed for an increase in the fluorescence of the organic compounds.9

With the hydrazinopyridine moiety behaving similar to the carbazolyl moiety; it is believed to be mimicking the π-π* transitions. The difference in the extent of π –conjugation between the naphthyl and the methoxy serves as a decider as to which one of the compounds is prone to have higher fluorescence than the other. In this case it accepted that compound **4** is much more luminescent than **5**.

7.3.4. Analysis of **Napht-SalH-Quin [6]** and **2oMe-Sal-Quin [7].**

Figure 7.10 depicts the respective absorption spectra of **Napht-SalH-Quin** [**6**] and **2oMe-SalH- Quin** [**8**]**.** The absorption nature of both **6** and **7** looks to be very broad, ranging from 350 nm to 600 nm for **6** and 350 nm to 550 nm for **7**.

The depicted spectra for **6** and **7** complexes in **Figure 7.10** are indicative of the same absorption identity with slight difference on the maxima absorbance peak. The exhibition in **Figure 7.10** clearly shows the three prominent absorption peaks from both **6** and **7**. The four observed prime peaks in **6**, indicated with black arrows, absorb at 365, 460, 554 and 578 nm respectively. The corresponding four prominent peaks in **7**, indicated in red arrows are 360, 404, 450 and 485 nm.

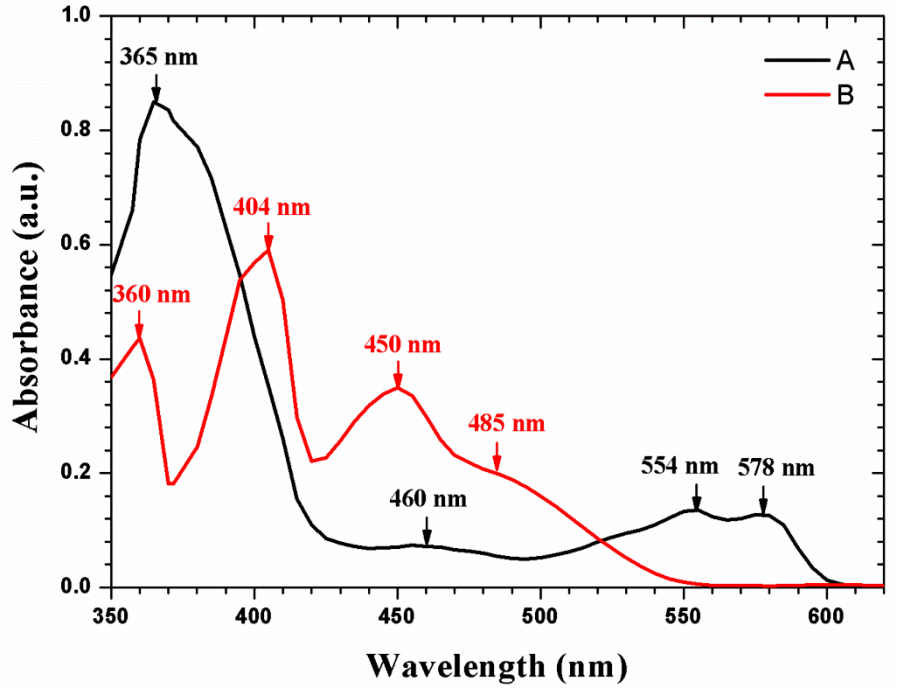

Figure 7.10: Absorption spectrum of (**A**)**Napht-SalH-Quin** [**6**] (**5.09 x10^{-6} M**) and (**B**) **2oMe-Sal-Quin** [**7**] (**2.04 x10^{-5} M**) in chloroform.

The observed absorption wavelength shift in **6** is assumed to be the aromatic influence by the highly absorbing naphthyl moeity compared to the methoxy (-OMe) moiety in **7**.

The comparison on the other end of the salicylidene backbone is of a quinolinol moiety for both **6** and **7**. Due to the extended π-conjugation imposed by the naphathyl moeity observed in **6**, it was observed that the absorption spectrum is red shifted to longer wavelengths.

The luminescence spectra below is the spectroscopic representation of the excitation and emission of **6**

The multiple excitation wavelengths range from 350 to 500 nm. The 400 nm peak appears to be the most prominent peak giving rise to the maximum emission peak at 549 nm of compound **6** as exhibited in **Figure 7.11**.

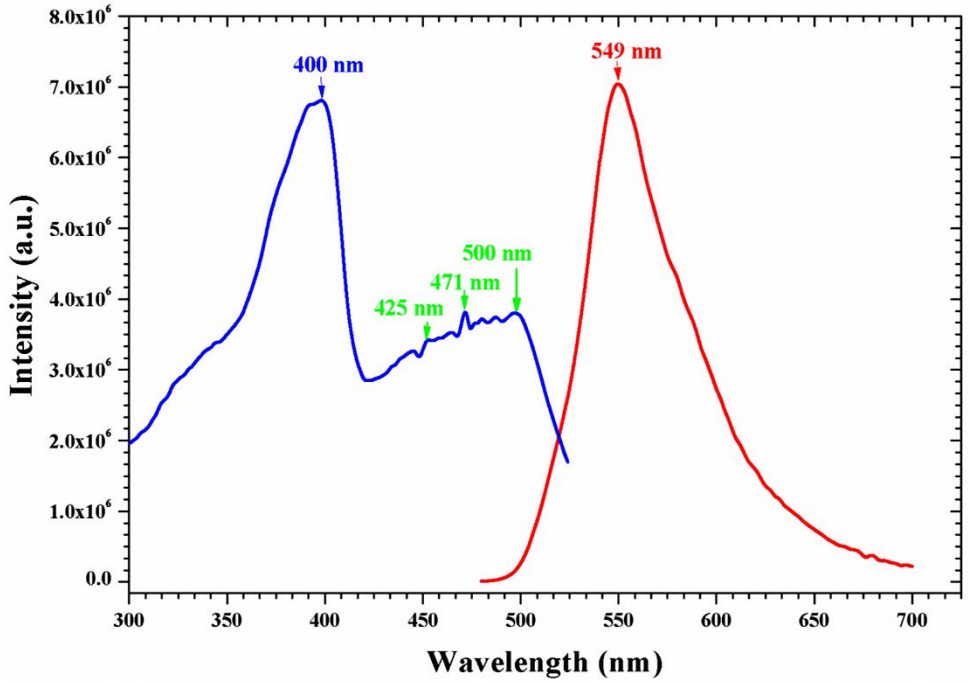

Figure 7.11: Excitation and emission spectra of **Napht-SalH-Quin** [**6**].

There are observed shoulder peaks on the excitation spectrum resonating at 425, 471 and 500 nm. The absorption maxima peak resonating at 400 seem to be far more prominent and bigger than the other excitation should peaks observed **Figure 7.11**. Moreover, it is blue shifted than the other ones.

The luminescence spectrum in **Figure 7.12** depicts the spectroscopic representation of the excitation and emission of **7**

The multiple excitation wavelengths potentially range from 350 to 550 nm. The 509 nm peak appears to be the most prominent peak giving rise to the maximum emission of 615 nm of compound **7** as exhibited in **Figure 7.12**.

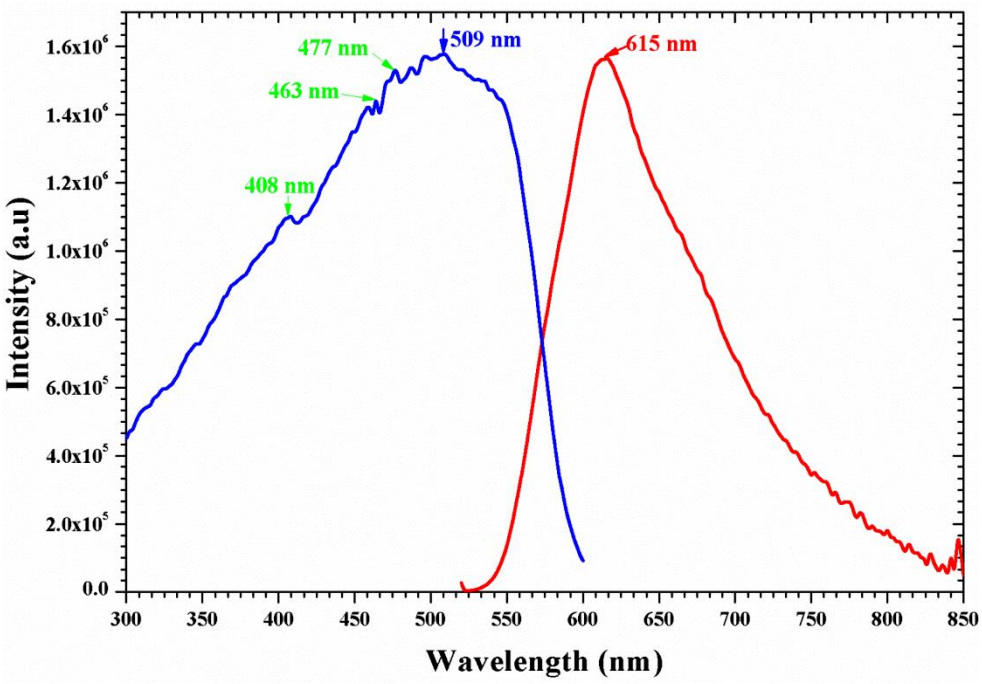

Figure 7.12: Excitation and emission spectra of **2oMe-SalH-Quin** [7].

There are observed shoulder peaks on the excitation spectrum resonating at 408, 463 and 477 nm. The emission spectrum of **7** is noticed to be also red shifted relative to **6** with the emission maximum of 615 nm. It is the electron donating ability of the methoxy influencing the emission spectral red shift compared to the naphthyl moiety.

The new quinolinol moiety on the other end of the salicylidene backbone is introduced in both **6** and **7**. This quinolinol moiety, known greatly for its flouretic endeavours,[Error! Bookmark not defined.] has an extended π –conjugation.

This quinolinol moiety behaves also similar to the carbazolyl moiety; it is believed to be mimicking the π-π* transitions. The difference in the extent of π –conjugation between the naphthyl and the methoxy, also serves as a decider between **6** and **7**. With the pattern observed from this chapter, it also accepted that compound **6** is much more luminescent than **7**.

7.3.5. Discussions

The absorption nature of the respective organic species appeared to be dependent on the respective molecular constituency. The absorption spectra of all the above discussed Schiff base ligands appeared to be broad in response to the absorbing nature of the aromatic systems used; like naphthalene, methoxy-benezene, hydrazinopyridine and 8-hydroxyquinoline moieties.

Only complexes with high emission intensity were considered for quantum yields measurements**.** The excitation and emission experiments were carried out in solid state. All the Schiff base ligands analyzed were found to give off fluorescence emissions. Very likely for organic scaffolds, both the excitation and emission curves were broad. All the recorded emission spectra resulted from the highest excitation peak. Most of the excitation spectra had multiple excitation peaks. The emission peaks across all the spectra are in the visible range between 436 and 615 nm.

The quantum yields of the samples **1**, **2** and **3** were measured at wavelengths close to their excitation maxima using an integrating sphere. The total excitation light was recorded using a reflective spectralon standard (reference), after which the excitation light reflected from the samples and their luminescence output up to 800 nm were measured under identical conditions.

The luminescence output (integrated area under the emission curve) was divided by the absorbed light (integrated difference of the reflection from the reference and the sample) to give the quantum yield. **Table 7.1** summarizes the quantum yield results.

Table 7.1: Quantum yields of the selected Schiff Base samples.

Ligands	Exc. Wavelength (nm)	QY (%)
Napht-SalH-Carba [**1**]	524	7.0
2oMe-SalH-Carba [**2**]	498	1.0
2oMe-SalH-Anil [**3**]	498	1.6

Figure 7.13 depicts the emission spectra of **1**, **2** and **3** with their respective emission wavelengths. These three molecules were found to have higher fluorescence than most of

other compounds reported above with **1** being the most luminous one giving QY of 7%. The area underneath **1** is sufficient for it have high quantum yield.

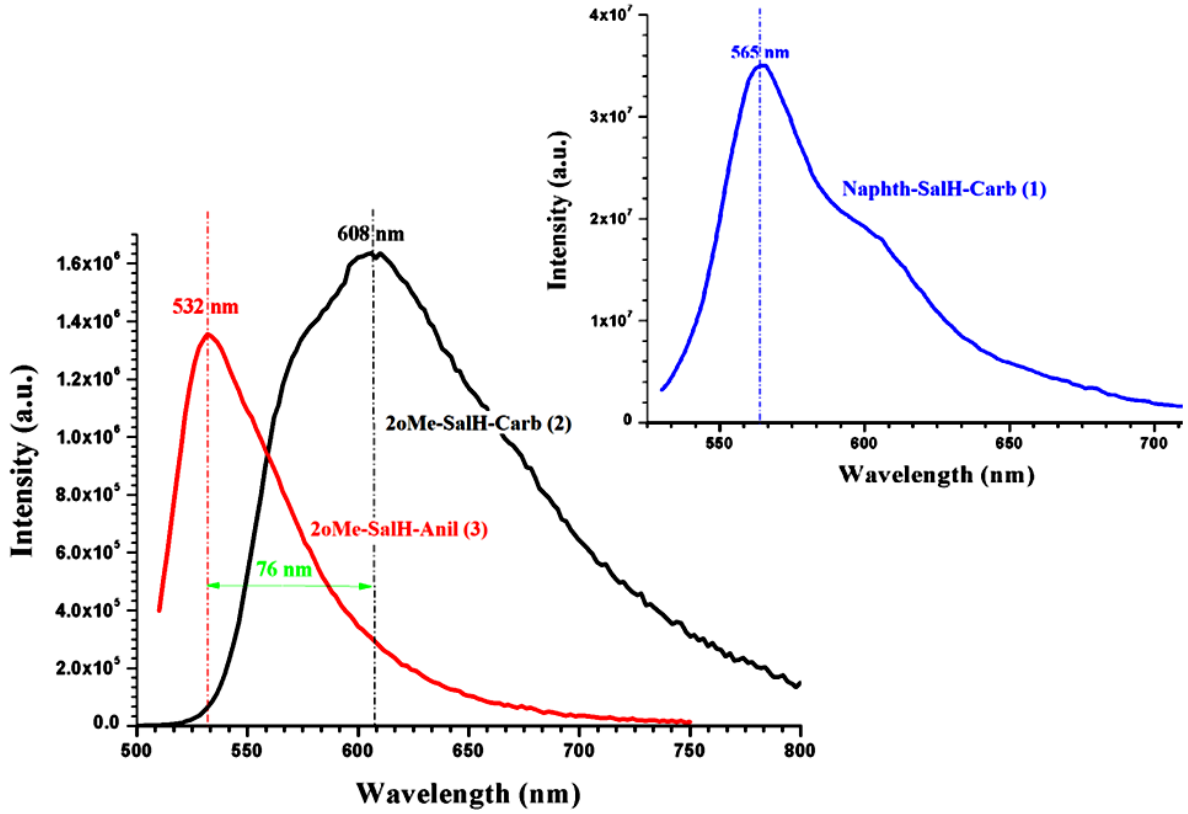

Figure 7.13: Selected emission spectra of **1, 2** and **3**. Both **2** and **3** are (x15) magnified on the vertical axis to match **1**.

Many of the ligands emission capacity above were affected by the excitation wavelength which generally appeared on the long wavelength side of a band, close to the emission peak. It is therefore clear that the respective constituents bonded to the salicylidene moiety have significant effect on the fluorescence properties in these compounds, although in general the quantum yields are not sufficiently high. Amongst all the complexes, compound **1** proved to have reasonably high quantum yield which is suitable for many applications. However, it is not as strong as many other well-known organic fluorophores.[10]

[10] Brink, A.; Kroon, R.E.; Visser, H.G.; van Rensburg C.E.J.; Roodt, A., New J. Chem., **2018**, DOI: 10.1039/c7nj04208f

7.4. Conclusions

The spectroscopic analysis of the array of synthesized bi-functional Schiff base chelators was successfully carried out in this chapter. The outlay analysis was based on the absorption, excitation and emission capacity of synthesized Schiff's organic entities and all the analysed ligands were successfully found to be fluorescent. The observed absorption behaviour of the analysed Schiff base ligands was somewhat responsive to the organic moieties constituting the ligand species. This effect further translates to the observed respective emission maxima red/blue shifts.

The quantum yield measurements presented compound **1** as the most emitting ligand species in the range with the yield of 7% followed by compound **2** and **3** which gave 1% and 1.6% respectively.

These Schiff organic scaffolds pose themselves as potential fluorophores for later use in many photoluminescence related applications. It is therefore necessary for further research to be exercised on this type of ligands in quest for high emitting complexes.

8 Photoluminescence Study of β-Diketonate Eu^{III} Based Complexes

In this chapter:
The spectroscopic analyses of the β-diketonate EuIII complexes are to be considered. Their excitation and emission abilities will be extensively discussed.

8.1. Introduction

Herein we look to illustrate and discuss the spectroscopic behaviour of the β-diketonate Eu^{III} based complexes. With different respective β-diketone ligand species used, it is believed that the Eu^{III} complex luminous behaviour could be attributed to the ligand properties; with respect to the steric and electronic effects they possess.

Since its earliest report of narrow red emission spectral profile,[1] Eu^{III} based complexes have gradually became of great concern across many scientific fields to-date.[2,3] Its success somewhat becomes a great interest for, ever evolving photoluminescence science in many scientific disciplines.[4,5] The luminous profile is prone to Eu^{III} metal ion conjugation to an organic matrix. However the degree of luminance thereof, triggered by different organic matrices, poses an interesting question. This phenomenon is called sensitization or the antenna effect.[6]

In this chapter, not only do we look to investigate the question posed above, but also to advance in looking at the influence of these ligands towards the spectral identity of the ternary β-diketonate Eu^{III} complexes.

Figure 8.1 illustrates the respective ternary europium β-diketonate complexes to be analyzed.

[1] Urbuin, G.; Hebd, C.R., *Acad. Sci*., **1906**, 142, 205-207.

[2] Casanova, D.; Bouzigues, C.; Nguyen, T.L.; Ramodiharilafy, R.O.; Bouzhir-Sima, L.; Gacoin, T.; Boilot, J.P.; Tharaux, P.L.; Alexandrou, A., *Nat. Nanotechnol.*, **2009**, 4, 581-585.

[3] Wu, S.W.; Han, G.; Milliron, D.J.; Aloni, S.; Altoe, V.; Talapin, D.V.; Cohen, B.E.; Schuck, P.J., *Proc. Natl. Acad. Sci. U.S.A.*, **2009**, 106, 10917-10921.

[4] Andres, J.; Hersch, R.D.; Moser, J.E.; Chauvin, A.S., *Adv. Funct. Mater*., **2014,** 24, 5029-5036.

[5] Rodriguez Burbano, D.C.; Naccache, R.; Capobianco, J.A.; *Handbook on the Physics and Chemistry of Rare Earths, Elsevier Science B.V*., Amsterdam, **2015**, 47, 273-347.

[6] Weissman, S.I., *J. Chem. Phys.*, **1942**, 10 , 214-217.

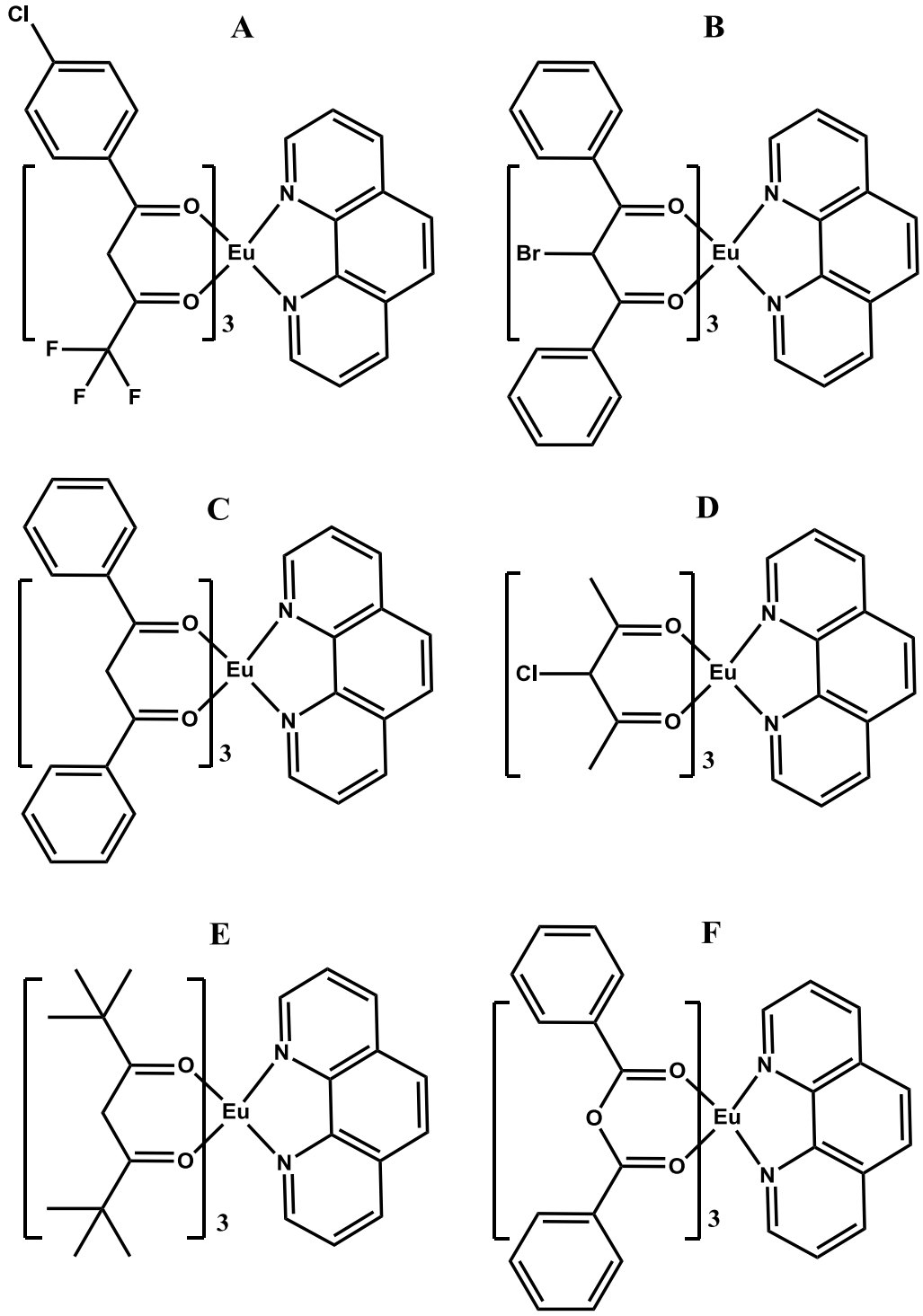

Figure 8.1: Schematic illustrations of synthesized Eu^{III} based *β*-diketonate complexes. **A**) [*tris*-(4,4,4-Trifluoro-1-chlorophenyl-butanedione) mono(1,10-phenanthroline) europium(III)], **B**) [*tris*-(2-Bromo-1,3-diphenyl-propanedione) mono(1,10-phenanthroline) europium(III)], **C**) [*tris*-(1,3-Diphenyl-propanedione) mono (1,10-phenanthroline) europium(III)], **D**) [*tris*-(3-Chloro-2,4-pentanedione) mono(1,10-phenanthroline) europium(III)], **E**) [*tris*-(2,2,6,6-Tetremethyl-heptanedione) mono(1,10-phenanthroline) europium(III)], **F**) [*tris*-(Benzoic Anhydride)-*mono*-(1,10-phenanthroline) europium(III)].

8.2. Experimental

8.2.1. Reagents and Solvents

All chemicals used for the synthesis and preparation of the complexes were of analytical grade and were purchased from Sigma-Aldrich, South Africa. Reaction solvents were of analytical grade and mostly used as received. In cases where anhydrous conditions were required, solvents were purified and dried according to literature procedures.[7]

8.2.2. Reflectance

Diffuse reflectance was measured using a Perkin Elmer Lambda 950 UV/Vis spectrophotometer with spectralon integrating sphere accessory.

8.2.3. Infrared

Solid state FT-IR spectra of samples were recorded on a Bruker Tensor 27 Fourier transform spectrometer (ATR), utilizing a He-Ne laser at 632.6 nm, in the range of 3000 to 600 cm^{-1}.

8.2.4. Photoluminescence

The measurements were made using an Edinburgh Instruments FLS980 photoluminescence spectrometer with double monochromators. Samples were excited by a 450 W xenon lamp and the luminescence was measured using a Hammamatsu R928P photomultiplier tube. All spectra were corrected for the spectral response of the system.The emission spectra were measured with a bandwith of 0,5 nm. The quantum yield was measured using an integrating sphere. The total excitation light was recorded using a reflective spectralon standard, after which the excitation light reflected from the sample and the luminescence were measured under identical conditions. The luminescence output (integrated area under the emission curve) was divided by the absorbed light (integrated difference of the reflection from the spectralon and the sample) to give the quantum yield.

[7] Perrin D.D., Armarego W.L.F., (**1988**). *Purification of Laboratory Chemicals, Pergamon Press,* Oxford, Great Britain.

8.3. Results and Discussions.

In this section we report the solid state luminescence analysis of the studied ternary *β*-diketonate Eu^{III} based complexes. The luminescence spectra of europium (III) compounds are more informative than the corresponding absorption spectra. These spectra will give an insight on the effect of the organic molecules coordinated to the Eu^{III} complexes and the identity thereof.

All the spectra were analysed with regard to the existence of the emission transitions (**Table 8.1**) and the splitting occurring in these transitions. Any occurring splitting in these transitions will be assessed in terms of **Table 8.2**, for further correlation with relative symmetry systems found in crystal structures (discussed in Chapter 6) of some of these complexes in this chapter.

Table 8.1: Transitions observed in luminescence spectra of europium (III) compounds.[8]

Transition[a]	Dipole Character	Wavelength range (nm)	Relative Intensity	Remarks
$^5D_0 \rightarrow {}^7F_0$	ED	570 - 585	vw to s	Only observed in C_n, C_{nv} and C_s symmetry
$^5D_0 \rightarrow {}^7F_1$	MD	585 - 600	s	Intensity largely independent of environment
$^5D_0 \rightarrow {}^7F_2$	ED	610 - 630	s to vs	Hypersensitive transition; intensity very strongly dependent on environment
$^5D_0 \rightarrow {}^7F_3$	ED	640 - 660	vw to w	Forbidden transition
$^5D_0 \rightarrow {}^7F_4$	ED	680 - 710	m to s	Intensity dependent on environment, but no hypersensitivity

[a] Only transitions starting from the $^5D_0$ level are shown.
[b] ED = induced magnetic dipole transition, MD = magnetic dipole transition.
[c] vw = very weak, w = weak, m = medum, s = strong, vs = very strong.

Table 8.2: Number of Sublevels in *J*-splitting for different symmetry classes.[8]

Symmetry Class	Point Groups	*J=0*	*J=1*	*J=2*	*J=3*	*J=4*
Icosahedral	I_h, I	1	1	1	2	2
Cubic	O_h, O, T_d, T_h, T	1	1	2	3	4
Octagonal	D_8, C_{8v}, S_8, D_{4d}	1	2	3	4	6
Hexagonal	D_{6h}, D_6, C_{6v}, C_{6h}, C_6, D_{3h}, C_{3h}	1	2	3	5	6
Pentagonal	D_{5h}, D_5, C_{5v}, C_{5h}, C_5	1	2	3	4	5
Tetragonal	D_{4h}, D_4, C_{4v}, C_{4h}, C_4, S_4, D_{2d}	1	2	3	5	7
Trigonal	D_{3d}, D_3, C_{3v}, C_{3i}, C_3	1	2	3	5	6
Orthorhombic	D_{2h}, D_2, C_{2c}	1	3	5	7	9
Monoclinic	C_{2h}, C_2, C_s	1	3	5	7	9
Triclinic	C_1, C_s	1	3	5	7	9

[8] Binnemans, K., *Coord. Chem. Rev.*, **2015**, 295, 1-45.

There are five characteristic sets of narrow spectral lines of $^5D_0 \rightarrow {}^7F_J$ transitions observed in all the emission spectra of the analysed complexes in this chapter. These observed europium (III) characteristic emission transitions of $^5D_0 \rightarrow {}^7F_0$, $^5D_0 \rightarrow {}^7F_1$, $^5D_0 \rightarrow {}^7F_2$, $^5D_0 \rightarrow {}^7F_3$, $^5D_0 \rightarrow {}^7F_4$; resonate approximately at 580, 592, 612, 652 and 703 nm respectively. However, the intensity of some of the transitions in the respective spectra is low; that behaviour is somewhat regulated by **Table 8.1**.

The crystal-field perturbation destroys the spherical symmetry of the Eu^{III} free ion and the $^{2S+1}L_J$ term splits up in a number of crystal-field levels (see **Figure 2.1**). Therefore, the extent to which the $2J+1$ degeneracy of a $^{2S+1}L_J$ term is removed depends on the symmetry class and not on the point group (see **Table 8.2**). For all the point groups within a symmetry class, the splitting of a *J*-term is identical.

It was learnt from Binnemans that the $^5D_0 \rightarrow {}^7F_0$ transition is useful in determining the number of non-equivalent Eu^{III} species. Any observation of more than one peak in that spectroscopic region signals more than one Eu^{III} species is present.[8] Furthermore, with $^5D_0 \rightarrow {}^7F_J$ (J=0, 3, 5) transition often found to have very weak intensities, the relative Stark splitting is somewhat dictated by the $^5D_0 \rightarrow {}^7F_1$ and $^5D_0 \rightarrow {}^7F_2$ transitions. These two transitions together with other pronounced transitions were used to configure the Stark splitting of the all complexes in this chapter.

The summary of the Stark splitting of all complexes is given in **Table 8.3**. This table is constructed for reasons pertaining clarity for the reader and will be frequently referred to later in the discussion sections in declaration of the relative Stark splitting of respective complexes therein.

Table 8.3: Summary of Stark splitting in the respective investigated complexes in this chapter.

	Number of Stark Splitting in Sub-levels				
Complex	$^7\mathbf{F_0}$ (*J=0*)	$^7\mathbf{F_1}$ (*J=1*)	$^7\mathbf{F_2}$ (*J=2*)	$^7\mathbf{F_3}$ (*J=3*)	$^7\mathbf{F_4}$ (*J=4*)
[Eu(TCPB)$_3$Phen] (A)	1	3	5	7	9
[Eu(DBBrM)$_3$Phen] (B)	1	3	5	7	9
[Eu(DBM)$_3$Phen] (C)	1	2	3	5	6
[Eu(DMC)$_3$Phen] (D)	1	2	3	5	6
[Eu(TMHD)$_3$Phen] (E)	1	3	5	7	9
[Eu(PCA)$_3$Phen] (F)	1	3	5	7	9
[Eu$_2$(PCA)$_6$(Phen)$_2$] (H)	1	2	3	5	6

8.3.1. Analysis of [Eu(TCPB)$_3$Phen] (A)

Figure 8.2 illustrates the excitation and emission spectra of [*tris*-(4,4,4-trifluoro-1-chlorophenyl-butanedione) mono(1,10-phenanthroline)] europium(III): **[Eu(TCPB)$_3$Phen]**.

There is a broad spectrum of excitation possibilities (green arrows) ranging from 240 to 380 nm. However, the prime excitation wavelength for maximum emission spectral profile is at 377 nm giving rise to the 611 nm emission peak as exhibited in **Figure 8.2**. There are higher excited states of $^5D_2 \leftarrow ^7F_0$ and $^5D_1 \leftarrow ^7F_0$ observed with low intensity resonating at 464 nm and 534 nm respectively.

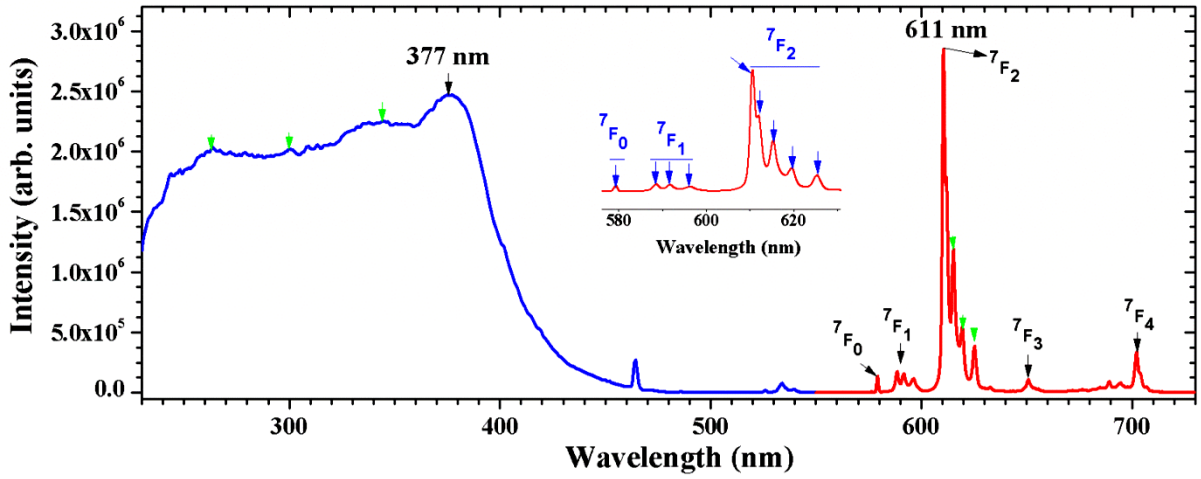

Figure 8.2: Excitation and emission spectra of **A.**

The spectral identity referred to in this chapter does not rely on the wavelength shift but on the actual Stark splitting of the $^5D_0 \rightarrow {}^7F_J$ transitions. With the $^5D_0 \rightarrow ^7F_0$ transition often found to be a singlet, the splitting pattern of the whole spectrum relies on the $^5D_0 \rightarrow ^7F_1$ transition.

Aided by **Table 8.2**, the number of Stark splitting accounted for in the $^5D_0 \rightarrow ^7F_1$ and $^5D_0 \rightarrow ^7F_2$ transitions (see the inset graph in **Figure 8.2**) is used to further determine the splitting on the $^5D_0 \rightarrow ^7F_3$ and $^5D_0 \rightarrow ^7F_4$ transitions. However, the medium to strong $^5D_0 \rightarrow ^7F_4$ transition (as per **Table 8.1**), which its intensity is dependent on the environment, is helpful in completing the pattern. Therefore once the splitting in $^5D_0 \rightarrow ^7F_1$, $^5D_0 \rightarrow ^7F_2$ and $^5D_0 \rightarrow ^7F_4$ is accounted for, the symmetry class in which the complex falls under will be identified and the corresponding splitting pattern undertaking in the sublevels.

The Stark splitting on the all the transitions were read-out from zoomed spectrums for accuracy purposes.

The singlet observed in the $^5D_0 \rightarrow ^7F_0$ transition is indicative of a singles Eu^{III} species in the complex. The number of Stark splitting (triplet, **3**) observed in the magnetic dipole $^5D_0 \rightarrow ^7F_1$ transition for [Eu(TCPB)$_3$Phen] was obtained to be a triplet (**3**) as given in **Figure 8.2**. Subsequently, that dictates the nature of splitting of the hypersensitive $^5D_0 \rightarrow ^7F_2$ transition to give a quintet (**5**) splitting.

With both the $^5D_0 \rightarrow ^7F_3$ and $^5D_0 \rightarrow ^7F_4$ transitions appear to be weak, the $^5D_0 \rightarrow ^7F_4$ transition slightly resolute to account for nonet (**9**). The high number of sub-levels suggests that the complex would stabilize in a low symmetry class as per **Table 8.**2. With the $^5D_0 \rightarrow ^7F_3$ left to have a septet (**7**) Stark splitting as per other resolved transitions above, the symmetry classes that which complex [Eu(TCPB)$_3$Phen] would stabilize in according to **Table 8.2** are *Orthorhombic*, *Monoclinic* and *Triclinic*.

The complete Stark splitting for [Eu(TCPB)$_3$Phen] is illustrated in **Table 8.3**.

8.3.2. Analysis of [Eu(DBBrM)$_3$Phen] [B].

Figure 8.3 illustrates the excitation and emission spectra of [*tris*-(2-Bromo-1,3-diphenyl-propanedione) mono(1,10-phenanthroline)] europium(III)**: [Eu(DBBrM)$_3$Phen**].

The excitation spectrum seems not too broad, ranging from 340 to 384 nm. However, the prime excitation wavelength for maximum emission spectral profile is at 373 nm as exhibited giving rise to the 611 nm emission peak as illustrated in **Figure 8.3**. The Eu^{III} *f-f* excitation lines are not observed in this spectrum.

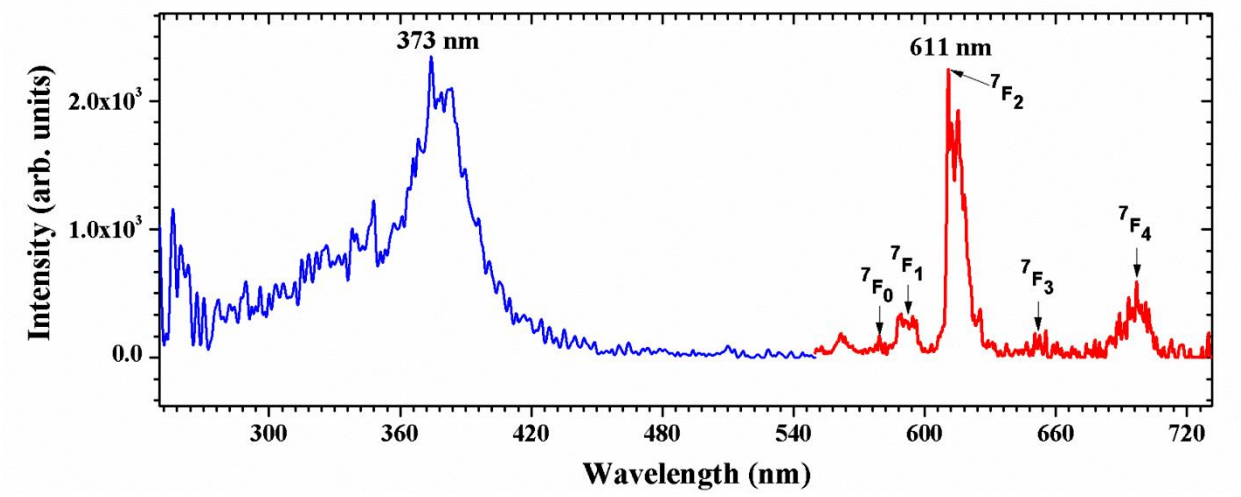

Figure 8.3: Excitation and emission spectra of **B.**

That is subsequent to the suspected nephelauxetic effect taking place in complex [Eu(DBBrM)$_3$Phen]. It is the effect wherein the crystal-field perturbation shifts the barycenters of the $^{2S+1}L_J$ levels. This is often translated to the red shift of the *4f-4f* transitions which is the case in this spectrum, hence their absence. Moreover, these above stated effect could result to the wavelength shift of the $^5D_0 \rightarrow {}^7F_0$ transition to 562 nm and that is common to hydrated complexes undergoing this effect.[9,10,11,12] However, it is not the case in this instance, instead, the transition is suspected to be of $^5D_1 \leftarrow {}^7F_0$ transition.[13]

The existence of splitting $^5D_0 \rightarrow {}^7F_0$ transitions at 580 nm condones the idea of existing possibility of more than one Eu^{III} ion in the complex [Eu(DBBrM)$_3$Phen] and this is observed in the overlapping spectra in **Figure 8.4**. The overlapping is indicated by the respective existence of a pair of a triplet splitting of the $^5D_0 \rightarrow {}^7F_1$ transition and a pair of quintet $^5D_0 \rightarrow {}^7F_2$ transition.

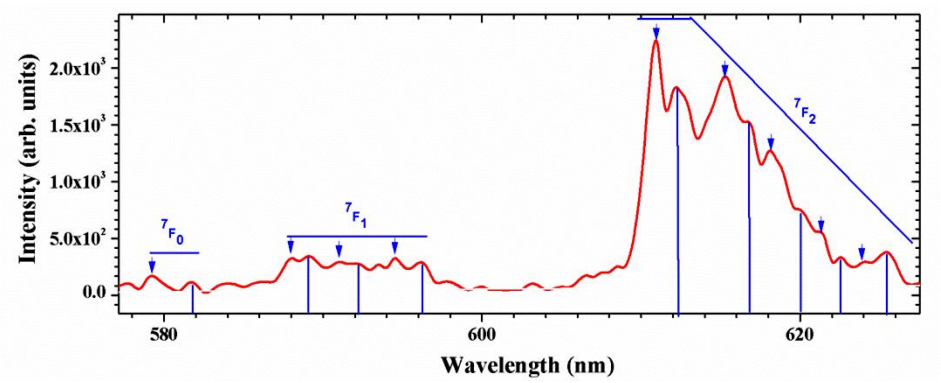

Figure 8.4: Illustration of the pairs of sublevel splitting for $^5D_0 \rightarrow {}^7F_0$, $^5D_0 \rightarrow {}^7F_1$ and $^5D_0 \rightarrow {}^7F_2$ transitions.

The doublet observed in $^5D_0 \rightarrow {}^7F_0$ transition at 580, is well indicative of two Eu^{III} species in the complex. Both the number of Stark splitting (triplet, **3**) observed in the magnetic dipole $^5D_0 \rightarrow {}^7F_1$ transitions for [Eu(DBBrM)$_3$Phen] were obtained to be a triplet (**3**) as given in **Figure 8.3**. Further nature of splitting of the hypersensitive $^5D_0 \rightarrow {}^7F_2$ transitions appears to give a quintet (**5**) splitting.

The $^5D_0 \rightarrow {}^7F_3$ and $^5D_0 \rightarrow {}^7F_4$ transitions appear to be weak; however, $^5D_0 \rightarrow {}^7F_4$ transition is slightly resolute to account for nonet (**9**).

[9] Holz, R.C.; Thompson, L.C., *Inorg. Chem*., **1993**, 32, 5251-5256.

[10] Van der Voort, D.; Blasse, G., *J. Phys. Chem. Solids*, **1991**, 52, 1149-1154.

[11] Choppin, G.R.; Wang, Z.M., *Inorg. Chem*., **1997**, 249-252.

[12] Carnall, W.T.; Fields, P.R; Rajnak, K., *J. Chem. Phys*., **1968**, 49, 4450-4455

[13] Tanner, P.A.; Yeung, Y.Y.; Ning, L., *J. Phys. Chem. A*., **2013**, 117, 2771-2781.

This complex suggests stabilizing in a low symmetry class as per **Table 8.2**. With the $^5D_0 \rightarrow {}^7F_3$ left to have a septet (**7**) Stark splitting in accord to other resolved transitions above, the symmetry classes that which complex [Eu(DBBrM)$_3$Phen] would stabilize in according to **Table 8.2** are also *Orthorhombic*, *Monoclinic* and *Triclinic*.

The complete Stark splitting for [Eu(DBBrM)$_3$Phen] is illustrated in **Table 8.3**.

8.3.3. Analysis of [Eu(DBM)$_3$Phen] (C).

Figure 8.5 illustrates the excitation and emission spectra of [*tris*-(1,3-Diphenyl-propanedione) mono(1,10-phenanthroline)] europium(III): **[Eu(DBM)$_3$Phen]**.

There is a broad spectrum of excitation possibilities ranging from 240 to 430 nm. However, the prime excitation wavelength for maximum emission spectral profile is at 401 nm giving rise to the 611 nm emission peak as exhibited in **Figure 8.5**. The excitation red shift (with respect to the above two discussed spectra) is highly noticeable in **C** and it is overlapping with the Eu^{III} $^5D_2 \leftarrow {}^7F_0$ transition at 464 nm. The $^5D_1 \leftarrow {}^7F_0$ excitation transition is observed with low intensity resonating at 534 nm.

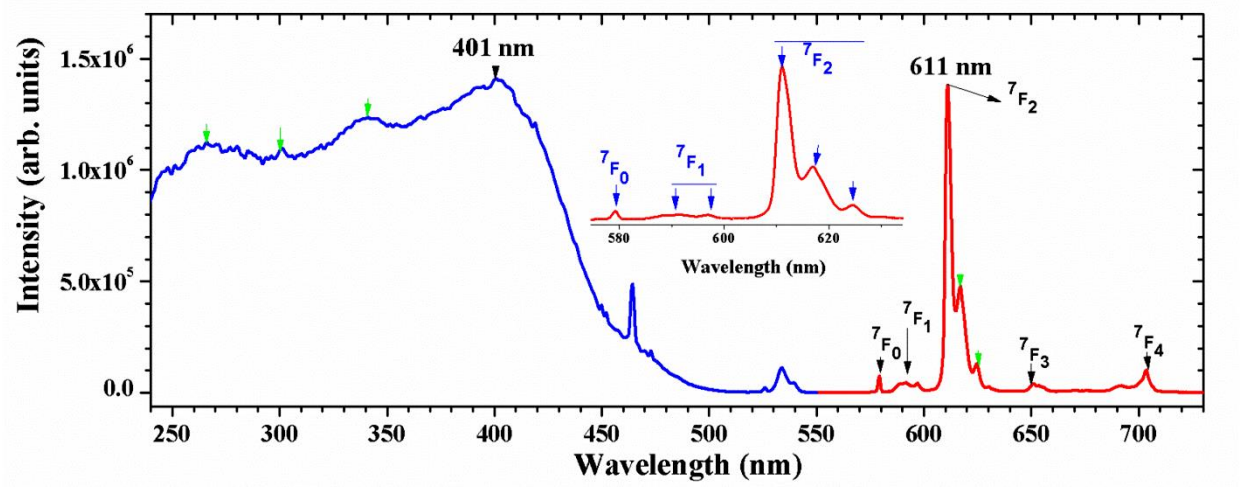

Figure 8.5: Excitation and emission spectra of **C.**

The $^5D_0 \rightarrow {}^7F_0$ emission transition in this europium complex is noticeably more intense than that of $^5D_0 \rightarrow {}^7F_1$ and that was also observed by Kirby et al.[14] The singlet observed in the $^5D_0 \rightarrow {}^7F_0$ transition is indicative of a single Eu^{III} species in the complex.

[14] Kirby, A.F.; Richardson, F.S., *J. Phys. Chem*., **1983**, 87, 2544-2556.

The number of Stark splitting sublevel (doublet, **2**) observed in the magnetic dipole $^5D_0 \rightarrow {}^7F_1$ transition for [Eu(DBM)$_3$Phen] was obtained as given in **Figure 8.5**. Subsequently, that dictates according to **Table 8.2** the splitting of the hypersensitive $^5D_0 \rightarrow {}^7F_2$ transition to give a triplet (**3**) splitting, which corresponds to what is observed in **Figure 8.5**.

The $^5D_0 \rightarrow {}^7F_3$ and $^5D_0 \rightarrow {}^7F_4$ transitions appear to be weak, however, the $^5D_0 \rightarrow {}^7F_4$ transition was observed to account for sextet (**6**) and the $^5D_0 \rightarrow {}^7F_3$ left to have a quintet (**5**) Stark splitting. The high number of sub-levels suggests that the complex would stabilize in a low symmetry class as per **Table 8.2**. The symmetry class which complex [Eu(DBM)$_3$Phen] would stabilize in according to **Table 8.2** is either *Trigonal* or *Hexagonal*. The similar symmetry class (with C_3 as the point group) was observed by Kirby and co-workers from their [Eu(DBM]$_3$(H_2O)] complex.[14]

The complete Stark splitting for [Eu(DBM)$_3$Phen] is illustrated in **Table 8.3**.

8.3.4. Analysis of [Eu(DMC)$_3$Phen] (D).

The illustration in **Figure 8.6** is of the excitation and emission spectra of [*tris*-(3-Chloro-2,4-pentanedione) mono(1,10-phenanthroline)] europium(III): **[Eu(DMC)$_3$Phen]**

There is a broad spectrum of excitation possibilities ranging from 240 to 350 nm. However, the prime excitation wavelength for maximum emission spectral profile is at 296 nm giving rise to the 615 nm emission peak as exhibited in **Figure 8.6**. The three f-f transitions of $^5L_6 \leftarrow {}^7F_{0,1}$, $^5D_2 \leftarrow {}^7F_0$ and $^5D_1 \leftarrow {}^7F_0$ are observed with low intensity resonating at 395, 464 and 534 nm respectively.

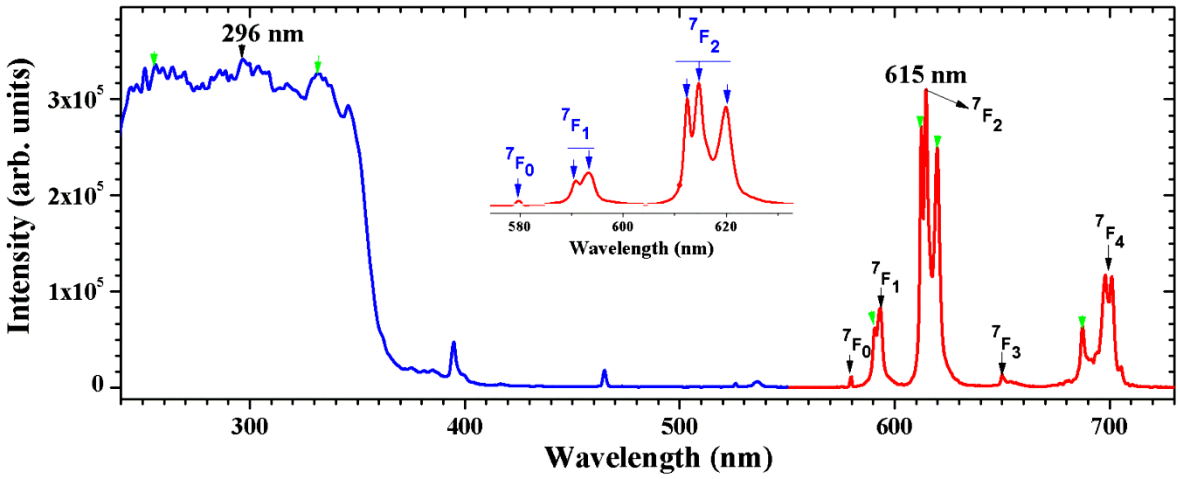

Figure 8.6: Excitation and emission spectra of **D.**

Unlike for complex **C**, there is a blue shift (with about 50 nm difference) in terms of broad ligand excitation spectrum of **D** separated from the Eu^{III} $^5D_2 \leftarrow ^7F_0$ excitation transition. Interestingly both the $^5D_2 \leftarrow ^7F_0$ and $^5D_1 \leftarrow ^7F_0$ transitions occur at longer wavelength relative to the excitation range in the UV range (<300 nm).

This singlet observed in the $^5D_0 \rightarrow ^7F_0$ emission transition is indicative of a single Eu^{III} species in the complex. The number of Stark splitting observed in the magnetic dipole $^5D_0 \rightarrow ^7F_1$ transition for $[Eu(DMC)_3Phen]$ was obtained to be a doublet (**2**) as given in **Figure 8.6**. Subsequently, that dictates the splitting of the hypersensitive $^5D_0 \rightarrow ^7F_2$ transition to give a triplet (**3**) splitting and that is nicely illustrated on the inset graph in **Figure 8.6**.

It was observed that the $^5D_0 \rightarrow ^7F_1$ and $^5D_0 \rightarrow ^7F_4$ transitions are very pronounced. However, it was learnt from Binnemans[8] that the intensity of the $^5D_0 \rightarrow ^7F_4$ transition should be compared to that of $^5D_0 \rightarrow ^7F_1$ and not in terms of absolute values. If that is the case, it is known that the total intensity of the $^5D_0 \rightarrow ^7F_1$ transition applies only to the total integrated intensity if the transition itself and not the crystal field components.[15]

The $^5D_0 \rightarrow ^7F_3$ transitions appear to be very weak. The $^5D_0 \rightarrow ^7F_4$ transition account for sextet (**6**) Stark splitting and the $^5D_0 \rightarrow ^7F_3$ give a quintet (**5**) Stark splitting. The symmetry class that which complex $[Eu(DMC)_3Phen]$ would stabilize in according to **Table 8.2** is either *Trigonal* or *Hexagonal*.

The complete Stark splitting for $[Eu(DMC)_3Phen]$ is illustrated in **Table 8.3**.

[15] Gorller-Walrand, C.; Fluyt, L.; Ceulemans, A.; Carnall, W.T., *J. Chem. Phys*., **1991**, 95, 3099-3106.

8.3.5. Analysis of [Eu(TMHD)$_3$Phen] (E).

The spectrum in **Figure 8.7** illustrates the excitation and emission spectra of [*tris*-(2,2,6-Trimethyl-3,5-heptanedione) mono (1,10-phenanthroline) europium(III)]: [**Eu(TMHD)$_3$Phen]**.

There is a broad spectrum of excitation possibilities ranging from 240 to 400 nm. However, the prime excitation wavelength for maximum emission spectral profile is at 332 nm giving rise to the 612 nm emission peak as exhibited in **Figure 8.7**. The ligand excitation red shift is noticeable in **E** relative to **D** with prominent *f-f* transitions $^5D_2 \leftarrow ^7F_0$ and $^5D_1 \leftarrow ^7F_0$ resonating at 464 and 534 nm respectively.

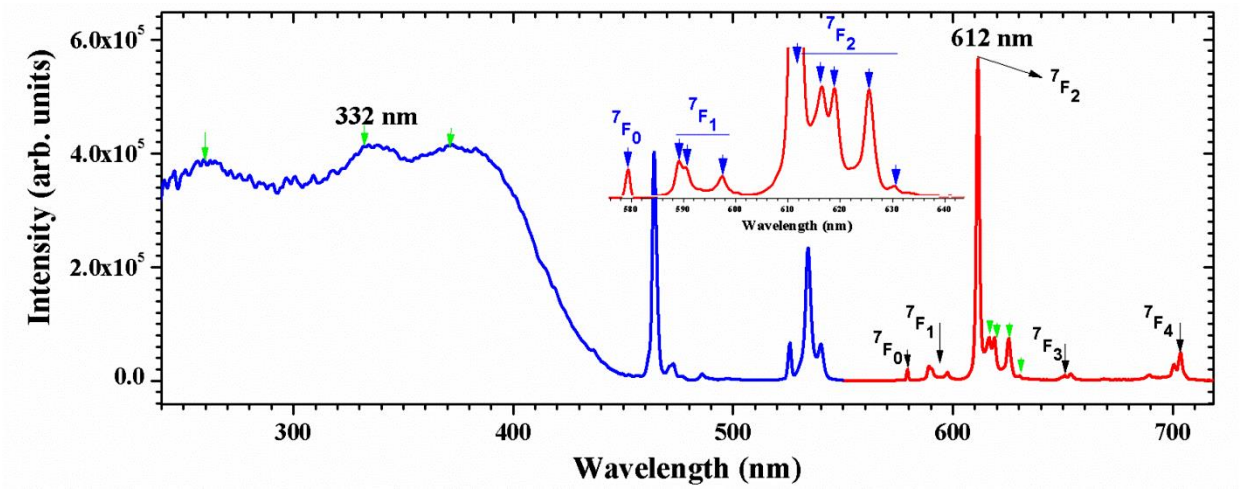

Figure 8.7: Excitation and emission spectra of **E.**

The singlet is also observed in this spectrum for the $^5D_0 \rightarrow ^7F_0$ transition and is indicative of a single Eu^{III} species in the complex. The number of Stark splitting observed in the magnetic dipole $^5D_0 \rightarrow ^7F_1$ transition for [Eu(TMHD)$_3$Phen] was found to be a triplet (**3**) as given in **Figure 8.7**. The nature of splitting (influenced by the $^5D_0 \rightarrow ^7F_1$ transition) in the hypersensitive $^5D_0 \rightarrow ^7F_2$ transition is a quintet (**5**).

Both the $^5D_0 \rightarrow ^7F_3$ and $^5D_0 \rightarrow ^7F_4$ transitions are weak, the $^5D_0 \rightarrow ^7F_4$ transition slightly resolute was deduces to have nonet (**9**) Stark splitting. The high number of sub-levels reflects that the complex would stabilize in a low symmetry class as per **Table 8.2**. The $^5D_0 \rightarrow ^7F_3$ transition must give a septet (**7**) Stark splitting as per other resolved transitions above, the symmetry classes that which complex [Eu(TMHD)$_3$Phen] would stabilize in according to **Table 8.2** are *Orthorhombic*, *Monoclinic* and *Triclinic*.

The complete Stark splitting for [Eu(TMHD)$_3$Phen] is illustrated in **Table 8.3**.

8.3.6. Analysis of [Eu $(PCA)_3$(Phen)] (F)

Figure 8.8 depicts the excitation and emission spectra of [*tris*-(benzoic acid) *bis*-(1,10-phenanthroline) europium(III)]: **[Eu$(PCA)_3$Phen]**.

The excitation range seems really to be short, ranging from 240 to 290 nm. However, the prime excitation wavelength for maximum emission spectral profile is at 286 nm giving rise to the 616 nm emission peak as exhibited in **Figure 8.8**. Due to the electron deficiency of the coordinated organic ligand; a large number of *f-f* tranasitions of the Eu ion are exposed for excitation. Nonetheless, the emission spectrum observed in **Figure 8.8** is excited from the organic molecule coordinated to the metal ion. However there are non-radiative relaxation or rather reduced sensitization effect for [Eu$(PCA)_3$Phen] and this phenomenon was also observed by da Silva et al.[16,17.]

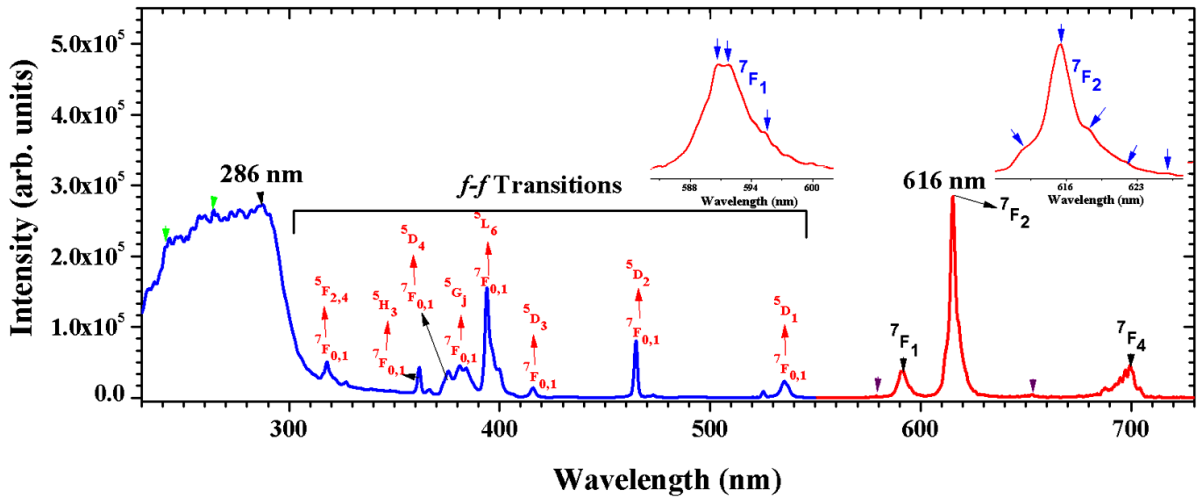

Figure 8.8: Excitation and emission spectra of **F.**

The ligands excitation spectrum blue shift is a result of electron deficiency or rather the minimal electron cloud from the organic matrix bonded to the metal ion. This phenomenon was observed by de Oliveira and co-workers.[18] Therefore it is deduced from this, that broad excitation peaks are a result of high electron efficiency from the organic matrix, preferably from aromatic constituency.

[16] da Silver, F.F.; da Menezes, F.L.; da Luz, L.L.; Alves, S., *New J. Chem*., **2014**, 38, 893-896.

[17] De Jesus, R.A.; da Luz, L.L.; Santos, D.O.; Santana, J.A., Navickiene, S.; Gatto, C.C.; Alves, S.; de Mesquita M.E., *Dalton Trans*., **2015**, 44, 17318-17325.

[18] de Oliveira, T.C; Santos, H.P.; Lahoud, M.G.; Franco, D.F.; Freire, R.O.; Dutra, J.D.L.; Cuin, A.; de Lima, J.F.; Marques, L.F., *J. Lumin*., **2016**, http://dx.doi.org/10.1016/j.jlumin.2016.09.024.

The $^5D_0 \rightarrow {}^7F_0$ and $^5D_0 \rightarrow {}^7F_3$ emission transitions are somewhat suppressed to none as observed above in **Figure 8.8**. Therefore the resolution of the entire spectrum relies on the Stark splitting occurring between the $^5D_0 \rightarrow {}^7F_1$, $^5D_0 \rightarrow {}^7F_2$ and the $^5D_0 \rightarrow {}^7F_4$ transition.

The number of Stark splitting observed in the magnetic dipole $^5D_0 \rightarrow {}^7F_1$ transition for $[Eu(PCA)_3Phen]$ was found to be a triplet (**3**) as given in **Figure 8.8**. The nature of splitting (influenced by the $^5D_0 \rightarrow {}^7F_1$ transition) in the hypersensitive $^5D_0 \rightarrow {}^7F_2$ transition is a quintet (**5**).

In the absence of the $^5D_0 \rightarrow {}^7F_3$ transition, the $^5D_0 \rightarrow {}^7F_4$ transition is well resolute to account for nonet (**9**) Stark splitting. The high number of sub-levels reflects that the complex would stabilize in a low symmetry class as per **Table 8.2**. The $^5D_0 \rightarrow {}^7F_3$ transition gives a septet (**7**) Stark splitting as per other resolved transitions above, the symmetry classes that which complex $[Eu(PCA)_3Phen]$ would stabilize in according to **Table 8.2** are *Orthorhombic*, *Monoclinic* and *Triclinic*.

The complete Stark splitting for $[Eu(PCA)_3Phen]$ is illustrated in **Table 8.3**.

8.3.7. Analysis of $[Eu_2(BCA)_6(Phen)_2]$ (G)

Figure 8.9 illustrates the excitation and emission spectra of {[*hexa*-(Benzyl carboxylic acid) *bis*-(1,10-phenanthroline) di-europium(III)]-μ-[κ^2-O,O'-(benzyl carboxylic acid)}: **{$[Eu_2(BCA)_6(Phen)_2]$-μ-[κ^2O,O'-BCA]$_2$}.**

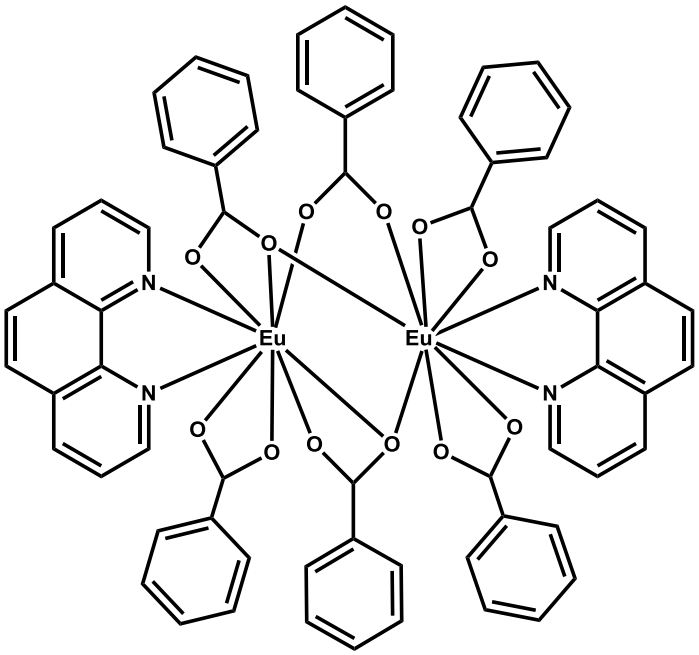

Figure 8.9: Schematic illustrations of Eu^{III} di-nuclear complex.

There is a broad spectrum of excitation possibilities ranging from 240 to 350 nm. However, the prime excitation wavelength for maximum emission spectral profile is at 334 nm giving rise to the 613 nm emission peak as exhibited in Figure 8.10. Unlike in complex **F**, there is a red shift (with about 50 nm difference) in terms of excitation spectra of **H**. Therefore, with more organic constituency around the Eu^{III} ions, the excitation wavelength broadened and resulted in overlapping with early higher excited states as observed in **Figure 8.8**.

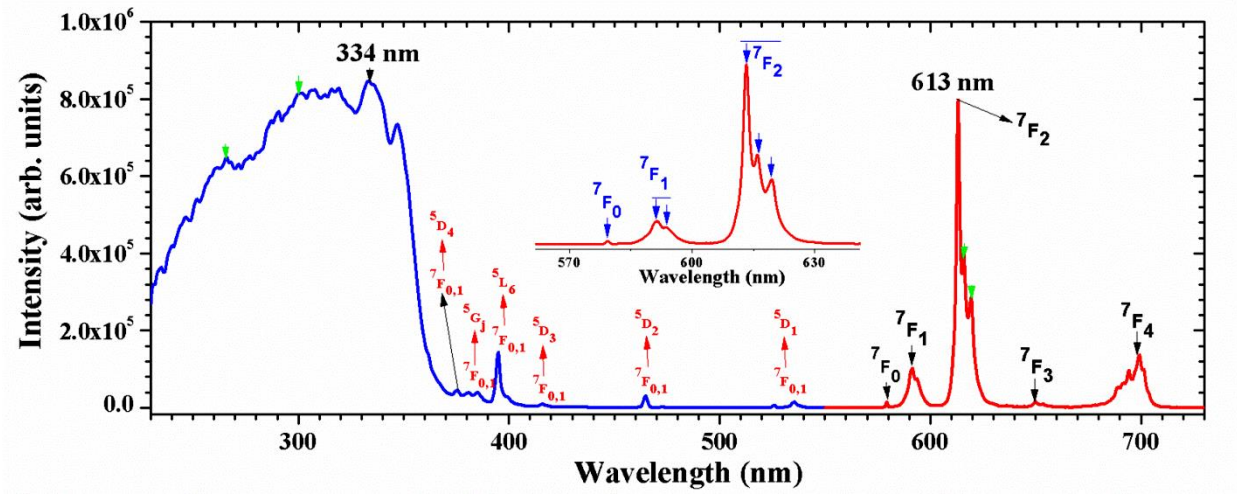

Figure 8.10: Excitation and emission spectra of **H.**

The number of Stark splitting observed in the magnetic dipole $^5D_0 \rightarrow {}^7F_1$ transition for $[Eu_2(PCA)_6(Phen)_2]$ was found to be a doublet (**2**) as given in **Figure 8.8**. The nature of splitting (influenced by the $^5D_0 \rightarrow {}^7F_1$ transition) in the hypersensitive $^5D_0 \rightarrow {}^7F_2$ transition is a triplet (**3**).

The $^5D_0 \rightarrow {}^7F_0$ and $^5D_0 \rightarrow {}^7F_3$ transitions are somewhat suppressed to none as observed above in **Figure 8.8**. The $^5D_0 \rightarrow {}^7F_3$ and $^5D_0 \rightarrow {}^7F_4$ transitions appear to be weak, however, the $^5D_0 \rightarrow {}^7F_4$ transition to account for sextet (**6**) and the $^5D_0 \rightarrow {}^7F_3$ in its low intensity is left to resonate with a quintet (**5**) Stark splitting. The symmetry class that which complex $[Eu_2(PCA)_6(Phen)_2]$ would stabilize in accordance to **Table 8.2** is *Trigonal* with D_{3d}, D_3, C_{3v}, C_{3i}, C_3 as point group choices.

The complete Stark splitting for $[Eu_2(PCA)_6(Phen)_2]$ is illustrated in **Table 8.3**.

8.4. Reflectance

Figure 8.13 gives the reflectance spectra of selected *β*-diketonate Eu^{III} complexes presented in this chapter.

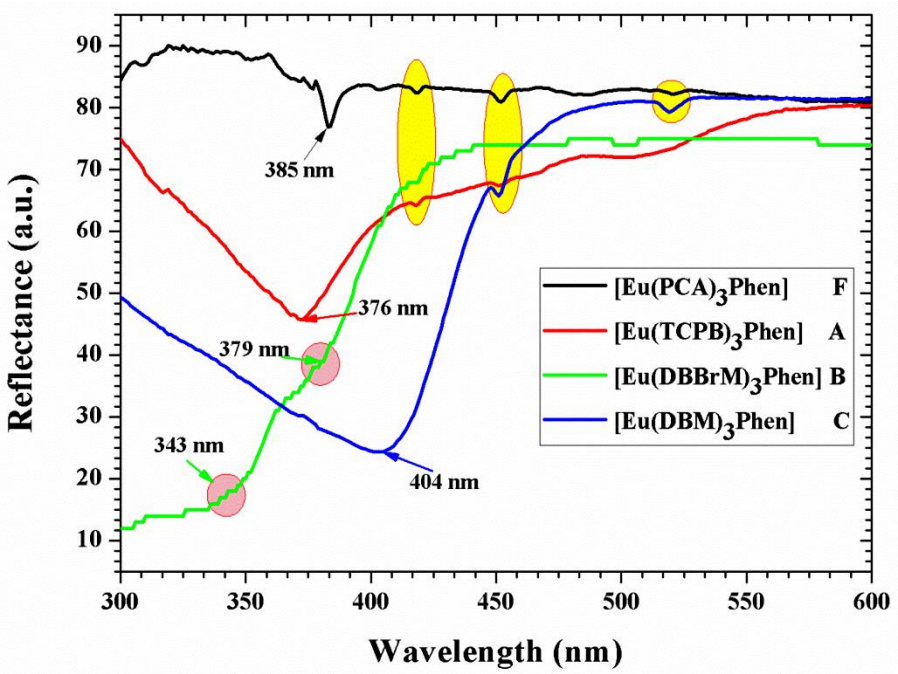

Figure 8. 11: Reflectance spectra of selected *β*-diketonate Eu^{III} complexes.

The illustrated reflectance data have minima (absorption) which correspond well with the relative excitation wavelengths of the respective complexes of concern. The primary excitation wavelength (286 nm) of **F** is out of range because the instrument tends to give artefacts in the shorter wavelength region. However, the absorption at 385 nm is close to the strongest *f-f* excitation band seen in **Figure 8.8**.

It is in **Figure 8.11** where there is also dual peak reflectance at the highlighted area in the **B** spectrum (green line). This behaviour somewhat corroborate the notion posed; on the possibility of having two metal ions sharing the same symmetry. Therefore with majority of the Eu^{III} complexes affected by the nephelauxitic effect (discussed in **Section 8.3.2**.) being hydrated, it is then suggested that the other molecule in the asymmetric unit cell is a diaqua Eu^{III} species and the other one is 1,10-phenanthroline substituted as an ancillary ligand.

Further observed in **Figure 8.13**, are the reflective higher excited states transitions of $^5D_1 \leftarrow ^7F_0$, $^5D_2 \leftarrow ^7F_0$ and $^5D_3 \leftarrow ^7F_0$ transitions as indicated in yellow oval markers. These transitions are in accordance to what was observed in the excitation spectra of respective complexes.

8.5. Quantum Yields

Only complexes with high emission intensity were considered for quantum yields measurements. The quantum yields of the samples **A**, **C**, **E** and **H** were measured for excitation at 340 nm using an integrating sphere. The data is shown in the **Figure 8.12** and **Table 8.4**. Sample **A** has an excellent quantum yield of 82% and that was due to the efficient energy transfer posed by the 1,10-phenanthroline ligand since it was observed to have the strongest bind to the Eu^{III} metal ion.[19] The lower absorption and significant output near 700 nm contribute to the quantum yield of sample **H** compared to sample **E**. The quantum yield at other wavelengths that may be of interest was also measured in a similar way and are given in the **Table 8.4**.

The direct excitation of Eu^{III} ions for sample **E** at the 464 nm *f-f* absorption line (see **Figure 8.7**) gives a quantum yield of 55%, significantly larger than for the shorter excitation wavelengths, because although output is similar the broadband absorption at shorter wavelengths is greater.

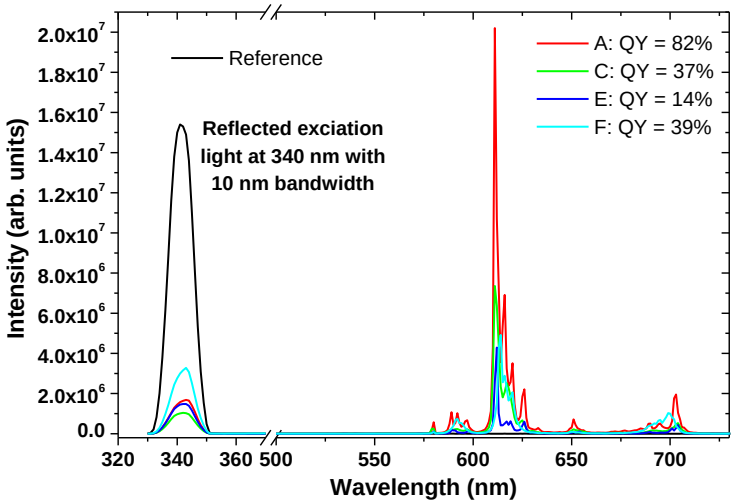

Figure 8.12: The quantum yield data of selected Eu^{III} based complexes excited at 340 nm.

Table 8.4: Quantum yields of the samples.

	Exc. 340 nm	Exc. 380 nm	Exc. 400 nm	Exc. 464 nm
Sample A	82%	73%		
Sample C	37%		29%	
Sample E	14%	13%		55%
Sample H	39%			

[19] Ishii, A.; Hasegawa, Miki, Scientific Reports | 5:11714 | DOI: 10.1038/srep11714.

8.6. Discussion and Conclusions

The analysis of the above discussed complexes was purely solid state based. The spectra given in **Figure 8.2** to **Figure 8.10** gave a wide insight on the relative excitation and emission nature of these Eu^{III} based β-diketonate complexes. All the used organic matrices have successfully helped in the sensitization of the Eu^{III} ion; some in the most luminous way and with lot of information but some had low luminescence capacity.

The main arguments made in the analysis were based on the emission spectral identity and also the nature of the emitting transitions of the respective complexes. The influence of β-diketones organic compounds on the Eu^{III} metal ion, using the 1,10-phenanthroline ligand as the ancillary ligands, was extensively explored and analysed in this chapter. It was further observed that each luminescence spectra had a different spectral identity which was the direct translation of the ligand effect coordinated to the metal ion. Different excitation and emission spectra observed in this chapter resulted from the symmetry these organic mediums impose on the metal ion and also the effect of the respective substituents on the backbone of these ligand species.

The excitation spectra of Eu^{III} complexes are composed of broad band assigned to the S_0-S_1 (π, π^*) transitions of the aromatic moiety and narrow bands assigned the f-f transition of the higher excited states. These absorption bands are originated from the $^7F_0$ ground state to the excited levels and remain approximately invariable in each Eu^{III} complexes. Their appearance in the excitation spectrum is subject to the electron cloud the organic matrices impose on the Eu^{III} metal ion.

The results obtained from this chapter will be further used to correlate with the crystallographic data obtained in chapter 6.

9 Luminescence and Crystallographic Correlation of Eu^{III} Complexes.

In this chapter:
A comparison between the obtained crystallographic and photoluminescence data for crystallized Eu^{III} based complexes in this project. Any two-way scientific influence of one field to the other.

9.1. Introduction

An overarching theme throughout the preceding chapters has focused on the investigation of various ligand effects on the photo-physics of the solid state properties of Eu^{III} β-diketonate complexes. According to the literature study reported in Chapter 2, it was clear that the organic ligand sensitized Europium (III) based complexes were used across different scientific fields. In some cases the metal is immersed in complex organic matrices. A comprehensive survey of the fundamental photo-physics of these Eu^{III} base complexes is essential for optimizing their optical properties and exploring new applications. Therefore the meaningful incorporation of crystallography to this survey could play an integral part to the study.

In Chapter 6 the crystallographic investigation of Eu^{III} β-diketonate complexes was discussed. The discussions entailed various solid state properties such as inter and intra-molecular interactions, solid-state crystal packing and coordination modes. This study sheds much light with relation to coordination preferences, stability of the compounds and the effects of ligand substituents on the crystal systems.

In Chapter 8 the photoluminescence investigations of Eu^{III} β-diketonate complexes was undertaken. Therein detailed analysis of the luminescence spectral identities, imposed by different organic matrices, of the respective Eu^{III} β-diketonate complexes was obtained.

In this chapter, the systematic integration of the photoluminescence and the crystallographic data is combined, compared and correlated for the selected Eu^{III} β-diketonate complexes. The subsections below attempt to systematically present the correlations drawn between the different properties of the complexes such as luminescence spectral splitting and crystallographic geometric conformations induced by the surrounding organic molecules around the metal centre.

9.2. Correlation of Results

The summary of the crystallographic data and number of Stark splitting sublevels of selected complexes is given in **Table 9.1**.

Table 9.1: The summary of results pertaining the analysis of complexes **1**, **2** and **3**.

Crystal Formula	**[Eu(TCPB)$_3$Phen] (1)**	**[Eu(TMHD)$_3$Phen] (2)**	**[Eu$_2$(BCA)$_6$(Phen)$_2$] (3)**
Empirical formula	$C_{42}H_{23}Cl_3EuF_9N_2O_6$	$C_{45}H_{65}EuN_2O_6$	$C_{66}H_{46}Eu_2N_4O_{12}$
Crystal system, Space Group	Monoclinic, $P2_1/n$	Triclinic, P-1	Triclinic, P-1
Temperature (K)	100 (2)	100 (2)	100 (2)
Unit Cell Dimensions			
***a* (Å)**	12.097(3)	10.860 (6)	10.761 (5)
***b* (Å)**	19.354(5)	12.285 (4)	11.865 (5)
***c* (Å)**	21.031(5)	18.398 (4)	12.275 (4)
α, β, γ (°)	90, 104.11(5), 90	80.39 (5), 87.58 (5), 68.76 (4)	105.04 (4), 93.81(5), 112.9 (4)
Volume (Å^3), Z	4528.6(16), 4	2255.3 (15), 2	1369,2 (10), 1
Density (g/cm^3)	1.585	1.299	1.687
Relative Point Groups			
Luminescence	C_{2h}	C_i	C_i
Crystallographic crystal	C_{2h}	C_i	C_i
Polyhedron Geometry	D_{2d}	D_{4d}	D_{3h}
Quantum Yields (%) (ex. 340 nm)	82	14	39
Number of Stark Splitting in Sub-levels			

Complex		^{7}**F$_0$** ($J=0$)	^{7}**F$_1$** ($J=1$)	^{7}**F$_2$** ($J=2$)	^{7}**F$_3$** ($J=3$)	^{7}**F$_4$** ($J=4$)
[Eu(TCPB)$_3$Phen]	**(1)**	1	3	5	7	9
[Eu(TMHD)$_3$Phen]	**(2)**	1	3	5	7	9
[Eu$_2$(PCA)$_6$(Phen)$_2$]	**(3)**	1	2	3	5	6

The relativeness in the point groups obtained from the luminescence, crystallography and the constructed polyhedrons is illustrated in **Figure 9.1**. The point groups of the crystal data corroborate well with that of photoluminescence, however, the point group deduced from the constructed polyhedrons differs. That is mainly because of the relative atomic orientation of ligands around the Eu^{III} metal centre, influenced by steric hindrance, somewhat distorts the polyhedrons to higher symmetry classes.

9.2.1 Correlation Analysis of [Eu(TCPB)$_3$Phen] (1)

The depiction in **Figure 9.1** illustrates the excitation and emission spectra of [*tris*-(4,4,4-trifluoro-1-chlorophenyl-butanedione) mono(1,10-phenanthroline)] europium(III): **[Eu(TCPB)$_3$Phen]**.

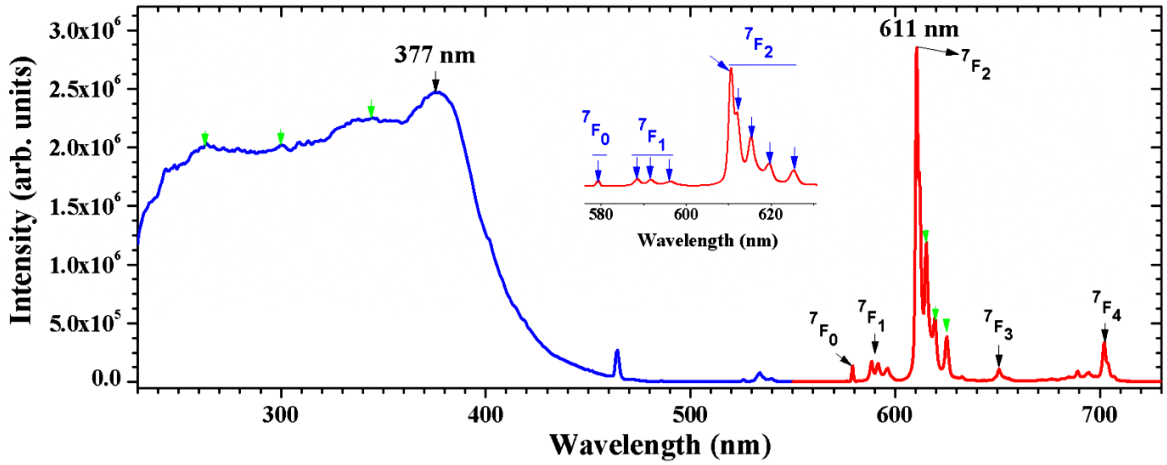

Figure 9.1: Excitation and emission spectra of **[Eu(TCPB)$_3$Phen]** (**1**).

The corresponding crystal structure is given in **Figure 9.2**.

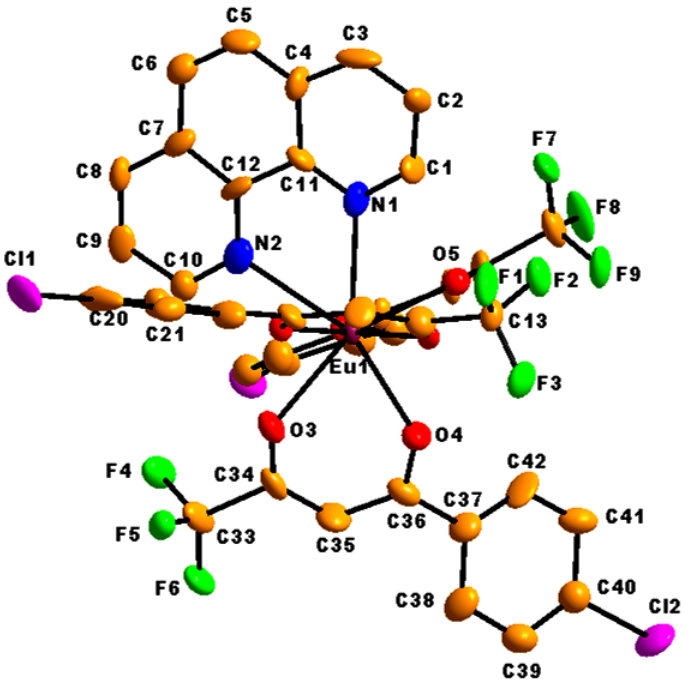

Figure 9.2: Crystal structure of **[Eu(TCPB)$_3$Phen]** (**1**).

The detailed analysis of the spectra exhibited in **Figure 9.1** (see **Section 8.3.1),** with regards to the extent to which Stark splitting occurs, yielded that the symmetry class in which this spectra belongs to is either *Orthorhombic*, *Triclinic* or *Monoclinic.*

A polyhedron was constructed in **Figure 9.3** portraying the coordination geometry of the organic ligands around the metal ion.

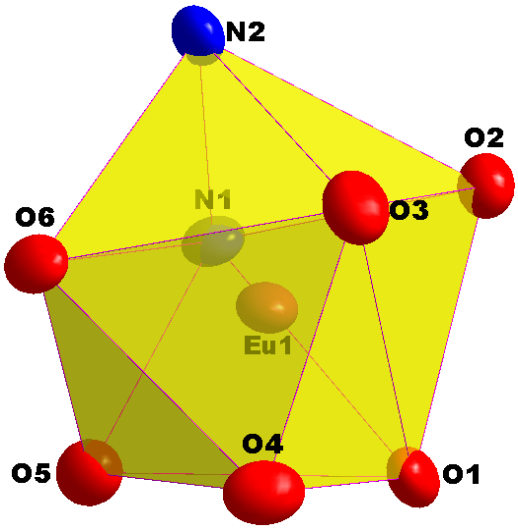

Figure 9.3: Schematic Illustration of coordination geometry of **1**.

The polyhedron is constituted by eight coordinated atoms, consisting of six oxygen and two nitrogen atoms. It therefore prefers either dodecahedron or squared antiprism as discussed in **Section 2.1.2.** However, the crystallographic data in **Table 9.1** indicates that complex **1** crystallized in a *monoclinic* crystal system in a $P2_1/n$ (C_{2h} point group) space group.

Moreover, the constructed polyhedron with 8 vertices, 12 triangle faces and 18 edges conforms to be of a *Snub Disphenoid* (D_{2d}),[1] which is a distorted sub class of dodecahedron polyhedron.

The results are in accord with the fact that, the existence of the $^5D_0 \rightarrow {}^7F_0$ transition is often indicative of the site (C_{nv}, C_n, *or* C_s) symmetry in which the Eu^{III} occupies.[2]

[1] Merkens, C.; Englert, U., *Dalton Trans*., **2012**, 41, 4664-4673.

[2] Binnemans, K.; Gorller-Walrand, C., *J. Rare Earths*., **1996**, 14, 173-180.

The measure of quantum yield for the complex in **Figure 9.2** was found to be 82%. The observed halide (Cl and F) atoms in the crystal structure may be allowing the strong bonding across molecules (via inter- and intra-molecular interaction) in the solid state, minimizing deformations and associated non-radiative transitions. Moreover, Tu et al., observed that the crystallographic symmetry site potentially influences the emission intensity of the crystal structure.[3] It is then observed in **Figure 9.4** that the screw axis drives through all the Eu^{III} atoms in the unit cell and therefore could contribute to the observed high quantum yield in **1**.

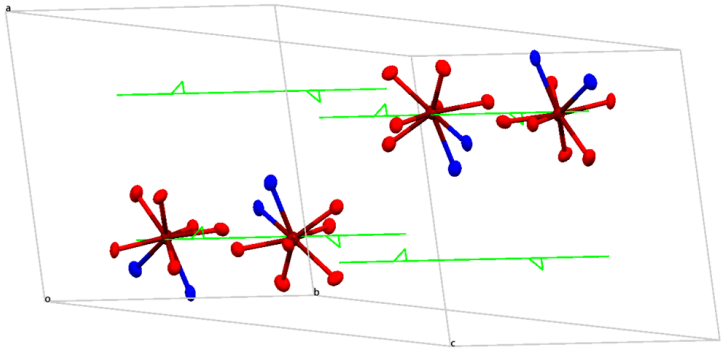

Figure 9.4: Molecular packing of **1** with the depiction of the screw axis symmetry element.

9.2.2 Correlation Analysis of [Eu(TMHD)$_3$Phen] (2)

The spectrum in **Figure 9.5** illustrates the excitation and emission spectra of [*tris*-(2,2,6-Trimethyl-3,5-heptanedione) mono (1,10-phenanthroline) europium(III)]: [**Eu(TMHD)$_3$Phen]**.

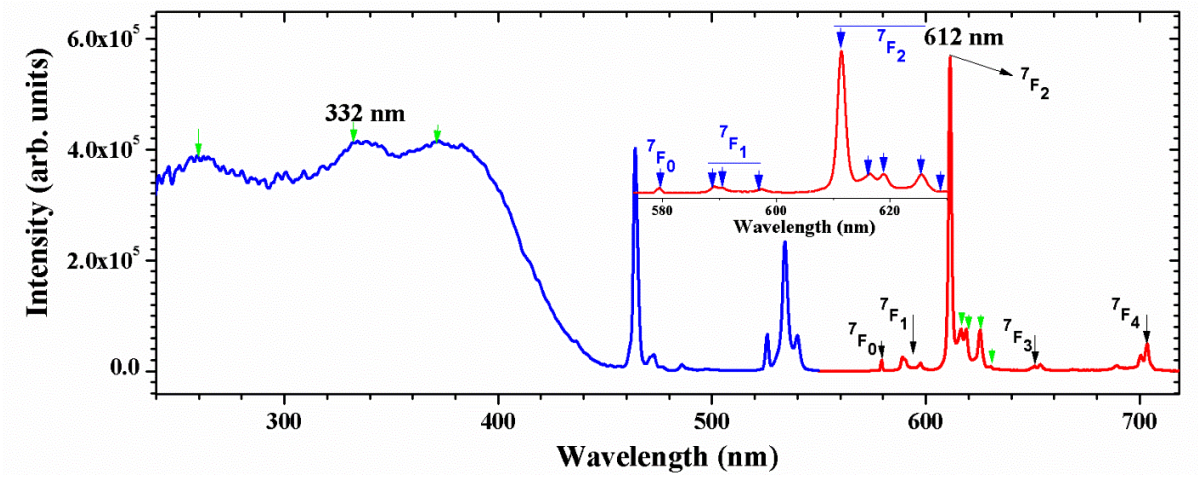

Figure 9.5: Excitation and emission spectra of **[Eu(TMHD)$_3$Phen]** (2).

[3] Tu, D.; Liu, Y.; Zhu, H.; Li, R.; Liu, L.; Chen, X., *Angewandte Chem.*, **2013**, 125 (4), 1166-1171.

The corresponding crystal structure is given in **Figure 9.6**.

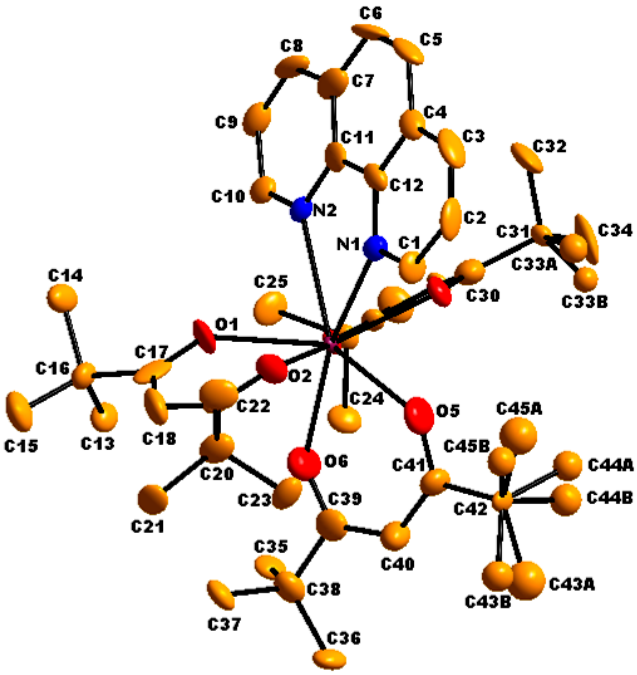

Figure 9.6: Crystal structure of **[Eu(TMHD)$_3$Phen]** (**2**).

The detailed analysis of the spectra exhibited in **Figure 9.5** (see **Section 8.3.5),** gave an indication that the symmetry class corresponding this spectra is either *Orthorhombic*, *Triclinic* or *Monoclinic* as per **Table 9.2**.

A polyhedron was constructed in **Figure 9.7** portraying the coordination geometry of the organic ligands around the metal ion.

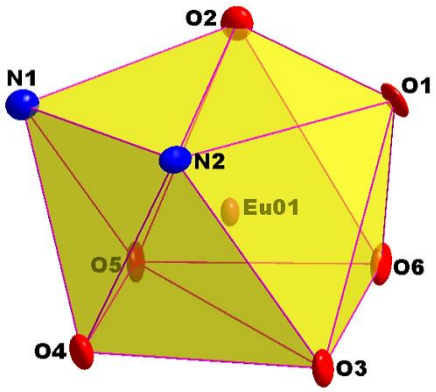

Figure 9.7: Schematic Illustration of coordination geometry of **2**.

The polyhedron is constructed around the six coordinated oxygens of three TMHD (2,2,6-Trimethyl-3,5-heptanedione) moieties and the two nitrogens of the 1,10-phenanthroline ancillary ligand. It therefore prefers either dodecahedron or squared antiprism as discussed in **Section 2.1.2.**

However, the crystallographic data in **Table 9.1** indicates that complex **2** crystallized in a *Triclinic* crystal system in a *P*-1 (C_i point group) space group.

The constructed polyhedron with 8 vertices, 8 triangle faces and 16 edges conforms to be of a *Square Antiprism* (D_{4d}).

The results are in accord with the fact that, the existence of the $^5D_0 \rightarrow {}^7F_0$ transition is often indicative of the site (C_{nv}, C_n, *or* C_s) symmetry in which the Eu^{III} occupies.

9.3. Correlation Analysis of {[$Eu_2(BCA)_6(Phen)_2$]- μ-[κ^2-O,O'-(BCA)]} (3)

The spectrum in **Figure 9.8** illustrates the excitation and emission spectra of {[*hexa*-(Benzyl carboxylic acid) *bis*-(1,10-phenanthroline) di-europium(III)]-μ-[κ^2-O,O'-(benzyl carboxylic acid)}: **{[$Eu_2(BCA)_6(Phen)_2$]- μ-[κ^2-O,O'-(BCA)]$_2$}** (**3**).

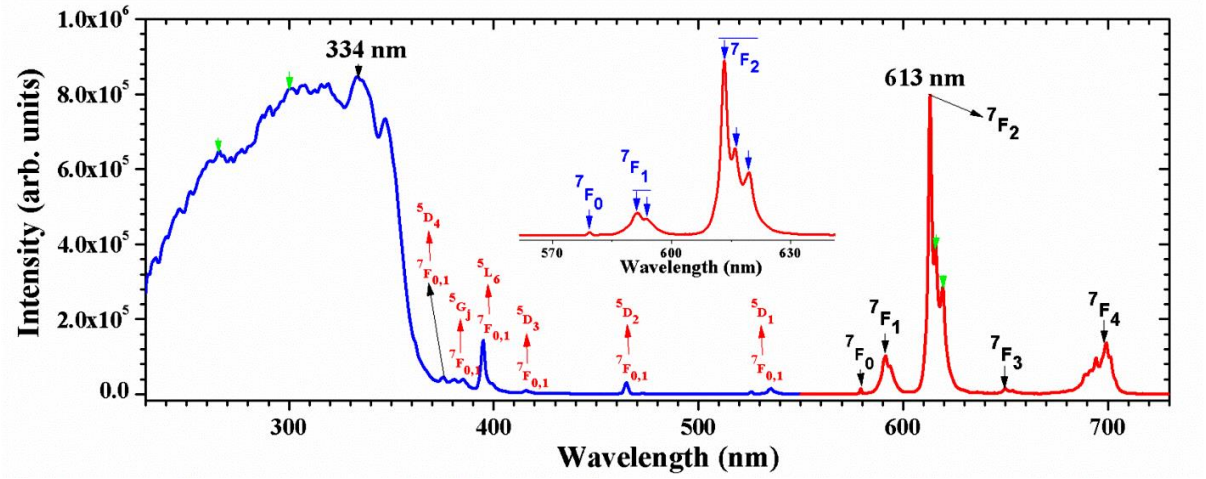

Figure 9.8: Excitation and emission spectra of **{[$Eu_2(BCA)_6(Phen)_2$]- μ-[κ^2-O,O'-(BCA)]$_2$}(3).**

The corresponding crystal structure is given in **Figure 9.5**.

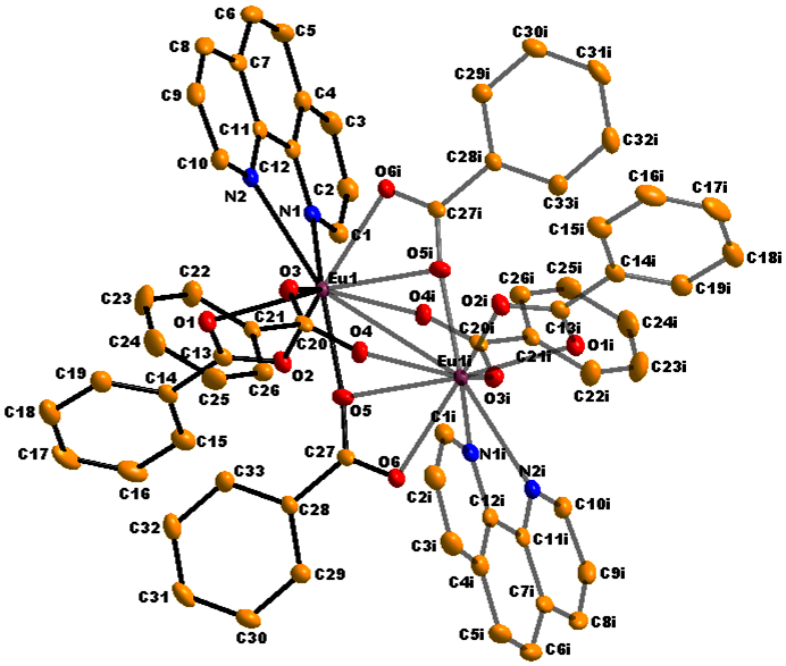

Figure 9.9: Crystal structure of **{[$Eu_2(BCA)_6(Phen)_2$]- μ-[κ^2-O,O'-(BCA)]$_2$}(3).**

The detailed analysis of the spectra exhibited in **Figure 9.8** (see **Section 8.3.7)**, gave an indication that the symmetry class corresponding to this spectra is either *hexagonal* or *trigonal.*

A polyhedron was constructed in **Figure 9.10** portraying the coordination geometry constituted by the organic ligands around the metal ions.

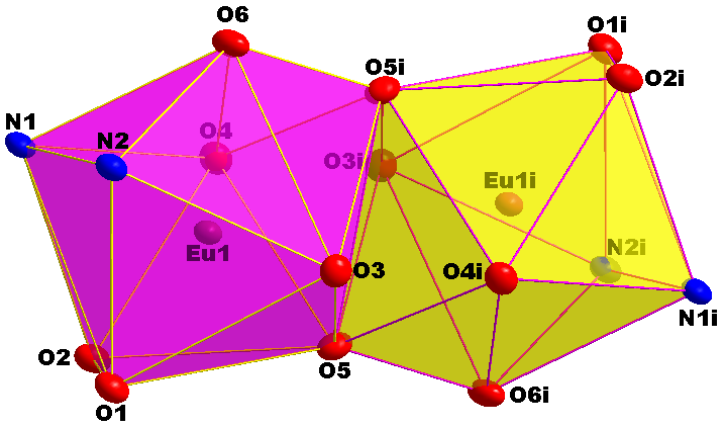

Figure 9.10: Schematic illustration of dual coordination geometry of **3**.

The polyhedral constructed around the dimeric structure is of coordination geometry around two Eu^{III} metal centres. There are nine coordinated atoms from the dimeric nature of the crystal.

The atomic orientation around the Eu^{III} ions consists of seven oxygen and two nitrogen atoms. The dual polyhedral geometries prefer either capped square antiprism or capped trigonal prism as discussed in **Section 2.1.2.**

The crystallographic data in **Table 9.1** indicates that complex **3** crystallized in a *Triclinic* crystal system in a *P*-1 (C_i point group) space group. However, the symmetry class from the crystallographic results is not in accordance with the spectral splitting of **3** as read from **Table 9.1** and **Figure 9.8**.

The polyhedron was then constructed for atoms only in the asymmetric unit cell with only one Eu^{III} centre as exhibited in **Figure 9.11**.

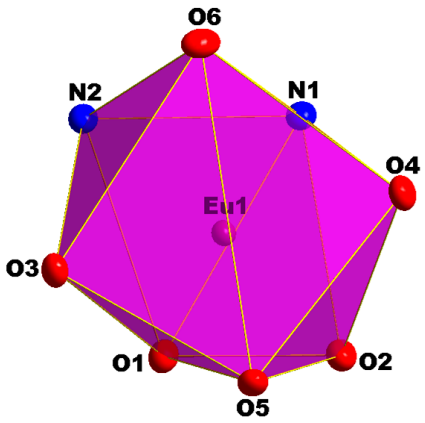

Figure 9.11 Schematic Illustration of mono coordination geometry of **3**.

The polyhedron constructed in **Figure 9.11** is of a distorted *Bicapped Trigonal Prism* (D_{4d}).[4,5] This polyhedron corroborates well with the D_{3h} point group in the *hexagonal* symmetry class.

However, the observation of the $^5D_0 \rightarrow {}^7F_0$ transition is an indication that the Eu^{III} ion occupies a site with C_{nv}, C_n *or* C_s symmetry. In principle, this means any other point group outside the restriction given both in the low (*trigonal)* and high (*hexagonal)* symmetry classes is not allowed. Nonetheless, Nieuwpoort and Blasse noticed that the $^5D_0 \rightarrow {}^7F_0$ transition always appears whenever it is allowed by the observed site symmetry.

[4] de Oliveira, T.C; Santos, H.P.; Lahoud, M.G.; Franco, D.F.; Freire, R.O.; Dutra, J.D.L.; Cuin, A.; de Lima, J.F.; Marques, L.F., *J. Lumin.*, **2016**, http://dx.doi.org/10.1016/j.jlumin.2016.09.024.

[5] Ma, J.; Liu, Y.; Yang, J.; Liu, Y.; Ma, J.F., *Cryst. Eng. Comm.*, **2011**, 13, 3498-3505.

Subsequently, it is believed that in di-nuclear complexes, the luminescence depends on the atomic orientation around the Eu^{III} ion in the asymmetric unit cell. The polyhedron constructed in **Figure 9.11** appears to be in high symmetry class and correlates with the luminescence spectral identity in **Figure 9.8**. However, it is the point group that is not in terms with the crystallographic data interpretations due to the selection rules governing the $^5D_0 \rightarrow {}^7F_J$ transitions.

9.4. Conclusions

There is a correlation between the luminescence spectra and the corresponding crystal structures. Moreover, the crystallographic data is more influential in completing and understanding the nature of the symmetry class and the respective corresponding point groups.

The tabled data below is of the complete data of the respective *J*-splitting for different symmetry classes for **1**, **2** and **3**

Table 9.2: Summary of the Final results of *J*-splitting for different symmetry classes for **1**, **2** and **3**.

		Number of Stark Splitting in Sub-levels				
Complex	**Point Group (crystallography)**	**$^7F_0$** (*J=0*)	**$^7F_1$** (*J=1*)	**$^7F_2$** (*J=2*)	**$^7F_3$** (*J=3*)	**$^7F_4$** (*J=4*)
[Eu(TCPB)$_3$Phen] (1)	C_{2h}	1	3	5	7	9
[Eu(TMHD)$_3$Phen] (2)	C_i	1	3	5	7	9
[Eu$_2$(PCA)$_6$(Phen)$_2$] (3)	C_i	1	2	3	5	6

It was deduced that the luminescence spectral identity can potentially hint at the relative symmetry class the complex can crystallize-in by its stark splitting patterns. Similarly, crystallography is somewhat influential in determining the exact point group of the complex which to some extent helps in the construction of structural geometric polyhedral to further understand the atomic orientation and the coordination pattern of the ligand species around the metal center.

The obtained crystal data of the Eu^{III} β-diketonate complexes offers a rare chance, unequivocally, of rubber stamping the template of predicting the relative crystal class in which a specific complex would crystalize in using the photoluminescence spectral splitting spectrum and vice versa.

Therefore it is deduced that there is a two-way lenience between crystallography and the photoluminescence studies with complimentary scientific results.

10 Evaluation of Study

In this chapter:
General assessment on the successes and failures of the study with respect to the initially proposed project aims. Outlines on possible future work deduced from relative failures in the project.

10.1. Results Obtained

One of the main aims of this study was to investigate the influence of the ligands coordinated to the Eu^{III} metal center towards the luminescence intensity and the luminescence spectral identity thereof. These aims were further incorporated with crystallographic study to thoroughly investigating the random effect of atomic orientations around the metal by constructing coordination polyhedrons and draw any correlations with respect to the luminescence given by these respective Eu^{III} complexes.

A stepwise evaluation entails:

1. Seven novel Schiff base ligand systems containing aromatic and biological active imino substituents were synthesized successfully. The ligands were fully characterized for structural confirmation. These Schiff base ligand species are widely utilized due to their relative ease of forming. The use of this ligand system was to explore the synthesis of a range of *N,O*-bidentate and *O,N,N'*-tridentate salicylidene ligands. They could be further utilized to evaluate their coordinating ability, in particular *N,O*-bidentate system, to the Eu^{III} metal ion and their relative influence towards their luminescence.

   Interestingly, through absorption (UV/Vis) measurements, the tautomerization phenomenon was observed for one of the most luminous ligand in the range.

   Solid state photoluminescence studies were carried out on all the Schiff base ligands synthesized and were all found to be fluorescent. Three of the seven ligands showed good luminescence intensity and therefore quantum yields were measured for those samples.

   Crystals suitable for single crystal X-ray diffraction were obtained. The crystallographic study addressed various intra- and inter-molecular interactions and packing effects of the salicylidene compounds including the rotation of the C=N

imine double bond which result in various orientations of the substituent's respectively. The planarity of the compounds was discussed as a result of this C=N rotations and somewhat reflected to the luminescence output if there is or not any correlation thereof.

2. The synthesis of Eu^{III} complexes of [Eu(β-diketone)$_3$ X] (X = 1,10-phenanthroline) type were successfully synthesized and the complexes were fully characterized. However, the synthesis of the [Eu(L,L'-Bid)$_3$ X] with synthesized Schiff base ligands were unsuccessful.

   The Eu^{III} complexes of [Eu(β-diketone)$_3$ X] were all analysed for photoluminescence. All of the obtained Eu^{III} complexes had five emissive transitions, essentially characteristic of Eu^{III} ion spectral emission profile. The relative spectral identities observed across all the complexes were resultant to the ligand effect imposed by the nature of the coordinated ligands to the Eu^{III} ion; subsequently, different spectral splitting patterns were observed for every analysed complexes.

   Moreover, some of the analysed complexes exhibited the nature of emission spectrum for systems with probably lower energy difference or that poses less electron cloud around the Eu^{III} metal center whereby the excitation wavelength range is far blue shifted giving rise to all the Eu^{III} *f-f* transitions to appear.

   All the emission spectra for all the complexes corroborated with literature in clearly indicating the symmetry class, through Stark splitting, in which the respective complexes would crystallize in.

   Quantum yields of four complexes with high luminescence intensity were carried out. One of the complexes interestingly yielded a quantum efficiency of 82% . A lot of aspects were addressed as a result of ligands effect from the [Eu(β-diketone)$_3$ X] complexes obtained.

   Crystals suitable for single crystal X-ray diffraction were obtained. The crystal structure of two of Eu^{III} complexes of [Eu(β-diketone)$_3$ X] and one of [Eu(O,O'-bidentate)$_6$ X$_2$] were analysed with X-ray diffraction. All the obtained crystals served the same purpose of outlaying the coordination nature of the respective ligands towards the Eu^{III} ion.

The crystallographic study addressed various intra- and inter-molecular interactions, coordination polyhedron and packing effects of the respective crystals obtained.

3. Correlations between the photoluminescence and the crystallographic results obtained from Eu^{III} complexes were carried out. Interestingly, it was obtained that the relative predictions of symmetry class deduced from the luminescence spectrum of Eu^{III} complexes via spectral Stark splitting embraced the relative crystal systems observed in crystallographic analysis.

   Moreover, the coordination polyhedrons exhibited the distortions, believed to have been caused by relative steric hindrance which influences the relative atomic orientations around the Eu^{III} ion. Knowing that the inversion center on the Eu^{III} ion would potentially impact the luminescence output of the that material, it is difficult to essentially rule out the possibility of any other symmetry elements in the vicinity of the Eu^{III} ion impacting the relative high emissions of the Eu complex.

   It was further deduced that dealing with dimeric or dinuclear complexes, it is best to correlate the relative spectral emission predictions with the constructed polyhedron of the molecule observed in the asymmetric unit cell than the dual polyhedron consisting of two metal centres.

10.2. Future Work

The use of Schiff organic framework with their ease of formation and their photochromic behaviour gives a huge hint in using them as potential fluorophores in tailoring Eu^{III} based complexes. Their easy concept of bifunctionality poses an interesting prospect in yielding highly luminescent Eu^{III} complexes. The reasons for rather bidentate than tridentate Schiff base ligand is merely because they pose a larger excitation cross-section which is influenced by the number of organic ligands in the first coordination sphere of the Eu^{III} ion.

It is thought to help a great deal in conducting some pKa studies in acquiring relative conducive pH conditions that would swiftly allow the coordination of the Schiff base bidentate ligands to Eu^{III} ion or any other lanthanide for that matter. When this is obtained, it will open a whole new venture in using Schiff base derivatives to explore their luminescence properties with the lanthanides. This could greatly benefit the biomedical science fraternity in

that many biologically active amines will be incorporated to these Schiff base ligands and later metalized to Eu^{III} ion or other lanthanides.

The highlight of this project was the successful direct correlation of the photoluminescence and the crystallographic result obtained. It would further help a great deal in incorporating powder X-ray diffraction technique in further analysing the relative symmetry class, stress and strain in the bulk material which could give reason at the observed distortions in single crystal x-ray crystallography. Furthermore, it will give thorough comparison from bulk powder for both luminescence and the powder x-ray diffraction.

With this stiff foundation laid by the [Eu(β-diketone)$_3$ X] (X = 1,10-phenanthroline) complexes in this project. More other fluorine substituted organic ligands are to be investigated on because of its good sublimation properties and lattice strength reinforcent with inter and intra-halide interactions it poses. It is further thought to use many other interesting organic ligands which are somewhat bulkier; to use similar methods used in this study in going about the spectral splitting analysis to get the relative symmetry class with the help of both single and powder x-ray diffraction to acquire more knowledge and further seek to tailor high emitting Eu^{III} complexes.

As was noted in Chapter 4, all of the syntheses were bench-top synthesis of various Eu^{III} based complexes which somewhat proved to yield numerous crystalline products. However, some of the compounds afforded crystals that were of too low quality to analyze via XRD analysis. Effort into the production of better quality crystals would greatly increase the possibility of structural characterization; while expanding on the knowledge base of europium (III) based analogues coordination behaviour properties.

It is worth noting that there are only four reported number of [Eu(β-diketone)$_3$ X] crystals in the Cambridge Structural Databse (CSD).[1] This clearly indicates that very little is known of the crystal structure and photoluminescence direct correlations and therefore we look to increase the structural database of these types of complexes.

[1] Cambridge Structural Database (CSD) Version 5.38, November 2016 update. Latest access date: 15/03/18.

APPENDIX

Supplementary data of Napht-SalH-Carba for the atomic coordinates, bond distance and angles and anisotropic displacement parameters are given in appendix tables A.

Table A.1: Atomic coordinates (x 10^4) and equivalent isotropic displacement parameters ($Å^2$x 10^3) for **Napht-SalH-Carba.** U(eq) is defined as one third of the trace of the orthogonalized U^{ij} tensor.

	x	y	z	U(eq)
O(1)	9049(1)	8846(2)	8497(1)	32(1)
N(1)	8213(1)	6101(2)	8918(1)	24(1)
N(2)	8258(1)	-1607(2)	10607(1)	25(1)
C(24)	8901(1)	-2984(3)	11078(1)	31(1)
C(25)	9285(1)	-2014(3)	11874(1)	39(1)
C(6)	7062(1)	12412(2)	7282(1)	25(1)
C(17)	7524(1)	3173(2)	9410(1)	23(1)
C(16)	7594(1)	1242(2)	9848(1)	21(1)
C(7)	6968(1)	10446(2)	7677(1)	22(1)
C(13)	8934(1)	3176(3)	9718(1)	26(1)
C(18)	7035(1)	-221(2)	10015(1)	23(1)
C(8)	6195(1)	9866(3)	7635(1)	31(1)
C(22)	5854(1)	-1970(3)	10058(1)	32(1)
C(12)	8199(1)	4143(2)	9343(1)	22(1)
C(15)	8343(1)	315(2)	10226(1)	23(1)
C(14)	9023(1)	1285(2)	10167(1)	26(1)
C(20)	7105(1)	-3665(3)	10759(1)	28(1)
C(3)	8394(1)	9904(3)	8106(1)	25(1)
C(1)	7592(1)	7201(2)	8522(1)	24(1)
C(19)	7469(1)	-1954(2)	10489(1)	24(1)
C(5)	7825(1)	13040(3)	7293(1)	30(1)
C(23)	6217(1)	-247(3)	9801(1)	28(1)
C(4)	8465(1)	11843(3)	7686(1)	31(1)
C(2)	7651(1)	9164(2)	8096(1)	22(1)
C(10)	5670(1)	13111(3)	6860(1)	36(1)
C(11)	6404(1)	13719(3)	6881(1)	31(1)
C(9)	5568(1)	11160(3)	7235(1)	38(1)
C(21)	6297(1)	-3646(3)	10535(1)	31(1)

Table A.2: Bond distances (Å) and angles (º) for **Napht-SalH-Carba.**

Bond	Distance (Å)	Bond Angle	Angle (º)
O(1)-C(3)	1.3271(18)	**C(3)-O(1)-H(1)**	109.5
O(1)-H(1)	0.84	**C(1)-N(1)-C(12)**	124.20(13)
N(1)-C(1)	1.2989(18)	**C(15)-N(2)-C(19)**	108.96(12)
N(1)-C(12)	1.414(2)	**C(15)-N(2)-C(24)**	124.95(13)
N(2)-C(15)	1.383(2)	**C(19)-N(2)-C(24)**	126.07(13)
N(2)-C(19)	1.3860(19)	**N(2)-C(24)-C(25)**	112.07(13)
N(2)-C(24)	1.4571(19)	**N(2)-C(24)-H(24A)**	109.2
C(24)-C(25)	1.507(2)	**C(25)-C(24)-H(24A)**	109.2
C(24)-H(24A)	0.99	**N(2)-C(24)-H(24B)**	109.2
C(24)-H(24B)	0.99	**C(25)-C(24)-H(24B)**	109.2
C(25)-H(25A)	0.98	**H(24A)-C(24)-H(24B)**	107.9
C(25)-H(25B)	0.98	**C(24)-C(25)-H(25A)**	109.5
C(25)-H(25C)	0.98	**C(24)-C(25)-H(25B)**	109.5
C(6)-C(11)	1.414(2)	**H(25A)-C(25)-H(25B)**	109.5
C(6)-C(7)	1.422(2)	**C(24)-C(25)-H(25C)**	109.5
C(6)-C(5)	1.423(2)	**H(25A)-C(25)-H(25C)**	109.5
C(17)-C(16)	1.391(2)	**H(25B)-C(25)-H(25C)**	109.5
C(17)-C(12)	1.391(2)	**C(11)-C(6)-C(7)**	120.24(14)
C(17)-H(17)	0.95	**C(11)-C(6)-C(5)**	120.51(14)
C(16)-C(15)	1.4162(19)	**C(7)-C(6)-C(5)**	119.25(13)
C(16)-C(18)	1.445(2)	**C(16)-C(17)-C(12)**	118.83(13)
C(7)-C(8)	1.416(2)	**C(16)-C(17)-H(17)**	120.6
C(7)-C(2)	1.444(2)	**C(12)-C(17)-H(17)**	120.6
C(13)-C(14)	1.379(2)	**C(17)-C(16)-C(15)**	120.05(13)
C(13)-C(12)	1.406(2)	**C(17)-C(16)-C(18)**	133.64(13)
C(13)-H(13)	0.95	**C(15)-C(16)-C(18)**	106.29(13)
C(18)-C(23)	1.399(2)	**C(8)-C(7)-C(6)**	117.12(13)
C(18)-C(19)	1.416(2)	**C(8)-C(7)-C(2)**	123.60(14)
C(8)-C(9)	1.372(2)	**C(6)-C(7)-C(2)**	119.28(13)
C(8)-H(8)	0.95	**C(14)-C(13)-C(12)**	122.56(14)
C(22)-C(23)	1.387(2)	**C(14)-C(13)-H(13)**	118.7
C(22)-C(21)	1.399(2)	**C(12)-C(13)-H(13)**	118.7
C(22)-H(22)	0.95	**C(23)-C(18)-C(19)**	119.08(14)
C(15)-C(14)	1.395(2)	**C(23)-C(18)-C(16)**	134.03(14)
C(14)-H(14)	0.95	**C(19)-C(18)-C(16)**	106.88(13)
C(20)-C(21)	1.383(2)	**C(9)-C(8)-C(7)**	121.17(15)
C(20)-C(19)	1.393(2)	**C(9)-C(8)-H(8)**	119.4

C(20)-H(20)	0.95	**C(7)-C(8)-H(8)**	119.4
C(3)-C(2)	1.410(2)	**C(23)-C(22)-C(21)**	120.71(15)
C(3)-C(4)	1.422(2)	**C(23)-C(22)-H(22)**	119.6
C(1)-C(2)	1.435(2)	**C(21)-C(22)-H(22)**	119.6
C(1)-H(1A)	0.95	**C(17)-C(12)-C(13)**	119.94(14)
C(5)-C(4)	1.352(2)	**C(17)-C(12)-N(1)**	124.72(13)
C(5)-H(5)	0.95	**C(13)-C(12)-N(1)**	115.34(13)
C(23)-H(23)	0.95	**N(2)-C(15)-C(14)**	129.23(13)
C(4)-H(4)	0.95	**N(2)-C(15)-C(16)**	109.17(12)
C(10)-C(11)	1.364(2)	**C(14)-C(15)-C(16)**	121.57(14)
C(10)-C(9)	1.400(3)	**C(13)-C(14)-C(15)**	117.04(13)
C(10)-H(10)	0.95	**C(13)-C(14)-H(14)**	121.5
C(11)-H(11)	0.95	**C(15)-C(14)-H(14)**	121.5
C(9)-H(9)	0.95	**C(21)-C(20)-C(19)**	117.63(14)
C(21)-H(21)	0.95	**C(21)-C(20)-H(20)**	121.2
		C(19)-C(20)-H(20)	121.2
		O(1)-C(3)-C(2)	122.31(14)
		O(1)-C(3)-C(4)	117.46(13)
		C(2)-C(3)-C(4)	120.24(13)
		N(1)-C(1)-C(2)	121.13(13)
		N(1)-C(1)-H(1A)	119.4
		C(2)-C(1)-H(1A)	119.4
		N(2)-C(19)-C(20)	129.45(13)
		N(2)-C(19)-C(18)	108.70(13)
		C(20)-C(19)-C(18)	121.85(14)
		C(4)-C(5)-C(6)	121.50(15)
		C(4)-C(5)-H(5)	119.2
		C(6)-C(5)-H(5)	119.2
		C(22)-C(23)-C(18)	119.09(14)
		C(22)-C(23)-H(23)	120.5
		C(18)-C(23)-H(23)	120.5
		C(5)-C(4)-C(3)	120.72(14)
		C(5)-C(4)-H(4)	119.6
		C(3)-C(4)-H(4)	119.6
		C(3)-C(2)-C(1)	119.36(13)
		C(3)-C(2)-C(7)	118.96(13)
		C(1)-C(2)-C(7)	121.65(13)
		C(11)-C(10)-C(9)	119.42(14)
		C(11)-C(10)-H(10)	120.3
		C(9)-C(10)-H(10)	120.3

	C(10)-C(11)-C(6)	120.84(15)
	C(10)-C(11)-H(11)	119.6
	C(6)-C(11)-H(11)	119.6
	C(8)-C(9)-C(10)	121.19(15)
	C(8)-C(9)-H(9)	119.4
	C(10)-C(9)-H(9)	119.4
	C(20)-C(21)-C(22)	121.62(15)
	C(20)-C(21)-H(21)	119.2
	C(22)-C(21)-H(21)	119.2

Table A.3: Anisotropic displacement parameters ($Å^2 \times 10^3$) for **Napht-SalH-Carba**. The anisotropic displacement factor exponent takes the form: $-2p^2[h^2 a^{*2} U^{11} + .. + 2 h k a^* b^* U^{12}]$

	U11	**U22**	**U33**	**U23**	**U13**	**U12**
O(1)	25(1)	35(1)	35(1)	6(1)	8(1)	1(1)
N(1)	27(1)	19(1)	24(1)	-1(1)	7(1)	2(1)
N(2)	26(1)	23(1)	25(1)	3(1)	6(1)	4(1)
C(24)	30(1)	27(1)	34(1)	7(1)	10(1)	9(1)
C(25)	33(1)	46(1)	32(1)	8(1)	4(1)	7(1)
C(6)	33(1)	23(1)	19(1)	-2(1)	8(1)	1(1)
C(17)	23(1)	22(1)	20(1)	-2(1)	4(1)	2(1)
C(16)	24(1)	20(1)	19(1)	-3(1)	5(1)	1(1)
C(7)	27(1)	21(1)	20(1)	-2(1)	8(1)	0(1)
C(13)	23(1)	26(1)	29(1)	-2(1)	8(1)	-1(1)
C(18)	28(1)	21(1)	18(1)	-1(1)	6(1)	1(1)
C(8)	29(1)	33(1)	34(1)	7(1)	13(1)	4(1)
C(22)	28(1)	36(1)	32(1)	-1(1)	8(1)	-4(1)
C(12)	27(1)	18(1)	22(1)	-2(1)	6(1)	1(1)
C(15)	27(1)	20(1)	21(1)	-2(1)	5(1)	2(1)
C(14)	23(1)	25(1)	28(1)	0(1)	5(1)	5(1)
C(20)	37(1)	24(1)	24(1)	1(1)	10(1)	2(1)
C(3)	26(1)	26(1)	24(1)	-3(1)	7(1)	1(1)
C(1)	25(1)	22(1)	23(1)	-3(1)	7(1)	-1(1)
C(19)	28(1)	22(1)	20(1)	-3(1)	7(1)	2(1)
C(5)	39(1)	25(1)	28(1)	2(1)	12(1)	-5(1)
C(23)	27(1)	29(1)	26(1)	2(1)	5(1)	2(1)
C(4)	30(1)	32(1)	32(1)	1(1)	11(1)	-7(1)
C(2)	27(1)	19(1)	20(1)	-2(1)	8(1)	1(1)
C(10)	36(1)	41(1)	30(1)	5(1)	9(1)	16(1)
C(11)	44(1)	24(1)	23(1)	4(1)	10(1)	6(1)
C(9)	28(1)	48(1)	39(1)	8(1)	13(1)	7(1)
C(21)	38(1)	28(1)	30(1)	0(1)	14(1)	-6(1)

Supplementary data of 3Methoxy-SalH-Carb for the atomic coordinates, bond distance and angles and anisotropic displacement parameters are given in appendix tables B.

Table B.1 Atomic coordinates (x 10^4) and equivalent isotropic displacement parameters ($Å^2$x 10^3) for **3Methoxy-SalH-Carb.** U(eq) is defined as one third of the trace of the orthogonalized U^{ij} tensor.

	x	y	z	U(eq)
O(1)	7228(1)	261(4)	3951(2)	31(1)
O(2)	7949(1)	-3447(4)	3930(2)	34(1)
N(1)	6502(1)	2929(5)	4918(2)	28(1)
N(2)	4827(1)	10040(5)	4612(2)	27(1)
C(17)	3934(1)	7179(7)	6959(2)	29(1)
C(18)	3716(1)	9269(7)	6461(2)	29(1)
C(16)	4428(1)	6122(7)	6676(2)	29(1)
C(15)	4713(1)	7187(6)	5871(2)	23(1)
C(19)	3982(1)	10348(6)	5660(3)	28(1)
C(22)	4370(2)	10857(7)	3008(3)	44(1)
C(7)	7147(1)	-1725(7)	6566(3)	31(1)
C(20)	4481(1)	9286(6)	5377(3)	25(1)
C(1)	6629(1)	1671(6)	5702(3)	29(1)
C(8)	8295(1)	-5645(7)	3863(3)	36(1)
C(6)	7511(2)	-3719(6)	6556(3)	32(1)
C(2)	7037(1)	-341(6)	5693(2)	27(1)
C(11)	5725(1)	8421(6)	3973(3)	28(1)
C(21)	4703(1)	11947(6)	3858(3)	30(1)
C(9)	6080(1)	4776(6)	4882(3)	23(1)
C(10)	6120(1)	6588(6)	4121(3)	27(1)
C(12)	5279(1)	8427(6)	4613(2)	24(1)
C(14)	5629(1)	4776(6)	5511(3)	25(1)
C(5)	7782(1)	-4371(7)	5680(3)	29(1)
C(4)	7689(1)	-3014(6)	4822(3)	26(1)
C(3)	7311(1)	-994(6)	4814(2)	24(1)
C(13)	5227(1)	6641(6)	5382(3)	23(1)

Table B.2: Bond distances (Å) and angles (º) for **3Methoxy-SalH-Carb.**

Bond	Distance (Å)	Bond Angle	Angle (º)
O(1)-C(3)	1.349(4)	**C(3)-O(1)-H(1)**	109.5
O(1)-H(1)	0.84	**C(4)-O(2)-C(8)**	117.4(3)
O(2)-C(4)	1.375(4)	**C(1)-N(1)-C(9)**	123.8(3)
O(2)-C(8)	1.432(4)	**C(1)-N(1)-H(1A)**	118.1
N(1)-C(1)	1.282(4)	**C(9)-N(1)-H(1A)**	118.1
N(1)-C(9)	1.415(4)	**C(12)-N(2)-C(20)**	108.0(3)
N(1)-H(1A)	0.88	**C(12)-N(2)-C(21)**	125.7(3)
N(2)-C(12)	1.389(4)	**C(20)-N(2)-C(21)**	125.8(3)
N(2)-C(20)	1.390(5)	**C(16)-C(17)-C(18)**	121.2(3)
N(2)-C(21)	1.456(4)	**C(16)-C(17)-H(17)**	119.4
C(17)-C(16)	1.381(5)	**C(18)-C(17)-H(17)**	119.4
C(17)-C(18)	1.390(5)	**C(19)-C(18)-C(17)**	121.3(3)
C(17)-H(17)	0.95	**C(19)-C(18)-H(18)**	119.4
C(18)-C(19)	1.380(4)	**C(17)-C(18)-H(18)**	119.4
C(18)-H(18)	0.95	**C(17)-C(16)-C(15)**	119.1(3)
C(16)-C(15)	1.402(5)	**C(17)-C(16)-H(16)**	120.5
C(16)-H(16)	0.95	**C(15)-C(16)-H(16)**	120.5
C(15)-C(20)	1.405(5)	**C(16)-C(15)-C(20)**	118.6(3)
C(15)-C(13)	1.446(5)	**C(16)-C(15)-C(13)**	134.7(3)
C(19)-C(20)	1.392(5)	**C(20)-C(15)-C(13)**	106.8(3)
C(19)-H(19)	0.95	**C(18)-C(19)-C(20)**	117.5(3)
C(22)-C(21)	1.515(5)	**C(18)-C(19)-H(19)**	121.2
C(22)-H(22A)	0.98	**C(20)-C(19)-H(19)**	121.2
C(22)-H(22B)	0.98	**C(21)-C(22)-H(22A)**	109.5
C(22)-H(22C)	0.98	**C(21)-C(22)-H(22B)**	109.5
C(7)-C(6)	1.372(5)	**H(22A)-C(22)-H(22B)**	109.5
C(7)-C(2)	1.406(5)	**C(21)-C(22)-H(22C)**	109.5
C(7)-H(7)	0.95	**H(22A)-C(22)-H(22C)**	109.5
C(1)-C(2)	1.451(5)	**H(22B)-C(22)-H(22C)**	109.5
C(1)-H(1B)	0.95	**C(6)-C(7)-C(2)**	120.6(3)
C(8)-H(8A)	0.98	**C(6)-C(7)-H(7)**	119.7
C(8)-H(8B)	0.98	**C(2)-C(7)-H(7)**	119.7
C(8)-H(8C)	0.98	**N(2)-C(20)-C(19)**	128.4(3)
C(6)-C(5)	1.394(5)	**N(2)-C(20)-C(15)**	109.2(3)
C(6)-H(6)	0.95	**C(19)-C(20)-C(15)**	122.4(3)
C(2)-C(3)	1.401(5)	**N(1)-C(1)-C(2)**	122.2(3)
C(11)-C(10)	1.377(5)	**N(1)-C(1)-H(1B)**	118.9
C(11)-C(12)	1.387(5)	**C(2)-C(1)-H(1B)**	118.9
C(11)-H(11)	0.95	**O(2)-C(8)-H(8A)**	109.5
C(21)-H(21A)	0.99	**O(2)-C(8)-H(8B)**	109.5
C(21)-H(21B)	0.99	**H(8A)-C(8)-H(8B)**	109.5
C(9)-C(14)	1.388(5)	**O(2)-C(8)-H(8C)**	109.5
C(9)-C(10)	1.400(5)	**H(8A)-C(8)-H(8C)**	109.5

C(10)-H(10)	0.95	**H(8B)-C(8)-H(8C)**	109.5
C(12)-C(13)	1.401(5)	**C(7)-C(6)-C(5)**	120.2(3)
C(14)-C(13)	1.396(5)	**C(7)-C(6)-H(6)**	119.9
C(14)-H(14)	0.95	**C(5)-C(6)-H(6)**	119.9
C(5)-C(4)	1.375(5)	**C(3)-C(2)-C(7)**	119.2(3)
C(5)-H(5)	0.95	**C(3)-C(2)-C(1)**	120.8(3)
C(4)-C(3)	1.406(5)	**C(7)-C(2)-C(1)**	120.0(3)
		C(10)-C(11)-C(12)	117.4(3)
		C(10)-C(11)-H(11)	121.3
		C(12)-C(11)-H(11)	121.3
		N(2)-C(21)-C(22)	112.2(3)
		N(2)-C(21)-H(21A)	109.2
		C(22)-C(21)-H(21A)	109.2
		N(2)-C(21)-H(21B)	109.2
		C(22)-C(21)-H(21B)	109.2
		H(21A)-C(21)-H(21B)	107.9
		C(14)-C(9)-C(10)	120.1(3)
		C(14)-C(9)-N(1)	123.8(3)
		C(10)-C(9)-N(1)	116.0(3)
		C(11)-C(10)-C(9)	122.1(3)
		C(11)-C(10)-H(10)	119
		C(9)-C(10)-H(10)	119
		C(11)-C(12)-N(2)	128.5(3)
		C(11)-C(12)-C(13)	121.9(3)
		N(2)-C(12)-C(13)	109.6(3)
		C(9)-C(14)-C(13)	118.8(3)
		C(9)-C(14)-H(14)	120.6
		C(13)-C(14)-H(14)	120.6
		C(4)-C(5)-C(6)	120.3(3)
		C(4)-C(5)-H(5)	119.8
		C(6)-C(5)-H(5)	119.8
		O(2)-C(4)-C(5)	124.9(3)
		O(2)-C(4)-C(3)	114.9(3)
		C(5)-C(4)-C(3)	120.3(3)
		O(1)-C(3)-C(2)	122.3(3)
		O(1)-C(3)-C(4)	118.2(3)
		C(2)-C(3)-C(4)	119.4(3)
		C(14)-C(13)-C(12)	119.7(3)
		C(14)-C(13)-C(15)	133.8(3)
		C(12)-C(13)-C(15)	106.4(3)

Table B.3: Anisotropic displacement parameters ($Å^2 \times 10^3$) for **3Methoxy-SalH-Carb**. The anisotropic displacement factor exponent takes the form: $-2p^2[h^2 a^{*2} U^{11} + .. + 2 h k a^* b^* U^{12}]$

	U11	U22	U33	U23	U13	U12
O(1)	31(2)	34(2)	27(2)	4(1)	0(1)	6(1)
O(2)	36(1)	36(1)	32(2)	1(1)	5(1)	9(1)
N(1)	28(2)	30(2)	25(2)	-7(2)	3(2)	-3(2)
N(2)	31(2)	24(2)	27(2)	4(2)	-1(2)	-1(2)
C(17)	29(2)	32(2)	27(2)	0(2)	1(2)	-5(2)
C(18)	24(2)	29(2)	34(2)	-6(2)	-1(2)	-1(2)
C(16)	35(2)	28(2)	24(2)	2(2)	-7(2)	-2(2)
C(15)	25(2)	25(2)	19(2)	-4(2)	-5(2)	-4(2)
C(19)	29(2)	24(2)	30(2)	-2(2)	-5(2)	-2(2)
C(22)	45(2)	54(3)	33(2)	8(2)	-11(2)	-4(2)
C(7)	27(2)	40(2)	24(2)	-1(2)	0(2)	-5(2)
C(20)	27(2)	24(2)	24(2)	-1(2)	-1(2)	-5(2)
C(1)	28(2)	32(2)	25(2)	-4(2)	0(2)	-5(2)
C(8)	35(2)	32(2)	40(2)	-3(2)	3(2)	5(2)
C(6)	28(2)	37(2)	31(2)	8(2)	-6(2)	-4(2)
C(2)	23(2)	31(2)	27(2)	0(2)	-1(2)	-3(2)
C(11)	33(2)	24(2)	27(2)	0(2)	-4(2)	-3(2)
C(21)	33(2)	25(2)	32(2)	4(2)	-2(2)	-1(2)
C(9)	25(2)	21(2)	24(2)	-5(2)	-5(2)	-1(2)
C(10)	29(2)	31(2)	22(2)	-7(2)	1(2)	-5(2)
C(12)	26(2)	21(2)	24(2)	-4(2)	-3(2)	-3(2)
C(14)	30(2)	23(2)	23(2)	0(2)	-4(2)	-3(2)
C(5)	25(2)	30(2)	31(3)	3(2)	-1(2)	0(2)
C(4)	24(2)	31(2)	24(2)	-3(2)	2(2)	-4(2)
C(3)	21(2)	28(2)	24(2)	4(2)	-4(2)	-3(2)
C(13)	25(2)	22(2)	23(2)	-5(2)	-4(2)	-6(2)

Supplementary data of 3Methoxy-SalH-Anil for the atomic coordinates, bond distance and angles and anisotropic displacement parameters are given in appendix tables C.

Table C.1: Atomic coordinates (x 10^4) and equivalent isotropic displacement parameters ($Å^2$x 10^3) for **3Methoxy-SalH-Anil.** U(eq) is defined as one third of the trace of the orthogonalized U^{ij} tensor.

	x	y	z	U(eq)
O(1)	-82(2)	5323(1)	5958(1)	21(1)
O(2)	-3295(2)	5716(1)	5125(1)	21(1)
N(1)	1484(2)	3812(1)	6927(1)	19(1)
C(1)	55(3)	2805(2)	6798(1)	20(1)
C(2)	-1556(3)	2963(2)	6289(1)	18(1)
C(3)	-1605(3)	4238(2)	5905(1)	17(1)
C(4)	-3336(3)	4419(2)	5461(1)	18(1)
C(5)	-5268(3)	6090(2)	4782(1)	26(1)
C(6)	-4923(3)	3328(2)	5391(1)	21(1)
C(7)	-4835(3)	2041(2)	5763(1)	22(1)
C(8)	-3178(3)	1870(2)	6208(1)	21(1)
C(9)	2927(3)	3645(2)	7457(1)	18(1)
C(10)	2340(3)	2879(2)	8014(1)	20(1)
C(11)	3852(3)	2765(2)	8512(1)	22(1)
C(12)	5931(3)	3400(2)	8462(1)	25(1)
C(13)	6489(3)	4180(2)	7915(1)	26(1)
C(14)	4988(3)	4319(2)	7415(1)	22(1)

Table C.2: Bond distances (Å) and angles (º) for **3Methoxy-SalH-Anil.**

Bond	Distance (Å)	Bond Angle	Angle (º)
O(1)-C(3)	1.3528(19)	**C(3)-O(1)-H(1)**	109.5
O(1)-H(1)	0.82	**C(4)-O(2)-C(5)**	116.40(13)
O(2)-C(4)	1.3706(18)	**C(1)-N(1)-C(9)**	120.11(13)
O(2)-C(5)	1.434(2)	**N(1)-C(1)-C(2)**	122.42(14)
N(1)-C(1)	1.286(2)	**N(1)-C(1)-H(1A)**	118.8
N(1)-C(9)	1.420(2)	**C(2)-C(1)-H(1A)**	118.8
C(1)-C(2)	1.450(2)	**C(8)-C(2)-C(3)**	119.76(14)
C(1)-H(1A)	0.93	**C(8)-C(2)-C(1)**	119.23(13)
C(2)-C(8)	1.406(2)	**C(3)-C(2)-C(1)**	120.87(14)

C(2)-C(3)	1.408(2)	**O(1)-C(3)-C(2)**	122.48(14)
C(3)-C(4)	1.411(2)	**O(1)-C(3)-C(4)**	118.36(13)
C(4)-C(6)	1.386(2)	**C(2)-C(3)-C(4)**	119.13(13)
C(5)-H(5A)	0.96	**O(2)-C(4)-C(6)**	124.83(14)
C(5)-H(5B)	0.96	**O(2)-C(4)-C(3)**	115.09(13)
C(5)-H(5C)	0.96	**C(6)-C(4)-C(3)**	120.08(13)
C(6)-C(7)	1.405(2)	**O(2)-C(5)-H(5A)**	109.5
C(6)-H(6)	0.93	**O(2)-C(5)-H(5B)**	109.5
C(7)-C(8)	1.377(2)	**H(5A)-C(5)-H(5B)**	109.5
C(7)-H(7)	0.93	**O(2)-C(5)-H(5C)**	109.5
C(8)-H(8)	0.93	**H(5A)-C(5)-H(5C)**	109.5
C(9)-C(14)	1.392(2)	**H(5B)-C(5)-H(5C)**	109.5
C(9)-C(10)	1.403(2)	**C(4)-C(6)-C(7)**	120.52(15)
C(10)-C(11)	1.390(2)	**C(4)-C(6)-H(6)**	119.7
C(10)-H(10)	0.93	**C(7)-C(6)-H(6)**	119.7
C(11)-C(12)	1.388(3)	**C(8)-C(7)-C(6)**	119.81(15)
C(11)-H(11)	0.93	**C(8)-C(7)-H(7)**	120.1
C(12)-C(13)	1.386(3)	**C(6)-C(7)-H(7)**	120.1
C(12)-H(12)	0.93	**C(7)-C(8)-C(2)**	120.66(14)
C(13)-C(14)	1.392(2)	**C(7)-C(8)-H(8)**	119.7
C(13)-H(13)	0.93	**C(2)-C(8)-H(8)**	119.7
C(14)-H(14)	0.93	**C(14)-C(9)-C(10)**	119.81(14)
		C(14)-C(9)-N(1)	117.05(14)
		C(10)-C(9)-N(1)	123.12(14)
		C(11)-C(10)-C(9)	119.51(15)
		C(11)-C(10)-H(10)	120.2
		C(9)-C(10)-H(10)	120.2
		C(12)-C(11)-C(10)	120.62(15)
		C(12)-C(11)-H(11)	119.7
		C(10)-C(11)-H(11)	119.7
		C(13)-C(12)-C(11)	119.69(15)
		C(13)-C(12)-H(12)	120.2
		C(11)-C(12)-H(12)	120.2
		C(12)-C(13)-C(14)	120.50(16)
		C(12)-C(13)-H(13)	119.8
		C(14)-C(13)-H(13)	119.8
		C(13)-C(14)-C(9)	119.83(15)
		C(13)-C(14)-H(14)	120.1
		C(9)-C(14)-H(14)	120.1

Table C.3: Anisotropic displacement parameters ($Å^2 \times 10^3$) for **3Methoxy-SalH-Anil**. The anisotropic displacement factor exponent takes the form: $-2p^2[h^2 a^{*2} U^{11} + .. + 2 h k a^* b^* U^{12}]$

	U11	U22	U33	U23	U13	U12
O(1)	23(1)	19(1)	22(1)	4(1)	-4(1)	-3(1)
O(2)	26(1)	17(1)	20(1)	4(1)	-4(1)	0(1)
N(1)	21(1)	20(1)	17(1)	2(1)	1(1)	3(1)
C(1)	26(1)	16(1)	17(1)	2(1)	0(1)	4(1)
C(2)	23(1)	16(1)	15(1)	0(1)	1(1)	2(1)
C(3)	21(1)	15(1)	16(1)	-1(1)	2(1)	1(1)
C(4)	24(1)	15(1)	14(1)	1(1)	2(1)	2(1)
C(5)	26(1)	25(1)	28(1)	8(1)	-5(1)	3(1)
C(6)	25(1)	20(1)	17(1)	-1(1)	-1(1)	-1(1)
C(7)	27(1)	18(1)	22(1)	0(1)	0(1)	-5(1)
C(8)	30(1)	16(1)	18(1)	2(1)	1(1)	-1(1)
C(9)	21(1)	15(1)	17(1)	-1(1)	-1(1)	3(1)
C(10)	21(1)	18(1)	20(1)	1(1)	1(1)	0(1)
C(11)	28(1)	19(1)	19(1)	1(1)	-1(1)	4(1)
C(12)	26(1)	23(1)	26(1)	-5(1)	-7(1)	5(1)
C(13)	20(1)	26(1)	31(1)	-6(1)	1(1)	-1(1)
C(14)	24(1)	21(1)	22(1)	0(1)	5(1)	-1(1)

Supplementary data of [Eu(TCPB)$_3$Phen] for the atomic coordinates, bond distance and angles and anisotropic displacement parameters are given in appendix tables D.

Table D.1: Atomic coordinates (x 10^4) and equivalent isotropic displacement parameters ($Å^2$x 10^3) for **[Eu(TCPB)$_3$Phen].** U(eq) is defined as one third of the trace of the orthogonalized U^{ij} tensor.

Atom	x	y	z	U(eq)
Eu1	2401.1(9)	5969.0(6)	2392.6(5)	30.7(6)
Cl3	3524(6)	4246(5)	6480(3)	62(2)
Cl1	907(7)	3199(5)	-1226(4)	87(3)
Cl2	-884(8)	8907(5)	4776(4)	84(3)
F9	4123(14)	8312(8)	3332(8)	75(5)
F2	2834(14)	8065(7)	1116(7)	67(4)
F3	1033(14)	8035(8)	715(8)	67(4)
F1	2184(16)	7701(8)	132(8)	74(5)
F6	-1204(13)	4458(8)	3173(8)	71(5)
F5	-838(13)	4194(8)	2248(8)	61(4)
F7	5570(13)	7699(8)	3278(9)	73(5)
O6	3017(12)	5671(8)	3535(7)	33(4)
O1	2032(11)	6895(7)	1616(7)	34(4)
O2	1880(12)	5422(9)	1334(7)	35(4)
O5	3557(12)	6915(8)	2943(7)	38(4)
F4	406(14)	3967(8)	3142(10)	78(6)
F8	5296(15)	7927(9)	4192(8)	85(6)
O3	901(14)	5202(9)	2484(7)	43(4)
O4	1095(14)	6635(8)	2864(8)	41(4)
C26	3516(18)	5981(11)	4034(10)	23(5)
C17	1550(17)	5027(14)	233(10)	35(6)
C27	3527(17)	5564(13)	4662(10)	29(6)
C16	1797(17)	5623(12)	771(11)	32(6)
N2	3496(16)	4741(10)	2460(8)	35(5)
C15	1838(18)	6353(13)	575(10)	33(6)
C25	4026(18)	6669(11)	4077(10)	30(5)
C14	1957(19)	6909(12)	999(12)	36(6)
N1	4271(16)	5988(10)	2002(9)	33(5)
C22	1181(18)	5181(14)	-420(11)	39(6)
C24	4083(19)	7053(12)	3556(12)	38(6)
C18	1726(18)	4283(13)	471(13)	43(6)
C1	4710(20)	6571(12)	1817(11)	33(6)

C20	1160(20)	3896(17)	-665(14)	57(9)
C42	850(20)	7590(13)	3850(12)	46(7)
C10	3090(20)	4167(12)	2680(10)	33(6)
C34	190(20)	5210(14)	2819(12)	51(7)
C11	4842(18)	5386(13)	2012(10)	31(6)
C30	3513(19)	4725(14)	5774(10)	45(6)
C13	2000(20)	7680(14)	736(13)	47(7)
C21	1000(20)	4637(18)	-864(13)	53(7)
C9	3700(30)	3491(14)	2717(11)	53(8)
C35	-100(20)	5793(15)	3160(13)	48(7)
C37	70(20)	7084(15)	3560(11)	47(7)
C2	5670(20)	6605(15)	1618(13)	51(7)
C4	5900(20)	5331(15)	1808(12)	44(7)
C19	1490(20)	3732(15)	-11(13)	50(7)
C36	350(20)	6498(15)	3146(13)	55(8)
C12	4447(19)	4707(13)	2263(11)	41(6)
C8	4700(30)	3448(13)	2576(12)	50(7)
C23	4820(30)	7761(15)	3628(17)	71(9)
C7	5120(20)	4080(15)	2316(13)	54(8)
C28	3040(20)	4855(16)	4637(14)	65(8)
C33	-390(20)	4458(15)	2842(15)	57(8)
C41	610(20)	8125(18)	4212(13)	61(9)
C6	6150(30)	4086(16)	2105(14)	62(8)
C5	6510(20)	4709(18)	1851(13)	66(8)
C29	3060(20)	4452(17)	5188(13)	58(8)
C38	-1060(30)	7080(20)	3662(13)	76(10)
C3	6250(20)	5980(20)	1601(14)	74(10)
C39	-1360(30)	7645(17)	4022(15)	73(8)
C40	-540(30)	8131(17)	4288(15)	65(8)
C31	4000(30)	5443(19)	5857(16)	79(10)
C32	3910(30)	5897(17)	5280(15)	72(9)

Table D.2: Bond distances (Å) and angles (º) for **[Eu(TCPB)$_3$Phen].**

Atom	Bond Distance (Å)	Atom	Angle/°
Eu1-O6	2.400(14)	**O1-Eu1-O6**	146.1(5)
Eu1-O1	2.324(15)	**O1-Eu1-O6**	141.9(5)
Eu1-O2	2.382(14)	**O1-Eu1-O1**	71.9(5)
Eu1-O5	2.350(15)	**O5-Eu1-O6**	70.9(5)
Eu1-O3	2.341(16)	**O5-Eu1-O1**	78.2(5)
Eu1-O4	2.395(16)	**O5-Eu1-O2**	139.7(5)
Eu1-N2	2.600(18)	**O3-Eu1-O6**	80.7(5)
Eu1-N1	2.588(19)	**O3-Eu1-O1**	118.5(5)
Cl3-C30	1.72(2)	**O3-Eu1-O2**	77.8(5)
Cl1-C20	1.72(2)	**O3-Eu1-O5**	141.6(5)
Cl2-C40	1.86(3)	**O4-Eu1-O6**	77.1(5)
F9-C23	1.37(3)	**O4-Eu1-O1**	83.4(5)
F2-C13	1.32(3)	**O4-Eu1-O2**	123.4(5)
F3-C13	1.33(3)	**O4-Eu1-O5**	78.0(5)
F1-C13	1.34(3)	**O4-Eu1-O3**	70.8(5)
F6-C33	1.33(3)	**N2-Eu1-O6**	73.6(5)
F5-C33	1.33(3)	**N2-Eu1-O1**	132.9(5)
F7-C33	1.30(4)	**N2-Eu1-O2**	72.6(5)
O6-C26	1.22(2)	**N2-Eu1-O5**	112.3(5)
O1-C14	1.28(3)	**N2-Eu1-O3**	82.5(6)
O2-C16	1.22(2)	**N2-Eu1-O4**	143.0(5)
O5-C24	1.31(3)	**N1-Eu1-O6**	103.8(5)
F4-C33	1.36(3)	**N1-Eu1-O1**	78.5(5)
F8-C23	1.22(3)	**N1-Eu1-O2**	76.2(5)
O3-C34	1.24(3)	**N1-Eu1-O5**	71.7(5)
O4-C36	1.22(3)	**N1-Eu1-O3**	142.1(6)
C26-C27	1.52(3)	**N1-Eu1-O4**	147.2(5)
C26-C25	1.40(3)	**N1-Eu1-O2**	63.6(6)
C17-C16	1.55(3)	**C26-O6-Eu1**	136.5(13)
C17-C22	1.37(3)	**C14-O1-Eu1**	133.0(13)
C17-C18	1.45(3)	**C16-O2-Eu1**	136.0(15)
C27-C28	1.42(4)	**C24-O5-Eu1**	135.4(14)
C27-C32	1.41(4)	**C34-O3-Eu1**	134.4(16)
C16-C15	1.41(3)	**C36-O4-Eu1**	137.4(17)
N2-C10	1.30(3)	**C27-C26-O6**	114.2(18)
N2-C12	1.32(3)	**C25-C26-O6**	126.6(19)
C15-C14	1.34(3)	**C25-C26-C27**	119.2(19)

C25-C24	1.32(3)	**C22-C17-C16**	123(2)
C14-C13	1.53(3)	**C18-C17-C16**	115.3(19)
N1-C1	1.29(3)	**C18-C17-C22**	122(2)
N1-C11	1.30(3)	**C28-C27-C26**	121(2)
C22-C21	1.35(4)	**C32-C27-C26**	121(2)
C24-C23	1.56(4)	**C32-C27-C28**	118(2)
C18-C19	1.41(3)	**C17-C16-O2**	117(2)
C1-C2	1.33(3)	**C15-C16-O2**	125(2)
C20-C21	1.42(4)	**C15-C16-C17**	118(2)
C20-C19	1.37(4)	**C10-N2-Eu1**	119.5(15)
C42-C37	1.36(4)	**C12-N2-Eu1**	119.8(15)
C42-C41	1.32(4)	**C12-N2-C10**	121(2)
C10-C9	1.43(3)	**C14-C15-C16**	122(2)
C34-C35	1.38(4)	**C24-C25-C26**	123(2)
C34-C34	1.56(4)	**C15-C14-O1**	129(2)
C11-C4	1.45(3)	**C13-C14-O1**	113(2)
C11-C12	1.48(3)	**C13-C14-C15**	118(2)
C30-C29	1.32(3)	**C1-N1-Eu1**	123.9(15)
C30-C31	1.44(4)	**C11-N1-Eu1**	119.0(14)
C9-C8	1.32(4)	**C11-N1-C1**	117(2)
C35-C36	1.41(4)	**C21-C22-C17**	120(3)
C37-C36	1.47(4)	**C25-C24-O5**	127(2)
C37-C38	1.44(4)	**C23-C24-O5**	113(2)
C2-C3	1.36(4)	**C23-C24-C25**	120(2)
C4-C5	1.35(4)	**C19-C18-C17**	116(2)
C4-C3	1.36(4)	**C2-C1-N1**	126(2)
C12-C7	1.39(3)	**C21-C20-Cl1**	121(2)
C8-C7	1.43(4)	**C19-C20-Cl1**	119(3)
C7-C6	1.43(4)	**C19-C20-C21**	119(2)
C28-C29	1.37(4)	**C41-C42-C37**	123(3)
C41-C40	1.43(4)	**C9-C10-N2**	119(2)
C6-C5	1.38(4)	**C35-C34-O3**	127(2)
C38-C39	1.38(4)	**C33-C34-O3**	113(2)
C39-C40	1.35(4)	**C33-C34-C35**	120(3)
C31-C32	1.45(4)	**C4-C11-N1**	124(2)
		C12-C11-N1	120.4(19)
		C12-C11-C4	116(2)
		C29-C30-Cl3	122(2)
		C31-C30-Cl3	116.6(19)
		C31-C30-C29	122(3)

	F3-C13-F2	107(2)
	F1-C13-F2	106(2)
	F1-C13-F3	107(2)
	C14-C13-F2	111(2)
	C14-C13-F3	111(2)
	C14-C13-F1	114(2)
	C20-C21-C22	121(2)
	C8-C9-C10	122(3)
	C36-C35-C34	124(2)
	C36-C37-C42	122(2)
	C38-C37-C42	121(2)
	C38-C37-C36	117(3)
	C3-C2-C1	118(3)
	C5-C4-C11	123(3)
	C3-C4-C11	113(2)
	C3-C4-C5	124(3)
	C20-C19-C18	121(3)
	C35-C36-O4	123(3)
	C37-C36-O4	116(2)
	C37-C36-C35	121(2)
	C11-C12-N2	117(2)
	C7-C12-N2	123(2)
	C7-C12-N11	120(2)
	C7-C8-C9	118(2)
	F7-C23-F9	104(2)
	F8-C23-F9	110(3)
	F8-C23-F7	110(3)
	C24-C25-F9	107(2)
	C24-C23-F7	109(3)
	C24-C23-F8	115(2)
	C8-C7-C12	117(2)
	C6-C7-C12	120(3)
	C6-C7-C8	123(3)
	C29-C28-C27	123(3)
	F5-C33-F6	108(2)
	F4-C33-F6	107(2)
	F4-C33-F5	106(2)
	C34-C33-F6	114(3)
	C34-C33-F5	112(2)
	C34-C33-F4	109(2)

	C40-C41-C42	115(3)
	C5-C6-C7	121(3)
	C6-C5-C4	121(3)
	C28-C29-C30	120(3)
	C39-C38-C37	118(3)
	C4-C3-C2	122(3)
	C40-C39-C38	117(3)
	C41-C42-Cl2	115(2)
	C39-C40-Cl2	119(2)
	C39-C40-C41	126(3)
	C32-C31-C30	119(3)
	C31-C32-C27	118(3)

Table D.3: Anisotropic displacement parameters ($Å^2 x\ 10^3$) for **[Eu(TCPB)$_3$Phen]**. The anisotropic displacement factor exponent takes the form: $-2p^2[\ h^2 a^{*2} U^{11} + .. + 2\ h\ k\ a^*\ b^* U^{12}]$

Atom	U11	U22	U33	U12	U13	U23
Eu1	38.7(9)	20.6(9)	32.4(9)	-3.5(5)	8.1(6)	1.2(5)
Cl3	68(5)	86(6)	29(4)	-12(4)	7(3)	14(3)
Cl1	89(6)	98(6)	81(6)	-50(5)	36(5)	-60(5)
Cl2	85(6)	101(7)	75(6)	23(5)	38(5)	-32(5)
F9	89(12)	26(8)	91(12)	7(8)	-15(10)	7(8)
F2	92(12)	38(9)	65(10)	-6(8)	5(9)	10(8)
F3	86(12)	41(9)	75(11)	20(9)	19(9)	20(8)
F1	142(16)	34(9)	59(10)	-6(9)	51(10)	2(8)
F6	60(10)	57(10)	102(13)	-15(8)	31(9)	22(9)
F5	55(9)	47(9)	83(12)	0(7)	17(9)	-12(8)
F7	61(11)	45(10)	120(14)	-19(8)	35(10)	-4(9)
O6	48(10)	29(9)	24(9)	1(8)	13(8)	8(8)
O1	32(9)	34(9)	32(10)	-2(7)	0(7)	-8(7)
O2	42(9)	36(10)	25(9)	-2(7)	6(7)	3(8)
O5	45(9)	40(10)	31(10)	3(8)	13(8)	2(8)
F4	62(11)	59(11)	111(15)	7(8)	17(10)	46(10)
F8	120(15)	55(11)	50(10)	-41(10)	-39(10)	2(9)
O3	53(11)	41(11)	35(9)	-14(8)	10(8)	4(8)
O4	43(10)	36(10)	51(10)	-1(8)	26(8)	5(8)
C26	35(13)	16(14)	15(13)	1(10)	0(10)	4(10)
C17	23(12)	57(19)	29(15)	-3(12)	12(10)	-9(13)
C27	27(12)	36(16)	29(13)	-11(11)	15(10)	-8(11)

C16	28(13)	31(15)	39(16)	-11(10)	14(11)	2(12)
N2	47(13)	34(12)	21(10)	2(10)	3(9)	-5(8)
C15	49(15)	38(16)	20(12)	1(12)	25(10)	4(12)
C25	44(14)	15(13)	28(13)	-8(11)	4(10)	-2(10)
C14	42(15)	37(15)	32(16)	-2(11)	15(11)	6(12)
N1	48(12)	23(12)	28(11)	6(10)	9(9)	7(8)
C22	35(14)	49(17)	35(16)	-4(12)	16(11)	-12(13)
C24	43(14)	18(14)	48(18)	-4(11)	0(12)	-9(13)
C18	32(14)	31(15)	62(18)	-1(12)	8(12)	-4(14)
C1	38(15)	21(16)	45(14)	2(11)	18(11)	15(11)
C20	23(14)	100(30)	60(20)	-15(14)	18(13)	-53(18)
C42	70(20)	39(15)	42(15)	13(14)	45(14)	-2(12)
C10	36(7)	29(7)	33(7)	-1(2)	8(2)	0(2)
C34	52(17)	48(18)	45(16)	-24(14)	-2(14)	7(14)
C11	27(13)	32(17)	37(14)	-11(12)	13(10)	4(11)
C13	69(19)	33(16)	42(17)	3(16)	19(14)	2(13)
C21	47(16)	70(20)	51(18)	8(15)	23(13)	13(17)
C9	80(20)	46(19)	19(13)	0(15)	-10(13)	-1(12)
C35	48(16)	50(20)	61(17)	-7(15)	39(13)	2(15)
C37	53(17)	53(18)	41(15)	4(15)	24(13)	-4(14)
C2	35(17)	46(19)	69(19)	5(14)	6(14)	16(14)
C4	61(18)	26(17)	48(16)	10(15)	17(13)	6(12)
C19	41(15)	48(16)	60(20)	0(13)	14(13)	-19(15)
C36	47(17)	70(20)	46(16)	-17(15)	11(14)	10(14)
C12	29(14)	53(18)	39(15)	14(13)	6(11)	-22(12)
C8	70(20)	28(17)	47(16)	4(14)	8(14)	3(12)
C23	80(20)	41(18)	80(30)	-22(17)	10(20)	10(17)
C7	53(17)	70(20)	42(16)	19(15)	10(13)	-15(14)
C28	80(11)	60(11)	55(10)	-2(5)	14(5)	-2(5)
C33	43(17)	40(19)	90(20)	-5(15)	11(17)	34(18)
C41	44(16)	90(30)	49(17)	6(16)	15(13)	18(18)
C6	63(11)	61(11)	62(11)	11(5)	16(5)	-2(5)
C5	51(18)	100(30)	57(19)	-3(18)	33(14)	-8(17)
C29	63(8)	57(9)	55(8)	-1(2)	16(3)	0(2)
C38	90(20)	90(30)	46(17)	20(20)	10(16)	-10(18)
C3	34(17)	140(30)	54(19)	-7(19)	24(14)	-17(18)
C39	57(19)	80(20)	80(20)	0(16)	22(17)	7(18)
C40	67(9)	64(9)	65(9)	1(2)	18(3)	-2(2)
C31	83(12)	88(13)	68(12)	-10(5)	20(5)	-1(5)
C32	77(12)	75(12)	65(11)	-9(5)	18(5)	-1(5)

Supplementary data of [Eu(TMHD)$_3$Phen] for the atomic coordinates, bond distance and angles and anisotropic displacement parameters are given in appendix tables E.

Table E.1: Atomic coordinates (x 10^4) and equivalent isotropic displacement parameters (Å^2 x 10^3) for **[Eu(TMHD)$_3$Phen].** U(eq) is defined as one third of the trace of the orthogonalized U^{ij} tensor.

Atom	x	y	z	U(eq)
Eu1	3440.1(3)	5868.8(2)	7300.67(15)	8.2(3)
O6	2128(5)	7039(4)	8118(3)	16.2(13)
O3	2218(5)	4709(5)	7791(3)	15.6(13)
O4	4910(5)	3928(4)	7717(3)	15.9(13)
O1	1484(5)	6910(4)	6564(3)	12.4(12)
O5	4871(5)	6163(4)	8122(3)	15.3(12)
O2	3572(5)	7676(5)	6685(3)	14.5(12)
N1	5569(6)	5335(5)	6493(3)	13.0(15)
N2	3521(6)	4658(5)	6243(3)	11.4(15)
C5	6120(9)	2820(7)	5118(4)	23(2)
C20	3164(9)	9721(7)	6612(4)	20(2)
C3	3776(9)	3021(7)	5311(4)	21(2)
C30	4865(8)	2921(8)	7995(4)	15(2)
C16	-642(8)	8328(7)	6200(4)	16.8(18)
C35	43(9)	7474(8)	9071(5)	24(2)
C2	2603(9)	3548(7)	5636(4)	21(2)
C1	2512(9)	4359(7)	6101(4)	17(2)
C27	1185(8)	3380(7)	8353(4)	17.2(19)
C17	823(7)	8006(7)	6396(4)	12.8(19)
C34	6196(8)	1917(7)	8114(4)	19.7(19)
C38	1005(7)	8147(6)	9024(4)	11.7(18)
C4	4857(8)	3310(6)	5434(4)	15.3(19)
C23	3892(9)	9439(8)	7373(5)	33(2)
C36	434(9)	9330(8)	8482(5)	29(2)
C39	2273(9)	7428(7)	8693(5)	12(2)
C12	4688(8)	4152(7)	5914(4)	10(2)
C11	5788(8)	4501(6)	6052(4)	12.7(19)
C24	625(9)	4130(9)	8959(5)	31(2)
C29	3694(8)	2746(7)	8170(4)	17(2)
C13	-1277(9)	7902(8)	6907(5)	31(2)
C28	2432(8)	3633(6)	8082(4)	13.4(18)
C40	3521(7)	7232(6)	8995(4)	14.7(18)

C41	4747(7)	6643(7)	8696(4)	11.0(18)
C9	7809(8)	5175(7)	6326(4)	24(2)
C6	7127(9)	3145(7)	5253(4)	24(2)
C37	1178(9)	8411(9)	9788(5)	32(2)
C42	6039(8)	6524(8)	9062(4)	23(2)
C14	-710(8)	7643(8)	5594(4)	26(2)
C10	6553(8)	5655(8)	6623(4)	19(2)
C19	2667(9)	8697(8)	6566(5)	16(2)
C7	7007(9)	3977(8)	5728(5)	17(2)
C18	1343(8)	8900(7)	6408(4)	17(2)
C22	4093(10)	9755(8)	5976(5)	34(2)
C8	8025(8)	4350(7)	5894(5)	25(2)
C25	1467(10)	2053(8)	8637(5)	37(3)
C15	-1398(8)	9691(7)	5921(5)	31(2)
C26	180(9)	3824(9)	7715(5)	33(3)
C21	2006(10)	10929(7)	6582(5)	30(2)
C32	6593(12)	1468(10)	7395(6)	70(4)
C31	6133(11)	895(10)	8700(6)	67(4)
C33B	7109(17)	2380(14)	8472(11)	23(4)
C33A	7400(20)	2430(20)	8054(14)	37(6)
C45B	7180(30)	6320(30)	8444(15)	31(7)
C44B	6750(20)	5143(18)	9383(12)	27(5)
C43B	5880(16)	7620(15)	9424(10)	37(4)
C44A	6460(20)	5490(20)	9629(13)	40(6)
C45A	6934(19)	6849(19)	8497(11)	39(5)
C43A	5870(30)	7040(30)	9776(16)	55(8)

Table E.2: Bond distances (Å) and angles (º) for **[Eu(TMHD)$_3$Phen].**

Atom	Bond Distance (Å)	Atom	Angle/°
Eu1-O6	2.400(14)	**O1-Eu1-O6**	146.1(5)
Eu1-O1	2.324(15)	**O1-Eu1-O6**	141.9(5)
Eu1-O2	2.382(14)	**O1-Eu1-O1**	71.9(5)
Eu1-O5	2.350(15)	**O5-Eu1-O6**	70.9(5)
Eu1-O3	2.341(16)	**O5-Eu1-O1**	78.2(5)
Eu1-O4	2.395(16)	**O5-Eu1-O2**	139.7(5)
Eu1-N2	2.600(18)	**O3-Eu1-O6**	80.7(5)

Eu1-N1	2.588(19)	**O3-Eu1-O1**	118.5(5)
Cl3-C30	1.72(2)	**O3-Eu1-O2**	77.8(5)
Cl1-C20	1.72(2)	**O3-Eu1-O5**	141.6(5)
Cl2-C40	1.86(3)	**O4-Eu1-O6**	77.1(5)
F9-C23	1.37(3)	**O4-Eu1-O1**	83.4(5)
F2-C13	1.32(3)	**O4-Eu1-O2**	123.4(5)
F3-C13	1.33(3)	**O4-Eu1-O5**	78.0(5)
F1-C13	1.34(3)	**O4-Eu1-O3**	70.8(5)
F6-C33	1.33(3)	**N2-Eu1-O6**	73.6(5)
F5-C33	1.33(3)	**N2-Eu1-O1**	132.9(5)
F7-C33	1.30(4)	**N2-Eu1-O2**	72.6(5)
O6-C26	1.22(2)	**N2-Eu1-O5**	112.3(5)
O1-C14	1.28(3)	**N2-Eu1-O3**	82.5(6)
O2-C16	1.22(2)	**N2-Eu1-O4**	143.0(5)
O5-C24	1.31(3)	**N1-Eu1-O6**	103.8(5)
F4-C33	1.36(3)	**N1-Eu1-O1**	78.5(5)
F8-C23	1.22(3)	**N1-Eu1-O2**	76.2(5)
O3-C34	1.24(3)	**N1-Eu1-O5**	71.7(5)
O4-C36	1.22(3)	**N1-Eu1-O3**	142.1(6)
C26-C27	1.52(3)	**N1-Eu1-O4**	147.2(5)
C26-C25	1.40(3)	**N1-Eu1-O2**	63.6(6)
C17-C16	1.55(3)	**C26-O6-Eu1**	136.5(13)
C17-C22	1.37(3)	**C14-O1-Eu1**	133.0(13)
C17-C18	1.45(3)	**C16-O2-Eu1**	136.0(15)
C27-C28	1.42(4)	**C24-O5-Eu1**	135.4(14)
C27-C32	1.41(4)	**C34-O3-Eu1**	134.4(16)
C16-C15	1.41(3)	**C36-O4-Eu1**	137.4(17)
N2-C10	1.30(3)	**C27-C26-O6**	114.2(18)
N2-C12	1.32(3)	**C25-C26-O6**	126.6(19)
C15-C14	1.34(3)	**C25-C26-C27**	119.2(19)
C25-C24	1.32(3)	**C22-C17-C16**	123(2)
C14-C13	1.53(3)	**C18-C17-C16**	115.3(19)
N1-C1	1.29(3)	**C18-C17-C22**	122(2)
N1-C11	1.30(3)	**C28-C27-C26**	121(2)
C22-C21	1.35(4)	**C32-C27-C26**	121(2)
C24-C23	1.56(4)	**C32-C27-C28**	118(2)
C18-C19	1.41(3)	**C17-C16-O2**	117(2)
C1-C2	1.33(3)	**C15-C16-O2**	125(2)
C20-C21	1.42(4)	**C15-C16-C17**	118(2)
C20-C19	1.37(4)	**C10-N2-Eu1**	119.5(15)

C42-C37	1.36(4)	**C12-N2-Eu1**	119.8(15)
C42-C41	1.32(4)	**C12-N2-C10**	121(2)
C10-C9	1.43(3)	**C14-C15-C16**	122(2)
C34-C35	1.38(4)	**C24-C25-C26**	123(2)
C34-C34	1.56(4)	**C15-C14-O1**	129(2)
C11-C4	1.45(3)	**C13-C14-O1**	113(2)
C11-C12	1.48(3)	**C13-C14-C15**	118(2)
C30-C29	1.32(3)	**C1-N1-Eu1**	123.9(15)
C30-C31	1.44(4)	**C11-N1-Eu1**	119.0(14)
C9-C8	1.32(4)	**C11-N1-C1**	117(2)
C35-C36	1.41(4)	**C21-C22-C17**	120(3)
C37-C36	1.47(4)	**C25-C24-O5**	127(2)
C37-C38	1.44(4)	**C23-C24-O5**	113(2)
C2-C3	1.36(4)	**C23-C24-C25**	120(2)
C4-C5	1.35(4)	**C19-C18-C17**	116(2)
C4-C3	1.36(4)	**C2-C1-N1**	126(2)
C12-C7	1.39(3)	**C21-C20-Cl1**	121(2)
C8-C7	1.43(4)	**C19-C20-Cl1**	119(3)
C7-C6	1.43(4)	**C19-C20-C21**	119(2)
C28-C29	1.37(4)	**C41-C42-C37**	123(3)
C41-C40	1.43(4)	**C9-C10-N2**	119(2)
C6-C5	1.38(4)	**C35-C34-O3**	127(2)
C38-C39	1.38(4)	**C33-C34-O3**	113(2)
C39-C40	1.35(4)	**C33-C34-C35**	120(3)
C31-C32	1.45(4)	**C4-C11-N1**	124(2)
		C12-C11-N1	120.4(19)
		C12-C11-C4	116(2)
		C29-C30-Cl3	122(2)
		C31-C30-Cl3	116.6(19)
		C31-C30-C29	122(3)
		F3-C13-F2	107(2)
		F1-C13-F2	106(2)
		F1-C13-F3	107(2)
		C14-C13-F2	111(2)
		C14-C13-F3	111(2)
		C14-C13-F1	114(2)
		C20-C21-C22	121(2)
		C8-C9-C10	122(3)
		C36-C35-C34	124(2)
		C36-C37-C42	122(2)

	C38-C37-C42	121(2)
	C38-C37-C36	117(3)
	C3-C2-C1	118(3)
	C5-C4-C11	123(3)
	C3-C4-C11	113(2)
	C3-C4-C5	124(3)
	C20-C19-C18	121(3)
	C35-C36-O4	123(3)
	C37-C36-O4	116(2)
	C37-C36-C35	121(2)
	C11-C12-N2	117(2)
	C7-C12-N2	123(2)
	C7-C12-N11	120(2)
	C7-C8-C9	118(2)
	F7-C23-F9	104(2)
	F8-C23-F9	110(3)
	F8-C23-F7	110(3)
	C24-C25-F9	107(2)
	C24-C23-F7	109(3)
	C24-C23-F8	115(2)
	C8-C7-C12	117(2)
	C6-C7-C12	120(3)
	C6-C7-C8	123(3)
	C29-C28-C27	123(3)
	F5-C33-F6	108(2)
	F4-C33-F6	107(2)
	F4-C33-F5	106(2)
	C34-C33-F6	114(3)
	C34-C33-F5	112(2)
	C34-C33-F4	109(2)
	C40-C41-C42	115(3)
	C5-C6-C7	121(3)
	C6-C5-C4	121(3)
	C28-C29-C30	120(3)
	C39-C38-C37	118(3)
	C4-C3-C2	122(3)
	C40-C39-C38	117(3)
	C41-C42-Cl2	115(2)
	C39-C40-Cl2	119(2)
	C39-C40-C41	126(3)

		C32-C31-C30	119(3)
		C31-C32-C27	118(3)

Table E.3: Anisotropic displacement parameters ($Å^2 x\ 10^3$) for **[Eu(TMHD)$_3$Phen]**. The anisotropic displacement factor exponent takes the form: $-2p^2[\ h^2 a^{*2} U^{11} + .. + 2\ h\ k\ a^*\ b^* U^{12}]$

Atom	U11	U22	U33	U12	U13	U23
Eu1	4.7(4)	8.3(4)	11.5(4)	-1.9(3)	0.5(2)	-2.2(2)
O6	5(3)	22(3)	22(3)	-4(2)	1(2)	-6(3)
O3	5(3)	15(4)	25(3)	-3(3)	0(2)	-1(3)
O4	9(3)	10(3)	24(3)	1(2)	1(2)	0(2)
O1	11(3)	3(3)	20(3)	2(3)	-4(2)	-1(2)
O5	4(3)	21(3)	20(3)	-2(2)	-1(2)	-5(3)
O2	15(3)	9(3)	20(3)	-5(3)	2(2)	-4(2)
N1	14(4)	13(4)	14(3)	-7(3)	0(3)	-2(3)
N2	12(4)	14(3)	11(3)	-9(3)	-2(3)	0(3)
C5	37(6)	10(5)	14(5)	4(4)	8(4)	-10(4)
C20	35(6)	11(5)	18(4)	-13(4)	-2(4)	0(4)
C3	41(6)	13(4)	8(4)	-10(4)	-1(4)	-2(3)
C30	14(5)	17(5)	13(4)	-1(4)	-1(4)	-7(4)
C16	15(5)	26(5)	9(4)	-8(4)	-2(3)	-1(3)
C35	13(5)	32(6)	31(6)	-10(4)	16(4)	-12(4)
C2	27(6)	18(5)	21(5)	-15(4)	-7(4)	5(4)
C1	22(5)	15(5)	11(5)	-7(4)	0(4)	4(4)
C27	13(5)	14(4)	28(5)	-9(4)	1(4)	-4(4)
C17	11(4)	27(6)	6(4)	-12(4)	11(3)	-9(3)
C34	22(5)	10(4)	25(5)	-5(4)	-2(4)	-1(4)
C38	12(5)	6(4)	19(4)	-2(4)	0(4)	-6(3)
C4	28(5)	9(4)	9(4)	-8(4)	-5(4)	1(3)
C23	48(6)	26(5)	36(5)	-25(5)	-13(5)	-1(4)
C36	19(5)	17(5)	43(6)	3(4)	9(5)	-6(4)
C39	20(6)	7(4)	11(5)	-8(4)	0(4)	-1(4)
C12	15(5)	6(4)	5(4)	-1(4)	0(4)	5(4)
C11	15(5)	7(4)	12(4)	-1(4)	1(4)	4(4)
C24	24(5)	44(6)	32(6)	-19(5)	17(5)	-10(5)
C29	14(5)	9(5)	28(5)	-5(4)	4(4)	-2(4)
C13	18(5)	40(6)	35(5)	-10(4)	0(4)	-8(4)
C28	17(5)	10(5)	14(4)	-6(4)	0(3)	-3(4)
C40	12(5)	17(4)	12(4)	0(4)	-2(4)	-6(3)
C41	7(5)	15(4)	13(4)	-5(4)	-1(3)	-6(4)
C9	6(5)	33(5)	29(5)	-6(4)	-9(4)	7(4)
C6	21(5)	17(5)	19(5)	8(4)	12(4)	-1(4)
C37	20(5)	42(6)	33(6)	-6(5)	10(4)	-23(5)

C42	10(5)	36(5)	24(5)	-6(4)	-2(4)	-14(4)
C14	13(5)	35(5)	29(5)	-3(4)	1(4)	-16(4)
C10	10(5)	27(5)	24(5)	-13(4)	-1(4)	-3(4)
C19	23(6)	20(6)	9(5)	-11(5)	7(4)	-7(4)
C7	14(5)	20(5)	12(4)	-3(4)	2(4)	5(4)
C18	11(5)	16(5)	14(4)	5(4)	-4(4)	3(3)
C22	43(6)	32(6)	42(6)	-29(5)	10(5)	-9(4)
C8	9(5)	28(5)	30(5)	1(4)	9(4)	0(4)
C25	30(6)	35(6)	50(6)	-22(5)	7(5)	1(5)
C15	16(5)	32(5)	35(5)	-4(4)	-2(4)	4(4)
C26	21(6)	56(7)	35(6)	-31(5)	5(4)	-6(5)
C21	48(6)	10(5)	35(6)	-13(5)	-9(5)	-1(4)
C32	65(9)	52(8)	50(7)	36(6)	3(6)	-23(6)
C31	38(7)	49(7)	65(8)	21(6)	2(6)	38(6)
C33B	13(7)	22(7)	32(8)	-1(4)	-11(4)	-5(4)
C33A	30(9)	36(9)	43(9)	-10(4)	2(5)	-8(5)
C45B	19(10)	34(10)	38(10)	-5(5)	-3(5)	-8(5)
C44B	19(8)	30(8)	30(9)	-6(4)	-1(4)	-7(4)
C43B	25(7)	39(7)	54(8)	-12(4)	2(4)	-22(4)
C44A	36(9)	43(9)	40(10)	-14(4)	-3(5)	-5(5)
C45A	29(8)	43(9)	48(8)	-15(4)	-1(4)	-7(5)
C43A	47(11)	61(11)	55(10)	-16(5)	-3(5)	-13(5)

6.1. Supplementary data of {[$Eu_2(BCA)_6(Phen)_2$]- μ-[κ^2-O,O'-(BCA)]$_2$} (3) for the atomic coordinates, bond distance and angles and anisotropic displacement parameters are given in appendix tables E.

6.2. Table F.1: Atomic coordinates (x 10^4) and equivalent isotropic displacement parameters ($Å^2$ x 10^3) for **{[$Eu_2(BCA)_6(Phen)_2$]- μ-[κ^2-O,O'-(BCA)]$_2$} (3).** U(eq) is defined as one third of the trace of the orthogonalized U^{ij} tensor.

Atom	x	y	z	U(eq)
Eu(1)	3638(1)	4385(1)	3535(1)	11(1)
O(2)	4266(2)	3192(1)	1809(1)	18(1)
O(3)	2566(1)	3644(1)	4991(1)	16(1)
O(5)	5022(2)	3608(1)	4363(1)	17(1)
O(6)	6569(2)	3616(1)	5633(1)	19(1)
C(28)	5336(2)	1668(2)	4128(2)	14(1)
N(1)	3111(2)	5138(2)	1829(1)	14(1)
C(29)	6279(2)	1175(2)	4345(2)	18(1)
N(2)	1144(2)	4285(2)	3073(1)	14(1)
C(33)	4076(2)	856(2)	3402(2)	18(1)
C(21)	1927(2)	2465(2)	6314(2)	14(1)
C(19)	1535(2)	24(2)	350(2)	20(1)
C(22)	556(2)	1840(2)	5766(2)	22(1)
C(2)	3941(2)	6158(2)	402(2)	21(1)
C(3)	2873(2)	6515(2)	352(2)	21(1)
C(14)	2834(2)	1024(2)	657(2)	16(1)
C(1)	4028(2)	5487(2)	1171(2)	18(1)
C(8)	-1201(2)	4773(2)	2940(2)	21(1)
C(26)	2330(2)	2142(2)	7250(2)	19(1)
C(13)	3146(2)	2227(2)	1630(2)	15(1)
C(4)	1874(2)	6157(2)	1030(2)	18(1)
C(27)	5663(2)	3043(2)	4740(2)	13(1)
C(20)	2963(2)	3476(2)	5908(2)	14(1)
C(11)	973(2)	4984(2)	2398(2)	14(1)
C(7)	-181(2)	5269(2)	2312(2)	18(1)
C(18)	1217(3)	-1063(2)	-590(2)	28(1)
C(10)	174(2)	3864(2)	3663(2)	18(1)
C(24)	21(2)	575(2)	7055(2)	25(1)
C(25)	1380(2)	1191(2)	7611(2)	23(1)
C(32)	3760(2)	-439(2)	2908(2)	24(1)

C(30)	5967(2)	-114(2)	3831(2)	22(1)
C(12)	2019(2)	5438(2)	1741(2)	14(1)
C(9)	-1022(2)	4080(2)	3620(2)	21(1)
C(17)	2237(3)	-1142(2)	-1202(2)	31(1)
C(6)	-263(2)	6048(2)	1620(2)	22(1)
C(31)	4702(3)	-920(2)	3120(2)	24(1)
C(23)	-389(2)	908(2)	6141(2)	27(1)
C(15)	3845(2)	922(2)	45(2)	22(1)
C(5)	715(2)	6475(2)	1006(2)	22(1)
C(16)	3540(3)	-170(2)	-884(2)	28(1)
O(1)	2249(1)	2233(1)	2258(1)	17(1)
O(4)	4148(1)	4096(1)	6518(1)	16(1)

Table F.2: Bond distances (Å) and angles (º) for **{[$Eu_2(BCA)_6(Phen)_2$]- μ-[κ^2-O,O'-(BCA)]$_2$} (3)**

Atom	Bond Distance (Å)	Atom	Angle/°
Eu(1)-O(5)	2.3364(15)	**O(5)-Eu(1)-O(3)**	73.54(6)
Eu(1)-O(3)	2.3668(15)	**O(5)-Eu(1)-O(4)#1**	79.77(6)
Eu(1)-O(4)#1	2.3800(16)	**O(3)-Eu(1)-O(4)#1**	134.69(5)
Eu(1)-O(1)	2.4187(16)	**O(5)-Eu(1)-O(1)**	89.64(6)
Eu(1)-O(6)#1	2.4296(17)	**O(3)-Eu(1)-O(1)**	86.06(6)
Eu(1)-O(2)	2.5146(16)	**O(4)#1-Eu(1)-O(1)**	130.15(5)
Eu(1)-N(1)	2.5906(19)	**O(5)-Eu(1)-O(6)#1**	126.83(5)
Eu(1)-N(2)	2.655(2)	**O(3)-Eu(1)-O(6)#1**	87.75(5)
Eu(1)-C(13)	2.824(2)	**O(4)#1-Eu(1)-O(6)#1**	79.71(6)
Eu(1)-O(5)#1	2.8379(17)	**O(1)-Eu(1)-O(6)#1**	139.18(5)
Eu(1)-C(27)#1	3.001(2)	**O(5)-Eu(1)-O(2)**	77.68(6)
Eu(1)-Eu(1)#1	4.0262(14)	**O(3)-Eu(1)-O(2)**	129.61(5)
O(2)-C(13)	1.254(3)	**O(4)#1-Eu(1)-O(2)**	77.08(5)
O(3)-C(20)	1.268(2)	**O(1)-Eu(1)-O(2)**	53.09(5)
O(5)-C(27)	1.272(2)	**O(6)#1-Eu(1)-O(2)**	142.04(5)
O(5)-Eu(1)#1	2.8379(17)	**O(5)-Eu(1)-N(1)**	145.86(5)
O(6)-C(27)	1.252(3)	**O(3)-Eu(1)-N(1)**	139.38(6)
O(6)-Eu(1)#1	2.4296(17)	**O(4)#1-Eu(1)-N(1)**	77.96(5)
C(28)-C(33)	1.392(3)	**O(1)-Eu(1)-N(1)**	85.31(6)
C(28)-C(29)	1.396(3)	**O(6)#1-Eu(1)-N(1)**	73.71(6)
C(28)-C(27)	1.494(3)	**O(2)-Eu(1)-N(1)**	72.35(6)
N(1)-C(1)	1.326(3)	**O(5)-Eu(1)-N(2)**	147.37(5)
N(1)-C(12)	1.359(3)	**O(3)-Eu(1)-N(2)**	76.97(5)

C(29)-C(30)	1.386(3)	**O(4)#1-Eu(1)-N(2)**	132.11(6)
C(29)-H(26)	0.93	**O(1)-Eu(1)-N(2)**	74.60(5)
N(2)-C(10)	1.321(3)	**O(6)#1-Eu(1)-N(2)**	64.70(5)
N(2)-C(11)	1.366(3)	**O(2)-Eu(1)-N(2)**	112.15(5)
C(33)-C(32)	1.388(3)	**N(1)-Eu(1)-N(2)**	62.47(5)
C(33)-H(30)	0.93	**O(5)-Eu(1)-C(13)**	82.39(6)
C(21)-C(22)	1.392(3)	**O(3)-Eu(1)-C(13)**	108.41(6)
C(21)-C(26)	1.395(3)	**O(4)#1-Eu(1)-C(13)**	103.43(6)
C(21)-C(20)	1.508(3)	**O(1)-Eu(1)-C(13)**	26.74(5)
C(19)-C(14)	1.382(3)	**O(6)#1-Eu(1)-C(13)**	150.27(5)
C(19)-C(18)	1.395(3)	**O(2)-Eu(1)-C(13)**	26.35(5)
C(19)-H(13)	0.93	**N(1)-Eu(1)-C(13)**	78.04(6)
C(22)-C(23)	1.385(3)	**N(2)-Eu(1)-C(13)**	94.08(6)
C(22)-H(19)	0.93	**O(5)-Eu(1)-O(5)#1**	78.26(6)
C(2)-C(3)	1.374(3)	**O(3)-Eu(1)-O(5)#1**	73.28(5)
C(2)-C(1)	1.404(3)	**O(4)#1-Eu(1)-O(5)#1**	65.79(5)
C(2)-H(2)	0.93	**O(1)-Eu(1)-O(5)#1**	158.27(5)
C(3)-C(4)	1.406(3)	**O(6)#1-Eu(1)-O(5)#1**	48.59(5)
C(3)-H(3)	0.93	**O(2)-Eu(1)-O(5)#1**	138.57(5)
C(14)-C(15)	1.388(3)	**N(1)-Eu(1)-O(5)#1**	114.74(5)
C(14)-C(13)	1.505(3)	**N(2)-Eu(1)-O(5)#1**	106.31(5)
C(1)-H(1)	0.93	**C(13)-Eu(1)-O(5)#1**	159.21(5)
C(8)-C(9)	1.367(3)	**O(5)-Eu(1)-C(27)#1**	103.18(6)
C(8)-C(7)	1.411(3)	**O(3)-Eu(1)-C(27)#1**	81.87(6)
C(8)-H(8)	0.93	**O(4)#1-Eu(1)-C(27)#1**	69.29(5)
C(26)-C(25)	1.391(3)	**O(1)-Eu(1)-C(27)#1**	159.04(5)
C(26)-H(23)	0.93	**O(6)#1-Eu(1)-C(27)#1**	23.81(5)
C(13)-O(1)	1.275(2)	**O(2)-Eu(1)-C(27)#1**	145.47(5)
C(4)-C(12)	1.409(3)	**N(1)-Eu(1)-C(27)#1**	92.74(6)
C(4)-C(5)	1.438(3)	**N(2)-Eu(1)-C(27)#1**	85.98(5)
C(27)-Eu(1)#1	3.001(2)	**C(13)-Eu(1)-C(27)#1**	169.48(5)
C(20)-O(4)	1.259(2)	**O(5)#1-Eu(1)-C(27)#1**	24.95(5)
C(11)-C(7)	1.413(3)	**O(5)-Eu(1)-Eu(1)#1**	43.64(4)
C(11)-C(12)	1.443(3)	**O(3)-Eu(1)-Eu(1)#1**	68.46(5)
C(7)-C(6)	1.431(3)	**O(4)#1-Eu(1)-Eu(1)#1**	66.91(4)
C(18)-C(17)	1.389(4)	**O(1)-Eu(1)-Eu(1)#1**	130.63(4)
C(18)-H(14)	0.93	**O(6)#1-Eu(1)-Eu(1)#1**	83.20(4)
C(10)-C(9)	1.407(3)	**O(2)-Eu(1)-Eu(1)#1**	113.87(4)
C(10)-H(10)	0.93	**N(1)-Eu(1)-Eu(1)#1**	140.84(4)
C(24)-C(23)	1.382(3)	**N(2)-Eu(1)-Eu(1)#1**	133.37(4)

C(24)-C(25)	1.384(3)	**C(13)-Eu(1)-Eu(1)#1**	125.60(4)
C(24)-H(21)	0.93	**O(5)#1-Eu(1)-Eu(1)#1**	34.62(3)
C(25)-H(22)	0.93	**C(27)#1-Eu(1)-Eu(1)#1**	59.55(4)
C(32)-C(31)	1.383(3)	**C(13)-O(2)-Eu(1)**	90.73(12)
C(32)-H(29)	0.93	**C(20)-O(3)-Eu(1)**	135.40(13)
C(30)-C(31)	1.388(3)	**C(27)-O(5)-Eu(1)**	172.75(14)
C(30)-H(27)	0.93	**C(27)-O(5)-Eu(1)#1**	84.73(12)
C(9)-H(9)	0.93	**Eu(1)-O(5)-Eu(1)#1**	101.74(6)
C(17)-C(16)	1.372(4)	**C(27)-O(6)-Eu(1)#1**	104.62(12)
C(17)-H(15)	0.93	**C(33)-C(28)-C(29)**	119.64(19)
C(6)-C(5)	1.349(3)	**C(33)-C(28)-C(27)**	121.05(18)
C(6)-H(6)	0.93	**C(29)-C(28)-C(27)**	119.20(18)
C(31)-H(28)	0.93	**C(1)-N(1)-C(12)**	117.85(18)
C(23)-H(20)	0.93	**C(1)-N(1)-Eu(1)**	120.98(14)
C(15)-C(16)	1.392(3)	**C(12)-N(1)-Eu(1)**	119.77(13)
C(15)-H(17)	0.93	**C(30)-C(29)-C(28)**	120.2(2)
C(5)-H(5)	0.93	**C(30)-C(29)-H(26)**	119.9
C(16)-H(16)	0.93	**C(28)-C(29)-H(26)**	119.9
O(4)-Eu(1)#1	2.3800(16)	**C(10)-N(2)-C(11)**	117.45(18)
		C(10)-N(2)-Eu(1)	123.20(14)
		C(11)-N(2)-Eu(1)	117.32(13)
		C(32)-C(33)-C(28)	119.9(2)
		C(32)-C(33)-H(30)	120.1
		C(28)-C(33)-H(30)	120.1
		C(22)-C(21)-C(26)	118.86(18)
		C(22)-C(21)-C(20)	120.76(18)
		C(26)-C(21)-C(20)	120.38(18)
		C(14)-C(19)-C(18)	120.7(2)
		C(14)-C(19)-H(13)	119.6
		C(18)-C(19)-H(13)	119.6
		C(23)-C(22)-C(21)	120.5(2)
		C(23)-C(22)-H(19)	119.8
		C(21)-C(22)-H(19)	119.8
		C(3)-C(2)-C(1)	118.4(2)
		C(3)-C(2)-H(2)	120.8
		C(1)-C(2)-H(2)	120.8
		C(2)-C(3)-C(4)	119.5(2)
		C(2)-C(3)-H(3)	120.2
		C(4)-C(3)-H(3)	120.2
		C(19)-C(14)-C(15)	119.5(2)

	C(19)-C(14)-C(13)	120.40(19)
	C(15)-C(14)-C(13)	120.11(19)
	N(1)-C(1)-C(2)	123.8(2)
	N(1)-C(1)-H(1)	118.1
	C(2)-C(1)-H(1)	118.1
	C(9)-C(8)-C(7)	119.6(2)
	C(9)-C(8)-H(8)	120.2
	C(7)-C(8)-H(8)	120.2
	C(25)-C(26)-C(21)	120.4(2)
	C(25)-C(26)-H(23)	119.8
	C(21)-C(26)-H(23)	119.8
	O(2)-C(13)-O(1)	121.49(18)
	O(2)-C(13)-C(14)	120.07(18)
	O(1)-C(13)-C(14)	118.44(18)
	O(2)-C(13)-Eu(1)	62.92(11)
	O(1)-C(13)-Eu(1)	58.61(10)
	C(14)-C(13)-Eu(1)	176.39(14)
	C(3)-C(4)-C(12)	117.82(19)
	C(3)-C(4)-C(5)	122.6(2)
	C(12)-C(4)-C(5)	119.54(19)
	O(6)-C(27)-O(5)	121.21(18)
	O(6)-C(27)-C(28)	118.45(17)
	O(5)-C(27)-C(28)	120.34(18)
	O(6)-C(27)-Eu(1)#1	51.56(10)
	O(5)-C(27)-Eu(1)#1	70.32(11)
	C(28)-C(27)-Eu(1)#1	166.46(13)
	O(4)-C(20)-O(3)	125.38(18)
	O(4)-C(20)-C(21)	117.10(18)
	O(3)-C(20)-C(21)	117.51(18)
	N(2)-C(11)-C(7)	122.90(19)
	N(2)-C(11)-C(12)	118.01(18)
	C(7)-C(11)-C(12)	119.09(19)
	C(8)-C(7)-C(11)	117.3(2)
	C(8)-C(7)-C(6)	123.1(2)
	C(11)-C(7)-C(6)	119.6(2)
	C(17)-C(18)-C(19)	119.0(2)
	C(17)-C(18)-H(14)	120.5
	C(19)-C(18)-H(14)	120.5
	N(2)-C(10)-C(9)	123.9(2)
	N(2)-C(10)-H(10)	118.1

	C(9)-C(10)-H(10)	118.1
	C(23)-C(24)-C(25)	119.7(2)
	C(23)-C(24)-H(21)	120.1
	C(25)-C(24)-H(21)	120.1
	C(24)-C(25)-C(26)	120.1(2)
	C(24)-C(25)-H(22)	119.9
	C(26)-C(25)-H(22)	119.9
	C(31)-C(32)-C(33)	120.2(2)
	C(31)-C(32)-H(29)	119.9
	C(33)-C(32)-H(29)	119.9
	C(29)-C(30)-C(31)	119.8(2)
	C(29)-C(30)-H(27)	120.1
	C(31)-C(30)-H(27)	120.1
	N(1)-C(12)-C(4)	122.47(19)
	N(1)-C(12)-C(11)	117.91(18)
	C(4)-C(12)-C(11)	119.62(18)
	C(8)-C(9)-C(10)	118.9(2)
	C(8)-C(9)-H(9)	120.6
	C(10)-C(9)-H(9)	120.6
	C(16)-C(17)-C(18)	120.6(2)
	C(16)-C(17)-H(15)	119.7
	C(18)-C(17)-H(15)	119.7
	C(5)-C(6)-C(7)	121.3(2)
	C(5)-C(6)-H(6)	119.4
	C(7)-C(6)-H(6)	119.4
	C(32)-C(31)-C(30)	120.3(2)
	C(32)-C(31)-H(28)	119.8
	C(30)-C(31)-H(28)	119.9
	C(24)-C(23)-C(22)	120.4(2)
	C(24)-C(23)-H(20)	119.8
	C(22)-C(23)-H(20)	119.8
	C(14)-C(15)-C(16)	120.0(2)
	C(14)-C(15)-H(17)	120
	C(16)-C(15)-H(17)	120
	C(6)-C(5)-C(4)	120.7(2)
	C(6)-C(5)-H(5)	119.6
	C(4)-C(5)-H(5)	119.6
	C(17)-C(16)-C(15)	120.1(2)
	C(17)-C(16)-H(16)	119.9
	C(15)-C(16)-H(16)	119.9

	C(13)-O(1)-Eu(1)	94.64(12)
	C(20)-O(4)-Eu(1)#1	139.80(13)

Table F.3: Anisotropic displacement parameters ($Å^2 \times 10^3$) for **{[Eu_2(BCA)$_6$(Phen)$_2$]- μ-[κ^2-O,O'-(BCA)]$_2$} (3)**. The anisotropic displacement factor exponent takes the form: $-2p^2[h^2 a^{*2} U^{11} + .. + 2 h k a^* b^* U^{12}]$

Atom	U11	U22	U33	U23	U13	U12
Eu(1)	11(1)	9(1)	12(1)	2(1)	3(1)	3(1)
O(2)	19(1)	13(1)	19(1)	3(1)	7(1)	5(1)
O(3)	14(1)	17(1)	17(1)	7(1)	5(1)	5(1)
O(5)	18(1)	16(1)	22(1)	9(1)	7(1)	10(1)
O(6)	17(1)	13(1)	23(1)	0(1)	-2(1)	6(1)
C(28)	16(1)	11(1)	13(1)	4(1)	4(1)	5(1)
N(1)	15(1)	11(1)	14(1)	0(1)	3(1)	5(1)
C(29)	18(1)	17(1)	19(1)	6(1)	4(1)	8(1)
N(2)	13(1)	12(1)	15(1)	1(1)	2(1)	4(1)
C(33)	18(1)	16(1)	19(1)	7(1)	1(1)	6(1)
C(21)	14(1)	11(1)	17(1)	4(1)	8(1)	5(1)
C(19)	24(1)	19(1)	16(1)	6(1)	1(1)	9(1)
C(22)	20(1)	21(1)	20(1)	9(1)	3(1)	3(1)
C(2)	24(1)	18(1)	19(1)	6(1)	8(1)	7(1)
C(3)	28(1)	18(1)	18(1)	8(1)	2(1)	8(1)
C(14)	22(1)	13(1)	12(1)	5(1)	2(1)	9(1)
C(1)	19(1)	15(1)	18(1)	4(1)	5(1)	7(1)
C(8)	16(1)	18(1)	26(1)	-2(1)	4(1)	9(1)
C(26)	17(1)	18(1)	24(1)	8(1)	5(1)	8(1)
C(13)	20(1)	14(1)	13(1)	5(1)	2(1)	8(1)
C(4)	19(1)	14(1)	17(1)	2(1)	0(1)	5(1)
C(27)	12(1)	12(1)	18(1)	6(1)	8(1)	6(1)
C(20)	15(1)	12(1)	17(1)	3(1)	9(1)	8(1)
C(11)	15(1)	11(1)	12(1)	-2(1)	-1(1)	4(1)
C(7)	18(1)	13(1)	17(1)	-3(1)	-1(1)	8(1)
C(18)	34(1)	17(1)	24(1)	3(1)	-7(1)	8(1)
C(10)	16(1)	16(1)	19(1)	3(1)	4(1)	4(1)
C(24)	25(1)	18(1)	29(1)	12(1)	12(1)	3(1)
C(25)	26(1)	23(1)	28(1)	17(1)	10(1)	12(1)
C(32)	25(1)	16(1)	20(1)	2(1)	-1(1)	2(1)
C(30)	30(1)	20(1)	22(1)	6(1)	8(1)	16(1)
C(12)	15(1)	12(1)	12(1)	-1(1)	0(1)	5(1)
C(9)	16(1)	19(1)	23(1)	1(1)	7(1)	5(1)
C(17)	55(2)	23(1)	16(1)	-3(1)	-4(1)	24(1)
C(6)	23(1)	21(1)	23(1)	0(1)	-1(1)	14(1)
C(31)	37(1)	13(1)	20(1)	2(1)	7(1)	10(1)
C(23)	17(1)	27(1)	28(1)	11(1)	4(1)	-1(1)

C(15)	29(1)	21(1)	20(1)	8(1)	8(1)	13(1)
C(5)	26(1)	19(1)	21(1)	6(1)	-1(1)	13(1)
C(16)	44(2)	29(1)	21(1)	7(1)	11(1)	26(1)
O(1)	16(1)	15(1)	17(1)	1(1)	5(1)	5(1)
O(4)	13(1)	15(1)	18(1)	5(1)	3(1)	2(1)